Breaking Barriers

Blood-brain barrier alterations in capillary cerebral amyloid angiopathy and Alzheimer's disease

Anna Carrano

VRIJE UNIVERSITEIT

Breaking Barriers
Blood-brain barrier alterations in capillary cerebral amyloid angiopathy and Alzheimer's disease

ACADEMISCH PROEFSCHRIFT

ter verkrijging van de graad Doctor aan
de Vrije Universiteit Amsterdam,
op gezag van de rector magnificus
prof.dr. F.A. van der Duyn Schouten,
in het openbaar te verdedigen
ten overstaan van de promotiecommissie
van de Faculteit der Geneeskunde
op maandag 23 september 2013 om 13.45 uur
in de aula van de universiteit,
De Boelelaan 1105

door

Anna Carrano

geboren te Varallo Sesia, Vercelli, Italië

promotoren: prof.dr. A.J.M Rozemuller-Kwakkel
                     prof.dr. H.E. de Vries
copromotoren: dr. J.J.M. Hoozemans
                     dr. J. van Horssen

"There are only two ways to live your life.
One is as though nothing is a miracle.
The other is as though everything is
a miracle."

Albert Einstein

Contents

1

part

1

chapter

General introduction

Anna Carrano

Alzheimer's disease

Alzheimer's disease (AD) is the most common form of dementia in the elderly population in the occidental world. Because of the ongoing increase in life expectancy, we can expect approximately 25% of people living in the Western hemisphere to be over 65 years of age by 2050. One third of these elderly people will likely develop AD and become affected with or will suffer from the consequences of this severe, disabling disorder, for which no cure exists yet. The first AD case was described by the German psychiatrist and neuropathologist Alois Alzheimer in 1907 (Alzheimer, 1907). Upon histopathological examination of the brain he described the common neuropathological hallmarks of the disease, which are to date still used to confirm the definite diagnosis of AD.

AD is clinically characterized by a gradual decline in memory and cognition that makes patients in the final stage of the disease bedridden and completely care dependent. Clinical symptoms begin with short term memory loss, and progress to more extensive cognitive and emotional dysfunction. Death occurs on average 9 years after clinical diagnosis, but the characteristic neuropathological changes that will eventually result in dementia occur decades before the first clinical symptoms appear. Neuroimaging and biochemical analysis of the cerebrospinal fluid, together with neuropsychological examination, are important tools to establish the diagnosis of "probable AD" during life. However, definite diagnosis of AD can only be obtained post-mortem by pathological examination of the brain, which is still the "gold standard" for AD diagnosis today.

Pathology

On a macroscopic level the main pathological hallmark of AD is severe atrophy of selective brain regions, such as the neocortex, hippocampus, amygdala and entorhinal cortex. The extensive neuronal loss results in widening of the sulci, narrowing of the gyri and enlargement of the ventricles (figure 1). Microscopically, the characteristic neuropathological lesions include senile plaques containing β-amyloid (Aβ) and intracellular neurofibrillary tangles (NFT) containing hyperphosphorylated-tau. Both lesions occur throughout the cerebral cortex and are commonly accompanied by deposition of Aβ in the brain vasculature also known as cerebral amyloid angiopathy (CAA) (figure 2). NFTs have not only been detected in brains of AD pa-
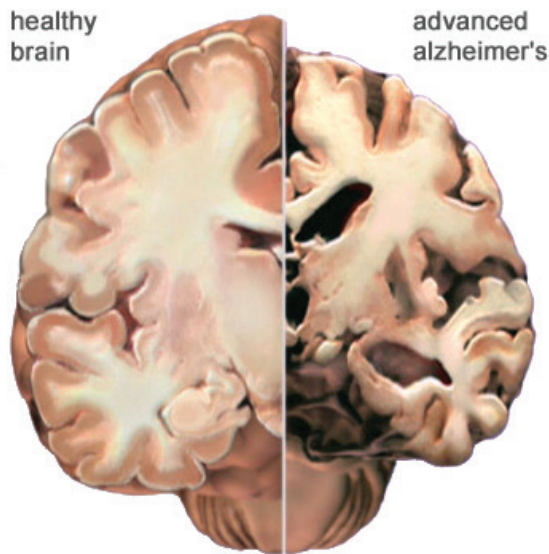
Figure 1. Macroscopical hallmarks of AD brain. A crosswise slice shows macroscopically the differences between a healthy brain and the severely affected AD brain. In the AD brain the cortex shrivels up, damaging areas involved in thinking, planning and memory. Atrophy is especially severe in the hippocampus, an area of the cortex that plays a key role in formation of new memories. Ventricles grow larger.

tients but also in patients suffering from other types of dementia. Extensive deposition of Aβ however exclusively occurs in AD pathology.

Although the pathological diagnosis of AD is based on the presence of insoluble Aβ plaques and by the number and distribution of neurofibrillary changes, clinicopathological studies suggest that three features in particular correlate with clinical dementia. They are 1) the number and distribution of neurofibrillary changes (Braak, et al., 2006; Braak and Braak, 1991) ; 2) a raised level of soluble Aβ in the brain (Lue, et al., 1999; McLean, et al., 1999) ; and 3) the severity of CAA (NGoM, 2001).

Neurofibrillary tangles

Neurofibrillary tangles (NFT) are formed by hyperphosphorylation of the microtubule-associated protein tau, causing it to aggregate intracellularly in an insoluble form in neurons. Under physiological conditions the primary function of tau is to bind to the microtubules and assists with their formation and stabilization in order to maintain effective axonal transport.

Under pathological conditions, an excessive disengagement of tau from the microtubules takes place due to abnormal post-translational hyperphosphorylation of tau. The detachment of tau from the microtubules leads to its intracellular accumulation compromising axonal transport and thus contributing to synaptic dysfunction and eventually neuronal death and neurodegeneration (Ballatore, et al., 2007).

The severity of NFT pathology is graded on a 0–6 scale (using Roman numerals 0-VI by convention) according to "Braak stages" (Braak and Braak, 1991), which pertain to the spread of NFTs in the brain.

NFT pathology relates to the severity of dementia, however, even though the neurofibrillary changes are closely related to dementia, they do not have a clear relationship to genetic factors in AD and they are thought to appear later in the disease progression, following Aβ deposition. Furthermore, NFT are also found in other neurodegenerative diseases, such as tauopathies, including progressive frontotemporal dementia subtypes, supranuclear palsy, corticobasal degeneration and Pick's disease.

In AD pathological events, such as Aβ-mediated neurotoxicity, oxidative stress and inflammation may be responsible to initiate or contribute directly or indirectly to tau mediated neurodegeneration; however, their precise positioning in the cascade of events that leads to neuronal loss remains unclear.
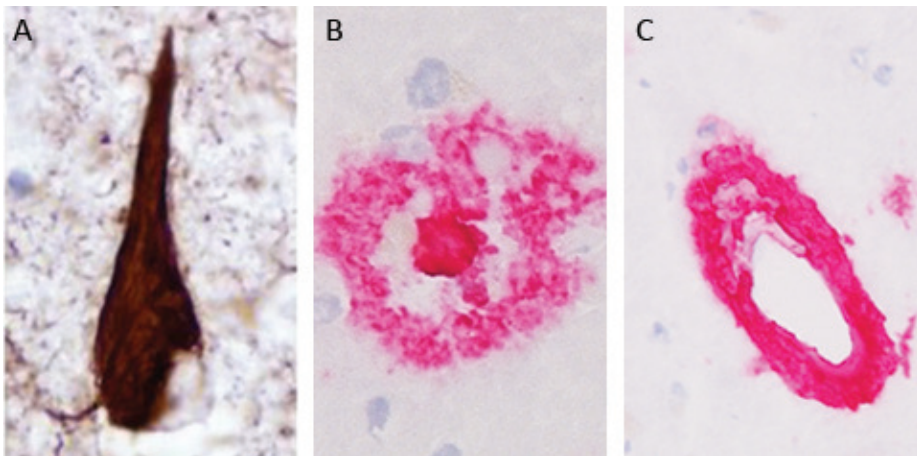

Figure 2. Microscopical hallmarks of AD. Immunohistochemical staining of the 3 hallmarks of AD: A) neurofibrillary tangle, B) neuritic plaque and C) cerebral amyloid angiopathy.

Amyloid Plaques

Plaques are characterized by extracellular deposition of Aβ and can be observed throughout the brain parenchyma. Full-length Aβ (Aβ1-40 or Aβ1-42) is derived from the amyloid precursor protein (APP) by sequential proteolytic activity of the β-secretase (or β-site AAP-cleaving enzyme, BACE) and the γ-secretase/presenilin complex (presenilin-1, nicastrin, APH1A and PEN2) (De Strooper 2003). After APP cleavage, Aβ peptides are secreted into the brain interstitial fluid (ISF) as monomers/dimers, where they are able to further polymerize into diffusible Aβ oligomers. The amino acid sequences of Aβ1-40 and Aβ1-42 are identical with the exception that the longer peptide contains 2 extra hydrophobic amino acids at the C-terminus, which render the Aβ1-42 more insoluble and prone to aggregation than Aβ1-40. In soluble states, Aβ is passively redistributed in brain parenchyma and cleared (Hardy and Selkoe, 2002). However, under pathological conditions Aβ starts to accumulate and because of its fibrillogenic characteristic forms protofibrils at first and eventually mature fibrils, which will deposit as insoluble plaques. Based on the importance of Aβ accumulation in AD pathogenesis, the amyloid cascade hypothesis has been formulated (for more details see figure 3).

Several forms of amyloid plaques can be distinguished in the brain parenchyma; the most common being compact and diffuse plaques. Diffuse plaques consist of amorphous extracellular deposits of Aβ and occur in large numbers in the same brain regions as neuritic plaques. Compact amyloid plaques (also called senile plaques or neuritic plaques) are roughly spherical in shape with a dense core of aggregated Aβ fibrils frequently surrounded by dystrophic axons and dendrites, activated microglia and reactive astrocytes. The severity of plaque pathology is scored according to a distinct metric, which is named after the Consortium to Establish a Registry for Alzheimer's Disease (CERAD) (Mirra, 1997). The CERAD scoring system is a four-tiered scale representing neocortical neuritic plaques density.
Amyloid plaques may also contain other proteins such as serum amyloid P component (SAP), activated complement proteins and clusterin (Eikelenboom, et al., 2011).

Cerebral Amyloid Angiopathy

CAA is defined by the deposition of a congophilic material (i.e. positive staining with a Congo-red dye) in cerebral leptomeningeal and intracortical arteries, arterioles and capillaries

and and can occasionnally be found in postcapillary venules and venes. CAA is caused by accumulation of Aβ peptide in the media and adventitia of cerebral blood vessels wall and occurs in about 98% of AD patients, with approximately 75% of these cases rated as severe CAA. Importantly, clinical studies reported a strong correlation between cognitive impairment and the severity of CAA (Attems, et al., 2011; Biffi and Greenberg, 2011; Thal, et al., 2008; Vinters, 1987).

The biologic overlap between CAA and AD is substantial as CAA is found, to some extent, in virtually all AD cases and correlated with AD severity (Thal, et al., 2008). Also genetically speaking the analogies between AD and CAA are undeniable. Mutations in the APP, PS1 and PS2 genes cause familial forms of AD and widespread CAA (Levy, et al., 2006; Mann, et al., 2001; Revesz, et al., 2003; St George-Hyslop, et al., 1987; Tanzi, et al., 1987). Most severe CAA is seen in cases with the Flemish, Iowa and Dutch mutations in the APP gene. Mutations in PS1 and PS2 genes can also lead to CAA in familial AD cases, especially those PS1-mutations beyond codon 200 (Revesz, et al., 2002).

Although non-invasive CAA diagnostic criteria have been developed and refined in the past decade, in order to both improve and standardize diagnosis during life (Boston criteria for CAA) (Knudsen, et al., 2001), a definitive CAA diagnosis can only be formulated after histological investigation of affected brain tissue, obtained at autopsy or via brain biopsy. Furthermore, positron emission tomography imaging with the Aβ-binding compound Pittsburgh Compound B can be used as a tool to distinguish between AD with or without CAA, as CAA generally favors occipital brain regions (Greenberg, et al., 2008) according to post mortem analysis of CAA pathology and radiographic analysis of CAA-related hemorrhages.

Common ApoE polymorphisms influence the risk of both sporadic CAA and sporadic AD (Biffi, et al., 2010). Based on localization, association to ApoE alleles and occurrence in AD patients, two types of sporadic CAA can be defined. CAA type 1 is characterized by Aβ accumulation in capillaries and is therefore often referred to as capillary CAA, although additional Aβ depositions in larger blood vessels, leptomeningeal and cortical arteries, arterioles, veins and venules can also be observed (Thal, et al., 2002). CAA type 1 has a strong association with Apolipoprotein E4 (ApoE4) genotype (46,7% allele frequency) (Richard, et al., 2010; Thal, et al., 2008) and correlates with severity of AD pathology (Attems and Jellinger, 2004). In CAA type 2, Aβ depositions are restricted to non-capillary blood vessels. CAA type 2 shows a higher frequency of the ApoE2 allele and is not associated with the ApoE4 genotype (Thal,
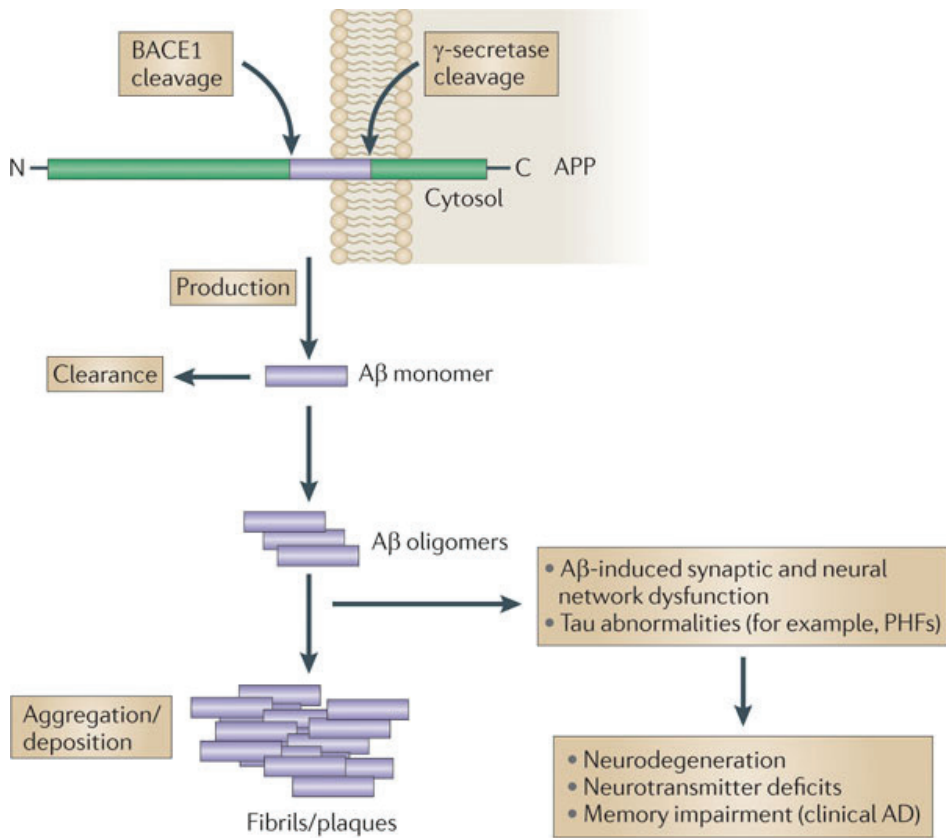
Figure 3. The amyloid cascade hypothesis. The amyloid cascade hypothesis posits that deposition of Aβ protein is the causative agent of AD pathology and that NFTs, neuronal cell loss, vascular damage follows as a direct result of this deposition that ultimately leads to AD dementia. The amyloid cascade hypothesis, first proposed by John Hardy in 1991, synthesizes histopathological and genetic information and has dominated AD research for the past twenty years.

The hypothesis started to take form in 1984 with the isolation of Aβ from leptomeningeal vessels (CAA) of an AD case and Down syndrome and later on with the identification of APP mutations as a cause of amyloid deposition in hereditary cerebral hemorrhage with amyloidosis Dutch type (a familiar form of CAA) (van Duinen et al. 1987; Levy et al. 1990; Van Broeckhoven et al. 1990). It was then clear that mutations in the APP gene (located on chromosome 21) could cause Aβ accumulation in some familiar cases and that these mutations likely induced an increase in Aβ production. We now know that mutations in APP, presenilin 1 (PS1) and presenilin 2 (PS2) are responsible for familiar forms of early onset AD (EOAD). These mutations indeed not only cause increased Aβ production, but, in addition, promote the release of more toxic forms of Aβ. Although these genetic alterations are not responsible for the more common late onset AD, accumulation of cerebral Aβ is still the key event in the pathogenesis of the sporadic form of the disease. Increased levels of Aβ can either be the result of increased production or alternatively by decreased clearance of Aβ. In sporadic AD Aβ accumulation is most likely due to an inefficient removal of Aβ rather than overproduction, as seen in EOAD. (Di Paolo et al., 2011).

et al., 2002). Interestingly ApoE2, which exerts a protective effect on AD risk, increases risk of intracerebral hemorrhage in CAA patients (Nicoll, et al., 1997). Based on the findings it seems that these two CAA types represent two different pathological entities. Furthermore, CAA type 1 appears to be more strictly related to AD pathology and it has even been postulated that CAA type 1 is a specific subtype of sporadic AD, defined by characteristic neuropathological features (Richard, et al., 2010) and genotype specific associations (Thal, et al., 2010).

The two types of CAA also differ with regard to the composition of Aβ species present in the vascular wall. The ratio between the two main forms of Aβ (1-40 and 1-42) has been reported to be different, with capCAA showing a ratio 1-40/1-42 significantly lower than in CAA type 2, a ratio much more similar to what found in parenchymal plaques. Thus, Aβ 1–40 has a greater tendency to be deposited in the larger vessel wall, whereas Aβ 1–42 is mainly deposited in senile plaques and CAA-affected capillaries (Attems and Jellinger, 2004; Roher, et al., 2003; Thal, et al., 2008). Nonetheless, it has to be noted that Aβ 1-40 is also present in capCAA and senile plaques as well and that the two Aβ isoforms are both present in amyloid-laden capillaries (Richard, et al., 2010).

In addition, N-terminal truncated forms of Aβ and other proteins including apoE are present in cerebrovascular Aβ depositions. Aβ is initially deposited in the abluminal portion of the tunica media surrounding smooth muscle cells (SMC) as well as in the adventitia. With increasing severity all layers of the vessel wall show Aβ depositions accompanied by a loss of SMC (Kawai, et al., 1993; Yamaguchi, et al., 1992). In capillaries, devoid of a smooth muscle cell layer, amyloid deposition also starts in the basement membrane, may extravasate into the neuropil and may also lead to capillary occlusion in severe cases (Thal, et al., 2008; Yamaguchi, et al., 1992).

In very severe stages of CAA the vascular architecture is disrupted potentially leading to microaneurysm formation, fibrinoid necrosis and Aβ depositions in the adjacent surrounding neuropil (i.e. dyshoric changes) (Attems, et al., 2011).

Frequently, dyshoric changes are seen surrounding capillaries as globose Aβ accumulation or flame like deposits and therefore some authors misleadingly use 'dyshoric CAA' as a synonym for capCAA.

The deposition of Aβ as CAA is probably due to the failure of two main mechanisms of Aβ

Historical notes

In 1907 Alois Alzheimer, a German pychiatrist, described, for the first time, the clinical symptoms and the typical plaques and tangles in a demented woman with presenile dementia (Alzheimer, 1907). In the same year, and without knowing the findings of Alzheimer, Oskar Fischer reported neuritic plaques in 12 cases of senile dementia (Fischer, 1907). These were landmark findings in the history of research in dementia because they delineated the clinico-pathological entity that is now known as Alzheimer's disease.

Cerebral amyloid angiopathy was probably observed for the first time in 1909 by Oppenheim when he described metachromasia in the core of plaques, which could also be found in nearby capillaries (Oppenheim, 1909). The amyloid nature of plaques was discovered by Divry in 1927, who also observed CAA (Divry, 1927), but the first systematic study was made by Scholz in 1938 (Scholz, 1938).

The term "angiopathy dyshorique" was originally introduced by Morel in 1950 (Morel, 1950) and interpreted as congophilic angiopathy (synonymous with CAA), with parenchymal lesions by Pantelakis in 1954 (Pantelakis, 1954). This terminology was derived from translating the original German description of CAA, which used the term *Drusige Entartung*, as used by Scholz, who reported that the substance in this specific form of angiopathy was the same as the main component of senile plaques. This term already made the link with amyloid plaques, which were called *Alzheimer Drusen* at that time, and meant the occurrence of plaque-like silver and Congo red stainable material in blood vessels (Richard, et al., 2010).

In 1984 Glenner and Wong isolated Aβ from cerebral blood vessels (Glenner and Wong, 1984b). Glenner and Wong were the first to isolate Aβ (called by them, beta amyloid) from the meningeal vessels of first a late onset sporadic AD case and then, based on the universal occurrence of AD in trisomy 21, from a Down syndrome brain (Glenner and Wong, 1984a).

Alzheimer, A. 1907. Über eine eigenartige Erkrankung der Hirnrinde. *Allgemeine Zeitschrift für Psychiatrie* 64, 146-8.

Divry, P. 1927. Etude histochimique des plaques séniles. *J Belge Neurol Psychiatry* 27, 643-57.

Fischer, O. 1907. Miliare Nekrosen mit drusigen Wucherunger der Neurofibrillen, eine regelmässige Veränderung der Hirnrinde bei seniler Demenz. *Monatsschr Psychiatr Neurol* 22, 361-72.

Glenner, G.G., Wong, C.W. 1984a. Alzheimer's disease and Down's syndrome: sharing of a unique cerebrovascular amyloid fibril protein. *Biochem Biophys Res Commun* 122(3), 1131-5.

Glenner, G.G., Wong, C.W. 1984b. Alzheimer's disease: initial report of the purification and characterization of a novel cerebrovascular amyloid protein. *Biochem Biophys Res Commun* 120(3), 885-90.

Morel, F. 1950. Petite contribution a l'etude d'une angiopathie apparement dyshorique et topistique. *Rev Mens Psychiat Neurol* 120, 352-7.

Oppenheim, G. 1909. Über 'drusige Nekrosen' in der Großhirnrinde. *Neurol Zbl* 8, 410-3.

Pantelakis, S. 1954. [A particular type of senile angiopathy of the central nervous system: congophilic angiopathy, topography and frequency]. *Monatsschr Psychiatr Neurol* 128(4), 219-56.

Richard, E., Carrano, A., Hoozemans, J.J., van Horssen, J., van Haastert, E.S., Eurelings, L.S., de Vries, H.E., Thal, D.R., Eikelenboom, P., van Gool, W.A., Rozemuller, A.J. 2010. Characteristics of dyshoric capillary cerebral amyloid angiopathy. *J Neuropathol Exp Neurol* 69(11), 1158-67.

Scholz, W. 1938. Studien zur Pathologie der Hirngefäße. II. Die drusige Entartung der Hirnarterien und -capillaren (Eine Form seniler Gefäßerkrankung). *Z Ges Neurol Psychiatr* 162, 694-715.

elimination from the brain: 1) the direct transport of Aβ into the blood via specific receptors at the BBB and 2) the perivascular drainage of Aβ with other solutes and interstitial fluid along capillary and artery walls. Deposition of Aβ within the perivascular space forms an obstacle and reduces the drainage capacity which can lead to CAA formation and also to increased parenchymal Aβ deposition (Weller, et al., 1998; Weller, et al., 2008).

Clearance of Aβ through the BBB is discussed in the following chapters.

The blood-brain barrier

The BBB is a complex structure within the brain and its main function is to provide and maintain a highly controlled microenvironment for neurotransmission to occur through the formation of a tight sealed barrier between the circulating blood and the CNS (figure 4). It is formed by a monolayer of brain microvascular endothelial cells, capillary basement membranes, astrocytic end feet and pericytes (Fig.2). The BBB is characterized, at least in part, by a specific phenotype of the endothelial cells, with adherens junctions as cell–cell interaction stabilizers, and tight junctions (TJ) that limit paracellular flow of water, ions and larger molecules into the brain.

TJ are domains of occluded intercellular clefts composed of protein complexes that seal the paracellular space. The sealing feature of the TJ is regulated by the expression of transmembrane proteins, such as occludin, claudins and junction adhesion molecules, anchored via accessory proteins, such as ZO-1-3 to the cytoskeleton. Occludin and the claudins consist of four transmembrane domains and two extracellular loops and form the TJ through homophilic protein-protein interactions mediated by the extracellular loops and are the most important membranous components of the junctions. The presence of intricate TJ complexes together with the lack of fenestrations are important characteristic of the BBB, which guarantee the low permeability of the barrier, impeding the entrance of plasma components, red blood cells, and leukocytes into the CNS, and conferring the high electrical resistance of the BBB.

The TJ have a valuable function not only in restricting paracellular permeability (gate function), but also in segregating the apical and basal domains of the cell membrane (fence function) so that the endothelium can take on the polarized (apical–basal) properties that are more commonly found in epithelia.

The supply of necessary substances into the brain needs therefore to be mediated by active transport. Several transporters for amino acid and nucleosides are present at the BBB along with the glucose transporter 1, allowing the maintenance of cerebral homeostasis.

BBB disruption is a common feature of virtually all neurodegenerative disorders and so, along with neuroinflammation, can be viewed as a key component in the process of neurodegeneration. The main question remains whether BBB dysfunction precedes neuropathological changes such as senile plaques and NFTs. Alternatively, impaired BBB function might be a secondary event and caused by the deposition of aberrant protein aggregates and concomitant inflammatory responses.

Histopathological studies have demonstrated that BBB changes are evident in the cerebral microvasculature of AD patients (Claudio, 1996; Farkas and Luiten, 2001). These include degeneration of perivascular cells, swollen astrocytic end feet (Higuchi, et al., 1987; Yamashita, et al., 1991), reduced expression of glucose transporter-1 protein, increased pinocytotic vesicles and decreased numbers of mitochondria. In addition, prominent thickening and local disruption of capillary basement membranes have been reported by several research groups analyzing either biopsy tissue or post mortem material (Farkas, et al., 2000; Perlmutter and Chui, 1990). Furthermore, the appearance of string vessels (collapsed and acellular membrane tubes), a reduction in capillary density, accumulation of collagen and perlecans in the basement membrane, loss of tight junctions and/or adherens junctions and BBB breakdown with leakage of blood-borne molecules have also been reported in AD (Zlokovic, 2011). Taken together, there is ample evidence that microvascular pathology is a commonly observed phenomenon in AD brains.

Because in capCAA accumulation of Aβ occurs at the interface of the CNS and the systemic circulation, affecting those location responsible for the transport or the clearance of Aβ into the venous or CSF compartments, the role of capCAA in affecting BBB function and integrity and therefore the involvement in Aβ clearance is of particular interest to understand AD pathophysiology.

Amyloid clearance

The low paracellular permeability of the BBB implies that, in order to cross the barrier, specific transporters and carriers are needed to allow the entrance of necessary metabolites and nu-

trients and the removal of toxic substances in order to maintain cerebral homeostatic balance. The brain endothelium does not allow free exchange of peptides, and this is also true for the passage of Aβ. The transport of Aβ is strictly regulated by specific (and less specific) transporters at the BBB, which play a crucial role in the clearance of Aβ from the brain.

The major influx transporter for Aβ across the BBB is the receptor for advanced glycation endproducts (RAGE). RAGE binds to different forms of Aβ and mediates its pathophysiologic cellular responses: not only can it transport Aβ across the BBB into the brain, but Aβ/RAGE interaction contributes to the neurotoxic effects directly by producing oxidative damage to RAGE-expressing neurons, and indirectly, by activating microglia (Yan, et al., 1996). The Aβ-enriched environment in AD brains increases RAGE expression at the BBB and in neurons, amplifying Aβ-mediated pathogenic responses.

Low-density lipoprotein receptor related protein 1 (LRP1), a member of the LDL receptor family, is the major efflux transporter of Aβ (Shibata, et al., 2000) and acts as a multifunctional scavenger and signaling receptor. Binding of Aβ to LRP1 at the abluminal side of the BBB initiates Aβ clearance from the brain to the systemic circulation via transcytosis across the BBB. LRP1 binds to Aβ either directly or via Aβ chaperones such as ApoE to mediate brain Aβ clearance.

ApoE mediates the clearance of Aβ and influence risk of developing AD affecting Aβ clearance in an isoform-dependent manner. The ApoE4 allele is in fact the isoform less effective in clearing Aβ when compared to ApoE2 and ApoE3 isoforms (Kim, et al., 2009). Notably, ApoE4 is the major genetic risk factor for sporadic AD, increasing risk and decreasing age at onset of AD dose-dependently, with the homozygotes having the higher risk (Castellano, et al., 2011).

Another apolipoprotein, ApoJ, also known as clusterin, is involved in the transport of Aβ across the BBB. ApoJ, as well as ApoE, can cluster to Aβ and facilitates its binding to LRP2. LRP2 quickly transports ApoJ across the BBB and eliminates Aβ as well when it is bound to ApoJ. Interestingly, also ApoJ has been reported to increase the risk of developing sporadic AD, emphasizing the importance of Aβ clearance in the development of AD.

The ABC (ATP-binding cassette) transporters belong to another class of transporters involved in the removal of Aβ from the brain. These are efflux transporters that are normally expressed at the BBB and limit the penetration of many drugs into the brain. Some ABC transporters,
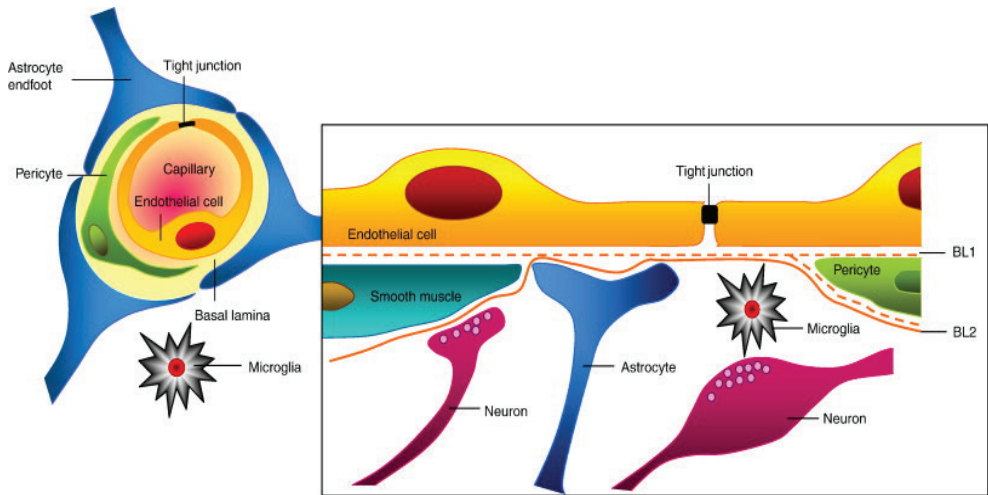
Figure 4. The Blood-Brain Barrier. The cerebral endothelial cells form tight junctions at their margins which seal the aqueous paracellular diffusional pathway between the cells. Pericytes are distributed discontinuously along the length of the cerebral capillaries and partially surround the endothelium. Both the cerebral endothelial cells and the pericytes are enclosed by, and contribute to, the local basement membrane which forms a distinct perivascular extracellular matrix (basal lamina 1, BL1), different in composition from the extracellular matrix of the glial endfeet bounding the brain parenchyma (BL2). Foot processes from astrocytes form a complex network surrounding the capillaries and this close cell association is important in induction and maintenance of the barrier properties. Axonal projections from neurons onto arteriolar smooth muscle contain vasoactive neurotransmitters and peptides and regulate local cerebral blood. BBB permeability may be regulated by release of vasoactive peptides and other agents from cells associated with the endothelium. Microglia are the resident immunocompetent cells of the brain. The movement of solutes across the BBB is facilitated by passive or active transporters in the endothelial cell membranes. Efflux transporters in the endothelium limit the CNS penetration of a wide variety of solutes including Aβ (Abbott et al., 2009).

including P-glycoprotein (P-gp), BCRP (breast cancer resistance protein) and MRP-1 (multidrug resistance-associated protein 1), are able to transport Aβ mediating its efflux from the brain endothelium to blood across the luminal side of the BBB.

Defective vascular clearance of Aβ from the brain and/or an increased re-entry of peripheral Aβ across the blood vessels into the brain result in elevated Aβ levels in the brain parenchyma and around cerebral blood vessels. At pathophysiological concentrations, Aβ forms neurotoxic oligomers and also self-aggregates, which leads to the development of CAA and plaques. Because of the pivotal role of Aβ removal in regulating the concentration of Aβ in the brain and therefore its accumulation, the transport of Aβ across the BBB might be a key event in the pathological cascade that leads to AD.

Inflammation

Inflammation and oxidative stress in the brain are concurrent with AD. Currently, there has been increasing evidence suggesting that inflammatory mechanisms are not merely bystanders in neurodegeneration but powerful pathogenetic forces in the disease process.

The innate immune response and resulting neuroinflammation appears to be responsible for local activation of microglia, astrocytes, and the complement system, the subsequent local initiating a pro-inflammatory cascade that results in the release of potentially cytotoxic molecules, cytokines, reactive oxygen species (ROS) and other related compounds, causing neurodegeneration (Yu and Tan, 2012).

Elevated levels of proinflammatory cytokines and acute phase proteins are localized around Aβ plaques in AD (Akiyama, et al., 2000), suggesting that the AD brain is in a chronic proinflammatory state. Oligomeric Aβ1-42 can also cause oxidative stress by integrating into membranes and catalytically generating the lipid peroxidation product, 4-hydroxynonenal (HNE), and through activation of the ROS-generating enzyme NADPH oxidase in microglia. On the other hand, inflammation and/or oxidative stress can themselves cause Aβ accumulation in the brain. APP, from which Aβ is cleaved, is transcriptionally regulated similarly to heat shock proteins and is responsive to the proinflammatory cytokine IL-1. Oxidative stress, on its turn, upregulates proteins involved in Aβ production, such as presenilin 1 (Oda, et al., 2010).

Several studies have suggested that amyloid associated proteins, such as clusterin and heat shock proteins, are involved directly and indirectly in numerous ways related to inflammation and immunities in the brain, regulating complement activation, inhibiting NF-κB, activating microglia and inducing release of proinflammatory cytokines (Bruinsma, et al., 2012; Erickson, et al., 2012).

Modest, transient upregulation of Aβ in the brain may serve as an antioxidant defense and promote clearance of damaged cells in the brain by microglia (Kontush, 2001; Neniskyte, et al., 2011). Under severe or chronic conditions of cellular stress, it is however feasible that Aβ accumulation could transition to pathological levels, resulting in formation of toxic oligomers that drive the AD process (Erickson, et al., 2012).

A prominent inflammatory response is found especially surrounding capCAA in which dyshoric changes are particularly severe. Furthermore CAA-related inflammation is of clinical importance since patients with this type of pathology present with cognitive decline, sei-

zures and headaches, that improve upon anti-inflammatory treatment (Chung, et al., 2011; Eng, et al., 2004; Kinnecom, et al., 2007). In addition, it has been suggested that especially capCAA dyshoric changes could contribute to a rapid clinical deterioration (Eurelings, et al., 2010), suggesting an important role of capCAA and dyshoric angiopathy, rather than plaques and CAA, in cognitive decline.

References

Abbott, N.J., Patabendige, A.A., Dolman, D.E., Yusof, S.R., Begley, D.J. 2010. Structure and function of the blood-brain barrier. *Neurobiol Dis* 37(1), 13-25.

Akiyama, H., Barger, S., Barnum, S., Bradt, B., Bauer, J., Cole, G.M., Cooper, N.R., Eikelenboom, P., Emmerling, M., Fiebich, B.L., Finch, C.E., Frautschy, S., Griffin, W.S., Hampel, H., Hull, M., Landreth, G., Lue, L., Mrak, R., Mackenzie, I.R., McGeer, P.L., O'Banion, M.K., Pachter, J., Pasinetti, G., Plata-Salaman, C., Rogers, J., Rydel, R., Shen, Y., Streit, W., Strohmeyer, R., Tooyoma, I., Van Muiswinkel, F.L., Veerhuis, R., Walker, D., Webster, S., Wegrzyniak, B., Wenk, G., Wyss-Coray, T. 2000. Inflammation and Alzheimer's disease. *Neurobiol Aging* 21(3), 383-421.

Alzheimer, A. 1907. Über eine eigenartige Erkrankung der Hirnrinde. *Allgemeine Zeitschrift für Psychiatrie* 64, 146-8.

Attems, J., Jellinger, K., Thal, D.R., Van Nostrand, W. 2011. Review: sporadic cerebral amyloid angiopathy. *Neuropathol Appl Neurobiol* 37(1), 75-93.

Attems, J., Jellinger, K.A. 2004. Only cerebral capillary amyloid angiopathy correlates with Alzheimer pathology--a pilot study. *Acta Neuropathol* 107(2), 83-90.

Bakker, A., Krauss, G.L., Albert, M.S., Speck, C.L., Jones, L.R., Stark, C.E., Yassa, M.A., Bassett, S.S., Shelton, A.L., Gallagher, M. 2012. Reduction of hippocampal hyperactivity improves cognition in amnestic mild cognitive impairment. *Neuron* 74(3), 467-74.

Ballatore, C., Lee, V.M., Trojanowski, J.Q. 2007. Tau-mediated neurodegeneration in Alzheimer's disease and related disorders. *Nat Rev Neurosci* 8(9), 663-72.

Biffi, A., Greenberg, S.M. 2011. Cerebral amyloid angiopathy: a systematic review. *J Clin Neurol* 7(1), 1-9.

Biffi, A., Sonni, A., Anderson, C.D., Kissela, B., Jagiella, J.M., Schmidt, H., Jimenez-Conde, J., Hansen, B.M., Fernandez-Cadenas, I., Cortellini, L., Ayres, A., Schwab, K., Juchniewicz, K., Urbanik, A., Rost, N.S., Viswanathan, A., Seifert-Held, T., Stoegerer, E.M., Tomas, M., Rabionet, R., Estivill, X., Brown, D.L., Silliman, S.L., Selim, M., Worrall, B.B., Meschia, J.F., Montaner, J., Lindgren, A., Roquer, J., Schmidt, R., Greenberg, S.M., Slowik, A., Broderick, J.P., Woo, D., Rosand, J. 2010. Variants at APOE influence risk of deep and lobar intracerebral hemorrhage. *Ann Neurol* 68(6), 934-43.

Braak, H., Braak, E. 1991. Neuropathological stageing of Alzheimer-related changes. *Acta Neuropathol* 82(4), 239-59.

Bruinsma, I.B., de Jager, M., Carrano, A., Versleijen, A.A., Veerhuis, R., Boelens, W.,

Rozemuller, A.J., de Waal, R.M., Verbeek, M.M. 2012. Small heat shock proteins induce a cerebral inflammatory reaction. *J Neurosci* 31(33), 11992-2000.

Castellano, J.M., Kim, J., Stewart, F.R., Jiang, H., DeMattos, R.B., Patterson, B.W., Fagan, A.M., Morris, J.C., Mawuenyega, K.G., Cruchaga, C., Goate, A.M., Bales, K.R., Paul, S.M., Bateman, R.J., Holtzman, D.M. 2011. Human apoE isoforms differentially regulate brain amyloid-beta peptide clearance. *Sci Transl Med* 3(89), 89ra57.

Chafekar, S.M., Baas, F., Scheper, W. 2008. Oligomer-specific Abeta toxicity in cell models is mediated by selective uptake. *Biochim Biophys Acta* 1782(9), 523-31.

Chung, K.K., Anderson, N.E., Hutchinson, D., Synek, B., Barber, P.A. 2011. Cerebral amyloid angiopathy related inflammation: three case reports and a review. *J Neurol Neurosurg Psychiatry* 82(1), 20-6.

Claudio, L. 1996. Ultrastructural features of the blood-brain barrier in biopsy tissue from Alzheimer's disease patients. *Acta Neuropathol* 91(1), 6-14.

Dahlgren, K.N., Manelli, A.M., Stine, W.B., Jr., Baker, L.K., Krafft, G.A., LaDu, M.J. 2002. Oligomeric and fibrillar species of amyloid-beta peptides differentially affect neuronal viability. *J Biol Chem* 277(35), 32046-53.

Di Paolo, G., Kim, T.W. 2011. Linking lipids to Alzheimer's disease: cholesterol and beyond. *Nat Rev Neurosci* 12(5), 284-96.

Eikelenboom, P., Veerhuis, R., van Exel, E., Hoozemans, J.J., Rozemuller, A.J., van Gool, W.A. 2011. The early involvement of the innate immunity in the pathogenesis of late-onset Alzheimer's disease: neuropathological, epidemiological and genetic evidence. *Curr Alzheimer Res* 8(2), 142-50.

Eng, J.A., Frosch, M.P., Choi, K., Rebeck, G.W., Greenberg, S.M. 2004. Clinical manifestations of cerebral amyloid angiopathy-related inflammation. *Ann Neurol* 55(2), 250-6.

Erickson, M.A., Dohi, K., Banks, W.A. 2012. Neuroinflammation: a common pathway in CNS diseases as mediated at the blood-brain barrier. *Neuroimmunomodulation* 19(2), 121-30.

Eurelings, L.S., Richard, E., Carrano, A., Eikelenboom, P., van Gool, W.A., Rozemuller, A.J. 2010. Dyshoric capillary cerebral amyloid angiopathy mimicking Creutzfeldt-Jakob disease. *J Neurol Sci* 295(1-2), 131-4.

Farkas, E., De Jong, G.I., de Vos, R.A., Jansen Steur, E.N., Luiten, P.G. 2000. Pathological features of cerebral cortical capillaries are doubled in Alzheimer's disease and Parkinson's disease. *Acta Neuropathol* 100(4), 395-402.

Farkas, E., Luiten, P.G. 2001. Cerebral microvascular pathology in aging and Alzheimer's disease. *Prog Neurobiol* 64(6), 575-611.

Greenberg, S.M., Grabowski, T., Gurol, M.E., Skehan, M.E., Nandigam, R.N., Becker, J.A., Garcia-Alloza, M., Prada, C., Frosch, M.P., Rosand, J., Viswanathan, A., Smith, E.E., Johnson, K.A. 2008. Detection of isolated cerebrovascular beta-amyloid with Pittsburgh compound B. *Ann Neurol* 64(5), 587-91.

Hardy, J., Selkoe, D.J. 2002. The amyloid hypothesis of Alzheimer's disease: progress and problems on the road to therapeutics. *Science* 297(5580), 353-6.

Higuchi, Y., Miyakawa, T., Shimoji, A., Katsuragi, S. 1987. Ultrastructural changes of blood vessels in the cerebral cortex in Alzheimer's disease. *Jpn J Psychiatry Neurol* 41(2), 283-90.

Kim, J., Basak, J.M., Holtzman, D.M. 2009. The role of apolipoprotein E in Alzheimer's disease. *Neuron* 63(3), 287-303.

Kinnecom, C., Lev, M.H., Wendell, L., Smith, E.E., Rosand, J., Frosch, M.P., Greenberg, S.M. 2007. Course of cerebral amyloid angiopathy-related inflammation. *Neurology* 68(17), 1411-6.

Knudsen, K.A., Rosand, J., Karluk, D., Greenberg, S.M. 2001. Clinical diagnosis of cerebral amyloid angiopathy: validation of the Boston criteria. *Neurology* 56(4), 537-9.

Kontush, A. 2001. Alzheimer's amyloid-beta as a preventive antioxidant for brain lipoproteins. *Cell Mol Neurobiol* 21(4), 299-315.

Levy, E., Prelli, F., Frangione, B. 2006. Studies on the first described Alzheimer's disease amyloid beta mutant, the Dutch variant. *J Alzheimers Dis* 9(3 Suppl), 329-39.

Mann, D.M., Pickering-Brown, S.M., Takeuchi, A., Iwatsubo, T. 2001. Amyloid angiopathy and variability in amyloid beta deposition is determined by mutation position in presenilin-1-linked Alzheimer's disease. *Am J Pathol* 158(6), 2165-75.

Mirra, S.S. 1997. The CERAD neuropathology protocol and consensus recommendations for the postmortem diagnosis of Alzheimer's disease: a commentary. *Neurobiol Aging* 18(4 Suppl), S91-4.

Neniskyte, U., Neher, J.J., Brown, G.C. 2011. Neuronal death induced by nanomolar amyloid beta is mediated by primary phagocytosis of neurons by microglia. *J Biol Chem* 286(46), 39904-13.

Nicoll, J.A., Burnett, C., Love, S., Graham, D.I., Dewar, D., Ironside, J.W., Stewart, J., Vinters,

H.V. 1997. High frequency of apolipoprotein E epsilon 2 allele in hemorrhage due to cerebral amyloid angiopathy. *Ann Neurol* 41(6), 716-21.

Oda, A., Tamaoka, A., Araki, W. 2010. Oxidative stress up-regulates presenilin 1 in lipid rafts in neuronal cells. *J Neurosci Res* 88(5), 1137-45.

Oda, T., Wals, P., Osterburg, H.H., Johnson, S.A., Pasinetti, G.M., Morgan, T.E., Rozovsky, I., Stine, W.B., Snyder, S.W., Holzman, T.F., et al. 1995. Clusterin (apoJ) alters the aggregation of amyloid beta-peptide (A beta 1-42) and forms slowly sedimenting A beta complexes that cause oxidative stress. *Exp Neurol* 136(1), 22-31.

Perlmutter, L.S., Chui, H.C. 1990. Microangiopathy, the vascular basement membrane and Alzheimer's disease: a review. *Brain Res Bull* 24(5), 677-86.

Revesz, T., Ghiso, J., Lashley, T., Plant, G., Rostagno, A., Frangione, B., Holton, J.L. 2003. Cerebral amyloid angiopathies: a pathologic, biochemical, and genetic view. *J Neuropathol Exp Neurol* 62(9), 885-98.

Revesz, T., Holton, J.L., Lashley, T., Plant, G., Rostagno, A., Ghiso, J., Frangione, B. 2002. Sporadic and familial cerebral amyloid angiopathies. *Brain Pathol* 12(3), 343-57.

Richard, E., Carrano, A., Hoozemans, J.J., van Horssen, J., van Haastert, E.S., Eurelings, L.S., de Vries, H.E., Thal, D.R., Eikelenboom, P., van Gool, W.A., Rozemuller, A.J. 2010. Characteristics of dyshoric capillary cerebral amyloid angiopathy. *J Neuropathol Exp Neurol* 69(11), 1158-67.

Roher, A.E., Kuo, Y.M., Esh, C., Knebel, C., Weiss, N., Kalback, W., Luehrs, D.C., Childress, J.L., Beach, T.G., Weller, R.O., Kokjohn, T.A. 2003. Cortical and leptomeningeal cerebrovascular amyloid and white matter pathology in Alzheimer's disease. *Mol Med* 9(3-4), 112-22.

Shibata, M., Yamada, S., Kumar, S.R., Calero, M., Bading, J., Frangione, B., Holtzman, D.M., Miller, C.A., Strickland, D.K., Ghiso, J., Zlokovic, B.V. 2000. Clearance of Alzheimer's amyloid-ss(1-40) peptide from brain by LDL receptor-related protein-1 at the blood-brain barrier. *J Clin Invest* 106(12), 1489-99.

St George-Hyslop, P.H., Tanzi, R.E., Polinsky, R.J., Haines, J.L., Nee, L., Watkins, P.C., Myers, R.H., Feldman, R.G., Pollen, D., Drachman, D., et al. 1987. The genetic defect causing familial Alzheimer's disease maps on chromosome 21. *Science* 235(4791), 885-90.

Tanzi, R.E., Gusella, J.F., Watkins, P.C., Bruns, G.A., St George-Hyslop, P., Van Keuren, M.L., Patterson, D., Pagan, S., Kurnit, D.M., Neve, R.L. 1987. Amyloid beta protein gene: cDNA, mRNA distribution, and genetic linkage near the Alzheimer locus. *Science* 235(4791), 880-4.

Thal, D.R., Ghebremedhin, E., Rub, U., Yamaguchi, H., Del Tredici, K., Braak, H. 2002. Two types of sporadic cerebral amyloid angiopathy. *J Neuropathol Exp Neurol* 61(3), 282-93.

Thal, D.R., Griffin, W.S., de Vos, R.A., Ghebremedhin, E. 2008. Cerebral amyloid angiopathy and its relationship to Alzheimer's disease. *Acta Neuropathol* 115(6), 599-609.

Thal, D.R., Papassotiropoulos, A., Saido, T.C., Griffin, W.S., Mrak, R.E., Kolsch, H., Del Tredici, K., Attems, J., Ghebremedhin, E. 2010. Capillary cerebral amyloid angiopathy identifies a distinct APOE epsilon4-associated subtype of sporadic Alzheimer's disease. *Acta Neuropathol* 120(2), 169-83.

Veerhuis, R., Boshuizen, R.S., Familian, A. 2005. Amyloid associated proteins in Alzheimer's and prion disease. *Curr Drug Targets CNS Neurol Disord* 4(3), 235-48.

Vinters, H.V. 1987. Cerebral amyloid angiopathy. A critical review. *Stroke* 18(2), 311-24.

Weller, R.O., Massey, A., Newman, T.A., Hutchings, M., Kuo, Y.M., Roher, A.E. 1998. Cerebral amyloid angiopathy: amyloid beta accumulates in putative interstitial fluid drainage pathways in Alzheimer's disease. *Am J Pathol* 153(3), 725-33.

Weller, R.O., Subash, M., Preston, S.D., Mazanti, I., Carare, R.O. 2008. Perivascular drainage of amyloid-beta peptides from the brain and its failure in cerebral amyloid angiopathy and Alzheimer's disease. *Brain Pathol* 18(2), 253-66.

Yamashita, K., Miyakawa, T., Katsuragi, S. 1991. Vascular changes in the brains with Alzheimer's disease. *Jpn J Psychiatry Neurol* 45(1), 79-84.

Yan, S.D., Chen, X., Fu, J., Chen, M., Zhu, H., Roher, A., Slattery, T., Zhao, L., Nagashima, M., Morser, J., Migheli, A., Nawroth, P., Stern, D., Schmidt, A.M. 1996. RAGE and amyloid-beta peptide neurotoxicity in Alzheimer's disease. *Nature* 382(6593), 685-91.

Yu, J.T., Tan, L. 2012. The role of clusterin in Alzheimer's disease: pathways, pathogenesis, and therapy. *Mol Neurobiol* 45(2), 314-26.

Zhan, S.-S., Veerhuis, R., Janssen, I., Kamphorst, W., Eikelenboom, P. 1994. Immunohistochemical distribution of the inhibitors of the terminal complement complex in Alzheimer's disease. *Neurodegeneration* 3, 111-7.

Zlokovic, B.V. 2011. Neurovascular pathways to neurodegeneration in Alzheimer's disease and other disorders. *Nat Rev Neurosci* 12(12), 723-38.

Outline of this thesis

Given the central role of the vascular and BBB compartments in the regulation of Aβ clearance the aim of the studies described in this thesis was to examine the role of Aβ transport proteins, as well as the expression of specific BBB/endothelial proteins in the AD/CAA brain and to elucidate the putative role of CAA in the evolution of AD pathology. To this end, my thesis focuses on vascular alterations presented in the capillary form of CAA and the common and not common features shared with "classical" AD, on proteins involved in Aβ transport across the BBB, including Aβ transporters and amyloid associated proteins, and a number of proteins that may play a significant role in the overall homeostasis and maintenance of the vascular endothelial and BBB compartment.

Chapter 2

This chapter describes the pathological characteristics of capCAA, the relationship between amyloid deposits in capCAA, CAA and plaques, and the distribution patterns of neurofibrillary changes, inflammatory markers, and ApoE around amyloid lesions.

Chapter 3

To investigate the differential expression of proteins between AD and capCAA brains a proteomics study was performed. We identified several proteins specifically upregulated in capCAA, the expression of which has been further validated with immunohistochemical techniques. We here investigated the expression and localization of laminin, clusterin, SAP and complement activation in capCAA and AD brains. Both laminin, clusterin, SAP and complement proteins colocalize with amyloid deposits in CAA and capCAA-affected tissue. Interestingly, we observed a more pronounced colocalization with vascular Aβ compared to amyloid plaques in AD brains.

Chapter 4

We investigated BBB alterations in CAA-affected capillaries with the emphasis on tight junction (TJ) changes and signs of neuroinflammation. We show that Aβ is toxic to brain endo-

thelial cells via binding to RAGE and concomitant ROS production, which ultimately leads to disruption of TJs and loss of BBB integrity, as shown by the leakage of fibrinogen in capCAA tissue.

Chapter 5

The expression and function of ABC transporters might be critical in the development of AD and (cap)CAA. We demonstrate that Pgp and BCRP are downregulated in capCAA, not in AD, and that Aβ and clusterin influence the expression level of P-gp. This might play a pivotal role in the development of the different amyloid deposits.

Chapter 6

In this chapter we summarize and discuss the results of this thesis.

2
part

CapCAA and Alzheimer's disease

2

chapter

Characteristics of Dyshoric Capillary Cerebral Amyloid Angiopathy

Anna Carrano, Edo Richard, Jeroen J. Hoozemans, Jack van Horssen, Elise S. van Haastert, Lisa S. Eurelings, Helga E. de Vries, Dietmar R. Thal, Piet Eikelenboom, Willem A. van Gool, and Annemieke J.M. Rozemuller

Characteristics of Dyshoric Capillary Cerebral Amyloid Angiopathy

Anna Carrano [1]*, Edo Richard [2]*, Jeroen J. Hoozemans [1], Jack van Horssen [3], Elise S. van Haastert [1], Lisa S. Eurelings [2], Helga E. de Vries [3], Dietmar R. Thal [4], Piet Eikelenboom [2], Willem A. van Gool [2], and Annemieke J.M. Rozemuller [1,5].

[1] *Department of Pathology, VU University Medical Center, Amsterdam, The Netherlands;* [2] *Department of Neurology, Academic Medical Center, University of Amsterdam, The Netherlands;* [3] *Department of Molecular Cell Biology and Immunology, VU University Medical Center, Amsterdam, The Netherlands;* [4] *Laboratory of Neuropathology, University of Ulm, Ulm, Germany; and* [5] *Department of Pathology, University Medical Center Utrecht, Utrecht, The Netherlands.*
* authors contributed equally to this work.

Abstract

Cerebral amyloid angiopathy (CAA) affects brain parenchymal and leptomeningeal arteries and arterioles but sometimes involves capillaries (capCAA) with spread of the amyloid into the surrounding neuropil, that is, dyshoric changes. We determined the relationship between capCAA and larger vessel CAA, A amyloid (Aβ) plaques, neurofibrillary changes, inflammation, and apolipoprotein E (APOE) in 22 cases of dyshoric capCAA using immunohistochemistry. The dyshoric changes contained predominantly Aβ1-40, whereas dense bulblike deposits adjacent to the capillary wall contained mostly Aβ1-42. There was an inverse local correlation between Aβ plaque load and capCAA severity (p = 0.01), suggesting that Aβ transport between the neuropil and the circulation may be mechanistically involved. Deposits of hyperphosphorylated tau and ubiquitin and clusters of activated microglia, resembling the changes around Aβ plaques, were found around capCAA but were absent around larger vessel CAA. In 14 cases for which APOE genotype was available, there was a high APOE-ε4 allele frequency (54%; 43% homozygous). The severity of CapCAA increased with the number of ε4-alleles; and APOE4 seemed to colocalize with capCAA by immunohistochemistry. These results suggest that capCAA is pathologically and possibly pathogenetically distinct from larger vessel CAA, and that it is associated with a high APOE- ε4 allele frequency.

Key Words: Alzheimer, Capillary cerebral amyloid angiopathy, Cerebral amyloid angiopathy, Dementia, Dyshoric, Neuroinflammation.

Introduction

Sporadic cerebral amyloid angiopathy (CAA) is characterized by deposits of A-amyloid (Aβ) in meningeal and parenchymal arteries, arterioles, and to a lesser extent, brain capillaries (Revesz, et al., 2003). Cerebral amyloid angiopathy is a common finding at autopsy, and its incidence increases with age and occurs in 70% to 100% of Alzheimer disease (AD) patients (Bergeron, et al., 1987; Ellis, et al., 1996). Cerebral amyloid angiopathy may occur in any region of the brain and spreads in a characteristic pattern starting in the neocortex, where the occipital lobe is a predilection site; it may involve other brain areas, including the diencephalon, striatum, and cerebellum (Alafuzoff, et al., 2009; Thal, et al., 2003). Sporadic CAA can be classified into CAA-type 1, involving cortical capillaries in addition to leptomeningeal and cortical arteries and arterioles, and CAA-type 2, not involving cortical capillaries (Thal, et al., 2002). Capillary CAA (CapCAA) can occur in any stage of CAA-type 1 and correlates with severity of AD pathology, whereas larger vessel CAA does not (Attems and Jellinger, 2004; Jellinger and Attems, 2005). A remarkably high apolipoprotein E- ε4 (APOE- ε4) allele frequency (46.7%) has been found in subjects with CAA-type 1 (6). Capillary CAA is relatively frequently found in subjects with advanced Aβ deposition in the brain, and severe capCAA in the absence of neuritic plaques has been described in a limited number of APOE-ε4 homozygous subjects (Thal, et al., 2008; Vidal, et al., 2000). In capCAA-affected capillaries, more than in larger CAA-affected vessels, flamelike amyloid deposits may extend beyond the vessel wall and radiate into the neuropil, that is, "dyshoric angiopathy" (Attems, 2005).

Although many capCAA-affected vessels exhibit dyshoric changes, they are not a prerequisite for capCAA. Here, we use the term dyshoric changes in capCAA to describe plaquelike AA aggregates attached to the basement membranes of capillaries entering the pericapillary neuropil. This is based upon the description of dyshoric angiopathy by Surbek (Surbek, 1961) in 1961, which distinguished capillaries with plaquelike amyloid deposits (dyshoric angiopathy) from parenchymal plaques. The term angiopathy dyshorique was originally introduced by Morel in 1950 (Morel, 1950) and interpreted as congophilic angiopathy (synonymous with CAA), with parenchymal lesions by Pantelakis (Pantelakis, 1954) in 1954. This terminology was derived from translating the original German description of CAA, which used the term Drusige Entartung, as used by Scholz (Scholz, 1938), who in 1938 first systematically reported that the substance in this specific form of angiopathy was the same as the main component

of senile plaques. This term already made the link with amyloid plaques, which were called Alzheimer Drusen at that time and meant the occurrence of plaquelike silver-and Congo red-stainable material in blood vessels. The vascular changes covered by this description were those in larger vessels as well as dyshoric changes in capillaries representing electron-dense amyloid material in the affected vessel walls (Schlote, 1965; Scholz, 1938). Here we use the term capCAA for amyloid laden capillaries and dyshoric changes to denote the amyloid deposits radiating into the neuropil. Some previous studies of capCAA report that Aβ1-42 is the most prominent isoform in globular deposits and that both Aβ1-40 and Aβ1-42 are present in the capillary wall; Aβ1-40 is mainly found in larger vessel CAA (Attems, et al., 2004; Jeynes and Provias, 2006; Oshima, et al., 2006). Little is known about the precise composition of the dyshoric changes. The presence of Aβ1-40 in capCAA has been reported to correlate with the amount of Aβ1-40 in plaques, but there are conflicting results for the correlation between capillary Aβ1-42 and plaque Aβ1-42 (i.e. some have found a positive correlation (Attems, et al., 2004), whereas this correlation was negative in other studies(Jeynes and Provias, 2006; Oshima, et al., 2006).

Neurofibrillary changes have been observed around Aβ-laden arteries and arterioles in CAA (Delacourte, et al., 1987; Williams, et al., 2005). Interestingly, the presence of tau-positive structures is correlated with perivascular Aβ deposits, but not with Aβ in the vessel wall, suggesting that parenchymal Aβ might trigger the tau pathology (Attems and Jellinger, 2004; Delacourte, et al., 1987; Oshima, et al., 2006; Oshima, et al., 2008; Rozemuller, et al., 1989; Williams, et al., 2005).

A neuroinflammatory response, as can be seen around classical plaques, is absent around larger vessel CAA (Akiyama, et al., 2000; Eikelenboom, et al., 2008; Yamada, et al., 1997). Whether dyshoric capCAA is accompanied by inflammatory changes has not been systematically investigated, but in addition to the parenchymal Aβ, perivascular tau deposits might elicit an inflammatory reaction similar to that observed around plaques. This study aims to further investigate the differences between dyshoric capCAA and larger vessel CAA, with respect to the distribution of different Aβ-isoforms, the relationship with plaques, the surrounding neurofibrillary changes, signs of inflammation, and the correlation with the APOE-ε4 allele.

Materials and Methods

Subjects and Clinical Data

Patient selection was based on neuropathologic findings at autopsy; collection of clinical data was performed retrospectively. Subjects with extensive capCAA and dyshoric changes were collected from 4 neuropathologic databases that contain autopsies between 2000 and 2007. The databases contain subjects with different types of dementia (mostly AD), and Parkinson disease (PD) and related disorders; subjects without dementia who donated their brains to the Netherlands Brain Bank; and subjects who died of a variety of nonneurological diseases in 1 academic hospital. Inclusion criteria were based on the neuropathologic finding of capCAA and not on clinical characteristics. Both subjects with and without dementia were included if there was marked capCAA. Subjects with very mild capCAA, with small number of Aβ-positive capillaries in some of the microscopic fields were excluded because this is a rather common finding in an aged population. All subjects or their legal representatives had signed an informed consent form for use of clinical data and tissue for scientific purposes before the information was added to the databases. In total, 22 patients with capCAA were included, with an average age of 77.9 years (SD, 7.7 years; range, 65-95 years); of these, 10 (46%) were men.

Neuropathologic Assessment

The brain specimens were obtained at autopsy with postmortem intervals of less than 15 hours. For neuropathologic diagnoses, blocks of 5 cortical areas, basal nuclei (including nucleus accumbens), thalamus, hippocampus, amygdala, mesencephalon, pons and medulla oblongata, and cerebellum were examined with routine stains (hematoxylin and eosin, periodic acid Schiff-Luxol fast blue). Hippocampus and cortical areas were also stained with methenamine silver and/or an antibody against Aβ 1-17, and either Gallyas or tau (AT8). All additional neuropathologic evaluations for this study were performed on formalin-fixed paraffin-embedded tissue from occipital pole cortex (Brodmann area 18/19).

Staging of neurofibrillary changes was done according to Braak and Braak (Braak, et al., 2006; Braak and Braak, 1991). To determine the CAA stage, temporal pole cortex, hippocampus (essentially CA1 and entorhinal area of the parahippocampal gyrus), cerebellum (vermis), and striatum (pallidum and caudatum), were analyzed, as described (Thal, et al., 2003).

Immunohistochemistry

Examinations were performed on 5-μm-thick sections of formalin-fixed (4%, 24 hours) par-

Table 1. Primary Antibodies

Primary Antibody	Antigen	dilution	method	ARS	Source
AT8	PHF-TAU	1:200	ABC	Na-citrate	Innogenetics (Gent, Belgium)
Anti-Aβ 1-17	Aβ 1-17	1:50	EV	FA	Dako (Glostrup, Denmark)
Anti-Aβ 1-40	Aβ 1-40	1:64000	ABC	FA	The Genetics Company (Schlieren, Switzerland)
Anti-A β1-42	Aβ 1-42	1:16000	ABC	FA	The Genetics Company (Schlieren, Switzerland)
Anti-ubiquitin	Ubiquitin	1:25600	PV	FA	Chemicon (Millipore, Temecula, CA, USA)
GFAP	GFAP	1:100	EV	Na-citrate	Monosan (Sanbio, Uden, The Netherlands)
LN3	HLA-DR	1:200	EV	Na-citrate	gift of Dr. J.H.M. Hilgers (VUMC, Amsterdam, The Netherlands)
Anti-APOE4	APOE4	1:200	EV	FA	MBL (Naka-ku Nagoya, Japan)

Aβ, A-amyloid; ABC, avidin-biotin-peroxidase complex method; ApoE4, apolipoprotein E4; EV, Envision method; FA, formic acid; GFAP, glial fibrillary acidic protein; Na citrate, sodium citrate; PHF-TAU, paired helical filament tau; PV, Power Vision method; ARS, antigen retrieval step; VUMC, VU Medical Center.

affin-embedded tissue. To quench endogenous peroxidase activity, sections were treated with 0.3% H_2O_2 in methanol for 30 minutes. Antigen retrieval was performed in either 10 mmol/L pH 6.0 sodium citrate buffer heated by microwave for 10 minutes and cooled to room temperature or formic acid for 15 minutes at room temperature and subsequently rinsed in water and PBS. Sections were stained using the avidin-biotin-peroxidase complex method, EnVision method, or Power Vision method, as described (Copani, et al., 2006; Hoozemans, et al., 2009). The primary antibodies, dilutions, and manufacturers of the antibodies are listed in Table 1. The sections stained for AT8 (anti-paired helical filament tau), ubiquitin, glial fibrillary acidic protein (GFAP), and HLA-DR (LN3) were costained with Congo red to visualize the relationship between these changes and the capCAA.

Immunofluorescent double staining for Aβ1-40 (mouse IgG2b) and Aβ1-42 (mouse IgG1) was performed by means of goat anti-mouse isotype-specific secondary antibodies to visualize the distribution of the different isoforms around the capillaries as previously described

Table 2. Patient Clinical and Neuropathologica Data

case	age	sex	clinical diagnosis	NP diagn	CAA stage	Braak T	ApoE	Disease duration (m)
1	71	f	CJD susp	AD	3	4	44	8
2	86	m	CJD susp	AD	2	6	33	3
3	78	f	CJD susp	AD	2	4	34	10
4	76	m	CJD susp	AD	2	4	n.d.	2
5	75	f	CJD susp	AD changes	3	3	n.d.	3
6	80	m	CJD susp	AD changes	2	2	n.d.	24
7	85	f	AD	AD	2	5	n.d.	48
8	73	m	AD	AD	2	4	44	120
9	72	m	AD	AD	2	6	32	120
10	85	f	AD	AD	2	5	44	120
11	65	m	AD	AD	3	5	33	84
12	75	f	AD	AD	3	5	44	144
13	83	f	AD	AD	2	3	n.d.	60
14	74	m	AD	AD	3	6	n.d.	72
15	89	f	AD	AD	3	5	33	36
16	70	f	PD	LBD-NT	3	3	44	rapid progressive
17	69	f	PD	LBD-NT	2	3	34	unknown
18	75	m	PD	LBD-NT	3	3	44	unknown
19	70	f	PD	LBD-NT	1	4	n.d.	18
20	95	f	no dementia	n.a.	2	3	n.d.	n.a.
21	79	m	no dementia	n.a.	2	1	33	n.a.
22	88	m	depression	n.a.	1	2	34	n.a.

AD, Alzheimer disease; ApoE, apolipoprotein E genotype; Braak T, Braak tangles; CAA, cerebral amyloid angiopathy; CJD susp, clinical suspicion of Creutzfeldt-Jakob disease; F, female; LBD-NT, Lewy body disease-neocortical type; M, male; n.a., not applicable; n.d., not determined; NP, neuropathologic diagnosis; PD, Parkinson disease.

(Pollio, et al., 2008).

Morphological Analysis and Quantification

Morphological analysis of capCAA and larger vessel CAA scores were determined in sections stained with antibodies against Aβ1-17, Aβ1-40, and Aβ1-42. Vessels smaller than 10 μm were defined as capillaries. Microscopic fields (n = 4) (capillaries, magnification 10×; larger vessels, magnification 2.5×) were analyzed. The Aβ-positive vessels were scored as follows: 0, none; 1, occasional positive vessel (<20%); 2, several positive vessels scattered throughout the field (20%-60%); 3, most vessels affected (>60%). The presence of Aβ plaques (plaque severity) was quantified in the same manner as the number of Aβ-positive larger vessels (0, none; 1, occasional plaque; 2, several plaques scattered throughout the field; 3, abundant presence of plaques).

The AT8 and ubiquitin immunostains were scored as follows: 0, none; 1, mild (occasional immunoreactivity [IR]); 2, moderate (scattered throughout the field); and 3, severe (surrounding most capillaries). All scoring was done by 2 raters (Edo Richard and Anna Carrano). Both raters assigned a score to every section, taking into account the whole section; the definite score was then assigned in consensus. The observers were blinded to the clinical diagnosis and any patient information.

Sections double stained with the primary antibodies and Congo red and for Aβ1-40/1-42 were evaluated in a qualitative way. Adjacent sections were stained for determination of colocalization of APOE4 and Aβ1-17.

Statistical Analysis

Because of the relatively small number of subjects in the study, and the use of ordinal scales to grade neuropathologic changes, nonparametric tests were used for all analyses. Spearman's rank correlation coefficients were calculated. Mann-Whitney U statistics was used for analyzing dichotomized variables.

Results

Subjects

Of the 22 patients with capCAA identified from the 4 databases based on the description of capCAA in the neuropathologic reports, 4 cases were found among 89 cases in a database of

subjects who were clinically suspected of having Creutzfeldt-Jakob disease (CJD), which was not confirmed at autopsy; 10 cases were from the database of the Netherlands Brain Bank (containing 380 subjects); 8 of these were diagnosed as AD and 2 had no neurological disease; 4 of 110 cases were from the database with PD and related disorders; and 2 cases were from the general pathology database of an academic hospital-one of these was diagnosed as AD, and one had no dementia (Table 2).

Neuropathologic Findings

All clinically diagnosed AD patients and 4 of 6 CJD-suspected cases fulfilled neuropathologic criteria for AD with respect to tau pathology, Braak tangle stage of IV, or higher. All clinically diagnosed PD cases had Lewy body pathology, in addition to moderate tau pathology. The 3 cases without dementia had Braak tangle scores of I to III.

Aβ Deposition

Dyshoric changes were mainly observed around the capillaries and only rarely around larger vessels. Both Aβ1-40 and Aβ 1-42 were detected around the capillaries, and they were highly correlated (Spearman ρ 0.855, p< 0.001), but their distributions differed. Aβ1-40 was the main component of the dyshoric changes; in addition to its main component in the vessel wall, it completely surrounded the capillary with extensive spread into the neuropil (Figs. 1A, C). On the other hand, Aβ1-42 was mainly present in dense bulblike deposits directly adjacent to and to a lesser extent in the capillary wall. To a much lesser degree than Aβ1-40, there were flame-like deposits radiating into the neuropil (Figs. 1B, C). This is the reverse of the distribution in plaques with a dense core consisting of Aβ1-40 and a diffuse spread around consisting of mainly Aβ1-42 (Figs. 1E, F).

The severity of capCAA correlated with the severity of larger vessel CAA (Spearman ρ 0.71, p < 0.001). Capillary CAA occurred in any stage of CAA, and no subjects had capCAA without any larger vessel CAA. There was a significant inverse correlation between capCAA severity and plaque density, with relatively few plaques in subjects with the most extensive capCAA (Spearman [rho] -0.52, p = 0.013; Fig. 2). When Aβ1-40 and Aβ1-42 were analyzed separately, this correlation was the same for both isoforms (Spearman [rho] -0.59, p = 0.004 vs -0.53, p = 0.011; Fig. 2). No significant correlation was found between larger vessel CAA and plaque load (Spearman [rho] -0.39, p = 0.076).
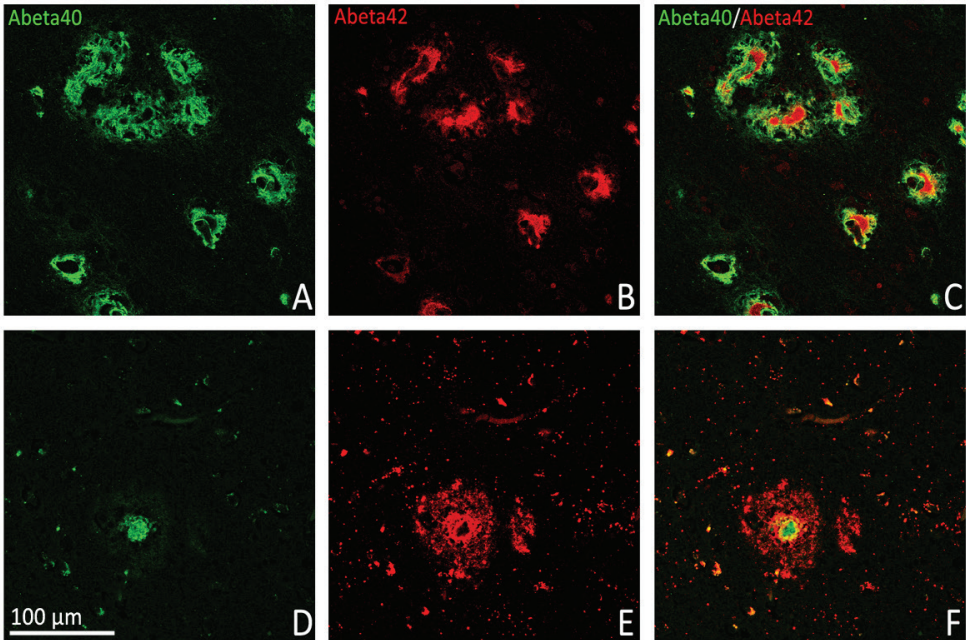
Figure 1. (A-F) Immunofluorescent double staining for β-amyloid (Aβ) 1-40 (green) and Aβ 1-42 (red), illustrating the distribution of the 2 isoforms in capillaries with the surrounding dyshoric changes (A-C) and plaques (D-F).
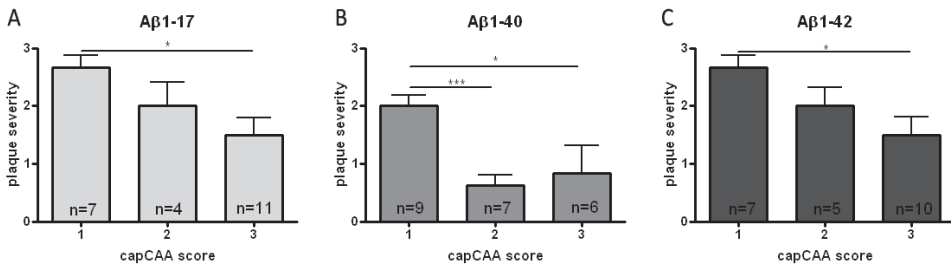
Figure 2. (A-C) Correlation between capillary cerebral amyloid angiopathy (capCAA) severity and plaque severity (scored as 0-3) analyzed for β-amyloid (Aβ) 1-17 (A), Aβ 1-40 (B), and Aβ 1-42 (C). Scale bars = mean +/- SEM. $*p < 0.05$, $***p < 0.001$.

Tau and Ubiquitin

Few or no neurofibrillary tangles were observed in the occipital cortex of any of the subjects, although they were present in other brain regions, particularly in the AD cases (Table 2, Braak tangle score). AT8 IR was observed surrounding Congo red-positive dyshoric capillaries and was virtually absent around the larger Congo red-positive vessels (Figs. 3J, K). Similarly, ubiq-

uitin-positive neuritic dystrophy was found around capCAA, but not around larger Congo red-positive vessels (Figs. 3M, N).

The extent of AT8 immunoreactivity correlated with the severity of ubiquitin reactivity (Spearman ρ 0.527, p = 0.03). The cases with little ubiquitin (score <=2) had significantly less AT8 IR than the cases with abundant ubiquitin (>2) (0.8 vs 2.4, p = 0.001). No cases had tau pathology in the absence of ubiquitin IR; whereas in 2 cases, ubiquitin IR without any tau pathology was observed around the dyshoric capCAA-affected vessels.

Glia Activation

Double staining for GFAP and Congo red demonstrated the presence of astrocytes around virtually all Aβ-laden vessels, albeit strongest around capillaries, in particular, in the presence of dyshoric changes, which were surrounded by clusters of GFAP-immunoreactive astrocytes (Figs. 3G, H). Clusters of HLA-DR-positive microglia were strongly associated with Aβ-laden capillaries with dyshoric changes but were only sporadically observed around larger vessels harboring CAA (Figs. 3D, E). Clusters of activated microglia and astrocytes were found around the classical plaques in the same region. In the control subjects, some GFAP IR was present, but no HLA-DR-positive microglia were seen.

APOE

The APOE genotype was available for 14 of 22 cases. The APOEε4 allele frequency in this cohort was 54%; 6 (43%) of 14 patients were homozygous for the APOEε4 allele. Of the 8 subjects in whom the APOE genotype was not determined, 7 had APOE4 IR compatible with the presence of at least 1 ε4 allele. When stratified for APOE genotype, subjects with at least 1 APOEε4 allele had higher scores for capillary Aβ1-17 (2.4 vs 2.0), Aβ1-40 (2.1 vs 1.4), and Aβ1-42 (2.3 vs 2.0) than subjects without an ε4 allele. In these small groups, none of these differences reached significance, but there was a trend (particularly for Aβ1-40) toward more severe capCAA depending on the number of ε4 alleles (Fig. 4). Subjects homozygous for the ε4 allele had the strongest association with capillary Aβ, as shown on adjacent sections stained for APOE4 and Aβ1-17 (Fig. 5).

Discussion

We describe neuropathologic changes accompanying the parenchymal Aβ surrounding cap-CAA with dyshoric changes in a series of 22 cases. Because different neuropathologic databases tend to contain disproportionate numbers of patients with specific diseases, subjects were selected from 4 different databases to obtain a sample with as little bias toward a specific category of subjects as possible. Despite this, selection bias might have contributed to an over-representation of subjects with dementia in our sample as a result of the relative overrepresentation of subjects with dementia in these databases. Therefore, clinical data of these subjects in relation to the neuropathologic findings should be interpreted with caution. The cases with clinical diagnosis of AD and PD were confirmed on neuropathologic analyses. All of the cases suspected of having CJD had rapidly progressive dementia, and at autopsy were found to have significant tangle pathology; in 4 cases, this fulfilled neuropathologic criteria for AD.

We found several neuropathologic differences between capCAA and larger vessel CAA. Consistent with previous reports, we demonstrated that in capCAA-affected vessels, Aβ1-42 is present within the walls of Aβ-laden capillaries and in dense bulblike deposits adjacent to the capillary wall (Attems, et al., 2004; Jeynes and Provias, 2006; Oshima, et al., 2006). In previous studies, Aβ1-42 was found to be the main isoform in capCAA as opposed to Aβ1-40 in larger vessel CAA. In capCAA in our cases, Aβ1-40 was mainly as dyshoric deposits spreading into the neuropil and to a relatively lesser degree in the vessel wall, whereas Aβ1-40 deposits were in the larger vessel wall CAA. A possible explanation for this difference with previous reports could be that few patients in previous series had abundant dyshoric changes (i.e. in which Aβ1-40 is the most prominent isoform); therefore, Aβ1-42 was described as the main isoform in capCAA.

The high APOEε4 allele frequency (54%) is similar to that found by Thal et al (Thal, et al., 2002) in their series of capCAA (46.7%). This frequency is much higher than that in the general population (14%) and in late-onset sporadic AD (37%) (Slooter and van Duijn, 1997). Moreover, the incidence of ε4/ε4 homozygous subjects of 43% is extraordinarily higher than that in the general population (3%) and in AD cases (13%) (Poirier, et al., 1993). It is also much higher than in the series of Thal et al (Thal, et al., 2002), in which 3 (20%) of 15 genotyped type 1 CAA subjects had the ε4/ε4 genotype. Taken together, these findings indicate that this specific genotype might represent a strong risk factor for the occurrence of capCAA, specifi-
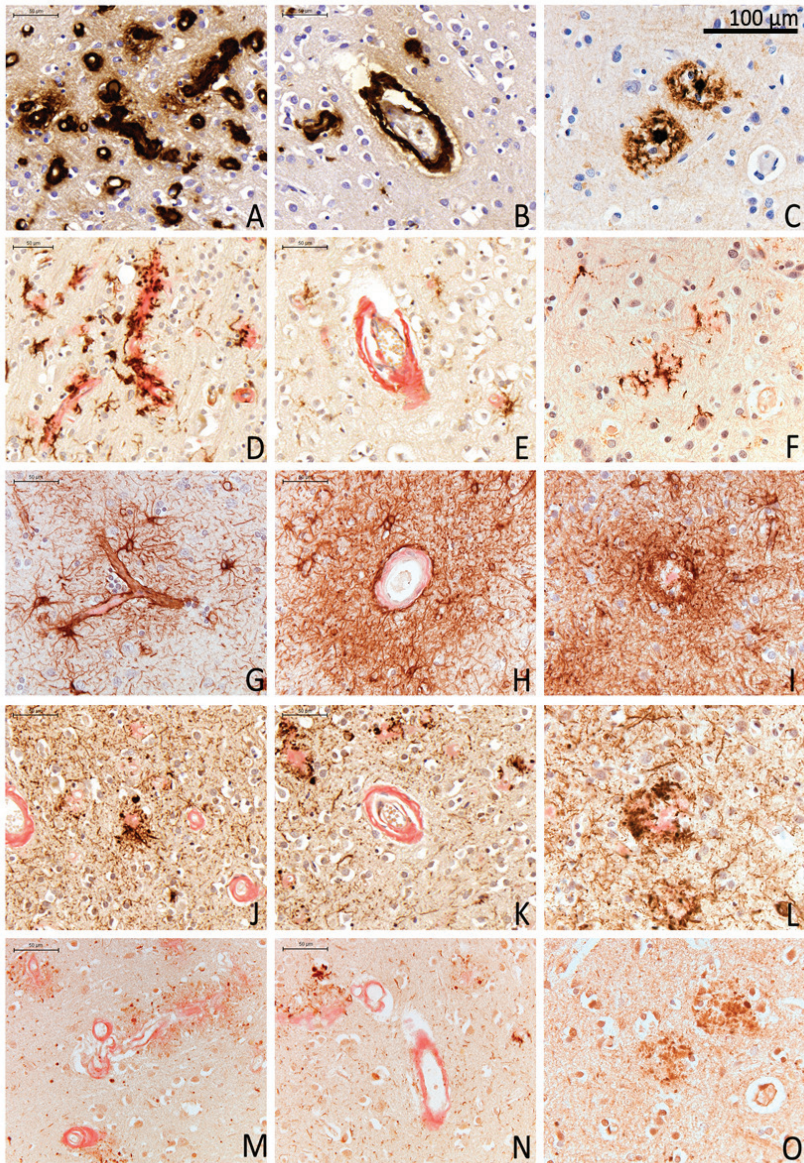
Figure 3. Immunoreactivity in capillary cerebral amyloid angiopathy (capCAA) (left column of panels), CAA (middle column of panels), and plaques (right column of panels). (D-O) Panels show double staining with Congo red. (A-C) β-Amyloid (Aβ) 1-17 staining. The dyshoric changes are found around the capillaries, and not the larger vessels. (D-F) Microglial activation (LN3 staining) around the capillaries, particularly when there are dyshoric changes. (G-I) Glial fibrillary acidic protein-positive reactive astrocytes are seen around both capillaries and larger vessels, mostly when there is a dyshoric component. (J-L) Hyperphosphorylated tau (AT8 staining) is seen only around the Aβ-laden capillaries and hardly around the larger vessels. (M-O) Ubiquitin is found around the Aβ-laden capillaries, mainly when there are dyshoric changes, and not around the larger vessels.

cally with concomitant dyshoric changes (Vidal, et al., 2000). The very high percentage of ε4/ε4 genotype might be explained by the fact that the subjects in our study were selected based on the recognition of widespread capCAA, thereby probably including more severe cases. The importance of the ε4 allele in the pathogenesis of capCAA is illustrated by the colocalization of APOE4 with capillary Aβ and the increasing severity of capCAA with increasing number of ε4 alleles. Although a strong genetic risk factor for dyshoric capCAA, the presence of an ε4 allele is not required because 5 (36%) of 14 genotyped subjects did not carry an ε4 allele.

The observation of tau pathology and ubiquitin IR around the capCAA-affected vessels in the occipital lobe, an area where few tangles are found (even in advanced AD), is remarkable. This supports the hypothesis that the tau pathology may be secondary to the Aβ deposits around the capillaries (Delacourte, et al., 1987; Oshima, et al., 2006; Oshima, et al., 2008; Williams, et al., 2005). Whether this relationship with tau-IR is different in other regions of the brain (e.g. with more neurofibrillary tangles) or whether capCAA in different regions can occur without any tau IR was not investigated. The presence of ubiquitin and tau close to the dyshoric changes closely resembles the changes that occur around classical plaques in AD. The fact that some cases exhibit ubiquitin without any tau pathology, but no cases exhibit tau pathology without any ubiquitin, suggests a sequence of events similar to what happens around Aβ plaques, where ubiquitin IR can be found before tau.

Also similar to the changes around Aβ plaques in AD are the clusters of activated microglia around the dyshoric Aβ-laden capillaries, indicating a strong inflammatory response, which is absent around larger Aβ-laden vessels (Arends, et al., 2000; Rozemuller, et al., 2005). The inflammatory reaction associated with Aβ plaques is thought to play a role in the pathogenesis of AD and likely contributes to the symptoms of cognitive decline (Arends, et al., 2000; Rozemuller, et al., 2005). Whereas larger vessel CAA is generally considered not to contribute to the development of cognitive decline, we hypothesize that the parenchymal Aβ in dyshoric capCAA with the associated deposits of tau and neuroinflammatory response, resembling the changes around Aβ plaques in AD, could contribute to cognitive decline.

The inverse local correlation between capCAA severity and plaque density around the capillaries is striking and provides a semiquantitative support for the speculation made by Surbek (Surbek, 1961) in 1961. Previous studies that have addressed this issue are contradictory, but this might be explained by different definitions of capCAA and by the fact that no clear distinction was made between capCAA with and without dyshoric changes (Attems and Jellinger,

2004; Jeynes and Provias, 2006; Oshima, et al., 2006). The inverse local correlation between plaques and capCAA is compatible with the hypothesis of Aβ transport between the neuropil and the circulation, that is, increased Aβ in and around capillaries might be accompanied by a decrease of Aβ plaques. This is consistent with the findings in a recent Aβ vaccination trial in AD patients, in which it was shown that a decrease in plaque load was accompanied by an increase in CAA severity (Boche, et al., 2008). Subsequently, CAA severity decreases again, suggesting that Aβ removal from plaques and clearance via the vascular system can occur and is a dynamic process (Boche, et al., 2008).

Several possible mechanisms of Aβ clearance have been hypothesized. There is clearance of Aβ via receptor-mediated transport across the blood-brain barrier (Deane and Zlokovic, 2007; Shibata, et al., 2000; Tanzi, et al., 2004) and another possible route of Aβ elimination is perivascular drainage of Aβ. Impaired clearance along this route might explain greater amounts of Aβ deposition in the brain that could ultimately lead to cognitive decline (Weller, et al., 2008). Our findings might be compatible with such a faulty blood-brain barrier clearance mechanism, resulting in accumulating deposits in and around the capillaries and leading to dyshoric angiopathy. They could also be consistent with obstruction of the perivascular route that would result in accumulation of Aβ as CAA and finally capCAA. However, Cap-CAA can occur with relatively little larger vessel CAA, suggesting that the problem does not necessarily start downstream from the capillaries, but rather with insufficient clearance at the blood-brain barrier in the capillaries.

Taken together, the pathological hallmarks of capCAA with dyshoric changes clearly differ from larger vessel CAA. This underscores the concept that CAA types 1 and 2 represent dis-
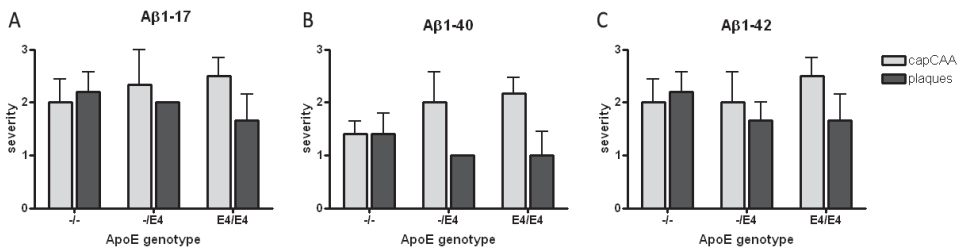
Figure 4. (A-C) Capillary cerebral amyloid angiopathy (capCAA) and plaque severity stratified for apolipoprotein E4 (APOE) genotype analyzed in the β-amyloid (Aβ) 1-17 (A), Aβ 1-40 (B), and Aβ 1-42 (C) stains show an apparent correlation between capCAA severity and APOE genotype. Values are presented as mean +/- SEM.
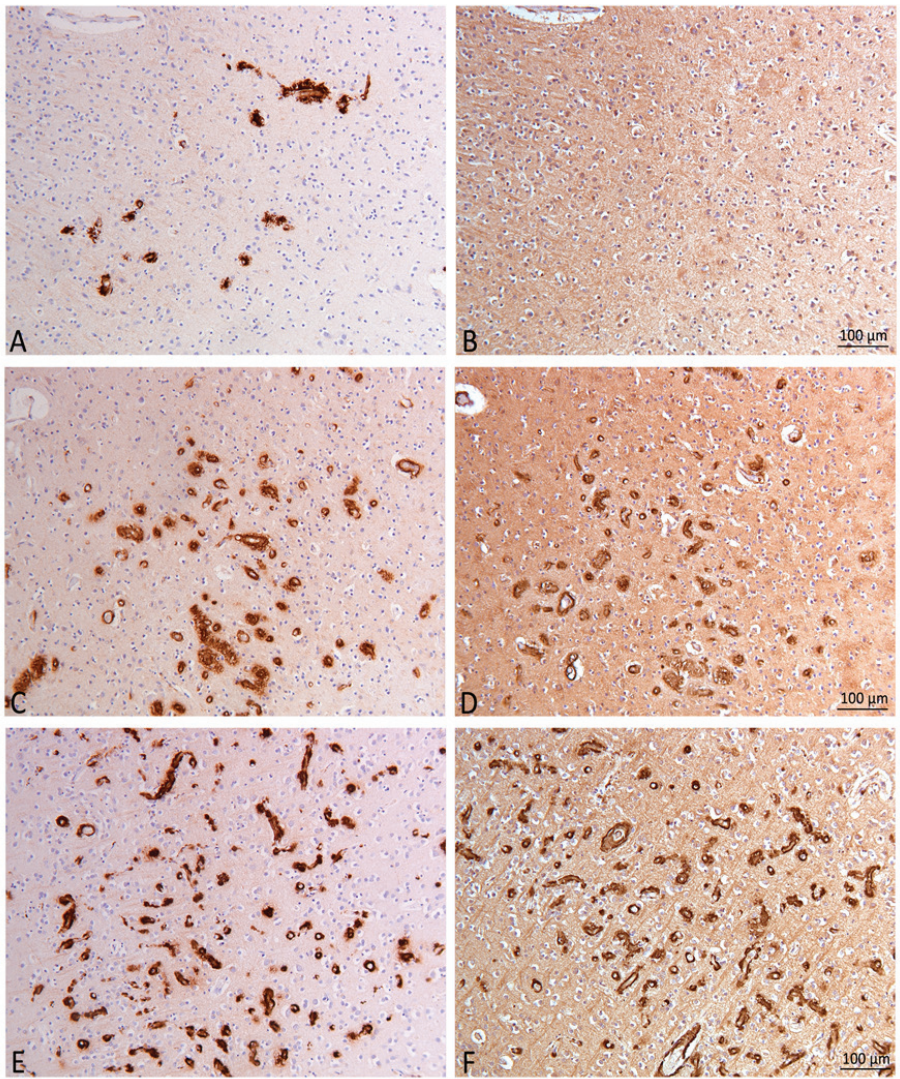
Figure 5. (A-F) Adjacent sections (10x) stained for β-amyloid (Aβ) 1-17 (A, C, E) and apolipoprotein E4 (APOE4) (B, D, F) in apatient with no ε4 allele (A, B), ε 4 heterozygous (C, D), and ε4 homozygous (E, F). The dyshoric capillary cerebral amyloid angiopathy severity is low in the ε4-negative subject, intermediate in the heterozygous subject, and high in the homozygous subject.

tinct neuropathologic entities. Several novel findings from the current study support this difference. We describe for the first time that Aβ1-42 is the main isoform in capCAA, as opposed to Aβ1-40 in larger vessel CAA. Although absent around larger vessel CAA without dyshoric changes, we show that capCAA is associated with tau deposits and clusters of activated microglia, closely resembling the hallmarks of parenchymal neuritic plaques in AD. In view of these

parenchymal changes, we hypothesize that dyshoric capCAA could possibly contribute to cognitive decline. We found a strong association with the APOE-ε4 allele, and the increasing capCAA severity with increasing number of ε4 alleles is remarkable and novel. Although the negative correlation between dyshoric capCAA and local plaque load was suggested as early as 1961, we confirm this finding based on a semiquantitative analysis. The strong association with APOE-ε4 and the negative correlation between dyshoric capCAA severity and the local plaque load suggest a role for faulty Aβ transport between the parenchyma and the capillary system in the pathogenesis of accumulation of Aβ in the neuropil surrounding the capillaries. Future studies on expression of proteins involved in transendothelial Aβ transport in subjects with capCAA with dyshoric changes may help clarify the underlying mechanisms.

References

Akiyama, H., Barger, S., Barnum, S., Bradt, B., Bauer, J., Cole, G.M., Cooper, N.R., Eikelenboom, P., Emmerling, M., Fiebich, B.L., Finch, C.E., Frautschy, S., Griffin, W.S., Hampel, H., Hull, M., Landreth, G., Lue, L., Mrak, R., Mackenzie, I.R., McGeer, P.L., O'Banion, M.K., Pachter, J., Pasinetti, G., Plata-Salaman, C., Rogers, J., Rydel, R., Shen, Y., Streit, W., Strohmeyer, R., Tooyoma, I., Van Muiswinkel, F.L., Veerhuis, R., Walker, D., Webster, S., Wegrzyniak, B., Wenk, G., Wyss-Coray, T. 2000. Inflammation and Alzheimer's disease. *Neurobiol Aging* 21(3), 383-421.

Alafuzoff, I., Thal, D.R., Arzberger, T., Bogdanovic, N., Al-Sarraj, S., Bodi, I., Boluda, S., Bugiani, O., Duyckaerts, C., Gelpi, E., Gentleman, S., Giaccone, G., Graeber, M., Hortobagyi, T., Hoftberger, R., Ince, P., Ironside, J.W., Kavantzas, N., King, A., Korkolopoulou, P., Kovacs, G.G., Meyronet, D., Monoranu, C., Nilsson, T., Parchi, P., Patsouris, E., Pikkarainen, M., Revesz, T., Rozemuller, A., Seilhean, D., Schulz-Schaeffer, W., Streichenberger, N., Wharton, S.B., Kretzschmar, H. 2009. Assessment of beta-amyloid deposits in human brain: a study of the BrainNet Europe Consortium. *Acta Neuropathol* 117(3), 309-20.

Arends, Y.M., Duyckaerts, C., Rozemuller, J.M., Eikelenboom, P., Hauw, J.J. 2000. Microglia, amyloid and dementia in alzheimer disease. A correlative study. *Neurobiol Aging* 21(1), 39-47.

Attems, J. 2005. Sporadic cerebral amyloid angiopathy: pathology, clinical implications, and possible pathomechanisms. *Acta Neuropathol* 110(4), 345-59.

Attems, J., Jellinger, K.A. 2004. Only cerebral capillary amyloid angiopathy correlates with Alzheimer pathology--a pilot study. *Acta Neuropathol* 107(2), 83-90.

Attems, J., Lintner, F., Jellinger, K.A. 2004. Amyloid beta peptide 1-42 highly correlates with capillary cerebral amyloid angiopathy and Alzheimer disease pathology. *Acta Neuropathol* 107(4), 283-91.

Bergeron, C., Ranalli, P.J., Miceli, P.N. 1987. Amyloid angiopathy in Alzheimer's disease. *Can J Neurol Sci* 14(4), 564-9.

Boche, D., Zotova, E., Weller, R.O., Love, S., Neal, J.W., Pickering, R.M., Wilkinson, D., Holmes, C., Nicoll, J.A. 2008. Consequence of Abeta immunization on the vasculature of human Alzheimer's disease brain. *Brain* 131(Pt 12), 3299-310.

Braak, H., Alafuzoff, I., Arzberger, T., Kretzschmar, H., Del Tredici, K. 2006. Staging of Alzheimer disease-associated neurofibrillary pathology using paraffin sections and immunocytochemistry. *Acta Neuropathol* 112(4), 389-404.

Braak, H., Braak, E. 1991. Neuropathological stageing of Alzheimer-related changes. *Acta Neuropathol* 82(4), 239-59.

Copani, A., Hoozemans, J.J., Caraci, F., Calafiore, M., Van Haastert, E.S., Veerhuis, R., Rozemuller, A.J., Aronica, E., Sortino, M.A., Nicoletti, F. 2006. DNA polymerase-beta is expressed early in neurons of Alzheimer's disease brain and is loaded into DNA replication forks in neurons challenged with beta-amyloid. *J Neurosci* 26(43), 10949-57.

Deane, R., Zlokovic, B.V. 2007. Role of the blood-brain barrier in the pathogenesis of Alzheimer's disease. *Curr Alzheimer Res* 4(2), 191-7.

Delacourte, A., Defossez, A., Persuy, P., Peers, M.C. 1987. Observation of morphological relationships between angiopathic blood vessels and degenerative neurites in Alzheimer's disease. *Virchows Arch A Pathol Anat Histopathol* 411(3), 199-204.

Eikelenboom, P., Veerhuis, R., Familian, A., Hoozemans, J.J., van Gool, W.A., Rozemuller, A.J. 2008. Neuroinflammation in plaque and vascular beta-amyloid disorders: clinical and therapeutic implications. *Neurodegener Dis* 5(3-4), 190-3.

Ellis, R.J., Olichney, J.M., Thal, L.J., Mirra, S.S., Morris, J.C., Beekly, D., Heyman, A. 1996. Cerebral amyloid angiopathy in the brains of patients with Alzheimer's disease: the CERAD experience, Part XV. *Neurology* 46(6), 1592-6.

Hoozemans, J.J., van Haastert, E.S., Nijholt, D.A., Rozemuller, A.J., Eikelenboom, P., Scheper, W. 2009. The unfolded protein response is activated in pretangle neurons in Alzheimer's disease hippocampus. *Am J Pathol* 174(4), 1241-51.

Jellinger, K.A., Attems, J. 2005. Prevalence and pathogenic role of cerebrovascular lesions in Alzheimer disease. *J Neurol Sci* 229-230, 37-41.

Jeynes, B., Provias, J. 2006. The possible role of capillary cerebral amyloid angiopathy in Alzheimer lesion development: a regional comparison. *Acta Neuropathol* 112(4), 417-27.

Morel, F. 1950. Petite contribution a l'etude d'une angiopathie apparemment dyshorique et topistique. *Rev Mens Psychiat Neurol* 120, 352-7.

Oshima, K., Akiyama, H., Tsuchiya, K., Kondo, H., Haga, C., Shimomura, Y., Iseki, E., Uchikado, H., Kato, M., Niizato, K., Arai, H. 2006. Relative paucity of tau accumulation in the small areas with abundant Abeta42-positive capillary amyloid angiopathy within a given cortical region in the brain of patients with Alzheimer pathology. *Acta Neuropathol* 111(6), 510-8.

Oshima, K., Uchikado, H., Dickson, D.W. 2008. Perivascular neuritic dystrophy associated with cerebral amyloid angiopathy in Alzheimer's disease. *Int J Clin Exp Pathol* 1(5), 403-8.

Pantelakis, S. 1954. [A particular type of senile angiopathy of the central nervous system: congophilic angiopathy, topography and frequency]. *Monatsschr Psychiatr Neurol* 128(4), 219-56.

Poirier, J., Davignon, J., Bouthillier, D., Kogan, S., Bertrand, P., Gauthier, S. 1993. Apolipoprotein E polymorphism and Alzheimer's disease. *Lancet* 342(8873), 697-9.

Pollio, G., Hoozemans, J.J., Andersen, C.A., Roncarati, R., Rosi, M.C., van Haastert, E.S., Seredenina, T., Diamanti, D., Gotta, S., Fiorentini, A., Magnoni, L., Raggiaschi, R., Rozemuller, A.J., Casamenti, F., Caricasole, A., Terstappen, G.C. 2008. Increased expression of the oligopeptidase THOP1 is a neuroprotective response to Abeta toxicity. *Neurobiol Dis* 31(1), 145-58.

Revesz, T., Ghiso, J., Lashley, T., Plant, G., Rostagno, A., Frangione, B., Holton, J.L. 2003. Cerebral amyloid angiopathies: a pathologic, biochemical, and genetic view. *J Neuropathol Exp Neurol* 62(9), 885-98.

Rozemuller, A.J., van Gool, W.A., Eikelenboom, P. 2005. The neuroinflammatory response in plaques and amyloid angiopathy in Alzheimer's disease: therapeutic implications. *Curr Drug Targets CNS Neurol Disord* 4(3), 223-33.

Rozemuller, J.M., Eikelenboom, P., Stam, F.C., Beyreuther, K., Masters, C.L. 1989. A4 protein in Alzheimer's disease: primary and secondary cellular events in extracellular amyloid deposition. *J Neuropathol Exp Neurol* 48(6), 674-91.

Schlote, W. 1965. Die Amyloidnatur der kongophilen, drusige entartung der Hirnarterien (Scholz) im Senium. *Acta Neuropathologica* 4, 449-68.

Scholz, W. 1938. Studien zur Pathologie der Hirngefäße. II. Die drusige Entartung der Hirnarterien und -capillaren (Eine Form seniler Gefäßerkrankung). *Z Ges Neurol Psychiatr* 162, 694-715.

Shibata, M., Yamada, S., Kumar, S.R., Calero, M., Bading, J., Frangione, B., Holtzman, D.M., Miller, C.A., Strickland, D.K., Ghiso, J., Zlokovic, B.V. 2000. Clearance of Alzheimer's amyloid-ss(1-40) peptide from brain by LDL receptor-related protein-1 at the blood-brain barrier. *J Clin Invest* 106(12), 1489-99.

Slooter, A.J., van Duijn, C.M. 1997. Genetic epidemiology of Alzheimer disease. *Epidemiol Rev* 19(1), 107-19.

Surbek, B. 1961. L'angiopathie dyshorique (Morel) de l'écorce cérébrale. Etude anatomo-clinique et statistique, aspect génétique. *Acta Neuropathologica* 1, 168-97.

Tanzi, R.E., Moir, R.D., Wagner, S.L. 2004. Clearance of Alzheimer's Abeta peptide: the many roads to perdition. *Neuron* 43(5), 605-8.

Thal, D.R., Ghebremedhin, E., Orantes, M., Wiestler, O.D. 2003. Vascular pathology in Alzheimer disease: correlation of cerebral amyloid angiopathy and arteriosclerosis/lipohyalinosis with cognitive decline. *J Neuropathol Exp Neurol* 62(12), 1287-301.

Thal, D.R., Ghebremedhin, E., Rub, U., Yamaguchi, H., Del Tredici, K., Braak, H. 2002. Two types of sporadic cerebral amyloid angiopathy. *J Neuropathol Exp Neurol* 61(3), 282-93.

Thal, D.R., Griffin, W.S., de Vos, R.A., Ghebremedhin, E. 2008. Cerebral amyloid angiopathy and its relationship to Alzheimer's disease. *Acta Neuropathol* 115(6), 599-609.

Vidal, R., Calero, M., Piccardo, P., Farlow, M.R., Unverzagt, F.W., Mendez, E., Jimenez-Huete, A., Beavis, R., Gallo, G., Gomez-Tortosa, E., Ghiso, J., Hyman, B.T., Frangione, B., Ghetti, B. 2000. Senile dementia associated with amyloid beta protein angiopathy and tau perivascular pathology but not neuritic plaques in patients homozygous for the APOE-epsilon4 allele. *Acta Neuropathol* 100(1), 1-12.

Weller, R.O., Subash, M., Preston, S.D., Mazanti, I., Carare, R.O. 2008. Perivascular drainage of amyloid-beta peptides from the brain and its failure in cerebral amyloid angiopathy and Alzheimer's disease. *Brain Pathol* 18(2), 253-66.

Williams, S., Chalmers, K., Wilcock, G.K., Love, S. 2005. Relationship of neurofibrillary pathology to cerebral amyloid angiopathy in Alzheimer's disease. *Neuropathol Appl Neurobiol* 31(4), 414-21.

Yamada, M., Itoh, Y., Suematsu, N., Otomo, E., Matsushita, M. 1997. Vascular variant of Alzheimer's disease characterized by severe plaque-like beta protein angiopathy. *Dement Geriatr Cogn Disord* 8(3), 163-8.

Supplementary Data

ELISA Aβ40 and Aβ42 (in collaboration with Alex Roher)

Immunoassays for Aβ40 and Aβ42 were performed on capCAA and AD cases, as illustrated in Fig. 1. In conformity with the neuropathological observations, quantitation of soluble and insoluble Aβ peptides demonstrated statistical differences between capCAA and AD, with respect to the ratio and amount of Aβ species. In the Tris-soluble samples (Fig. 1A) the capCAA cases demonstrated a strikingly greater mean value of both Aβ40 (capCAA = 1466 pg/mg total protein; AD = 112 pg/mg total protein; $p = 0.0002$) and Aβ42 (capCAA = 218 pg/mg total protein; AD = 70 pg/mg total protein; $p = 0.0114$). A similar difference between capCAA and AD was observed in the Guanidine-HCl soluble samples (Fig. 1B) for levels of Aβ40 (capCAA = 205632 pg/mg total protein; AD = 16973 pg/mg total protein; $p = 0.0524$) and Aβ42 (capCAA = 270840 pg/mg total protein; AD = 91606 pg/mg total protein; $p = 0.0213$).
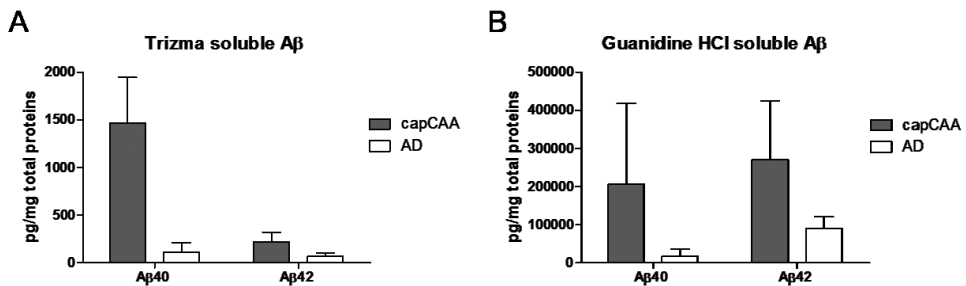
Supplementary Figure 1. Elisa quantification of Aβ40 and Aβ42 in capCAA and comparison with AD. A. Trizma soluble Aβ levels shows a striking increase of Aβ40 in capCAA respect to AD, with a ratio Aβ40:Aβ42 4.2 times higher in capCAA. A similar ratio Aβ40:Aβ42 is observed in the Guanidine-HCl fractions (4.09 times higher in capCAA respect to AD). All values are adjusted for total protein. The statistical analysis used was an unpaired, 2-tailed t-test. capCAA= capillary cerebral amyloid angiopathy, AD= Alzheimer's disease

All steps were performed at 4°C. Occipital lobe tissue pieces (100 mg) were homogenized in 6 volumes (600 μl) of 20 mM Tris-HCl, 5 mM EDTA, pH 7.8, protease inhibitor cocktail (PIC, Roche Diagnostics, Mannheim, Germany) with a Teflon tissue grinder. The homogenate was centrifuged in a TLA 120.2 rotor (Beckman) for 20 min at $435,000 \times g$. The Tris-HCl-soluble supernatant was collected and total protein measured with the Micro BCA protein assay kit

from Pierce (Rockford, IL). The remaining pellet was dissolved in 600 µl of 90% glass distilled formic acid (GDFA) with an electric grinder (Omni TH, Kennesaw, GA) and incubated for 1 h. The GDFA homogenates were then centrifuged at 435,000 × g in a TLA 120.2 rotor for 20 min. The supernatant was collected and dialyzed 3 times, 30 min each against deionized water then twice for 1 h against 0.1 M ammonium bicarbonate and lyophilized. The lyophilized material was reconstituted in 500 µl 5 M guanidine hydrochloride (GHCl), 50 mM Tris-HCl, pH 8.0, PIC (Roche), shaken for 3 h, centrifuged at 435,000 × g in a TLA 120.2 rotor for 20 min, the supernatant collected and total protein determined with Pierce's Micro BCA protein assay kit. Aβ40 and Aβ42 were quantified with ELISA kits from Invitrogen according the manufacturers' instructions.
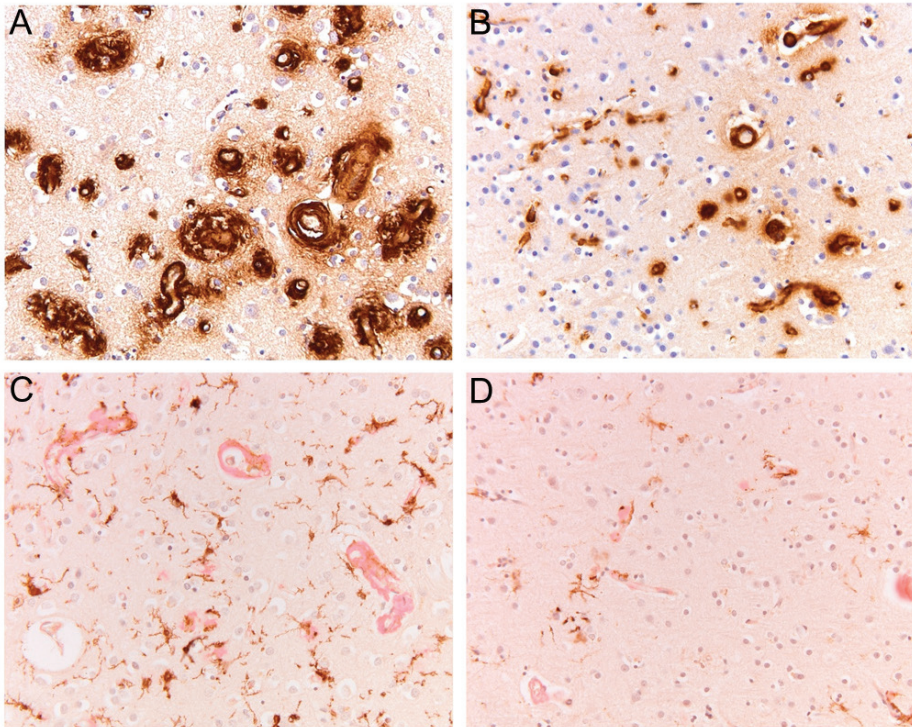
Supplementary Figure 2. Microglia activation around diverse dyshoric Aβ deposits: flames vs. bulbs. A, C depict adjacent tissue slices of a capCAA case showing severe flame-like vascular Aβ deposits. B, D present a case with severe bulb-like vascular Aβ. Aβ staining is visible in brown in A and B. In C and D activated microglia are shown in brown around capCAA microvessels loaded with Aβ (in pink, stained with Congo red)

Microglia activation

Microglia are strongly activated around dyshoric changes. Especially the flame-like Aβ deposits evoke a severe inflammatory reaction, when compared to the mild glia activation in response to the more compact and contained bulb-like deposits as shown in Fig. 2.

Activated microglia surrounding capCAA lack the expression of microglia marker CD45 (Fig. 3). CD45, also known as leukocyte common antigen (LCA), is expressed constitutively by resting microglia and it is further inducible at the cell surface during activation (Carson, et al., 1998; Sedgwick, et al., 1991). CD45 negative microglia have a proinflammatory phenotype (release more cytokines) and have less phagocytic abilities in an AD mouse model (Zhu, et al., 2011).
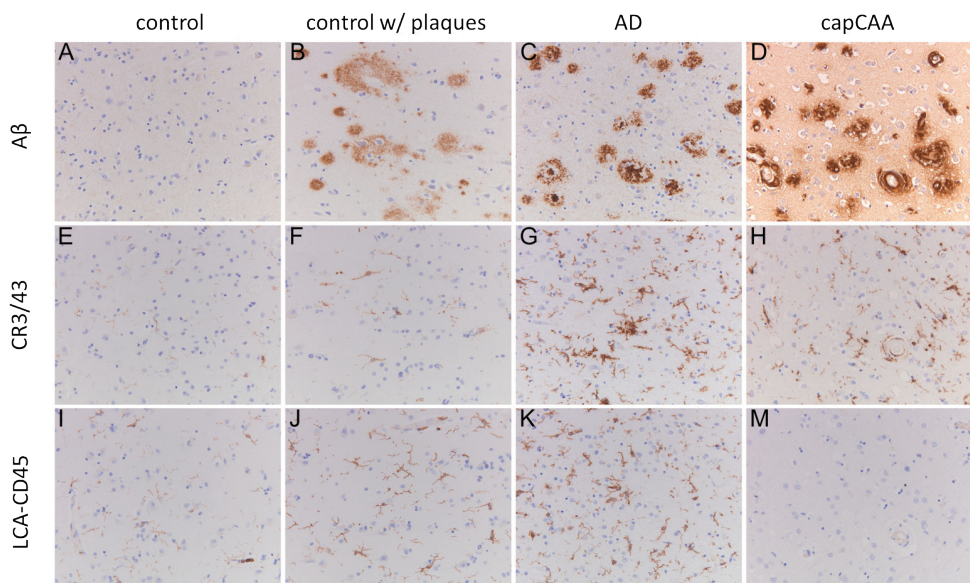
Supplementary Figure 3. CD45 expression in activated microglia. A, B, C, D show in brown Aβ staining. E, F, G, H, show in brown CR3/43 (a MHC class II marker) positive activated microglia. I, J, K, M show in brown CD45 positive activated microglia. In control cases glia activation is absent or negligible (A, E, I). In non demented cases that presents with plaques glia activation is already present (B, F, J) although is not as strong as in full blown AD (C, G, K) or capCAA (D, H, M). Also notice the striking lack of CD45 positivity in activated microglia around capCAA (M). LCA (leukocyte common antigen) = CD45

References

Carson, M.J., Reilly, C.R., Sutcliffe, J.G., Lo, D. 1998. Mature microglia resemble immature antigen-presenting cells. Glia 22(1), 72-85.

Sedgwick, J.D., Schwender, S., Imrich, H., Dorries, R., Butcher, G.W., ter Meulen, V. 1991. Isolation and direct characterization of resident microglial cells from the normal and inflamed central nervous system. Proc Natl Acad Sci U S A 88(16), 7438-42.

Zhu, Y., Hou, H., Rezai-Zadeh, K., Giunta, B., Ruscin, A., Gemma, C., Jin, J., Dragicevic, N., Bradshaw, P., Rasool, S., Glabe, C.G., Ehrhart, J., Bickford, P., Mori, T., Obregon, D., Town, T., Tan, J. 2011. CD45 deficiency drives amyloid-beta peptide oligomers and neuronal loss in Alzheimer's disease mice. J Neurosci 31(4), 1355-65.

3

chapter

Proteome of Cerebral Capillary Amyloid Angiopathy: relevance for amyloid clearance in Alzheimer's disease

Anna Carrano, Davide Chiasserini, Jeroen J. Hoozemans, Jack van Horssen, Silvina Fratantoni, Sander R. Piersma, Thang Pham, Helga E. de Vries, Annemieke J.M. Rozemuller, Connie R. Jimenez and Saskia M. van der Vies

Proteome of Cerebral Capillary Amyloid Angiopathy: relevance for amyloid clearance in Alzheimer's disease

Anna Carrano[1], Davide Chiasserini[2], Jeroen J.M. Hoozemans[1], Jack van Horssen[3], Silvina Fratantoni[2], Sander R. Piersma[2], Thang Pham[2], Helga E. de Vries[3], Annemieke J.M. Rozemuller[1], Connie R. Jimenez[2] and Saskia M. van der Vies[1].

[1]Department of Pathology, [2]Oncoproteomics Laboratory and [3]Department of Molecular Cell Biology and Immunology, VU University Medical Center, Neuroscience Campus Amsterdam, The Netherlands.

Abstract

Alzheimer's disease (AD) is characterized by progressive cognitive impairment associated with accumulation of amyloid β (Aβ) in the brain parenchyma such as plaques and in cerebral blood vessels as cerebral amyloid angiopathy (CAA). Over half of the number of AD cases show presence of Aβ accumulation in and around cortical capillaries, which is referred to as capillary CAA (capCAA). CapCAA cases exhibit a compromised blood-brain barrier (BBB), which might contribute to impaired Aβ clearance observed in AD cases. With this exploratory proteomic analysis using human *post-mortem* brain tissue we aimed to identify differentially expressed proteins in cases with profound capCAA pathology compared to AD, in order to reveal specific insight in underlying molecular mechanisms resulting in disturbed clearance of Aβ across the BBB. Furthermore, by profiling the proteomes of capCAA patients and comparing them with AD cases, we aimed to identify proteins and (patho-)biological processes that are involved in the pathogenesis of capCAA and novel biomarkers for the differential diagnosis of capCAA and AD. Using mass-spectrometry we identified 1547 proteins in total, of which 29 were differentially regulated in capCAA compared to AD and controls, including clusterin (ApoJ), serum amyloid P component (SAP) and laminin β2. Immunohistochemical evaluation revealed that these proteins co-localized with Aβ deposits, predominantly microvascular over parenchymal. Interestingly, previous studies have demonstrated that these proteins are involved in Aβ aggregation and clearance from the brain, implying the involvement of altered clearance mechanisms in the pathophysiology of capCAA.

Introduction

Alzheimer's disease (AD) is the most common form of dementia in the elderly affecting 10% of the population aged over 65 years (de Jong, et al., 2007). AD is characterized by accumulation of amyloid β (Aβ) protein in the brain parenchyma and in the cerebrovasculature. Excessive deposition of Aβ is thought to be the result of an imbalance between Aβ production and Aβ removal and increasing evidence suggests that in sporadic late-onset AD this process is driven by an impaired clearance of Aβ (Goos, et al., 2012).

The blood-brain-barrier (BBB) plays an essential role in the clearance of Aβ from the brain to periphery. A disturbance in Aβ clearance across the BBB is illustrated in cases that exhibit deposition of Aβ in and around cortical capillaries, also referred to as capillary cerebral amyloid angiopathy (capCAA). CapCAA is observed in up to 51% of AD cases and is associated with the clinical progression of AD (Thal, et al., 2008). Little is known about the molecular mechanism leading to capCAA in AD pathogenesis and how amyloid deposition in the vessel wall affects disease development. Considerable effort has been made in understanding the pathogenesis of AD and the development of novel therapeutic approaches. However to date, there is no effective treatment that can prevent, delay or cure the disease and most of the latest clinical trials focusing on decreasing Aβ load in the brain have been failing. Interestingly, anti-Aβ immunization therapies while able to reduce the amount of plaque in the brain parenchyma led, in some patients, to increased accumulation in the vasculature and consequent vasogenic edema (Alzheimer, 1907; Dierksen, et al., 2010). Clinical diagnosis of "probable AD" is based on neuropsychological examination together with neuroimaging and biochemical analysis of the cerebrospinal fluid. Although guidelines to diagnose CAA during life exist (Boston criteria) (Fischer, 1907), these are not specific for capCAA. Hence currently, it is not possible to clinically define whether an AD case has signs of ongoing or progressive capCAA. Recently, we neuropathologically defined clinical AD cases which show extensive capCAA pathology without presence of senile plaques and only minor tau depositions as tangles (Richard, et al., 2010). These cases are characterized by extensive activated NOX-positive glia recruited around vascular Aβ deposits and a damaged BBB showing a reduced expression of tight junction proteins (Carrano, et al., 2011a; Carrano, et al., 2012). Identification of differentially expressed proteins in cases that only show capCAA pathology might reveal insight in the underlying molecular mechanism resulting in the disturbed clearance of Aβ across the

BBB and the identification of specific biomarker for capCAA.

The use of proteomics gives information about changes in the total protein network of a tissue or cell and in the recent years it has become extremely useful to study complex diseases, such as AD.

Proteomics studies focusing on the identification of AD biomarkers for early diagnosis or disease progression and for the validation of new targets for treatment are reviewed by Juhasz (Juhasz, et al., 2011). Although proteomics analysis of AD brain and AD animal models are rather abundant, to date there is no study that analyzed the capCAA proteome. Hence, we used a proteomic approach to identify differential changes in the proteome of *post-mortem* brain tissue of patients with exclusive capCAA pathology and compared these finding with AD and age-matched non-demented controls.

Analysis of the mass spectrometry data resulted in the identification of 1547 proteins in total. A number of proteins that are known to have an altered expression profile in AD compared to controls were identified, indicating the value of this approach. Interestingly, we could identify and validate proteins that were differentially upregulated in capCAA compared to AD, including clusterin (ApoJ), serum amyloid P component (SAP) and laminin β2.

This is the first proteomic analysis on human *post-mortem* capCAA tissue to date. By profiling the proteomes of capCAA patients and comparing them with AD and control cases, we identified proteins and processes that are involved in the pathogenesis of capCAA. More research is needed to confirm our findings and to demonstrate whether differentially expressed proteins can be used as possible candidate biomarkers for the differential diagnosis of capCAA.

Material and Methods

Post-mortem tissue

Two patients with neuropathologically diagnosed pure capCAA without senile plaques, 2 AD cases without capCAA and 2 age-matched nondemented controls were selected for the proteomics analysis. These cases were also analyzed by immunohistochemical staining. A total of 5 patients with neuropathologically diagnosed capCAA, 5 AD cases without capCAA and 2 age-matched nondemented controls were selected for the validation of differentially ex-

pressed proteins by immunohistochemistry. Cases were selected on the basis of the clinical and neuropathological diagnosis and immunohistochemical characterization of Aβ aggregates. Human brain specimens were obtained at autopsy with a short post-mortem interval (The Netherlands Brain Bank, Amsterdam, The Netherlands and University Medical Centre in Utrecht, The Netherlands). Neuropathological evaluation was performed on frozen tissue and formalin-fixed, paraffin-embedded tissue from occipital pole cortex. capCAA score was defined as follows: severe (+++), moderate (++), mild (+). Staging of AD was evaluated on thin paraffin embedded routine slices according to Braak and Braak (Braak, et al., 2006; Braak and Braak, 1991) and CERAD (Mirra, et al., 1991). Age, gender, post-mortem delay (PMD), Braak, CERAD and capCAA scores and cause of death are listed in Table 1.

Tissue Homogenization and Fractionation Using Gel Electrophoresis

Tissue from the occipital pole cortex was used for proteomics analysis. For homogenization, we cut a cortical piece of ˍ20 mg in a bath of liquid nitrogen in smaller parts. The proteins in the tissue were solubilized in 800 μl of 1× reducing SDS sample buffer (containing 62.5 mM Tris-HCl, 2% w/v SDS, 10% v/v glycerol, and 0.0025% bromphenol blue, 100 mM DTT, pH 6.8) using a Pellet Pestles microgrinder system (Kontes glassware, Vineland, NJ). Subsequently, proteins were denatured by heating at 100 °C for 10 min. Any insoluble debris was removed by centrifuging for 15 min at maximum speed (16.1 relative centrifugal force) in a benchtop centrifuge.

Proteins were fractionated using one-dimensional SDS-PAGE. 25 μl of each homogenized sample (containing about 50 μg of protein) was loaded on a well of a precast NuPAGE 4–12% w/v Bis-Tris 1.5-mm minigel (Invitrogen). The stacking gel contained 4% (w/v) acrylamide/Bis-Tris. Electrophoresis was carried out at 200 V in NuPAGE MES SDS running buffer (50 mM Tris base, 50 mM MES, 0.1% w/v SDS, 1 mM EDTA, pH 7.3) until the dye front reached the end of the gel. Following electrophoresis, the gels were fixed with a solution of 50% ethanol and 3% phosphoric acid. Staining was carried out in a solution of 34% methanol, 3% phosphoric acid, 15% ammonium sulfate, and 0.1% Coomassie Blue G-250 (Bio-Rad) with subsequent destaining in MilliQ water.

In-gel Digestion

The gel lanes were cut in 10 bands, and each band was processed for in-gel digestion as previ-

ously described (Piersma, et al., 2010). Briefly, the bands were washed and dehydrated three times in 50 mM ammonium bicarbonate, pH 7.9, 50 mM ammonium bicarbonate, and 50% ACN. Subsequently, cysteine bonds were reduced with 10 mM DTT for 1 h at 56 °C and alkylated with 50 mM iodoacetamide for 45 min at room temperature in the dark. After two subsequent wash/dehydration cycles, bands were dried for 10 min in a vacuum centrifuge and incubated overnight with 0.06 μg/μl trypsin at 25 °C. The peptides were extracted once in 1% formic acid and subsequently twice in 50% ACN in 5% formic acid. The volume was reduced to 50 μl in a vacuum centrifuge prior to LC-MS analysis.

Table 1. Patients details

Patient #	Age (years)	sex	PMD (hrs:min)	Braak	CERAD	capCAA	cause of death
capCAA 1	71	F	< 24	IV	B	+++	pneumonia
capCAA 2	75	F	6:00	V	0	+++	dehydration
capCAA 3	65	M	7:00	V	C	++/+++	pneumonia
capCAA 4	89	F	6:55	V	B	++/+++	cachexia, pneumonia
capCAA 5	74	M	3:25	V	C	+++	died suddenly
AD 1	90	F	3:50	VI	C	-	cachexia/dehydration
AD 2	44	M	4:25	VI	C	-	unknown
AD 3	86	F	5:00	VI	C	-	uremia based on pneumonia
AD 4	83	F	7:20	VI	C	-	cachexia/dehydration
AD 5	70	F	4:20	VI	C	-	cachexia/dehydration
Control 1	75	M	n.d.	0	A	-	myocardial infarct
Control 2	72	F	n.d.	0	A	-	lung cancer, broncho-pneumonia

n.d. : no date, F: female, M: male
Note: CERAD classification can be mistaken in capCAA cases, as neuritic changes around amyloid are not necessarily neuritic plaques but can be neurofibrillary degeneration around capCAA. This is probably the case in classification CERAD A, B and C in severe capCAA cases.

Nano-LC-MS/MS

Peptides were separated by an Ultimate 3000 nano-LC system (Dionex LC-Packings, Amsterdam, The Netherlands) equipped with a 20-cm × 75-μm inner diameter fused silica column custom packed with 3-μm 100 Å ReproSil Pur C18 aqua (Dr. Maisch GMBH, Ammer-

buch-Entringen, Germany) as described before (Bergeron, et al., 1987). After injection, the peptides were trapped at 30 μl/min on a 0.5-cm × 300-μm inner diameter Pepmap C18 cartridge (Dionex LC-Packings, Amsterdam, The Netherlands) at 2% buffer B (buffer A, 0.05% formic acid in MQ; buffer B, 80% ACN and 0.05% formic acid in MQ) and separated at 300 nl/min in a 10–40% buffer B gradient in 60 min. Eluting peptides were ionized at 1.7 kV in a Nanomate Triversa chip-based nanospray source using a Triversa LC coupler (Advion, Ithaca, NJ). Intact peptide mass spectra and fragmentation spectra were acquired on a LTQ-FT hybrid mass spectrometer (Thermo Fisher, Bremen, Germany). Intact masses were measured at resolution 50,000 in the ICR cell using a target value of 1×106 charges. In parallel, following an FT prescan, the top five peptide signals (charge states 2+ and higher) were submitted to MS/MS in the linear ion trap (3-atomic mass unit isolation width, 30-ms activation, 35% normalized activation energy, Q value of 0.25, and a threshold of 5,000 counts). Dynamic exclusion was applied with a repeat count of 1 and an exclusion time of 30 s.

Table 1. Antibodies

Primary Antibody	species raised in	Isotype	dilution	source
Lamininβ2 clone C4	mouse	IgG1	1:1000	R&D systems
SAP	mouse	-	1:200	SSI Diagnostica
Factor VIII	rabbit	-	1:50	DAKO
Clusterin clone G7	mouse	IgG1	1:100	Dept of Clinical Chemistry, Vumc Amsterdam
Anti Aβ 4G8	mouse	IgG2b	1:200	Signet

Database Searching

MS/MS spectra were searched against the human IPI database 3.31 using Sequest (version 27, rev 12), which is part of the BioWorks 3.3 data analysis package (Thermo Fisher, San Jose, CA). MS/MS spectra were searched with a maximum allowed deviation of 10 ppm for the precursor mass and 1 amu for fragment masses. Methionine oxidation and cysteine carboxamidomethylation were allowed as variable modifications, two missed cleavages were allowed and the minimum number of tryptic termini was 1. After database searching, the DTA and OUT files were imported into Scaffold (versions 1.07 and 2.01) (Proteome software, Portland, OR). Scaffold was used to organize the data and to validate peptide identifications using the PeptideProphet algorithm, and only identifications with a probability >95% were retained.

Subsequently, the ProteinProphet algorithm was applied and protein identifications with a probability of >99% with 2 peptides or more in at least one of the samples were retained (Alafuzoff, et al., 2009; Ellis, et al., 1996). Proteins that contained similar peptides and could not be differentiated based on MS/MS analysis alone were grouped. For each protein identified, the number of spectral counts (the number of MS/MS associated with an identified protein) was exported to Excel. For quantitative analysis across samples, spectral counts were normalized on the sum of the spectral counts per biological sample.

Each sample was separated in 10 fractions that were subjected to nano LC-MS/MS. Spectral counts for identified proteins in a sample were summed across all fractions for each sample and were normalized on the total sum of spectral counts for that sample (a similar approach has been used in (Jellinger and Attems, 2005). This gives the relative spectral count (SpC) contribution of protein i to all spectral counts in the sample (Vidal, et al., 2000). When comparing different data sets, these normalized spectral counts are used to calculate fold changes.

Spectral Count Normalization and Statistics

Normalization was performed as described previously (Pham, et al., 2010; Surbek, 1961). The spectral counts of each protein were divided by the total spectral counts of all proteins within a sample. This number was multiplied with a constant equal to the average of total spectral counts of all samples to obtain a normalized spectral count value in the same range as the non-normalized spectral counts. The beta-binomial test (Pham, et al., 2010) was applied to find proteins that show significant differences in spectral count numbers between the diseased group and the reference group. Proteins with a p value less than 0.05 were designated as being significant.

Unsupervised and supervised cluster analysis of identified proteins was performed using hierarchical clustering in R. The protein abundances were normalized to zero mean and unit variance for each individual protein. Subsequently, the Euclidean distance measure was used for protein clustering.

Network analysis

To gain insight into the possible interactions of differentially expressed proteins in capCAA tissue we used the database STRING (Pantelakis, 1954) to retrieve functional and physical interaction. First, a general network of all identified proteins was created using medium strin-

gency settings and experimental, database, and co-expression interactions, with a number of maximum interactors for each node of 100. Text mining interactions were excluded. Network data were exported to a text file and loaded in Cytoscape v 2.8.3 for network visualization and analysis. The proteins showing differential expression in the three groups comparison were selected together with their first interactors, limiting the selection to the interactors which showed at least a fold change of 2 for the comparisons capCAA vs controls or capCAA vs AD. Proteins for which interactions were not present in the STRING database were excluded from the analysis. Clustering of the final network was obtained with the clusterMaker plugin v 1.1 (Morris, et al., 2011) using the Markov Cluster (MCL) algorithm (Enright, et al., 2002), while ontologies for each cluster were obtained using BINGO plug-in (Schlote, 1965).

Immunohistochemistry analysis for validation of differentially expressed proteins

5 μm cryosections were mounted on coated glass slides (Menzel Gläzer super frost PLUS, Brainschweig, Germany) and dried O/N. Sections were incubated in thioflavin S solution (100 mg/ml) for 5 minutes to stain Aβ fibrils and washed subsequently 3 times in ethanol 70%. Sections were preincubated with normal goat serum 1:10 for 10 minutes and overnight with a mix of primary antibodies (see table 2) diluted in PBS containing 1% bovine serum albumin. Next, sections were incubated with secondary antibodies for 30 minutes.

In some cases an incubation step of 1 h with Streptavidine-Alexa633 followed. For all stainings peroxidase labelling was visualized by reaction with rhodamine-tyramide (1:3000) in the presence of 0.01% H_2O_2 for 5 minutes. After washing, slides were covered with Vectashield (Vector laboratories, Burlington, CA, USA). Between all incubation steps, sections were extensively washed with PBS (pH 7.4). Fluorescent analysis was performed with a Leica TCS SP2 AOBS confocal laser-scanning microscope (Leica Microsystem, Heidelberg, Germany). Quantification of fluorescent signal was performed by ImageJ software. Four 100 times magnified fields per slides were quantified and an average was calculated.

Table 3. (Page 72) Three group comparison. List of differentially expressed proteins (p< 0.05) in the occipital cortex of capCAA patients compared with Alzheimer's disease cases and controls ranked on fold change (capCAA versus controls). Abbreviations: CAA = capillary cerebral amyloid angiopathy; AD = Alzheimer's disease; C = control; nc= normalized spectral counts; fc = fold change

Gene Symbol	AD1 nc	AD2 nc	capCAA1 nc	capCAA2 nc	C1 nc	C2 nc	fc.cap-CAA/C	fc.cap-CAA/AD	fc. AD/C	fc. max	pvalues	Protein name
NPTN	1,94	3,63	1,00	0,00	0,00	0,00	∞	-5,58	∞	∞	0,0204	Isoform 3 of Neuroplastin
S100B	3,89	2,72	1,00	2,14	0,00	0,00	∞	-2,10	∞	∞	0,0121	Protein S100-B
APCS	0,97	0,00	3,00	3,21	0,00	0,00	∞	6,39	∞	∞	0,0132	Serum amyloid P-component
HUWE1	0,00	0,00	3,00	1,07	0,00	0,00	∞	∞	1,00	∞	0,0245	482 kDa protein
AKAP12	13,61	6,35	9,98	7,50	1,10	0,98	8,43	-1,14	9,62	9,62	0,0038	A kinase (PRKA) anchor protein 12 isoform 2
SUB1	3,89	4,54	4,99	3,21	0,00	0,98	8,38	-1,03	8,61	8,61	0,0209	Activated RNA polymerase II transcriptional coactivator p15
APP	0,97	7,26	7,99	12,85	2,19	1,96	5,02	2,53	1,98	5,02	0,0431	Isoform APP770 of Amyloid beta A4 protein (Fragment)
AGRN	3,89	5,44	3,00	1,07	0,00	0,98	4,15	-2,29	9,53	9,53	0,0263	Agrin
CLU	9,72	15,43	25,96	24,64	8,77	4,89	3,70	2,01	1,84	3,70	0,0021	Clusterin
LAMB2	0,00	0,00	2,00	4,28	0,00	2,94	2,14	∞	-∞	∞	0,0335	Laminin subunit beta-2
ABR	0,00	0,00	2,00	3,21	5,48	1,96	-1,43	∞	-∞	∞	0,0088	Isoform Long of Active breakpoint cluster region-related protein
LDHA	44,72	36,30	28,96	24,64	38,36	38,18	-1,43	-1,51	1,06	1,51	0,0473	L-lactate dehydrogenase
CUL3	1,94	1,81	4,99	3,21	7,67	6,85	-1,77	2,18	-3,86	3,86	0,0332	Isoform 1 of Cullin-3
CORO1C	0,00	0,00	3,00	1,07	4,38	2,94	-1,80	∞	-∞	∞	0,0081	cDNA FLJ50992, highly similar to Coronin-1C
ME3	3,89	1,81	6,99	3,21	10,96	9,79	-2,03	1,79	-3,64	3,64	0,0188	NADP-dependent malic enzyme, mitochondrial
ALDH9A1	10,69	15,43	7,99	6,43	18,63	14,68	-2,31	-1,81	-1,28	2,31	0,0301	aldehyde dehydrogenase 9A1
PCSK1N	9,72	9,98	3,99	3,21	10,96	8,81	-2,74	-2,73	-1,00	2,74	0,0248	ProSAAS
ACTR3	6,80	8,17	3,99	2,14	8,77	9,79	-3,02	-2,44	-1,24	3,02	0,0364	Actin-related protein 3
PPA1	5,83	2,72	0,00	1,07	2,19	1,96	-3,87	-7,99	2,06	7,99	0,0437	Inorganic pyrophosphatase
MAP1LC3A	2,92	2,72	1,00	2,14	7,67	4,89	-4,00	-1,80	-2,23	4,00	0,0468	Isoform 1 of Microtubule-associated proteins 1A/1B light chain 3A
CPNE5	0,97	0,00	1,00	1,07	4,38	3,92	-4,01	2,13	-8,54	8,54	0,0241	Copine-5
ENDOD1	0,00	0,00	1,00	0,00	3,29	1,96	-5,25	∞	-∞	∞	0,0226	Endonuclease domain-containing 1 protein
NDUFAF3	0,00	0,00	0,00	1,07	2,19	3,92	-5,70	∞	-∞	∞	0,0160	Uncharacterized protein C3orf60
ACTN2	0,97	1,81	2,00	0,00	8,77	3,92	-6,35	-1,40	-4,55	6,35	0,0289	Alpha-actinin-2
TIMM13	3,89	2,72	0,00	0,00	1,10	0,98	-∞	-∞	3,19	∞	0,0110	Mitochondrial import inner membrane translocase subunit Tim13
PIP4K2B	1,94	3,63	0,00	0,00	2,19	0,00	-∞	-∞	2,54	∞	0,0326	Isoform 1 of Phosphatidylinositol-5-phosphate 4-kinase type-2 beta
CAMK2D	1,94	1,81	0,00	0,00	17,54	1,96	-∞	-∞	-5,19	∞	0,0334	Isoform Delta 6 of Calcium/calmodulin-dependent protein kinase type II delta chain
PLD3	0,00	0,00	0,00	0,00	1,10	1,96	-∞	-1,00	-∞	∞	0,0360	Phospholipase D3
KIAA1244	0,00	0,00	0,00	0,00	2,19	0,98	-∞	-1,00	-∞	∞	0,0370	Brefeldin A-inhibited guanine nucleotide-exchange protein 3

Results

Differential protein expression in capCAA, AD and controls

Our primary goal was to determine the differences in protein expression profiles between capCAA, AD and control brain tissue in a small scale feasibility study with very well documented material. For comparative protein profiling, we employed a label-free workflow based on protein fractionation by gel electrophoresis coupled to nano-LC-MS/MS of in-gel digested proteins and spectral counting that has shown its validity for candidate biomarkers discovery (Albrethsen, et al., 2010) (van Dijk, et al., 2012).

To identify proteins associated with capCAA and AD, we compared the protein expression profiles in 2 severe capCAA cases with 2 AD cases and 2 age-matched controls. The protein band patterns obtained after gel electrophoresis of the 6 brain lysates and Coomassie staining were similar in terms of overall pattern and intensity (Fig.1a), thereby ensuring reliable label free comparison.

In total 1546 proteins were identified across all 6 samples (Fig. 1b) (see supplementary table 1 for the full list of identified proteins). The number of proteins identified in the capCAA brain samples was 1487, with 1235 identified in both samples, indicating acceptable reproducibility of protein identification and quantification across different biological samples. Similar values were obtained for the AD and control brain samples (see Fig. 1b).

44 proteins were not identified in the controls samples; most of these proteins are shared between the capCAA and AD group, 8 proteins are unique to capCAA, while 10 are found only in AD cases.

To obtain a global overview of the data set, we performed unsupervised hierarchical clustering using the normalized spectral count data from the identified proteins that were significantly differentially expressed in the 3 groups (capCAA, AD and controls, p value < 0.05) (Fig. 1 c). Supervised hierarchical clustering using 29 differentially expressed proteins clearly showed 2 different groups that clustered according to their pathological status as diseased (capCAA and AD) and non-diseased (controls). The diseased cluster further separated in capCAA and AD. (Fig. 1d)

Identification of known markers for AD and related diseases

Aβ was significantly upregulated in both AD and capCAA brain lysates, with a fold change of

1.9 and 5.0 respectively, whereas tau protein was only significantly up-regulated in AD brains (fold change 2.3) not in capCAA samples (fold change 1.7, p value: 0.15).

ApoE, the most important genetic risk factor for the sporadic form of AD and CAA, was also identified in our data set. ApoE was found significantly up-regulated in the capCAA brains and in 1 of the AD cases (fold change 3.1 and 3.6 respectively). These findings underscore the validity of our proteomics approach to identify proteins associated with AD and related pathology.

Differentially expressed proteins in capCAA cases.
We identified 29 proteins that were differentially expressed in capCAA cases compared to AD and control cases (table 3). In addition, we conducted a GO enrichment analysis to identify functions, cellular localization and pathways that are differently activated between two different proteomes. The 29 significant proteins were compared to the whole list of proteins in our dataset for the GO enrichment analysis (Fig. 2).

Of the 29 proteins that were significantly different between the 3 groups, 10 were found to be upregulated and 19 downregulated in capCAA compared to controls (table 3). Because of our interest in discovering proteins specifically and differentially expressed in capCAA and AD, we also compared the expression rate between capCAA and AD samples. Of the proteins upregulated in capCAA respect to controls, only 5 revealed higher spectral counts when we compared capCAA to AD. These five proteins include amyloid precursor protein (APP), clusterin, serum amyloid P component, laminin β2, and HUWE1. Interestingly, HUWE1 was only expressed in capCAA cases and absent in the other samples.
Of the 19 proteins downregulated in capCAA respect to controls, the expression levels of 10 were also lower when we compared them to AD profile. In this class of proteins we identified 2 dehydrogenases, aldehyde dehydrogenase 9A1 (ALDH91A) and L-lactate dehydrogenase (LDHA) (fold change -2.3 and -1.4 versus control); and 3 cytoskeleton proteins, actin-related protein 3 (ACTR3), alpha-actinin-2 (ACTN2) and microtubule-associated proteins 1A/1B light chain 3A (MAP1LC3A) (fold change -3.0, 6.4 and 4.0 versus control).

Network and pathway analysis
To obtain an interaction network of the differentially expressed proteins in the three groups
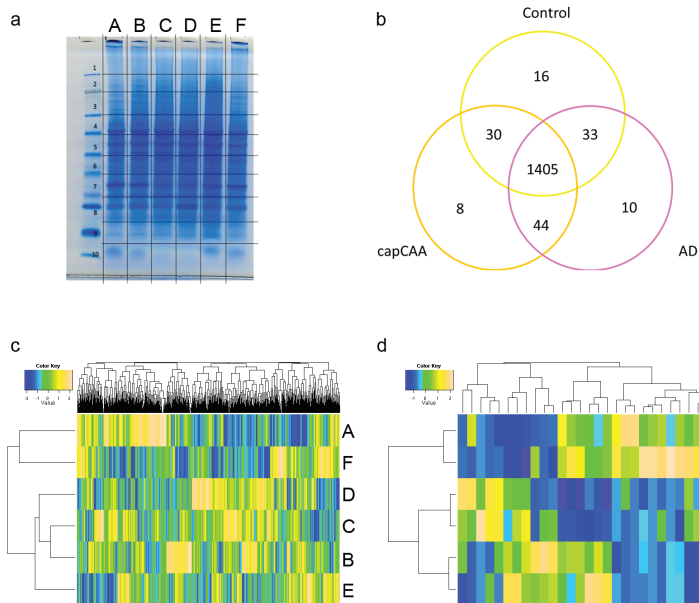
Figure 1. (a) SDS gel showing protein band patterns of the 6 brain lysates. A,D: controls; B,E: AD cases: C,F: capCAA cases. (b) Numbers of proteins identified in proteomics analysis of capCAA, AD and controls brain samples. (c) Unsupervised cluster analysis of the entire data set. (d) Supervised cluster analysis of the 29 proteins significantly differentially expressed in the 3 group comparison.

we used different tools and databases. First a total interaction network of all identified proteins was built using the online database STRING. Network visualization and analysis was carried out with the Cytoscape software. The total network of interactions consisted of 1212 nodes, representing proteins and 9017 edges representing experimental or functional interactions. To gain insight into the possible co-modulation of neighboring proteins for the differentially expressed proteins in capCAA we built a subnetwork of proteins which showed differential regulation in capCAA patients with respect to AD and control subjects with their first inter-actors. This subnetwork included 65 proteins and 132 interactions (figure 2). Of the 65 pro-teins, 12 proteins showed differential expression in capCAA vs control subjects while 10 were differential when compared to AD patients. APP was one of the most interconnected nodes in the network, showing experimental interaction with APOE and clusterin (CLU). These three proteins were all significantly up-regulated in capCAA patients with respect to controls (figure 2a) while only CLU was up-regulated significantly in capCAA when compared to AD (figure 2b). APP showed experimental interactions also with annexin 1 (ANXA1) which was

significantly up-regulated in capCAA vs AD comparison (figure 2b, fold change 7.9) and with alpha actinin 1 (ACTN1) which was decreased in capCAA patients with respect to controls (fold change -6.3).

Using cluster analysis we found 12 modules of proteins showing high interconnection. To verify if these modules were involved in specific pathways we searched for enrichment of biological processes for each of the subnetworks. The subnetwork which included the majority of differentially expressed proteins was the one with APP, CLU and APOE, mainly involved in lipid transport (figure 2c), followed by negative regulation of ubiquitin-protein ligase activity. The third sub-network, for which gene ontology analysis evidenced enrichment in cell-substrate adhesion processes, included laminin β2 (LAMB2) and serum amyloid P component (SAP or APCS) proteins both differentially regulated in capCAA. Subnetwork number 4, involved in cell signaling and protein phosphorylation, included CAMK2D, which was significantly reduced in capCAA with respect to both AD and controls subjects (fold change = -100 for both the comparisons), but also STAT1, increased significantly in capCAA vs AD comparison (fold change = 100). The complete gene ontology enrichment analysis of the 12 clusters is reported in supplementary table 2.

Validation by immunohistochemical staining

To verify the expression of proteins upregulated in the occipital cortex of capCAA cases, immunohistochemical staining for clusterin, SAP (serum amyloid P component) and LAMB2 (laminin β2) was performed on brain tissue slices from occipital pole cortex of capCAA, AD and controls. Protein selection was based on significances (pvalue lower than 0.05), fold change (higher than 2) and readily availability of antibodies. Furthermore these proteins, interestingly, have the ability to bind Aβ and modulate Aβ aggregation and clearance at the BBB.

To demonstrate the relationships between the mass spectrometry expression and the expression observed for the same proteins by immunostaining, we compared the fold change expression measured in the two analyses. Immunohistochemical analysis showed that clusterin, SAP and laminin β2 were abundantly expressed in capCAA cases and colocalized with microvascular amyloid deposits. Laminin β2, which is normally expressed in the vascular basal lamina, was predominantly increased in capCAA cases, specifically around Aβ-laden vessels, were the structure of the basal lamina was altered and appeared as a double barrel. In contrast,
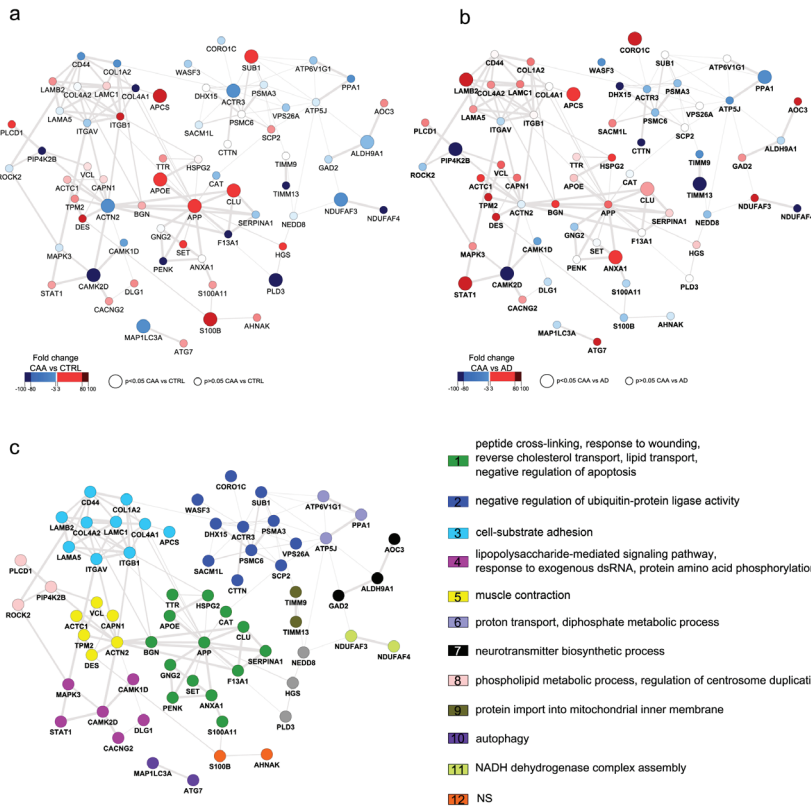
Figure 2. Interaction network of differentially expressed proteins in capCAA patients. Functional and experimental intereactions were retrieved from STRING database and the proteins which showed differential expression in the 3 groups comparison were selected with their first interactors. a) fold change capCAA vs controls b) fold change capCAA vs AD, c) cluster analysis of the network. Twelve clusters were identified including a maximum of 14 proteins and a minimum of 2 proteins. On the right the most significant biological process for each clusters is reported . NS = not significant.

in AD tissue laminin expression was severely reduced, especially in the microvasculature.

SAP immunostaining revealed that this protein clearly colocalized with vascular amyloid in capCAA cases, whereas SAP was weakly expressed in and around classical plaques of AD cases and absent in control cases.

Clusterin markedly accumulated in capCAA-affected vessels and colocalized with amyloid deposits in capCAA and AD cases. However, in capCAA the expression was significantly increased compared to AD cases as clusterin not only localized to vascular amyloid deposits but also accumulated as a halo around Aβ-laden microvessels. Clusterin immunoreactivity was lacking in control cases.

Discussion

In the present study, we aimed to identify proteins that are associated with capCAA pathology. Because some capCAA is observed in up to 51% of AD cases (Thal, et al., 2008), we were specifically interested in proteins differently expressed between AD cases without capCAA and pure capCAA without amyloid plaques. Clinically pure capCAA cases can mimic Creutzfeldt-Jakob disease (CJD) (Eurelings, et al., 2010). Identification of differently expressed proteins might reveal novel biomarkers or targets for therapeutic intervention. To this end, we analyzed protein profiles of pure capCAA, AD and control brain samples using a high resolution tandem mass spectrometry-based proteomics approach. We identified 1547 proteins, of which 29 were significantly differentially regulated between the 3 groups. To our knowledge, this is the first proteomics analysis of capCAA and comparison with AD cases lacking microvascular amyloid deposition. We here showed that the protein expression profiles of AD and capCAA are significantly different, and particularly that such differentially expressed proteins might reveal distinct pathogenic pathways leading to these 2 subtypes of AD. Furthermore, we have demonstrated that our method based on the selection of pure severe cases is a valid approach for the identification of proteins and pathological processes important for the characterization of diverse Aβ-related diseases.

Classical AD markers

Although accumulation of hyperphosphorylated tau in dystrophic neurites is commonly seen surrounding Aβ-laden capillaries (Richard, et al., 2010), the lower Braak stage (tau pathology) and the low frequency of tau tangles in our capCAA cases might explain why tau expression is not significantly altered in capCAA cases.

ApoE is strongly associated with AD and capCAA and ApoE4 is a major genetic risk factor for AD, increasing risk and decreasing age at onset of AD dose-dependently, with the homozygotes having a higher risk (Glenner and Wong, 1984), and an even higher frequency in capCAA cases (Richard, et al., 2010; Thal, et al., 2008). ApoE is an amyloid associated protein found in all types of Aβ deposits. The apoE levels measured with our proteomic analysis reflected Aβ expression and, although up-regulated compared to controls, were not significantly different between capCAA and AD. Our small case selection was not base on ApoE genotype, but considering the influence of ApoE4 allele on AD and capCAA, this can be an interesting

approach for future studies.

Disturbed amyloid clearance

In the present study we observed specifically in capCAA an upregulation of proteins affecting the clearance of Aβ, a process thought to be severely compromised in AD and capCAA. Alterations in the mechanisms regulating Aβ clearance would, in fact, lead to a misbalance situation in which accumulated cerebral Aβ start aggregating and depositing as plaques or vascular CAA (Weller, et al., 2008).

Laminin β2, SAP and clusterin were all strongly upregulated in capCAA cases, even when we compared it to AD.
Laminin, among other proteins, is present at the cerebrovascular basement membrane (Mirra, et al., 1991) and it has been suggested that basement membrane alterations may play a role
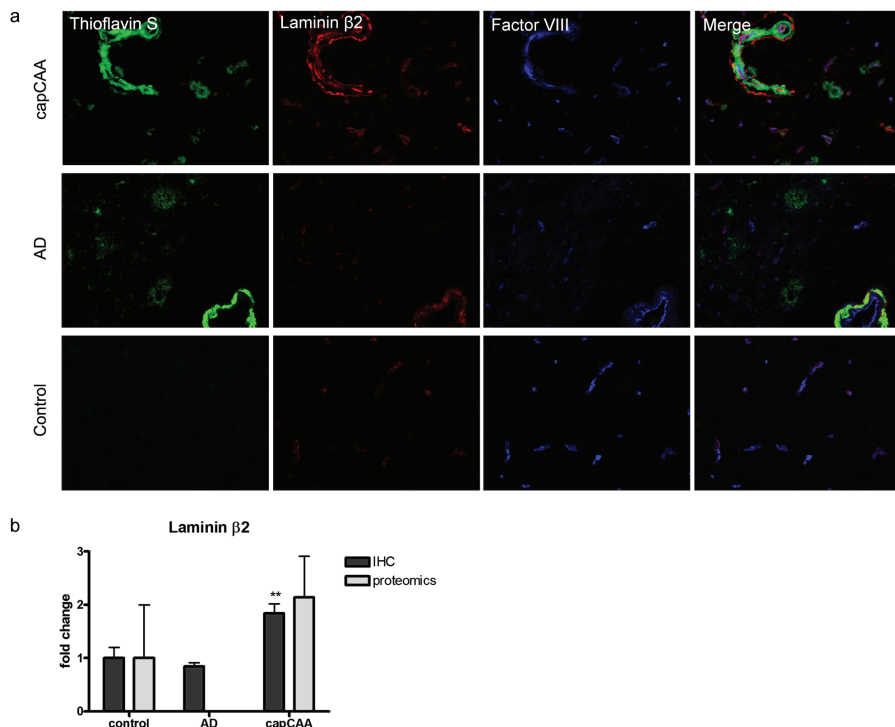
Figure 3. Validation - Lamininβ2 immunostaining (a) and quantification (b) show that lamininβ2 expression is increased in capCAA cases specifically in and around blood vessels affected by Aβ deposition. Lamininβ2 is expressed on the abluminal side of the vasculature where the basement membrane is located and can colocalize with vascular Aβ in capCAA and CAA, but does not colocalize with parenchymal plaques.
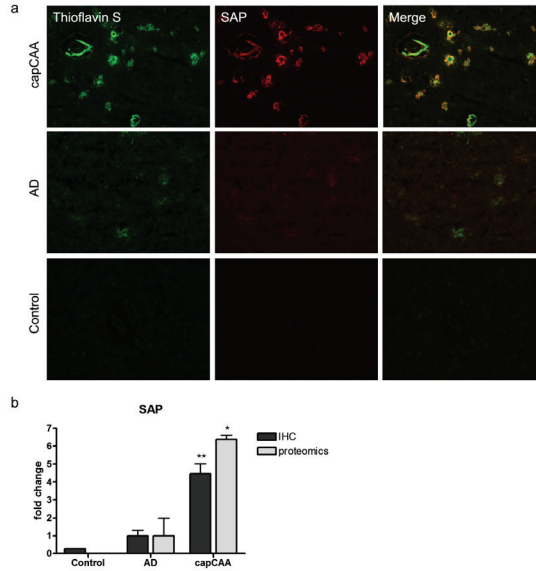
Figure 4. Validation - SAP immunostaining (a) and quantification (b) show control cases. SAP is significantly more abundant in capCAA, where it colocalizes with vascular Aβ, whereas it is only moderately expressed in parenchymal plaques.
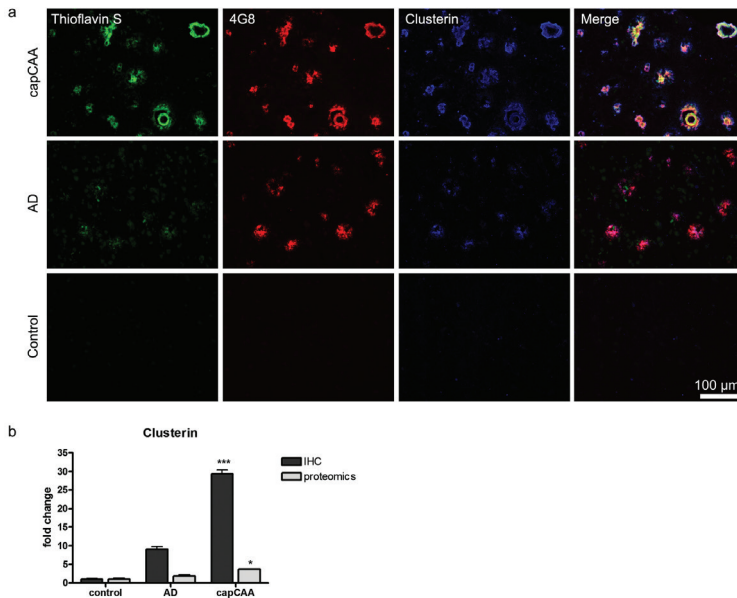
Figure 5. Validation - Clusterin immunostaining (a) and quantification (b) show that clusterin is present in virtually all Aβ deposits both in capCAA and AD. Immunoreactivity was lacking in control cases. Clustering expression is significantly higher in capCAA compared to AD. In capCAA cases, clusterin is found colocalizing with vascular Aβ and accumulating as a halo around Aβ-laden microvessels.

in the aetiology of CAA (Juhasz, et al., 2011). Changes in the basal membrane structure, such as thickening, reduplication and vacuolization, have been reported in AD brains (Carrano, et al., 2011b; Sedgwick, et al., 1991). Basal membrane proteins have been shown to interact directly with Aβ influencing its aggregation. Laminin, for instance, is capable of preventing Aβ aggregation and promoting disaggregation of pre-formed fibrils (Carson, et al., 1998; Verbeek, et al., 1998; Zhu, et al., 2011).

The expression pattern that we observed for the β2 subunit of laminin is of particular interest, since not only laminin β2 is upregulated in capCAA but it appears to be decreased in the vasculature of AD brains. A diagnostic marker with such characteristics might be useful to discriminate capCAA from AD and could potentially find clinical use since change in brain laminin levels could be reflected in the CSF (Matsuda, et al., 2002).

SAP is a plasma glycoprotein that can bind a variety of ligands, including Aβ (Hartz, et al., 2012) and is a universal component of amyloid deposits (Menon and Kidwell, 2009; Verbeek, et al., 1998). SAP levels are elevated in AD brain (Raposo, et al., 2011; Zipfel, et al., 2009) and it has been suggested that SAP plays a role in AD pathogenesis by binding to Aβ, accelerating fibril formation and inhibiting Aβ proteolysis (Eurelings, et al., 2010; C. Mulder, et al., 2010). (Raposo, et al., 2011; Ryu and McLarnon, 2009; Zipfel, et al., 2009). On the other hand SAP, in combination with Aβ and complement proteins, in particular C1q, promotes the release of pro-inflammatory cytokines enhancing inflammation around Aβ deposits (Veerhuis, et al., 2003). SAP was strongly upregulated in capCAA cases respect to AD, as measured by our proteomics analysis. Immunohistochemistry revealed that microvascular Aβ deposits harbour significantly more SAP than parenchymal plaques, which might initiate or, at least, contribute to severe glial activation associated with capCAA (Carrano, et al., 2011a; Richard, et al., 2010). Furthermore, as for laminin, SAP levels can be monitored in CSF. Although no differences in CSF SAP levels have been reported between AD and controls (S.D. Mulder, et al., 2010), it is possible, considering the higher degree of SAP positivity detected in capCAA versus AD, that capCAA cases would show significant changes in CSF SAP levels compared to controls.

Clusterin is a well-known amyloid associated protein present in amyloid plaques and we here show that its expression is significantly increased in capCAA cases. Clusterin is a glycoprotein involved in the clearance of Aβ peptides and fibrils by binding to megalin receptors and en-

hancing endocytosis of fibrils into glial cells. The binding of Aβ to clusterin should promote its clearance and the overexpression of clusterin could be a compensatory mechanism to the high abundance of cerebral Aβ. On the other hand the presence of clusterin can alter the aggregation of the amyloid, this results in the formation of slowly sedimenting, non-fibrillar Aβ complexes that are highly toxic to neurons (Bibl, et al., 2008; Goos, et al., 2009). Increase in clusterin might be beneficial in the initial stage of the disease, however when the disease progresses it might promote accumulation of toxic Aβ complexes.

Laminin, SAP and clusterin were found to co-localize with Aβ deposits, predominantly microvascular over parenchymal. Although, these proteins can be defined as Aβ-associated proteins, the levels measured in our proteomics analysis were not directly reflective of total Aβ levels. It appears that they strongly colocalize with fibrillar amyloid deposits, thioflavin-S positive, which are the main component of capCAA and CAA. This might suggest that laminin, SAP and clusterin are not directly related to the abundance of cerebral Aβ in general, but they might contribute to the formation of highly fibrillar vascular Aβ deposits (capCAA), instead of parenchymal plaques. Taken together the differential expression of proteins such as laminin, SAP and clusterin, might represent a crucial step in the pathogenesis of capCAA, affecting Aβ fibrilization, Aβ transport across the BBB and Aβ-driven neuroinflammation. Whether these Aβ-associated proteins can be used in a clinical setting as diagnostic markers remains to be investigated and warrants further studies.

Other potential candidate markers

In addition to clusterin, SAP and laminin β2, we observed reduced expression of various other proteins, including proprotein convertase subtilisin/kexin type 1 (proSAAS), lactate dehydrogenase A (LDHA), aldehyde dehydrogenase 9A (ALDH9A1), specific cytoskeleton proteins, calcium/calmodulin-dependent protein kinase type II delta chain (CAMK2D) and phosphatidylinositol-5-phosphate 4-kinase type-2 beta (PIP4K2B). ProSAAS is a prohormone expressed in synaptic vesicles (Delacourte, et al., 1987) and it has been shown that proSAAS fragments accumulate in tau-positive Pick bodies and other tauopathies (Oshima, et al., 2008; Williams, et al., 2005). ProSAAS was repeatedly identified as a potential AD marker and found upregulated in AD CSF (Braak, et al., 2006; Eikelenboom, et al., 2008; Yamada, et al., 1997). Interestingly, we showed that proSAAS is upregulated in AD brains, but markedly

downnregulated in capCAA cases. This might be explained by the low frequency of tau tangles in capCAA cases and might imply that the pathological processes leading to tau pathology in AD are likely not involved in capCAA, where the disease is, instead, centred on the compromised Aβ clearance at the BBB.

The dehydrogenases LDHA and ALDH9A1 are both specifically downregulated in capCAA, not in AD. LDHA is a mediator of aerobic glycolysis, an enzyme responsible for the conversion of pyruvate to lactate (Poirier, et al., 1993). Changes in LDHA levels have been associated to amyloid pathology as its expression is decreased in AD transgenic mice and in primary cortical neurons exposed to Aβ (Boche, et al., 2008). Remarkably, we found no alterations in LDHA expression in AD brains, whereas LDHA expression was significantly decreased in capCAA. When LDHA expression decreases, glycolytic metabolism is taken over by the mitochondria leading to increased free radical production, consequent oxidative stress and cell death, and ultimately cognitive impairment (Boche, et al., 2008). ALDH9A1 is a detoxification enzyme participating in the oxidation of aldehydes and in the metabolism of gamma-aminobutyric acid (GABA) and dopamine. Lack of ALDH would lead to increased accumulation of toxic aldehydes (Tanzi, et al., 2004). Decreased function and/or expression of ALDH, as we have specifically observed in capCAA brain, may play an important role in the pathophysiology of capCAA and might promote neurotoxicity and neuronal death.

Conclusions

In this study, we are able to demonstrate the occurrence of significant differences between capCAA and AD proteomes, despite the overlap of these two pathological conditions. Impaired Aβ clearance, altered synaptic plasticity, accumulation of toxic metabolites appeared to be the main pathways affected in capCAA. Proteins specifically up- or downregulated in capCAA (and not in AD) might underscore altered pathogenic pathways explaining why Aβ accumulates around the brain vasculature instead of depositing as plaques in the brain parenchyma, as it is observed in AD. The identification of proteins that are differentially expressed comparing AD and capCAA cases offers the opportunity to diagnose the two AD subtypes and to develop differential approaches for treatment, as different therapeutic targets can be identified for the two conditions. This not only would allow optimize treatments but would help us in the designing of clinical trials and in the selection of specific (more homogenous)

patients groups minimizing the variability of clinical outcome. It is now important to continue in the direction of assessing the validity and feasibility of such proteins for use as biomarkers, for instance analysing their modulation *in vivo* during disease progression in animal models and in human cases, e.g. by extending our proteomics analysis to more cases with diverse profiles (apoE genotypes, mild versus severe cases) and by CSF analysis.

Disclosure Statement

There is no actual or potential conflict of interest for any author concerning this manuscript.

References

Alafuzoff, I., Thal, D.R., Arzberger, T., Bogdanovic, N., Al-Sarraj, S., Bodi, I., Boluda, S., Bugiani, O., Duyckaerts, C., Gelpi, E., Gentleman, S., Giaccone, G., Graeber, M., Hortobagyi, T., Hoftberger, R., Ince, P., Ironside, J.W., Kavantzas, N., King, A., Korkolopoulou, P., Kovacs, G.G., Meyronet, D., Monoranu, C., Nilsson, T., Parchi, P., Patsouris, E., Pikkarainen, M., Revesz, T., Rozemuller, A., Seilhean, D., Schulz-Schaeffer, W., Streichenberger, N., Wharton, S.B., Kretzschmar, H. 2009. Assessment of beta-amyloid deposits in human brain: a study of the BrainNet Europe Consortium. *Acta Neuropathol* 117(3), 309-20.

Albrethsen, J., Knol, J.C., Piersma, S.R., Pham, T.V., de Wit, M., Mongera, S., Carvalho, B., Verheul, H.M., Fijneman, R.J., Meijer, G.A., Jimenez, C.R. 2010. Subnuclear proteomics in colorectal cancer: identification of proteins enriched in the nuclear matrix fraction and regulation in adenoma to carcinoma progression. *Mol Cell Proteomics* 9(5), 988-1005.

Alzheimer, A. 1907. Über eine eigenartige Erkrankung der Hirnrinde. *Allgemeine Zeitschrift für Psychiatrie* 64, 146-8.

Bergeron, C., Ranalli, P.J., Miceli, P.N. 1987. Amyloid angiopathy in Alzheimer's disease. *Can J Neurol Sci* 14(4), 564-9.

Bibl, M., Mollenhauer, B., Esselmann, H., Schneider, M., Lewczuk, P., Welge, V., Gross, M., Falkai, P., Kornhuber, J., Wiltfang, J. 2008. Cerebrospinal fluid neurochemical phenotypes in vascular dementias: original data and mini-review. *Dement Geriatr Cogn Disord* 25(3), 256-65.

Boche, D., Zotova, E., Weller, R.O., Love, S., Neal, J.W., Pickering, R.M., Wilkinson, D., Holmes, C., Nicoll, J.A. 2008. Consequence of Abeta immunization on the vasculature of human Alzheimer's disease brain. *Brain* 131(Pt 12), 3299-310.

Braak, H., Alafuzoff, I., Arzberger, T., Kretzschmar, H., Del Tredici, K. 2006. Staging of Alzheimer disease-associated neurofibrillary pathology using paraffin sections and immunocytochemistry. *Acta Neuropathol* 112(4), 389-404.

Braak, H., Braak, E. 1991. Neuropathological stageing of Alzheimer-related changes. *Acta Neuropathol* 82(4), 239-59.

Carrano, A., Hoozemans, J.J., van der Vies, S.M., Rozemuller, A.J., van Horssen, J., de Vries, H.E. 2011a. Amyloid beta Induces Oxidative Stress-Mediated Blood-Brain Barrier Changes in Capillary Amyloid Angiopathy. *Antioxid Redox Signal*.

Carrano, A., Hoozemans, J.J., van der Vies, S.M., van Horssen, J., de Vries, H.E., Rozemuller, A.J. 2011b. Neuroinflammation and blood-brain barrier changes in capillary amyloid angiopathy. *Neurodegener Dis* 10(1-4), 329-31.

Carrano, A., Hoozemans, J.J., van der Vies, S.M., van Horssen, J., de Vries, H.E., Rozemuller, A.J. 2012. Neuroinflammation and blood-brain barrier changes in capillary amyloid angiopathy. *Neurodegener Dis* 10(1-4), 329-31.

Carson, M.J., Reilly, C.R., Sutcliffe, J.G., Lo, D. 1998. Mature microglia resemble immature antigen-presenting cells. *Glia* 22(1), 72-85.

de Jong, D., Kremer, B.P., Olde Rikkert, M.G., Verbeek, M.M. 2007. Current state and future directions of neurochemical biomarkers for Alzheimer's disease. *Clin Chem Lab Med* 45(11), 1421-34.

Delacourte, A., Defossez, A., Persuy, P., Peers, M.C. 1987. Observation of morphological relationships between angiopathic blood vessels and degenerative neurites in Alzheimer's disease. *Virchows Arch A Pathol Anat Histopathol* 411(3), 199-204.

Dierksen, G.A., Skehan, M.E., Khan, M.A., Jeng, J., Nandigam, R.N., Becker, J.A., Kumar, A., Neal, K.L., Betensky, R.A., Frosch, M.P., Rosand, J., Johnson, K.A., Viswanathan, A., Salat, D.H., Greenberg, S.M. 2010. Spatial relation between microbleeds and amyloid deposits in amyloid angiopathy. *Ann Neurol* 68(4), 545-8.

Eikelenboom, P., Veerhuis, R., Familian, A., Hoozemans, J.J., van Gool, W.A., Rozemuller, A.J. 2008. Neuroinflammation in plaque and vascular beta-amyloid disorders: clinical and therapeutic implications. *Neurodegener Dis* 5(3-4), 190-3.

Ellis, R.J., Olichney, J.M., Thal, L.J., Mirra, S.S., Morris, J.C., Beekly, D., Heyman, A. 1996. Cerebral amyloid angiopathy in the brains of patients with Alzheimer's disease: the CERAD experience, Part XV. *Neurology* 46(6), 1592-6.

Enright, A.J., Van Dongen, S., Ouzounis, C.A. 2002. An efficient algorithm for large-scale detection of protein families. *Nucleic Acids Res* 30(7), 1575-84.

Eurelings, L.S., Richard, E., Carrano, A., Eikelenboom, P., van Gool, W.A., Rozemuller, A.J. 2010. Dyshoric capillary cerebral amyloid angiopathy mimicking Creutzfeldt-Jakob disease. *J Neurol Sci* 295(1-2), 131-4.

Fischer, O. 1907. Miliare Nekrosen mit drusigen Wucherunger der Neurofibrillen, eine regelmässige Veränderung der Hirnrinde bei seniler Demenz. *Monatsschr Psychiatr Neurol* 22, 361-72.

Glenner, G.G., Wong, C.W. 1984. Alzheimer's disease: initial report of the purification and characterization of a novel cerebrovascular amyloid protein. *Biochem Biophys Res Commun* 120(3), 885-90.

Goos, J.D., Kester, M.I., Barkhof, F., Klein, M., Blankenstein, M.A., Scheltens, P., van der Flier,

W.M. 2009. Patients with Alzheimer disease with multiple microbleeds: relation with cerebrospinal fluid biomarkers and cognition. *Stroke* 40(11), 3455-60.

Goos, J.D., Teunissen, C.E., Veerhuis, R., Verwey, N.A., Barkhof, F., Blankenstein, M.A., Scheltens, P., van der Flier, W.M. 2012. Microbleeds relate to altered amyloid-beta metabolism in Alzheimer's disease. *Neurobiol Aging* 33(5), 1011 e1-9.

Hartz, A.M., Bauer, B., Soldner, E.L., Wolf, A., Boy, S., Backhaus, R., Mihaljevic, I., Bogdahn, U., Klunemann, H.H., Schuierer, G., Schlachetzki, F. 2012. Amyloid-beta contributes to blood-brain barrier leakage in transgenic human amyloid precursor protein mice and in humans with cerebral amyloid angiopathy. *Stroke* 43(2), 514-23.

Jellinger, K.A., Attems, J. 2005. Prevalence and pathogenic role of cerebrovascular lesions in Alzheimer disease. *J Neurol Sci* 229-230, 37-41.

Juhasz, G., Foldi, I., Penke, B. 2011. Systems biology of Alzheimer's disease: How diverse molecular changes result in memory impairment in AD. *Neurochem Int*.

Matsuda, K., Tashiro, K., Hayashi, Y., Monji, A., Yoshida, I., Mitsuyama, Y. 2002. Measurement of laminins in the cerebrospinal fluid obtained from patients with Alzheimer's disease and vascular dementia using a modified enzyme-linked immunosorbent assay. *Dement Geriatr Cogn Disord* 14(3), 113-22.

Menon, R.S., Kidwell, C.S. 2009. Neuroimaging demonstration of evolving small vessel ischemic injury in cerebral amyloid angiopathy. *Stroke* 40(12), e675-7.

Mirra, S.S., Heyman, A., McKeel, D., Sumi, S.M., Crain, B.J., Brownlee, L.M., Vogel, F.S., Hughes, J.P., van Belle, G., Berg, L. 1991. The Consortium to Establish a Registry for Alzheimer's Disease (CERAD). Part II. Standardization of the neuropathologic assessment of Alzheimer's disease. *Neurology* 41(4), 479-86.

Morris, J.H., Apeltsin, L., Newman, A.M., Baumbach, J., Wittkop, T., Su, G., Bader, G.D., Ferrin, T.E. 2011. clusterMaker: a multi-algorithm clustering plugin for Cytoscape. *BMC Bioinformatics* 12, 436.

Mulder, C., Verwey, N.A., van der Flier, W.M., Bouwman, F.H., Kok, A., van Elk, E.J., Scheltens, P., Blankenstein, M.A. 2010. Amyloid-beta(1-42), total tau, and phosphorylated tau as cerebrospinal fluid biomarkers for the diagnosis of Alzheimer disease. *Clin Chem* 56(2), 248-53.

Mulder, S.D., Hack, C.E., van der Flier, W.M., Scheltens, P., Blankenstein, M.A., Veerhuis, R. 2010. Evaluation of intrathecal serum amyloid P (SAP) and C-reactive protein (CRP) synthesis in Alzheimer's disease with the use of index values. *J Alzheimers Dis* 22(4), 1073-9.

Oshima, K., Uchikado, H., Dickson, D.W. 2008. Perivascular neuritic dystrophy associated

with cerebral amyloid angiopathy in Alzheimer's disease. *Int J Clin Exp Pathol* 1(5), 403-8.

Pantelakis, S. 1954. [A particular type of senile angiopathy of the central nervous system: congophilic angiopathy, topography and frequency]. *Monatsschr Psychiatr Neurol* 128(4), 219-56.

Pham, T.V., Piersma, S.R., Warmoes, M., Jimenez, C.R. 2010. On the beta-binomial model for analysis of spectral count data in label-free tandem mass spectrometry-based proteomics. *Bioinformatics* 26(3), 363-9.

Piersma, S.R., Fiedler, U., Span, S., Lingnau, A., Pham, T.V., Hoffmann, S., Kubbutat, M.H., Jimenez, C.R. 2010. Workflow comparison for label-free, quantitative secretome proteomics for cancer biomarker discovery: method evaluation, differential analysis, and verification in serum. *J Proteome Res* 9(4), 1913-22.

Poirier, J., Davignon, J., Bouthillier, D., Kogan, S., Bertrand, P., Gauthier, S. 1993. Apolipoprotein E polymorphism and Alzheimer's disease. *Lancet* 342(8873), 697-9.

Raposo, N., Viguier, A., Cuvinciuc, V., Calviere, L., Cognard, C., Bonneville, F., Larrue, V. 2011. Cortical subarachnoid haemorrhage in the elderly: a recurrent event probably related to cerebral amyloid angiopathy. *Eur J Neurol* 18(4), 597-603.

Richard, E., Carrano, A., Hoozemans, J.J., van Horssen, J., van Haastert, E.S., Eurelings, L.S., de Vries, H.E., Thal, D.R., Eikelenboom, P., van Gool, W.A., Rozemuller, A.J. 2010. Characteristics of dyshoric capillary cerebral amyloid angiopathy. *J Neuropathol Exp Neurol* 69(11), 1158-67.

Ryu, J.K., McLarnon, J.G. 2009. A leaky blood-brain barrier, fibrinogen infiltration and microglial reactivity in inflamed Alzheimer's disease brain. *J Cell Mol Med* 13(9A), 2911-25.

Schlote, W. 1965. Die Amyloidnatur der kongophilen, drusige entartung der Hirnarterien (Scholz) im Senium. *Acta Neuropathologica* 4, 449-68.

Sedgwick, J.D., Schwender, S., Imrich, H., Dorries, R., Butcher, G.W., ter Meulen, V. 1991. Isolation and direct characterization of resident microglial cells from the normal and inflamed central nervous system. *Proc Natl Acad Sci U S A* 88(16), 7438-42.

Surbek, B. 1961. L'angiopathie dyshorique (Morel) de l'écorce cérébrale. Etude anatomo-clinique et statistique, aspect génétique. *Acta Neuropathologica* 1, 168-97.

Tanzi, R.E., Moir, R.D., Wagner, S.L. 2004. Clearance of Alzheimer's Abeta peptide: the many roads to perdition. *Neuron* 43(5), 605-8.

Thal, D.R., Griffin, W.S., de Vos, R.A., Ghebremedhin, E. 2008. Cerebral amyloid angiopathy

and its relationship to Alzheimer's disease. *Acta Neuropathol* 115(6), 599-609.

van Dijk, K.D., Berendse, H.W., Drukarch, B., Fratantoni, S.A., Pham, T.V., Piersma, S.R., Huisman, E., Breve, J.J., Groenewegen, H.J., Jimenez, C.R., van de Berg, W.D. 2012. The proteome of the locus ceruleus in Parkinson's disease: relevance to pathogenesis. *Brain Pathol* 22(4), 485-98.

Veerhuis, R., Van Breemen, M.J., Hoozemans, J.M., Morbin, M., Ouladhadj, J., Tagliavini, F., Eikelenboom, P. 2003. Amyloid beta plaque-associated proteins C1q and SAP enhance the Abeta1-42 peptide-induced cytokine secretion by adult human microglia in vitro. *Acta Neuropathol* 105(2), 135-44.

Verbeek, M.M., Otte-Holler, I., Veerhuis, R., Ruiter, D.J., De Waal, R.M. 1998. Distribution of A beta-associated proteins in cerebrovascular amyloid of Alzheimer's disease. *Acta Neuropathol* 96(6), 628-36.

Vidal, R., Calero, M., Piccardo, P., Farlow, M.R., Unverzagt, F.W., Mendez, E., Jimenez-Huete, A., Beavis, R., Gallo, G., Gomez-Tortosa, E., Ghiso, J., Hyman, B.T., Frangione, B., Ghetti, B. 2000. Senile dementia associated with amyloid beta protein angiopathy and tau perivascular pathology but not neuritic plaques in patients homozygous for the APOE-epsilon4 allele. *Acta Neuropathol* 100(1), 1-12.

Weller, R.O., Subash, M., Preston, S.D., Mazanti, I., Carare, R.O. 2008. Perivascular drainage of amyloid-beta peptides from the brain and its failure in cerebral amyloid angiopathy and Alzheimer's disease. *Brain Pathol* 18(2), 253-66.

Williams, S., Chalmers, K., Wilcock, G.K., Love, S. 2005. Relationship of neurofibrillary pathology to cerebral amyloid angiopathy in Alzheimer's disease. *Neuropathol Appl Neurobiol* 31(4), 414-21.

Yamada, M., Itoh, Y., Suematsu, N., Otomo, E., Matsushita, M. 1997. Vascular variant of Alzheimer's disease characterized by severe plaque-like beta protein angiopathy. *Dement Geriatr Cogn Disord* 8(3), 163-8.

Zhu, Y., Hou, H., Rezai-Zadeh, K., Giunta, B., Ruscin, A., Gemma, C., Jin, J., Dragicevic, N., Bradshaw, P., Rasool, S., Glabe, C.G., Ehrhart, J., Bickford, P., Mori, T., Obregon, D., Town, T., Tan, J. 2011. CD45 deficiency drives amyloid-beta peptide oligomers and neuronal loss in Alzheimer's disease mice. *J Neurosci* 31(4), 1355-65.

Zipfel, G.J., Han, H., Ford, A.L., Lee, J.M. 2009. Cerebral amyloid angiopathy: progressive disruption of the neurovascular unit. *Stroke* 40(3 Suppl), S16-9.

Supplementary Data
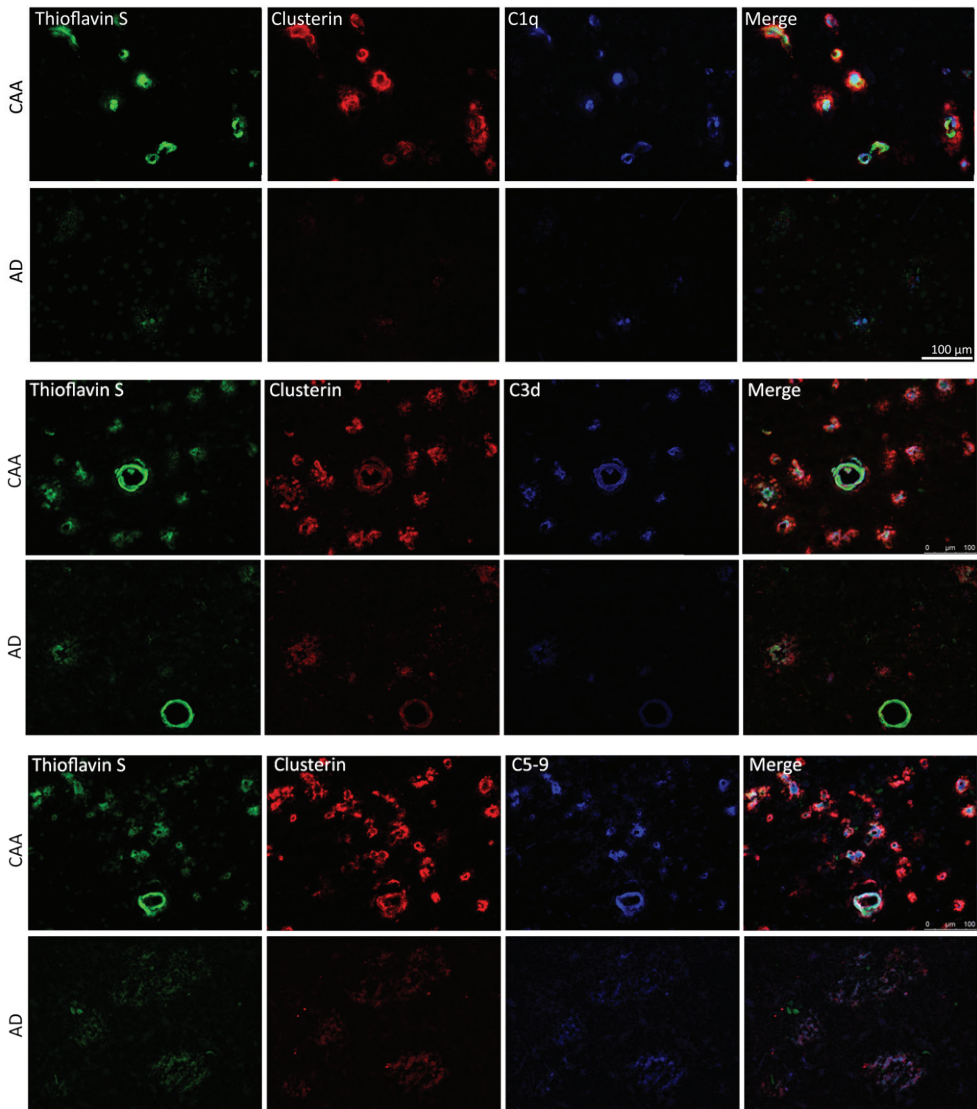
Supplementary Figure 1. Expression of complement proteins C1q, C3d, C5-9 in capCAA and AD. Clusterin and SAP are both amyloid associated proteins and both modulate the complement system. SAP can bind to C1q and initiate activation of the classical pathway of the complement. Clusterin is a complement inhibitor and can suppress complement activation suppressing the formation of complex C5-9.

Therefore we analyze the expression of several complement proteins located at different stages of the cascade in post-mortem occipital cortices from capCAA and AD cases. Immunohistochemistry analysis reveals that C1q, C3d and C5-9 colocalize with the most fibrillar Aβ deposits, showing significantly higher levels in capCAA compared to AD.
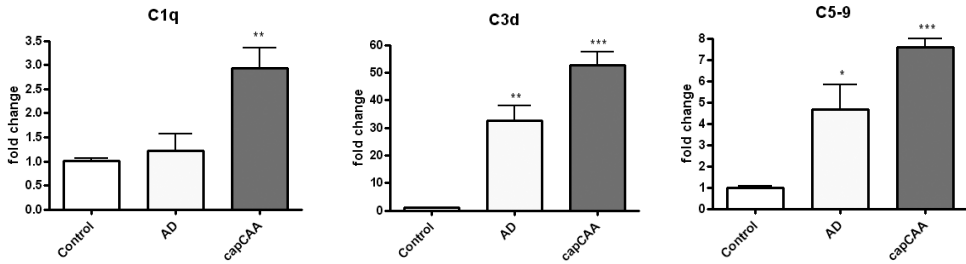
Supplementary Figure 2. Quantification of complement proteins C1q, C3d and C5-9 expression in cap-CAA, AD and controls. Fluorescent analysis was performed with confocal laser-scanning microscope and quantification of fluorescent intensity was performed by ImageJ software. Quantification confirmed that these complement proteins are markedly upregulated in capCAA compared to AD and controls.

Supplementary Table 1. (Page 94-130). List of identified proteins (p< 0.05) in the occipital cortex of capCAA patients compared with Alzheimer's disease cases and controls ranked on pvalue. Abbreviations: CAA = capillary cerebral amyloid angiopathy; AD = Alzheimer's disease; C = control; nc= normalized spectral counts; fc = fold change

Gene Symbol	AD1 nc	AD2 nc	capCAA1 nc	capCAA2 nc	C1 nc	C2 nc	fc.cap-CAA/C	fc.capCAA/AD	fc. AD/C	fc. max	pvalues	Protein name
CLU	9,72	15,43	25,96	24,64	8,77	4,89	3,70	2,01	1,84	3,70	0,00	Clusterin
AKAP12	13,61	6,35	9,98	7,50	1,10	0,98	8,43	-1,14	9,62	9,62	0,00	A kinase (PRKA) anchor protein 12 isoform 2
CORO1C	0,00	0,00	3,00	1,07	4,38	2,94	-1,80	∞	-∞	∞	0,01	cDNA FLJ50992, highly similar to Coronin-1C
ABR	0,00	0,00	2,00	3,21	5,48	1,96	-1,43	∞	-∞	∞	0,01	Isoform Long of Active breakpoint cluster region-related protein
TIMM13	3,89	2,72	0,00	0,00	1,10	0,98	-∞	-∞	3,19	∞	0,01	Mitochondrial import inner membrane translocase subunit Tim13
S100B	3,89	2,72	1,00	2,14	0,00	0,00	∞	-2,10	∞	∞	0,01	Protein S100-B
APCS	0,97	0,00	3,00	3,21	0,00	0,00	∞	6,39	∞	∞	0,01	Serum amyloid P-component
NDUFAF3	0,00	0,00	0,00	1,07	2,19	3,92	-5,70	∞	-∞	∞	0,02	Uncharacterized protein C3orf60
ME3	3,89	1,81	6,99	3,21	10,96	9,79	-2,03	1,79	-3,64	3,64	0,02	NADP-dependent malic enzyme, mitochondrial
NPTN	1,94	3,63	1,00	0,00	0,00	0,00	∞	-5,58	∞	∞	0,02	Isoform 3 of Neuroplastin
SUB1	3,89	4,54	4,99	3,21	0,00	0,98	8,38	-1,03	8,61	8,61	0,02	Activated RNA polymerase II transcriptional coactivator p15
ENDOD1	0,00	0,00	1,00	0,00	3,29	1,96	-5,25	∞	-∞	∞	0,02	Endonuclease domain-containing 1 protein
CPNE5	0,97	0,00	1,00	1,07	4,38	3,92	-4,01	2,13	-8,54	8,54	0,02	Copine-5
HUWE1	0,00	0,00	3,00	1,07	0,00	0,00	∞	∞	1,00	∞	0,02	482 kDa protein
PCSK1N	9,72	9,98	3,99	3,21	10,96	8,81	-2,74	-2,73	-1,00	2,74	0,02	ProSAAS
AGRN	3,89	5,44	3,00	1,07	0,00	0,98	4,15	-2,29	9,53	9,53	0,03	Agrin
ACTN2	0,97	1,81	2,00	0,00	8,77	3,92	-6,35	-1,40	-4,55	6,35	0,03	Alpha-actinin-2
ALDH9A1	10,69	15,43	7,99	6,43	18,63	14,68	-2,31	-1,81	-1,28	2,31	0,03	aldehyde dehydrogenase 9A1
PIP4K2B	1,94	3,63	0,00	0,00	0,00	0,00	-∞	-∞	∞	∞	0,03	Isoform 1 of Phosphatidylinositol-5-phosphate 4-kinase type-2 beta
CUL3	1,94	1,81	4,99	3,21	7,67	6,85	-1,77	2,18	-3,86	3,86	0,03	Isoform 1 of Cullin-3
CAMK2D	1,94	1,81	0,00	0,00	17,54	1,96	-∞	-∞	-5,19	∞	0,03	Isoform Delta 6 of Calcium/calmodulin-dependent protein kinase type II delta chain
LAMB2	0,00	0,00	2,00	4,28	0,00	2,94	2,14	∞	-∞	∞	0,03	Laminin subunit beta-2
PLD3	0,00	0,00	0,00	0,00	1,10	1,96	-∞	-1,00	-∞	∞	0,04	Phospholipase D3
ACTR3	6,80	8,17	3,99	2,14	8,77	9,79	-3,02	-2,44	-1,24	3,02	0,04	Actin-related protein 3
KIAA1244	0,00	0,00	0,00	0,00	2,19	0,98	-∞	-1,00	-∞	∞	0,04	Brefeldin A-inhibited guanine nucleotide-exchange protein 3
APP	0,97	7,26	7,99	12,85	2,19	1,96	5,02	2,53	1,98	5,02	0,04	Isoform APP770 of Amyloid beta A4 protein (Fragment)
PPA1	5,83	2,72	0,00	1,07	2,19	1,96	-3,87	-7,99	2,06	7,99	0,04	Inorganic pyrophosphatase
MAP1LC3A	2,92	2,72	1,00	2,14	7,67	4,89	-4,00	-1,80	-2,23	4,00	0,05	Isoform 1 of Microtubule-associated proteins 1A/1B light chain 3A
LDHA	44,72	36,30	28,96	24,64	38,36	38,18	-1,43	-1,51	1,06	1,51	0,05	L-lactate dehydrogenase
GNG3	6,80	3,63	3,00	2,14	1,10	0,98	2,48	-2,03	5,03	5,03	0,05	Guanine nucleotide-binding protein G(I)/G(S)/G(O) subunit gamma-3
STAT1	0,00	0,00	2,00	2,14	1,10	0,98	1,99	∞	-∞	∞	0,05	Isoform Alpha of Signal transducer and activator of transcription 1-alpha/beta
RPL6	0,00	0,00	1,00	0,00	1,10	2,94	-4,04	∞	-∞	∞	0,05	60S ribosomal protein L6
RBP1	6,80	5,44	1,00	2,14	4,38	1,96	-2,02	-3,90	1,93	3,90	0,05	retinol binding protein 1, cellular isoform a
RARS	0,00	0,00	0,00	1,07	1,10	2,94	-3,76	∞	-∞	∞	0,05	Isoform Complexed of Arginyl-tRNA synthetase, cytoplasmic
GNG7	4,86	4,54	1,00	1,07	0,00	2,94	-1,42	-4,54	3,20	4,54	0,06	Guanine nucleotide-binding protein G(I)/G(S)/G(O) subunit gamma-7
SNIP	5,83	1,81	4,99	5,36	1,10	0,98	4,99	1,35	3,69	4,99	0,06	Isoform 2 of p130Cas-associated protein
PTPN11	0,00	0,91	0,00	0,00	3,29	0,98	-∞	-∞	-4,70	∞	0,06	Isoform 2 of Tyrosine-protein phosphatase non-receptor type 11
C4B	7,78	11,80	9,98	19,28	7,67	1,96	3,04	1,50	2,03	3,04	0,06	Complement component 4B
HNRNPA2B1	28,19	18,15	18,97	21,42	8,77	15,66	1,65	-1,15	1,90	1,90	0,06	Isoform B1 of Heterogeneous nuclear ribonucleoproteins A2/B1
SLC1A2	80,68	99,81	87,87	80,33	31,78	73,42	1,60	-1,07	1,72	1,72	0,06	Isoform 1 of Excitatory amino acid transporter 2
PGM1	21,39	24,50	26,96	26,78	15,34	16,64	1,68	1,17	1,43	1,68	0,06	Isoform 1 of Phosphoglucomutase-1
PSMC5	0,97	2,72	1,00	2,14	0,00	0,00	∞	-1,18	∞	∞	0,06	26S protease regulatory subunit 8
HSPB1	13,61	23,59	10,98	22,49	7,67	7,83	2,16	-1,11	2,40	2,40	0,07	Heat shock protein beta-1

Gene Symbol	AD1 nc	AD2 nc	capCAA1 nc	capCAA2 nc	C1 nc	C2 nc	fc.cap-CAA/C	fc.capCAA/AD	fc. AD/C	fc. max	pvalues	Protein name
PGM2L1	3,89	0,91	4,99	2,14	17,54	5,87	-3,28	1,49	-4,88	4,88	0,07	Glucose 1,6-bisphosphate synthase
STOM	1,94	1,81	1,00	1,07	6,58	2,94	-4,60	-1,82	-2,53	4,60	0,07	Erythrocyte band 7 integral membrane protein
P4KA	0,97	0,00	3,00	3,21	1,10	4,89	1,04	6,39	-6,16	6,39	0,08	Isoform 1 of Phosphatidylinositol 4-kinase alpha
C19orf10	1,94	1,81	1,00	1,07	0,00	0,00	∞	-1,82	∞	∞	0,08	UPF0556 protein C19orf10
RPLP1	1,94	1,81	1,00	1,07	0,00	0,00	∞	-1,82	∞	∞	0,08	60S acidic ribosomal protein P1
CACNA2D1	10,69	15,43	6,99	6,43	15,34	10,77	-1,95	-1,95	1,00	1,95	0,08	Dihydropyridine receptor alpha 2 subunit
AHNAK	11,66	26,31	15,98	8,57	2,19	8,81	2,23	-1,55	3,45	3,45	0,08	Neuroblast differentiation-associated protein AHNAK
GPI	54,44	68,05	55,91	65,34	50,41	42,09	1,31	-1,01	1,32	1,32	0,08	Glucose-6-phosphate isomerase
HEPACAM	5,83	14,52	4,99	3,21	2,19	4,89	1,16	-2,48	2,87	2,87	0,08	Isoform 1 of Hepatocyte cell adhesion molecule
DUT	0,97	2,72	0,00	0,00	0,00	1,96	-∞	-∞	1,89	∞	0,08	Isoform 1 of Deoxyuridine 5'-triphosphate nucleotidohydrolase, mitochondrial
HADHA	16,53	19,96	22,96	25,71	30,69	27,41	-1,19	1,33	-1,59	1,59	0,08	Trifunctional enzyme subunit alpha, mitochondrial
HAPLN1	8,75	4,54	5,99	5,36	0,00	3,92	2,90	-1,17	3,39	3,39	0,08	Hyaluronan and proteoglycan link protein 1
APOE	10,69	48,09	46,93	48,20	17,54	12,73	3,14	1,62	1,94	3,14	0,08	Apolipoprotein E
SERPINA1	4,86	5,44	5,99	9,64	24,11	8,81	-2,11	1,52	-3,19	3,19	0,08	Isoform 1 of Alpha-1-antitrypsin
GLS	14,58	16,33	21,97	28,92	19,73	22,51	1,20	1,65	-1,37	1,65	0,08	Isoform KGA of Glutaminase kidney isoform, mitochondrial
PSMD3	2,92	0,91	0,00	0,00	0,00	1,96	-∞	-∞	1,95	∞	0,09	26S proteasome non-ATPase regulatory subunit 3
CKB	174,97	207,79	172,74	185,30	138,09	170,32	1,16	-1,07	1,24	1,24	0,09	Creatine kinase B-type
NDRG4	4,86	6,35	4,99	7,50	1,10	2,94	3,10	1,11	2,78	3,10	0,09	Isoform 2 of Protein NDRG4
CNTNAP2	1,94	3,63	4,99	4,28	0,00	1,96	4,74	1,66	2,85	4,74	0,09	Isoform 1 of Contactin-associated protein-like 2
ACLY	3,89	2,72	7,99	4,28	12,06	5,87	-1,46	1,86	-2,71	2,71	0,09	ATP-citrate synthase
ALDH5A1	16,53	16,33	21,97	20,35	26,30	26,43	-1,25	1,29	-1,60	1,60	0,09	Succinate-semialdehyde dehydrogenase, mitochondrial
H2AFY	0,97	0,91	3,00	3,21	0,00	0,98	6,34	3,30	1,92	6,34	0,09	H2A histone family, member Y isoform 2
NDUFS2	7,78	6,35	14,98	12,85	7,67	16,64	1,14	1,97	-1,72	1,97	0,10	NADH dehydrogenase [ubiquinone] iron-sulfur protein 2, mitochondrial
SPTA1	1,94	0,91	0,00	0,00	2,19	0,98	-∞	-∞	-1,11	∞	0,10	spectrin, alpha, erythrocytic 1
ARMC10	1,94	0,91	0,00	0,00	2,19	0,98	-∞	-∞	-1,11	∞	0,10	Isoform 1 of Armadillo repeat-containing protein 10
GIT1	0,97	1,81	2,00	1,07	0,00	0,00	∞	1,10	∞	∞	0,10	Isoform 1 of ARF GTPase-activating protein GIT1
KGHG1	25,27	10,89	33,95	27,85	28,49	24,47	1,17	1,71	-1,46	1,71	0,10	Putative uncharacterized protein DKFZp686P15220
GNB1	93,32	112,52	81,87	103,90	84,39	75,37	1,16	-1,11	1,29	1,29	0,10	Guanine nucleotide-binding protein G(I)/G(S)/G(T) subunit beta-1
SLC4A1	1,94	0,91	1,00	4,28	3,29	7,83	-2,10	1,85	-3,90	3,90	0,10	Solute carrier family 4 anion exchanger member 1 variant
IDH3G	2,92	0,91	3,99	4,28	3,29	10,77	-1,70	2,17	-3,68	3,68	0,10	Isocitrate dehydrogenase [NAD] subunit gamma, mitochondrial
ALDH1L1	13,61	21,78	13,98	13,92	9,86	9,79	1,42	-1,27	1,80	1,80	0,10	10-formyltetrahydrofolate dehydrogenase
MINK1	0,00	0,00	2,00	0,00	2,19	0,98	-1,59	-∞	-∞	∞	0,10	mishapen/NIK-related kinase isoform 4
TRAP1	5,83	1,81	4,99	6,43	12,06	6,85	-1,66	1,49	-2,47	2,47	0,10	Heat shock protein 75 kDa, mitochondrial
NCKIPSD	0,97	0,00	3,99	3,21	0,00	3,92	1,84	7,41	-4,03	7,41	0,10	Isoform 1 of NCK-interacting protein with SH3 domain
STAM	0,00	0,00	1,00	0,00	2,19	0,98	-3,18	∞	∞	∞	0,10	Isoform 1 of Signal transducing adapter molecule 1
ERO1L	0,00	0,00	1,00	2,14	1,10	0,00	2,87	∞	-∞	∞	0,10	ERO1-like protein alpha
ATP5F1	12,64	10,89	20,97	16,07	16,44	21,54	-1,03	1,57	-1,61	1,61	0,10	ATP synthase subunit b, mitochondrial
SFRS3	4,86	3,63	3,99	3,21	0,00	1,96	3,68	-1,18	4,34	4,34	0,10	Splicing factor, arginine/serine-rich 3
LAMP1	0,97	0,91	2,00	6,43	3,29	2,94	1,35	4,48	-3,31	4,48	0,10	Lysosome-associated membrane glycoprotein 1
ROBLD3	2,92	3,63	2,00	2,14	0,00	0,98	4,23	-1,58	6,69	6,69	0,11	Isoform 1 of Mitogen-activated protein-binding protein-interacting protein
CUL5	0,97	0,91	1,00	4,28	4,38	3,92	-1,57	2,81	-4,42	4,42	0,11	Cullin-5
EPS15L1	0,97	1,81	0,00	0,00	0,00	2,94	-∞	-∞	-1,05	∞	0,11	cDNA FLJ60624, highly similar to Epidermal growth factor receptor substrate 15-like 1
OPA1	12,64	15,43	13,98	19,28	23,01	22,51	-1,37	1,19	-1,62	1,62	0,11	Isoform 1 of Dynamin-like 120 kDa protein, mitochondrial

Gene Symbol	AD1 nc	AD2 nc	capCAA1 nc	capCAA2 nc	C1 nc	C2 nc	fc.cap-CAA/C	fc.capCAA/AD	fc. AD/C	fc. max	pvalues	Protein name
DDT	6,80	9,98	3,99	3,21	2,19	6,85	-1,25	-2,33	1,86	2,33	0,11	D-dopachrome decarboxylase
GLOD4	9,72	11,80	4,99	5,36	12,06	6,85	-1,83	-2,08	1,14	2,08	0,12	Uncharacterized protein C17orf25
ANXA6	63,18	50,81	62,90	86,76	70,14	72,44	1,05	1,31	-1,25	1,31	0,12	Annexin A6
KCNAB2	6,80	3,63	2,00	3,21	0,00	2,94	1,77	-2,00	3,55	3,55	0,12	Isoform 1 of Voltage-gated potassium channel subunit beta-2
PAFAH1B3	3,89	3,63	0,00	1,07	4,38	0,00	-4,09	-7,02	1,71	7,02	0,12	Platelet-activating factor acetylhydrolase IB subunit gamma
NDUFC2	0,97	0,91	0,00	0,00	2,19	0,98	∞	-∞	-1,69	∞	0,12	NADH dehydrogenase [ubiquinone] 1 subunit C2
MAPRE1	0,97	0,91	2,00	1,07	0,00	0,00	∞	1,63	∞	∞	0,12	Microtubule-associated protein RP/EB family member 1
FAT2	1,94	0,00	2,00	1,07	0,00	0,00	∞	1,58	∞	∞	0,12	Protocadherin Fat2
HLA-A	0,00	1,81	1,00	2,14	0,00	0,00	∞	1,73	∞	∞	0,12	HLA class I histocompatibility antigen, A-1 alpha chain
GSTZ1	1,94	0,00	1,00	2,14	0,00	0,00	∞	1,62	∞	∞	0,12	glutathione transferase zeta 1 isoform 1
UBB;UBC;RPS27A	30,13	29,94	16,97	26,78	24,11	17,62	1,05	-1,37	1,44	1,44	0,12	ubiquitin and ribosomal protein S27a precursor
GCSH;LOC730107	0,00	0,00	3,00	0,00	1,10	0,98	1,44	∞	-∞	1,44	0,12	Glycine cleavage system H protein, mitochondrial
PFKP	39,85	28,13	37,94	39,63	58,08	40,13	-1,27	1,14	-1,44	1,44	0,12	6-phosphofructokinase type C
WDR1	4,86	1,81	5,99	2,14	7,67	7,83	-1,91	1,22	-2,32	2,32	0,12	Isoform 2 of WD repeat-containing protein 1
CALM2;CALM3;CALM1	31,11	39,02	26,96	26,78	28,49	21,54	1,07	-1,30	1,40	1,40	0,13	Calmodulin
HPCAL4	4,86	5,44	2,00	1,07	4,38	2,94	-2,39	-3,36	1,41	3,36	0,13	Hippocalcin-like protein 4
DHX9	7,78	2,72	2,00	1,07	1,10	2,94	-1,31	-3,42	2,60	3,42	0,13	ATP-dependent RNA helicase A
GPD2	6,80	9,98	11,98	16,07	4,38	10,77	1,85	1,67	1,11	1,85	0,13	Isoform 1 of Glycerol-3-phosphate dehydrogenase, mitochondrial
CNN3	0,97	1,81	0,00	0,00	1,10	0,98	-∞	∞	1,34	∞	0,13	Calponin-3
PSMD7	1,94	0,91	0,00	0,00	1,10	0,98	-∞	-∞	1,37	∞	0,13	26S proteasome non-ATPase regulatory subunit 7
WASF1	0,97	1,81	2,00	0,00	0,00	0,00	∞	-1,40	∞	∞	0,13	Wiskott-Aldrich syndrome protein family member 1
HSPA9	37,91	39,93	43,93	55,70	44,93	56,77	-1,02	1,28	-1,31	1,31	0,14	Stress-70 protein, mitochondrial
IQSEC1	1,94	0,91	0,00	0,00	0,00	0,98	-∞	∞	2,91	∞	0,14	Isoform 1 of IQ motif and SEC7 domain-containing protein 1
C19orf70	0,97	1,81	3,99	0,00	1,10	0,00	∞	-∞	2,54	∞	0,14	Protein QIL1
SFXN5	0,97	1,81	0,00	0,00	1,10	0,00	-∞	-∞	2,54	∞	0,14	Sideroflexin-5
ITPA	0,97	1,81	1,00	0,00	1,10	0,00	-∞	-∞	2,54	∞	0,14	Inosine triphosphate pyrophosphatase
BOLA2;BOLA2B	1,94	0,91	1,00	0,00	0,00	0,00	∞	-2,86	∞	∞	0,14	BolA-like protein 2
CNTFR	0,97	1,81	1,00	0,00	0,00	0,00	∞	-2,79	∞	∞	0,14	Ciliary neurotrophic factor receptor alpha
SSB	0,97	0,91	3,99	0,00	0,00	0,00	∞	2,13	∞	∞	0,14	Lupus La protein
IMMT	16,53	20,87	21,97	28,92	26,30	29,37	-1,09	1,36	-1,49	1,49	0,14	Isoform 1 of Mitochondrial inner membrane protein
NEBL	5,83	7,26	7,99	2,14	0,00	3,92	2,59	-1,29	3,34	3,34	0,14	nebulette non-muscle isoform
TPM1	9,72	9,98	11,98	21,42	12,06	9,79	1,53	1,70	-1,11	1,70	0,15	tropomyosin 1 alpha chain isoform 2
SLC1A3	53,46	58,07	49,92	43,91	30,69	50,90	1,15	-1,19	1,37	1,37	0,15	Excitatory amino acid transporter 1
ERC2	3,89	3,63	1,00	1,07	1,10	1,96	-1,48	-3,63	2,46	3,63	0,15	Isoform 1 of ERC protein 2
MAP4	3,89	3,63	3,00	0,00	1,10	0,98	1,44	-2,51	3,62	3,62	0,15	Isoform 1 of Microtubule-associated protein 4
ATP5J	6,80	5,44	3,99	0,00	1,10	4,89	-1,50	-3,07	2,04	3,07	0,15	ATP synthase-coupling factor 6, mitochondrial
GSTM5	0,00	2,72	0,00	0,00	1,10	0,98	-∞	-∞	1,31	∞	0,15	Glutathione-S-transferase Mu 5
CTNNB1	4,86	10,89	11,98	9,64	17,54	11,75	-1,35	1,37	-1,86	1,86	0,15	Isoform 1 of Catenin beta-1
RPN1	0,97	0,91	3,00	0,00	3,29	3,92	-2,40	1,59	-3,83	3,83	0,15	Dolichyl-diphosphooligosaccharide–protein glycosyltransferase subunit 1 precursor
GAPDH	195,39	226,85	186,71	219,57	190,69	169,34	1,13	-1,04	1,17	1,17	0,15	Glyceraldehyde-3-phosphate dehydrogenase
MAPT	36,94	77,13	26,96	58,91	24,11	24,47	1,77	-1,33	2,35	2,35	0,16	Isoform Tau-E of Microtubule-associated protein tau
SLC25A1	0,97	0,00	1,00	0,00	4,38	0,98	-5,37	1,03	-5,52	5,52	0,16	Tricarboxylate transport protein, mitochondrial
XRCC5	2,92	0,00	0,00	0,00	1,10	0,98	-∞	-∞	1,41	∞	0,16	ATP-dependent DNA helicase 2 subunit 2

Gene Symbol	AD1 nc	AD2 nc	capCAA1 nc	capCAA2 nc	C1 nc	C2 nc	fc.capCAA/C	fc.capCAA/AD	fc.AD/C	fc.max	pvalues	Protein name
MTHFD1	4,86	0,91	7,99	5,36	4,38	0,00	3,04	2,31	1,32	3,04	0,16	C-1-tetrahydrofolate synthase, cytoplasmic
GPM6A	30,13	39,02	32,95	20,35	26,30	22,51	1,09	-1,30	1,42	1,42	0,16	Neuronal membrane glycoprotein M6-a
FHL1	6,80	3,63	6,99	5,36	14,25	6,85	-1,71	1,18	-2,02	2,02	0,16	cDNA FLJ55259, highly similar to Four and a half LIM domains protein 1
ATP1B3	3,89	1,81	1,00	3,21	0,00	0,98	4,30	-1,35	5,83	5,83	0,17	Sodium/potassium-transporting ATPase subunit beta-3
SPTB	0,97	0,00	3,00	1,07	2,19	2,94	-1,26	4,18	-5,28	5,28	0,17	Isoform 2 of Spectrin beta chain, erythrocyte
HSD17B10	7,78	2,72	5,99	10,71	9,86	10,77	-1,24	1,59	-1,97	1,97	0,17	Isoform 1 of 3-hydroxyacyl-CoA dehydrogenase type-2
PPP1CB	11,66	5,44	13,98	11,78	15,34	13,70	-1,13	1,51	-1,70	1,70	0,17	Serine/threonine-protein phosphatase PP1-beta catalytic subunit
DHRS7	0,97	0,00	3,99	0,00	2,19	3,92	-1,53	4,11	-6,28	6,28	0,17	Isoform 1 of Dehydrogenase/reductase SDR family member 7
HBG2;HBG1	2,92	5,44	0,00	2,14	3,29	0,00	-1,53	-3,90	2,54	3,90	0,17	Hemoglobin subunit gamma-2
PPP2R5D	2,92	2,72	2,00	1,07	0,00	0,98	3,13	-1,84	5,76	5,76	0,17	Isoform Delta-1 of Serine/threonine-protein phosphatase 2A 56 kDa regulatory subunit delta isoform
TGM2	0,00	0,00	1,00	1,07	0,00	1,96	1,06	∞	-∞	∞	0,17	Isoform 1 of Protein-glutamine gamma-glutamyltransferase 2
ATP8A2	0,00	0,00	1,00	1,07	2,19	0,00	-1,06	∞	-∞	∞	0,17	ATPase, aminophospholipid transporter-like, Class I, type 8A, member 2
WFS1	0,00	0,00	2,00	0,00	1,10	0,98	-1,04	∞	-∞	∞	0,17	Wolframin
RUFY3	7,78	8,17	9,98	9,64	16,44	11,75	-1,44	1,23	-1,77	1,77	0,17	Isoform 1 of Protein RUFY3
DBN1	4,86	2,72	3,99	2,14	1,10	0,98	2,96	-1,24	3,65	3,65	0,17	Putative uncharacterized protein DBN1
PGK1	83,60	89,83	80,88	101,75	70,14	78,31	1,23	1,05	1,17	1,23	0,18	Phosphoglycerate kinase 1
GAD2	1,94	0,00	2,00	2,14	4,38	2,94	-1,77	2,13	-3,77	3,77	0,18	Glutamate decarboxylase 2
DLAT	14,58	13,61	19,97	20,35	18,63	23,49	-1,04	1,43	-1,49	1,49	0,18	Dihydrolipoyllysine-residue acetyltransferase component of pyruvate dehydrogenase complex, mitochondrial
TF	11,66	11,80	10,98	22,49	21,92	16,64	-1,15	1,43	-1,64	1,64	0,18	Serotransferrin
SLC6A11	2,92	1,81	5,99	4,28	2,19	1,96	2,48	2,17	1,14	2,48	0,18	Sodium- and chloride-dependent GABA transporter 3
S100A13	1,94	3,63	3,00	0,00	0,00	0,98	2,96	-1,86	5,69	5,69	0,18	Protein S100-A13
NAP1L4	4,86	0,91	0,00	1,07	1,10	0,00	-1,02	-5,38	5,26	5,38	0,19	cDNA FLJ59403, highly similar to Nucleosome assembly protein 1-like 4
PEA15	4,86	14,52	4,99	2,14	10,96	5,87	-2,36	-2,72	1,15	2,72	0,19	Astrocytic phosphoprotein PEA-15
IVD	0,97	0,91	1,00	0,00	2,19	2,94	-5,14	-1,88	-2,73	5,14	0,19	Isovaleryl-CoA dehydrogenase, mitochondrial
KIAA0174	1,94	0,00	2,00	3,21	1,10	0,00	4,75	2,68	1,77	4,75	0,19	Isoform 1 of IST1 homolog
COL4A2	1,94	1,81	3,99	4,28	2,19	7,83	-1,21	2,20	-2,67	2,67	0,19	Collagen alpha-2(IV) chain
ORM1	0,97	2,72	2,00	5,36	6,58	3,92	-1,43	1,99	-2,84	2,84	0,19	Alpha-1-acid glycoprotein 1
NDUFA11	0,97	0,91	3,99	1,07	0,00	0,98	5,17	2,69	1,92	5,17	0,19	Isoform 1 of NADH dehydrogenase [ubiquinone] 1 alpha subcomplex subunit 11
COL4A1	0,00	0,00	0,00	0,00	0,00	1,96	-∞	-1,00	-∞	∞	0,19	Putative uncharacterized protein COL4A1
FGF12	0,00	0,00	0,00	0,00	0,00	1,96	-∞	-1,00	-∞	∞	0,19	Isoform 1 of Fibroblast growth factor 12
LRRC8A	0,00	0,00	1,00	0,00	0,00	1,96	-∞	-1,00	-∞	∞	0,19	Leucine-rich repeat-containing protein 8A
F13A1	0,00	0,00	0,00	0,00	0,00	1,96	-∞	-1,00	-∞	∞	0,19	Coagulation factor XIII A chain
PDHA1	14,58	10,89	19,97	19,28	12,06	23,49	1,10	1,54	-1,40	1,54	0,20	Mitochondrial PDHA1
HSD17B8	0,00	0,00	2,00	0,00	0,00	0,00	∞	∞	1,00	∞	0,20	Estradiol 17-beta-dehydrogenase 8
STXBP1	2,92	1,81	6,99	4,28	0,00	4,89	2,30	2,38	-1,03	2,38	0,20	Isoform 2 of Syntaxin-binding protein 1
NIPSNAP3A	4,86	1,81	3,99	5,36	7,67	6,85	-1,55	1,40	-2,18	2,18	0,20	Protein NipSnap homolog 3A
IDH2	35,97	41,74	47,93	42,84	47,13	53,84	-1,11	1,17	-1,30	1,30	0,21	Isocitrate dehydrogenase [NADP], mitochondrial
DPP6	11,66	18,15	22,96	9,64	28,49	20,56	-1,50	1,09	-1,65	1,65	0,21	Isoform DPPX-S of Dipeptidyl aminopeptidase-like protein 6
ARHGEF2	1,94	0,00	0,00	0,00	1,10	0,98	-∞	∞	-1,07	∞	0,21	Isoform 1 of Rho guanine nucleotide exchange factor 2
TM9SF2	0,97	0,91	2,00	0,00	0,00	0,00	∞	1,06	∞	∞	0,21	Transmembrane 9 superfamily member 2
PSMB5	2,92	0,91	5,99	3,21	1,10	2,94	2,28	2,41	-1,05	2,41	0,21	Proteasome subunit beta type-5
COX7B	0,00	0,00	3,00	0,00	0,00	0,00	∞	∞	1,00	∞	0,21	Cytochrome c oxidase subunit 7B, mitochondrial
SND1	0,00	0,00	3,00	0,00	0,00	0,00	∞	∞	1,00	∞	0,21	Staphylococcal nuclease domain-containing protein 1

Gene Symbol	AD1 nc	AD2 nc	capCAA1 nc	capCAA2 nc	C1 nc	C2 nc	fc.cap-CAA/C	fc.capCAA/AD	fc. AD/C	fc. max	pvalues	Protein name
MYH9	22,36	17,24	25,96	29,99	17,54	25,45	1,30	1,41	-1,09	1,41	0,21	Isoform 1 of Myosin-9
MAP2	85,54	55,35	59,91	23,56	28,49	55,80	-1,01	-1,69	1,67	1,69	0,21	Isoform 1 of Microtubule-associated protein 2
ACTBL2	0,00	1,81	0,00	0,00	0,00	0,00	1,00	-∞	∞	∞	0,22	Beta-actin-like protein 2
VPS26B	2,92	2,72	3,99	3,21	1,10	0,98	3,47	1,28	2,72	3,47	0,22	Vacuolar protein sorting-associated protein 26B
USP5	5,83	6,35	7,99	10,71	16,44	6,85	-1,25	1,53	-1,91	1,91	0,22	Isoform Long of Ubiquitin carboxyl-terminal hydrolase 5
CALD1	0,00	0,00	0,00	2,14	0,00	0,00	∞	∞	1,00	∞	0,22	Isoform 1 of Caldesmon
EHD2	0,00	0,00	0,00	2,14	0,00	0,00	∞	∞	1,00	∞	0,22	EH domain-containing protein 2
KRT4	0,00	0,00	0,00	2,14	0,00	0,00	∞	∞	1,00	∞	0,22	keratin 4
DES	0,00	0,00	0,00	2,14	0,00	0,00	∞	∞	1,00	∞	0,22	Desmin
-	0,00	0,00	3,00	0,00	0,00	0,98	3,06	∞	-∞	∞	0,22	AVLL5809
GNG2	3,89	9,07	3,00	3,21	4,38	2,94	-1,18	-2,09	1,77	2,09	0,22	Guanine nucleotide-binding protein G(I)/G(S)/G(O) subunit gamma-2
CCDC6	0,00	0,00	0,00	0,00	2,19	0,00	-∞	-1,00	-∞	∞	0,22	Coiled-coil domain-containing protein 6
CPT2	0,00	0,00	0,00	0,00	2,19	0,00	-∞	-1,00	-∞	∞	0,22	Carnitine O-palmitoyltransferase 2, mitochondrial
MCAM	0,00	0,00	0,00	0,00	2,19	0,00	-∞	-1,00	-∞	∞	0,22	Isoform 1 of Cell surface glycoprotein MUC18
FAH	0,00	0,00	0,00	0,00	2,19	0,00	-∞	-1,00	-∞	∞	0,22	Fumarylacetoacetase
RASAL1	0,00	0,00	0,00	0,00	2,19	0,00	-∞	-1,00	-∞	∞	0,22	Isoform 2 of RasGAP-activating-like protein 1
CAPN2	0,00	0,00	0,00	0,00	2,19	0,00	-∞	-1,00	-∞	∞	0,22	Calpain-2 catalytic subunit
ABI2	0,00	0,00	0,00	0,00	2,19	0,00	-∞	-1,00	-∞	∞	0,22	ArgBPIB protein
CTSB	1,94	1,81	3,99	1,07	0,00	0,98	5,17	1,35	3,84	5,17	0,22	Cathepsin B
PENK	0,00	0,00	0,00	0,00	3,29	0,00	-∞	-1,00	-∞	∞	0,22	Proenkephalin-A
SRM	0,00	0,00	0,00	0,00	3,29	0,00	-∞	-1,00	-∞	∞	0,22	Spermidine synthase
EPB41L1	14,58	13,61	18,97	10,71	6,58	11,75	1,62	1,05	1,54	1,62	0,22	Isoform 1 of Band 4.1-like protein 1
FERMT2	0,00	0,91	1,00	0,00	2,19	1,96	-4,16	1,10	-4,57	4,57	0,23	Isoform 1 of Fermitin family homolog 2
GPHN	0,97	0,00	1,00	0,00	1,10	2,94	-4,04	1,03	-4,15	4,15	0,23	Isoform 1 of Gephyrin
GABRG2	0,97	0,91	3,00	1,07	0,00	0,98	4,15	4,18	-1,01	4,18	0,23	Gamma-aminobutyric acid receptor subunit gamma-2
ANXA1	0,00	0,91	3,99	3,21	0,00	6,85	1,05	7,94	-7,55	7,94	0,23	Annexin A1
NECAB2	0,00	0,00	0,00	0,00	8,77	0,00	-∞	-1,00	-∞	∞	0,23	N-terminal EF-hand calcium-binding protein 2
-	5,83	6,35	5,99	3,21	1,10	3,92	1,84	-1,32	2,43	2,43	0,23	Diazepam binding inhibitor, splice form 1D
CD44	0,00	0,91	0,00	1,07	3,29	0,98	-3,98	1,18	-4,70	4,70	0,23	Isoform 12 of CD44 antigen
VAMP1	6,80	6,35	5,99	6,43	1,10	4,89	2,07	-1,06	2,20	2,20	0,23	Isoform 1 of Vesicle-associated membrane protein 1
SYN2	17,50	29,94	31,95	28,92	42,74	27,41	-1,15	1,28	-1,48	1,48	0,23	synapsin II isoform IIb
C11orf2	1,94	0,91	3,00	2,14	1,10	0,00	4,69	1,80	2,60	4,69	0,23	Isoform 1 of Protein fat-free homolog
EFHD2	10,69	6,35	9,98	13,92	5,48	7,83	1,80	1,40	1,28	1,80	0,23	EF-hand domain-containing protein D2
CCBL2	1,94	0,00	0,00	0,00	0,00	0,00	1,00	-∞	∞	∞	0,23	Isoform 1 of Kynurenine--oxoglutarate transaminase 3
DIP2B	1,94	0,00	0,00	0,00	0,00	0,00	1,00	-∞	∞	∞	0,23	Isoform 1 of Disco-interacting protein 2 homolog B
SEMA7A	1,94	0,00	0,00	0,00	0,00	0,00	1,00	-∞	∞	∞	0,23	Semaphorin-7A
AP1M1	1,94	0,00	0,00	0,00	0,00	0,00	1,00	-∞	∞	∞	0,23	AP-1 complex subunit mu-1
C12orf5	1,94	0,00	0,00	0,00	0,00	0,00	1,00	-∞	∞	∞	0,23	Probable fructose-2,6-bisphosphatase TIGAR
CTTN	1,94	0,00	0,00	0,00	0,00	0,00	1,00	-∞	∞	∞	0,23	Src substrate cortactin
DHX15	1,94	0,00	0,00	0,00	0,00	0,00	1,00	-∞	∞	∞	0,23	Putative pre-mRNA-splicing factor ATP-dependent RNA helicase DHX15
OGT	2,92	0,00	0,00	0,00	0,00	0,00	1,00	-∞	∞	∞	0,23	Isoform 3 of UDP-N-acetylglucosamine--peptide N-acetylglucosaminyltransferase 110 kDa subunit
BAZ2B	2,92	0,00	0,00	0,00	0,00	0,00	1,00	-∞	∞	∞	0,23	Isoform 2 of Bromodomain adjacent to zinc finger domain protein 2B
APOD	6,80	5,44	8,99	12,85	9,86	8,81	1,17	1,78	-1,52	1,78	0,24	Apolipoprotein D

Gene Symbol	AD1 nc	AD2 nc	capCAA1 nc	capCAA2 nc	C1 nc	C2 nc	fc.cap-CAA/C	fc.capCAA/AD	fc. AD/C	fc. max	pvalues	Protein name
MAP2K4	4,86	1,81	1,00	1,07	3,29	2,94	-3,01	-3,23	1,07	3,23	0,24	Mitogen-activated protein kinase kinase 4, isoform CRA_c
ACAA2	4,86	0,00	3,99	3,21	5,48	5,87	-1,58	1,48	-2,34	2,34	0,24	3-ketoacyl-CoA thiolase, mitochondrial
CAPZA1	0,97	1,81	3,00	2,14	5,48	2,94	-1,64	1,84	-3,02	3,02	0,24	F-actin-capping protein subunit alpha-1
ALDH4A1	9,72	11,80	5,99	9,64	8,77	17,62	-1,69	-1,38	-1,23	1,69	0,24	Delta-1-pyrroline-5-carboxylate dehydrogenase, mitochondrial
ALDOC	85,54	99,81	97,85	110,32	78,91	94,95	1,20	1,12	1,07	1,20	0,24	Fructose-bisphosphate aldolase
FBXO41	0,00	0,00	1,00	0,00	0,00	1,96	-1,96	∞	-∞	∞	0,24	F-box protein 41
ATG7	0,00	0,00	2,00	0,00	0,00	0,98	2,04	∞	-∞	∞	0,24	Isoform 1 of Autophagy-related protein 7
LANCL1	9,72	7,26	15,98	7,50	13,15	14,68	-1,19	1,38	-1,64	1,64	0,24	LanC-like protein 1
APEH	0,97	1,81	3,00	2,14	6,58	1,96	-1,66	1,84	-3,06	3,06	0,24	Acylamino-acid-releasing enzyme
TPPP	27,22	24,50	17,97	18,21	21,92	20,56	-1,17	-1,43	1,22	1,43	0,24	Tubulin polymerization-promoting protein
TPM2	0,00	0,00	0,00	2,14	0,00	0,98	2,19	∞	-∞	∞	0,25	Isoform 2 of Tropomyosin beta chain
AOC3	0,00	0,00	0,00	2,14	0,00	0,98	2,19	∞	-∞	∞	0,25	Membrane primary amine oxidase
PTRF	0,00	0,00	0,00	3,21	0,00	0,98	3,28	∞	-∞	∞	0,25	Isoform 1 of Polymerase I and transcript release factor
HDHD2	2,92	5,44	3,00	7,50	1,10	2,94	2,60	1,26	2,07	2,60	0,25	Isoform 1 of Haloacid dehalogenase-like hydrolase domain-containing protein 2
CADPS	12,64	6,35	13,98	7,50	14,25	15,66	-1,39	1,13	-1,58	1,58	0,25	Isoform 1 of Calcium-dependent secretion activator 1
SLC17A6	0,00	0,00	1,00	0,00	2,19	0,00	-2,20	∞	-∞	∞	0,25	Vesicular glutamate transporter 2
DNAJA4	0,00	0,00	1,00	0,00	2,19	0,00	-2,20	∞	-∞	∞	0,25	DnaJ (Hsp40) homolog, subfamily A, member 4 isoform 1
AK2	0,00	1,81	0,00	0,00	0,00	1,96	-1,17	∞	-1,08	2,16	0,25	Isoform 1 of Adenylate kinase 2, mitochondrial
SLC9A3R1	5,83	5,44	2,00	3,21	3,29	3,92	-2,16	-2,16	1,85	2,16	0,25	Na(+)/H(+) exchange regulatory cofactor NHE-RF1
PPP3CA	50,55	57,17	52,92	55,70	42,74	45,03	1,24	1,01	1,23	1,24	0,25	Isoform 1 of Serine/threonine-protein phosphatase 2B catalytic subunit alpha isoform
CADM3	9,72	13,61	11,98	9,64	15,34	17,62	-1,52	-1,08	-1,41	1,52	0,26	Isoform 2 of Cell adhesion molecule 3
LGI1	0,97	0,91	3,99	2,14	1,10	3,92	1,22	3,26	-2,67	3,26	0,26	Isoform 1 of Leucine-rich glioma-inactivated protein 1
IDH1	3,89	3,63	2,00	1,07	1,10	1,96	1,00	-2,45	2,46	2,46	0,26	Isocitrate dehydrogenase [NADP] cytoplasmic
KIF5B	0,00	0,00	1,00	0,00	3,29	0,00	-3,29	∞	-∞	∞	0,26	Kinesin-1 heavy chain
SHANK3	0,97	0,00	3,00	3,21	5,48	6,85	-1,99	∞	-2,01	∞	0,26	SH3 and multiple ankyrin repeat domains 3
ARPC2	3,89	2,72	3,00	22,49	14,25	9,79	-1,06	1,11	-1,87	1,99	0,26	Actin-related protein 2/3 complex subunit 2
PGD	16,53	16,33	13,98	22,49	14,25	9,79	1,52	1,01	1,37	1,52	0,26	6-phosphogluconate dehydrogenase, decarboxylating
OGDHL	4,86	0,00	6,99	2,14	4,38	7,83	-1,34	1,88	-2,51	2,51	0,26	2-oxoglutarate dehydrogenase E1 component-like, mitochondrial
GSTM1	1,94	13,61	11,98	2,14	19,73	11,75	-2,23	-1,10	-2,02	2,23	0,26	Isoform 1 of Glutathione S-transferase Mu 1
UFM1	0,97	0,00	2,00	0,00	0,00	0,00	∞	2,05	∞	∞	0,26	Ubiquitin-fold modifier 1
C1orf93	0,97	0,00	1,00	0,00	0,00	0,00	∞	2,05	∞	∞	0,26	Chromosome 1 open reading frame 93, isoform CRA_d
GDPD1	0,97	0,00	2,00	0,00	0,00	0,00	∞	2,05	∞	∞	0,26	Isoform 1 of Glycerophosphodiester phosphodiesterase domain-containing protein 1
SLC32A1	4,86	2,72	3,00	1,07	6,58	3,92	-2,58	-1,86	-1,38	2,58	0,26	Vesicular inhibitory amino acid transporter
NPM1	4,86	3,63	3,00	2,14	1,10	1,96	1,68	-1,65	2,78	2,78	0,27	Isoform 2 of Nucleophosmin
LINGO1	0,00	0,00	2,00	0,00	3,29	0,00	-1,65	∞	-∞	∞	0,27	Isoform 1 of Leucine-rich repeat and immunoglobulin-like domain-containing nogo receptor-interacting protein 1
COL6A2	0,00	0,00	0,00	1,07	0,00	4,89	-4,57	∞	-∞	∞	0,27	Isoform 2C2A of Collagen alpha-2(VI) chain
NSF	81,65	93,46	89,86	93,19	108,50	97,89	-1,13	-1,10	-1,18	1,18	0,27	Vesicle-fusing ATPase
EIF4G1	0,00	0,91	0,00	0,00	2,19	0,00	-∞	-2,05	-2,42	∞	0,27	eukaryotic translation initiation factor 4 gamma, 1 isoform 4
NCKAP1	10,69	8,17	17,97	6,43	16,44	14,68	-1,28	1,29	-1,65	1,65	0,27	Isoform 1 of Nck-associated protein 1
MAP1A	55,41	35,39	44,93	26,78	29,59	32,30	1,16	-1,27	1,47	1,47	0,27	331 kDa protein
TMEM30A	0,00	0,91	0,00	0,00	3,29	0,00	-∞	-∞	-3,62	∞	0,27	Isoform 1 of Cell cycle control protein 50A
C20orf103	0,00	0,91	0,00	0,00	3,29	0,00	-∞	-∞	-3,62	∞	0,27	Isoform 1 of LAMP family protein C20orf103
SIRPA	21,39	35,39	37,94	29,99	32,88	45,03	-1,15	1,20	-1,37	1,37	0,27	signal-regulatory protein alpha precursor

Gene Symbol	AD1 nc	AD2 nc	capCAA1 nc	capCAA2 nc	C1 nc	C2 nc	fc.cap-CAA/C	fc.capCAA/AD	fc. AD/C	fc. max	pvalues	Protein name
ITGB1	0.00	1.81	0.00	2.14	0.00	0.00	∞	1.18	∞	∞	0.27	Isoform Beta-1A of Integrin beta-1
OGN	0.00	0.00	0.00	5.36	0.00	4.89	1.09	-∞	-∞	∞	0.27	cDNA FLJ59205, highly similar to Mimecan
KIAA0513	4.86	3.63	3.00	3.21	0.00	2.94	2.11	-1.37	2.89	2.89	0.27	Isoform 1 of Uncharacterized protein KIAA0513
MACROD1	4.86	4.54	4.99	4.28	0.00	3.92	2.37	-1.01	2.40	2.40	0.27	MACRO domain-containing protein 1
HNRNPM	5.83	3.63	4.99	4.28	2.19	1.96	2.24	-1.02	2.28	2.28	0.27	Isoform 1 of Heterogeneous nuclear ribonucleoprotein M
COL6A1	0.00	0.00	0.00	3.21	0.00	6.85	-2.13	∞	-∞	∞	0.27	Collagen alpha-1(VI) chain
LIN7A	6.80	3.63	5.99	2.14	0.00	3.92	2.08	-1.28	2.66	2.66	0.28	Lin-7 homolog A
DLD	34.02	26.31	36.94	36.42	30.69	46.99	-1.06	1.22	-1.29	1.29	0.28	Dihydrolipoyl dehydrogenase, mitochondrial
HADHB	6.80	6.35	11.98	4.28	8.77	13.70	-1.38	1.24	-1.71	1.71	0.28	Trifunctional enzyme subunit beta, mitochondrial
PADI2	8.75	20.87	10.98	9.64	8.77	8.81	1.17	-1.44	1.69	1.69	0.28	Protein-arginine deiminase type-2
HSPA4	25.27	18.15	17.97	15.00	33.97	17.62	-1.56	-1.32	-1.19	1.56	0.28	Heat shock 70 kDa protein 4
MAP6	18.47	10.89	11.98	6.43	12.06	14.68	-1.45	-1.59	1.10	1.59	0.28	Isoform 1 of Microtubule-associated protein 6
LYNX1	2.92	1.81	1.00	0.00	0.00	2.94	-2.94	-4.74	1.61	4.74	0.28	Ly-6/neurotoxin-like protein 1
CNN1	0.00	0.00	0.00	10.71	0.00	5.87	1.82	∞	-∞	∞	0.28	Calponin-1
GSTM4	0.00	1.81	1.00	0.00	0.00	0.00	∞	-1.82	∞	∞	0.28	Isoform 1 of Glutathione S-transferase Mu 4
UCRC	3.89	0.91	1.00	2.14	0.00	0.98	3.21	-1.53	4.90	4.90	0.28	Cytochrome b-c1 complex subunit 9
PC	5.83	0.91	12.98	2.14	6.58	12.73	-1.28	2.24	-2.86	2.86	0.28	Pyruvate carboxylase, mitochondrial
CIT	2.92	0.00	1.00	0.00	0.00	0.00	∞	-2.92	∞	∞	0.28	Isoform 1 of Citron Rho-interacting kinase
FLNA	1.94	5.44	10.98	56.77	3.29	37.20	1.67	9.17	-5.48	9.17	0.28	Isoform 2 of Filamin-A
SLC25A6	54.44	49.00	51.92	42.84	48.22	70.48	-1.25	-1.09	-1.15	1.25	0.28	ADP/ATP translocase 3
GYG1	0.00	1.81	0.00	1.07	0.00	0.00	∞	-1.69	∞	∞	0.28	Isoform GN-1L of Glycogenin-1
MAPK3	0.97	0.91	3.00	1.07	4.38	1.96	-1.56	2.16	-3.37	3.37	0.29	Mitogen-activated protein kinase 3
NDUFAF4	1.94	0.00	0.00	0.00	0.00	0.98	-∞	-∞	1.99	∞	0.29	Protein HRPAP20
DDX6	1.94	0.00	0.00	0.00	0.00	0.98	-∞	-∞	1.99	∞	0.29	Probable ATP-dependent RNA helicase DDX6
SFPQ	3.89	1.81	5.99	1.07	0.00	1.96	3.61	1.24	2.91	3.61	0.29	Isoform Long of Splicing factor, proline- and glutamine-rich
NDUFAB1	3.89	2.72	2.00	2.14	2.19	0.00	1.89	-1.60	3.02	3.02	0.29	Acyl carrier protein, mitochondrial
ATP5EP2	1.94	0.00	1.00	0.00	0.00	0.00	∞	-1.95	∞	∞	0.29	ATP synthase subunit epsilon-like protein, mitochondrial
TOMM40	1.94	0.00	1.00	1.07	0.00	0.00	∞	-1.95	∞	∞	0.29	Isoform 1 of Mitochondrial import receptor subunit TOM40 homolog
CAPN1	2.92	0.91	3.99	5.36	4.38	1.96	1.47	2.45	-1.66	2.45	0.29	Calpain-1 catalytic subunit
COPS4	6.80	3.63	3.99	1.07	3.29	1.96	-1.04	-2.06	1.99	2.06	0.29	COP9 signalosome complex subunit 4
UCHL1	34.99	39.93	35.95	29.99	50.41	36.22	-1.31	-1.14	-1.16	1.31	0.29	Ubiquitin carboxyl-terminal hydrolase isozyme L1
ANLN	0.00	0.00	1.00	1.07	5.48	0.00	-5.12	∞	-∞	∞	0.29	Isoform 2 of Actin-binding protein anillin
RABGAP2	1.94	0.00	0.00	0.00	2.19	0.00	-∞	-∞	-1.13	∞	0.29	Isoform 1 of Rab3 GTPase-activating protein non-catalytic subunit
AMPD2	1.94	0.00	0.00	0.00	2.19	0.00	-∞	-∞	-1.13	∞	0.29	Adenosine monophosphate deaminase 2
PSMD6	1.94	0.00	0.00	0.00	2.19	0.00	-∞	-∞	-1.13	∞	0.29	26S proteasome non-ATPase regulatory subunit 6
PSPC1	1.94	0.00	0.00	1.07	0.00	0.00	∞	-1.82	∞	∞	0.29	Isoform 2 of Paraspeckle component 1
SUCLA2	1.94	0.00	0.00	1.07	0.00	0.00	∞	-1.82	∞	∞	0.29	cDNA FLJ54097, highly similar to Succinyl-CoA ligase (ADP-forming) beta-chain, mitochondrial
CAB39L	1.94	0.00	0.00	0.00	1.10	0.00	-∞	-∞	1.77	∞	0.29	Calcium-binding protein 39-like
SHGL1	1.94	0.00	0.00	0.00	1.10	0.00	-∞	-∞	1.77	∞	0.29	cDNA, FLJ96508, Homo sapiens SH3-domain GRB2-like 1 (SH3GL1), mRNA
ACADM	1.94	0.00	0.00	0.00	1.10	0.00	-∞	-∞	1.77	∞	0.29	Medium-chain specific acyl-CoA dehydrogenase, mitochondrial
KIF21A	3.89	1.81	3.99	2.14	6.58	4.89	-1.87	1.08	-2.01	2.01	0.30	Isoform 1 of Kinesin-like protein KIF21A
ATL1	3.89	3.63	6.99	5.36	5.48	8.81	-1.16	1.64	-1.90	1.90	0.30	Atlastin-1
TIMM9	2.92	0.91	1.00	0.00	0.00	0.98	1.02	-3.83	3.91	3.91	0.30	Mitochondrial import inner membrane translocase subunit Tim9

Gene Symbol	AD1 nc	AD2 nc	capCAA1 nc	capCAA2 nc	C1 nc	C2 nc	fc.cap-CAA/C	fc.capCAA/AD	fc. AD/C	fc. max	pvalues	Protein name
C6orf174	1,94	1,81	1,00	0,00	1,10	0,00	-1,10	-3,76	3,43	3,76	0,30	Uncharacterized protein C6orf174
NANS	1,94	1,81	1,00	0,00	1,10	0,00	-1,10	-3,76	3,43	3,76	0,30	Sialic acid synthase
HNRPDL	1,94	1,81	1,00	0,00	0,00	0,98	1,02	-3,76	3,84	3,84	0,30	Isoform 1 of Heterogeneous nuclear ribonucleoprotein D-like
S100A16	1,94	1,81	0,00	1,07	0,00	0,98	1,09	-3,51	3,84	3,84	0,30	Protein S100-A16
MAP6D1	1,94	1,81	0,00	1,07	0,00	0,98	1,09	-3,51	3,84	3,84	0,30	MAP6 domain-containing protein 1
ATP2B2	88,46	90,74	91,86	59,98	30,69	90,06	1,26	-1,18	1,48	1,48	0,30	Isoform WB of Plasma membrane calcium-transporting ATPase 2
DYNLL2	13,61	9,98	9,98	4,28	7,67	13,70	-1,50	-1,65	1,10	1,65	0,30	Dynein light chain 2, cytoplasmic
OGDH	14,58	5,44	21,97	10,71	12,06	27,41	-1,21	1,63	-1,97	1,97	0,30	2-oxoglutarate dehydrogenase E1 component, mitochondrial
PSMD2	3,89	1,81	3,00	0,00	4,38	3,92	-2,77	-1,90	-1,46	2,77	0,31	26S proteasome non-ATPase regulatory subunit 2
GPD1	0,97	0,00	0,00	0,00	6,58	0,00	-∞	-∞	-6,76	∞	0,31	Glycerol-3-phosphate dehydrogenase [NAD+], cytoplasmic
PRDX3	13,61	15,43	13,98	18,21	17,54	23,49	-1,27	1,11	-1,41	1,41	0,31	Thioredoxin-dependent peroxide reductase, mitochondrial
HSPA12A	51,52	29,94	49,92	53,55	43,84	44,05	1,18	1,27	-1,08	1,27	0,31	Heat shock 70 kDa protein 12A
CA1	16,53	10,89	10,98	18,21	14,25	26,43	-1,39	1,06	-1,48	1,48	0,31	Carbonic anhydrase 1
PRDX1	31,11	39,02	26,96	26,78	36,17	24,47	-1,13	-1,30	1,16	1,30	0,31	Peroxiredoxin-1
OXR1	12,64	6,35	12,98	2,14	0,00	7,83	1,93	-1,26	2,42	2,42	0,31	cDNA FLJ56044, highly similar to Oxidation resistance protein 1
PA2G4	0,97	0,00	2,00	1,07	3,29	0,98	-1,39	3,16	-4,39	4,39	0,31	PA2G4 protein (Fragment)
PVRL1	0,97	0,00	1,00	2,14	2,19	1,96	-1,32	3,23	-4,27	4,27	0,31	Isoform Delta of Poliovirus receptor-related protein 1
TSFM	0,97	0,00	2,00	1,07	2,19	1,96	-1,35	3,16	-4,27	4,27	0,31	Isoform 1 of Elongation factor Ts, mitochondrial
SBF1	0,97	0,00	2,00	2,14	1,10	1,96	1,36	4,26	-3,14	4,26	0,31	Isoform 1 of Myotubularin-related protein 5
SH3GL2	21,39	28,13	18,97	18,21	18,63	19,58	-1,03	-1,33	1,30	1,33	0,31	Endophilin-A1
MYO1RA	6,80	0,91	3,00	2,14	1,10	0,98	2,48	-1,50	3,72	3,72	0,31	Isoform 1 of Myosin-XVIIIa
YWHAG	43,74	58,07	40,94	44,99	39,45	44,05	1,03	-1,18	1,22	1,22	0,31	14-3-3 protein gamma
CALR	6,80	12,70	8,99	7,50	6,58	4,89	1,44	-1,18	1,70	1,70	0,31	Calreticulin
BSG	10,69	11,80	11,98	10,71	7,67	6,85	1,56	1,01	1,55	1,56	0,32	Isoform 2 of Basigin
-	3,89	4,54	5,99	5,36	0,00	4,89	2,32	1,35	1,72	2,32	0,32	cDNA FLJ54694, highly similar to Pleckstrin and Sec7 domain-containing protein 3
ADD3	20,41	24,50	18,97	18,21	16,44	15,66	1,16	-1,21	1,40	1,40	0,32	Isoform 2 of Gamma-adducin
MACF1	7,78	7,26	8,99	0,00	2,19	3,92	1,47	-1,67	2,46	2,46	0,32	Isoform 2 of Microtubule-actin cross-linking factor 1, isoforms 1/2/3/5
IARS2	1,94	0,91	3,99	2,14	2,19	4,89	-1,15	2,15	-2,49	2,49	0,32	Isoleucyl-tRNA synthetase, mitochondrial
ARHGDIA	7,78	9,98	7,99	7,50	17,54	7,83	-1,64	-1,15	-1,43	1,64	0,32	Rho GDP-dissociation inhibitor 1
GSS	1,94	0,91	3,00	4,28	5,48	0,98	1,13	2,55	-2,26	2,55	0,32	Glutathione synthetase
TAGLN2	5,83	7,26	7,99	13,92	8,77	9,79	1,18	1,67	-1,42	1,67	0,33	Transgelin-2
ARL6IP1	2,92	0,91	0,00	1,07	2,19	1,96	-3,87	-3,57	-1,09	3,87	0,33	ADP-ribosylation factor-like protein 6-interacting protein 1
RAB8B	1,94	1,81	0,00	1,07	3,29	0,98	-3,98	-3,51	-1,14	3,98	0,33	Ras-related protein Rab-8B
PFKL	9,72	7,26	6,99	3,21	10,96	6,85	-1,75	-1,66	-1,05	1,75	0,33	Isoform 1 of 6-phosphofructokinase, liver type
FARSB	3,89	0,91	6,99	0,00	4,38	8,81	-1,89	1,46	-2,75	2,75	0,33	Phenylalanyl-tRNA synthetase beta chain
CRABP1	0,97	0,00	3,00	0,00	1,10	2,94	-1,35	3,08	-4,15	4,15	0,33	Cellular retinoic acid-binding protein 1
HIST2H4A;HIST1 H4J;HIST1H4B;H1 ST1H4E;HIST1H4 1H5T1H4H;HIST 1HA4;HIST2H4B; HIST1H4D;HIST1 H4C;HIST4H4;HIS T1H4E;HIST1H4L; HIST1H4K	34,02	41,74	29,95	39,63	30,69	28,39	1,18	-1,09	1,28	1,28	0,33	Histone H4
HSD12	3,89	2,72	4,99	2,14	7,67	4,89	-1,76	1,08	-1,90	1,90	0,33	Isoform 1 of Hydroxysteroid dehydrogenase-like protein 2

Gene Symbol	AD1 nc	AD2 nc	capCAA1 nc	capCAA2 nc	C1 nc	C2 nc	fc.cap-CAA/C	fc.capCAA/AD	fc.AD/C	fc.max	pvalues	Protein name
SLC44A2	2,92	3,63	4,99	2,14	7,67	4,89	-1,76	1,09	-1,92	1,92	0,33	Isoform 2 of Choline transporter-like protein 2
AMPH	36,94	27,22	29,95	29,99	17,54	30,34	1,25	-1,07	1,34	1,34	0,33	Isoform 1 of Amphiphysin
CCT7	11,66	7,26	8,99	10,71	15,34	12,73	-1,42	1,04	-1,48	1,48	0,33	T-complex protein 1 subunit eta
CYB5R3	7,78	6,35	6,99	9,64	13,15	9,79	-1,38	1,18	-1,62	1,62	0,33	cDNA FLJ56301, highly similar to NADH-cytochrome b5 reductase
EHD3	12,64	11,80	13,98	15,00	8,77	9,79	1,56	1,19	1,32	1,56	0,33	EH domain-containing protein 3
PTPRZ1	22,36	31,76	26,96	16,07	23,01	17,62	1,06	-1,26	1,33	1,33	0,33	Isoform Long of Receptor-type tyrosine-protein phosphatase zeta
PGRMC1	4,86	4,54	2,00	2,14	4,38	1,96	-1,53	-2,27	1,48	2,27	0,34	Membrane-associated progesterone receptor component 1
NPTX1	1,94	7,26	3,00	1,07	2,19	2,94	-1,26	-2,26	1,79	2,26	0,34	Neuronal pentraxin-1
ATP6V0C	1,94	0,91	3,99	0,00	3,29	3,92	-1,80	1,40	-2,53	2,53	0,34	V-type proton ATPase 16 kDa proteolipid subunit
PPAP2B	1,94	2,72	2,00	0,00	3,29	2,94	-3,12	-2,34	-1,33	3,12	0,34	Lipid phosphate phosphohydrolase 3
RAP1GDS1	10,69	9,98	12,98	18,21	13,15	11,75	1,25	1,51	-1,20	1,51	0,34	RAP1, GTP-GDP dissociation stimulator 1 isoform 4
TINAGL1	0,97	1,81	3,99	3,21	1,10	2,94	1,79	2,59	-1,45	2,59	0,34	Isoform 1 of Tubulointerstitial nephritis antigen-like
SEPT11	26,25	32,67	35,95	22,49	14,25	28,39	1,37	-1,01	1,38	1,38	0,34	cDNA FLJ53574, highly similar to Septin-11
ARL6IP5	8,75	7,26	5,99	3,21	5,48	4,89	-1,13	-1,74	1,54	1,74	0,35	PRA1 family protein 3
MDH2	92,35	105,26	88,86	104,97	87,68	84,18	1,13	-1,02	1,15	1,15	0,35	Malate dehydrogenase, mitochondrial
TLN1	7,78	8,17	7,99	18,21	7,67	12,73	1,28	1,64	-1,28	1,64	0,35	Talin-1
PTPLAD1	4,86	4,54	3,00	1,07	5,48	1,96	-1,83	-2,31	1,26	2,31	0,35	Protein tyrosine phosphatase-like protein PTPLAD1
ITSN1	2,92	0,91	3,99	2,14	0,00	1,96	3,13	1,60	1,95	3,13	0,35	Isoform 4 of Intersectin-1
PLLP	1,94	1,81	2,00	4,28	1,10	0,98	3,03	1,67	1,81	3,03	0,35	Plasmolipin
NDUFS1	47,63	39,93	49,92	40,70	42,74	65,58	-1,20	1,04	-1,24	1,24	0,35	NADH-ubiquinone oxidoreductase 75 kDa subunit
LHPP	1,94	5,44	1,00	3,21	2,19	0,98	1,33	-1,75	2,33	2,33	0,35	Phospholysine phosphohistidine inorganic pyrophosphate phosphatase
MPI	0,97	0,91	3,00	2,14	2,19	2,94	1,00	2,73	-2,73	2,73	0,35	Isoform 1 of Mannose-6-phosphate isomerase
CA2	33,05	20,87	13,98	24,64	30,69	21,54	-1,35	-1,40	1,03	1,40	0,35	Carbonic anhydrase 2
FLOT2	1,94	9,07	5,99	3,21	3,29	0,98	2,16	-1,20	2,58	2,58	0,35	flotillin 2
ALDH1A1	3,89	4,54	8,99	6,43	2,19	3,92	2,03	1,47	1,38	2,03	0,35	Retinal dehydrogenase 1
ATP1B2	8,75	9,07	8,99	11,78	3,29	8,81	1,72	1,17	1,47	1,72	0,35	Sodium/potassium-transporting ATPase subunit beta-2
PLXNA1	0,97	0,91	1,00	0,00	1,10	2,94	-4,04	-1,88	-2,15	4,04	0,35	Plexin-A1
FUNDC2	1,94	0,00	1,00	0,00	1,10	2,94	-4,04	-1,95	-2,07	4,04	0,35	FUN14 domain-containing protein 2
ATAD3A	1,94	0,00	1,00	0,00	1,10	2,94	-4,04	-1,95	-2,07	4,04	0,35	Isoform 2 of ATPase family AAA domain-containing protein 3A
SH3BGRL3	0,97	0,91	0,00	0,00	2,19	1,96	-4,16	-1,88	-2,21	4,16	0,35	Putative uncharacterized protein
CARS	0,97	0,91	0,00	1,07	3,29	0,98	-3,98	-1,75	-2,27	3,98	0,35	cysteinyl-tRNA synthetase isoform c
FTL	18,47	17,24	15,98	13,92	17,54	24,47	-1,40	-1,19	-1,18	1,40	0,35	Ferritin
WBP2	0,97	0,91	2,00	0,00	3,29	1,96	-2,63	1,06	-2,79	2,79	0,35	WW domain-binding protein 2
PLCD1	0,00	1,81	2,00	2,14	1,10	0,00	3,78	2,28	1,66	3,78	0,35	1-phosphatidylinositol-4,5-bisphosphate phosphodiesterase delta-1
ADAM23	1,94	0,00	1,00	3,21	0,00	0,98	4,30	2,17	1,99	4,30	0,35	Isoform Alpha of Disintegrin and metalloproteinase domain-containing protein 23
SYNE1	1,94	0,00	3,00	2,14	1,10	0,98	2,48	2,64	-1,07	2,64	0,35	Isoform 4 of Nesprin-1
HPX	0,97	0,91	0,00	2,14	1,10	3,92	-2,34	1,14	-2,67	2,67	0,36	Hemopexin
ANXA2	5,83	8,17	7,99	15,00	6,58	16,64	-1,01	1,64	-1,66	1,66	0,36	annexin A2 isoform 1
CSE1L	1,94	0,91	3,00	2,14	4,38	2,94	-1,42	1,80	-2,57	2,57	0,36	Isoform 1 of Exportin-2
RGS7	2,92	3,63	2,00	0,00	0,00	4,89	-2,45	-3,28	1,34	3,28	0,36	Isoform 1 of Regulator of G-protein signaling 7
PDHX	1,94	0,91	2,00	2,14	1,10	5,87	-1,68	1,45	-2,44	2,44	0,36	Pyruvate dehydrogenase protein X component, mitochondrial
ACTN1	51,52	51,72	51,92	62,12	29,59	57,75	1,31	1,10	1,18	1,31	0,36	actinin, alpha 1 isoform a
CHL1	4,86	7,26	4,99	1,07	6,58	1,96	-1,41	-2,00	1,42	2,00	0,36	Isoform 2 of Neural cell adhesion molecule L1-like protein

Gene Symbol	AD1 nc	AD2 nc	capCAA1 nc	capCAA2 nc	C1 nc	C2 nc	fc.cap-CAA/C	fc.capCAA/AD	fc. AD/C	fc. max	pvalues	Protein name
PRDX5	13,61	25,41	11,98	15,00	12,06	18,60	-1,14	-1,45	1,27	1,45	0,36	Isoform Mitochondrial of Peroxiredoxin-5, mitochondrial
FH	14,58	16,33	15,98	26,78	15,34	25,45	1,05	1,38	-1,32	1,38	0,36	Isoform Mitochondrial of Fumarate hydratase, mitochondrial
RPS8	4,86	2,72	3,00	1,07	3,29	5,87	-2,25	-1,86	-1,21	2,25	0,36	40S ribosomal protein S8
IGSF8	37,91	43,55	42,93	29,99	53,70	39,15	-1,27	-1,12	-1,14	1,27	0,36	Isoform 1 of Immunoglobulin superfamily member 8
UQCRQ	5,83	4,54	3,99	2,14	2,19	2,94	1,20	-1,69	2,02	2,02	0,36	Cytochrome b-c1 complex subunit 8
COX6C	7,78	7,26	5,99	6,43	3,29	4,89	1,52	-1,21	1,84	1,84	0,36	Cytochrome c oxidase subunit 6C
PHPT1	4,86	7,26	3,99	2,14	4,38	4,89	-1,51	-1,98	1,31	1,98	0,37	14 kDa phosphohistidine phosphatase
LRPPRC	13,61	6,35	15,98	10,71	13,15	15,66	-1,08	1,34	-1,44	1,44	0,37	Leucine-rich PPR motif-containing protein, mitochondrial
PKM2	215,80	209,61	205,69	204,58	206,04	181,09	1,06	-1,04	1,10	1,10	0,37	Isoform M1 of Pyruvate kinase isozymes M1/M2
UGP2	7,78	5,44	4,99	11,78	4,38	4,89	1,81	1,27	1,42	1,81	0,37	cDNA FLJ56155, highly similar to UTP--glucose-1-phosphate uridylyltransferase 2
AHCYL1	12,64	13,61	17,97	9,64	13,15	23,49	-1,33	1,05	-1,40	1,40	0,37	Isoform 1 of Putative adenosylhomocysteinase 2
AGK	4,86	0,91	6,99	4,28	2,19	5,87	1,40	1,95	-1,40	1,95	0,37	Isoform 1 of Acylglycerol kinase, mitochondrial
AP2A1	59,30	58,07	65,90	73,91	44,93	72,44	1,19	1,19	-1,00	1,19	0,37	Isoform B of AP-2 complex subunit alpha-1
FREQ	2,92	4,54	3,99	2,14	2,19	0,98	1,94	-1,21	2,35	2,35	0,37	Neuronal calcium sensor 1
ATP5B	169,14	187,83	188,71	186,37	149,05	185,99	1,12	1,05	1,07	1,12	0,37	ATP synthase subunit beta, mitochondrial
KIAA1045	4,86	5,44	9,98	7,50	6,58	7,83	1,21	1,70	-1,40	1,70	0,37	Protein KIAA1045
VAPB	3,89	4,54	3,99	0,00	0,00	3,92	1,02	-2,11	2,15	2,15	0,38	Isoform 1 of Vesicle-associated membrane protein-associated protein B/C
UBE2D2	1,94	3,63	1,00	1,07	3,29	1,96	-2,53	-2,69	1,06	2,69	0,38	ubiquitin-conjugating enzyme E2D 2 isoform 2
NRCAM	20,41	36,30	21,97	19,28	21,92	32,30	-1,31	-1,37	1,05	1,37	0,38	Isoform 1 of Neuronal cell adhesion molecule
KCTD12	1,94	0,91	1,00	0,00	3,29	0,98	-4,27	-2,86	-1,50	4,27	0,38	BTB/POZ domain-containing protein KCTD12
AGT	1,94	0,91	0,00	1,07	2,19	1,96	-3,87	-2,66	-1,46	3,87	0,38	Angiotensinogen
LOC201229	1,94	0,91	1,00	0,00	2,19	1,96	-4,16	-2,86	-1,46	4,16	0,38	UPF0631 protein HSD24
PCDH1	1,94	0,91	3,00	1,07	0,00	0,98	4,15	1,43	2,91	4,15	0,38	Isoform 1 of Protocadherin-1
LY6H	1,94	4,54	3,00	3,21	6,58	4,89	-1,85	-1,04	-1,77	1,85	0,38	lymphocyte antigen 6 complex, locus H isoform b
ARHGAP1	0,97	7,26	1,00	2,14	2,19	0,00	1,43	-2,62	3,76	3,76	0,38	cDNA FLJ60782, highly similar to Rho-GTPase-activating protein 1
VAT1L	0,00	4,54	1,00	3,21	28,49	1,96	-7,23	-1,08	-6,71	7,23	0,38	Synaptic vesicle membrane protein VAT-1 homolog-like
VAPA	9,72	7,26	6,99	3,21	4,38	6,85	-1,10	-1,66	1,51	1,66	0,38	Vesicle-associated membrane protein-associated protein A
CADM4	7,78	9,07	4,99	6,43	5,48	4,89	1,10	-1,48	1,62	1,62	0,38	Cell adhesion molecule 4
CAMK2G	17,50	9,07	18,97	12,85	3,29	15,66	1,68	1,20	1,40	1,68	0,39	Isoform 5 of Calcium/calmodulin-dependent protein kinase type II gamma chain
SLC44A1	4,86	6,35	5,99	2,14	16,44	3,92	-2,50	-1,38	-1,82	2,50	0,39	Isoform 1 of Choline transporter-like protein 1
HINT1	6,80	9,07	3,99	5,36	5,48	5,87	-1,21	-1,70	1,40	1,70	0,39	Histidine triad nucleotide-binding protein 1
AIFM1	2,92	1,81	3,00	2,14	4,38	4,89	-1,81	1,09	-1,96	1,96	0,39	Isoform 1 of Apoptosis-inducing factor 1, mitochondrial
ALCAM	3,89	5,44	3,00	4,28	8,77	4,89	-1,88	-1,28	-1,46	1,88	0,39	Isoform 1 of CD166 antigen
PRDX6	47,63	49,00	46,93	34,28	40,55	40,13	1,01	-1,19	1,20	1,20	0,39	Peroxiredoxin-6
ATIC	2,92	6,35	6,99	6,43	2,19	4,89	1,89	1,45	1,31	1,89	0,39	Bifunctional purine biosynthesis protein PURH
C3orf10	3,89	2,72	3,00	4,28	1,10	1,96	2,38	1,10	2,16	2,38	0,39	Isoform 1 of Probable protein BRICK1
PALM	4,86	1,81	3,99	3,21	0,00	2,94	2,45	1,08	2,27	2,45	0,39	Isoform 1 of Paralemmin
MATR3	14,58	6,35	8,99	5,36	2,19	8,81	1,30	-1,46	1,90	1,90	0,39	Matrin-3
LONP1	2,92	5,44	8,99	4,28	7,67	6,85	-1,09	1,59	-1,74	1,74	0,39	Lon protease homolog, mitochondrial
DCXR	4,86	1,81	3,99	5,36	6,58	5,87	-1,33	1,40	-1,86	1,86	0,39	L-xylulose reductase
RPS25	2,92	2,72	2,00	0,00	1,10	1,96	-1,53	-2,82	1,85	2,82	0,40	40S ribosomal protein S25
PDCD5	1,94	3,63	2,00	0,00	2,19	0,98	-1,59	-2,79	1,76	2,79	0,40	Programmed cell death protein 5
PSMA1	2,92	2,72	0,00	3,21	1,10	0,98	1,55	-1,75	2,72	2,72	0,40	Isoform Short of Proteasome subunit alpha type-1

Gene Symbol	AD1 nc	AD2 nc	capCAA1 nc	capCAA2 nc	C1 nc	C2 nc	fc.capCAA/C	fc.capCAA/AD	fc. AD/C	fc. max	pvalues	Protein name
NAP1L1	2,92	2,72	1,00	2,14	1,10	0,98	1,51	-1,80	2,72	2,72	0,40	Nucleosome assembly protein 1-like 1
NUDT21	3,89	1,81	1,00	2,14	1,10	0,98	1,51	-1,82	2,75	2,75	0,40	Cleavage and polyadenylation specificity factor subunit 5
MYH11	0,97	0,00	1,00	23,56	0,00	5,87	4,18	25,27	-6,04	25,27	0,40	Myosin-11
GSTP1	19,44	29,94	17,97	19,28	21,92	22,51	-1,19	-1,33	1,11	1,33	0,40	Glutathione S-transferase P
VCAN	56,38	54,44	28,96	50,34	66,85	33,28	-1,26	-1,40	1,11	1,40	0,40	Isoform V0 of Versican core protein
DDX1	2,92	0,91	3,00	2,14	3,29	4,89	-1,59	1,34	-2,14	2,14	0,40	ATP-dependent RNA helicase DDX1
ANXA11	1,94	6,35	3,99	4,28	2,19	1,96	1,99	-1,00	2,00	2,00	0,40	cDNA FLJ55482, highly similar to Annexin A11
ALDOC	4,86	3,63	3,99	4,28	1,10	2,94	2,05	-1,03	2,11	2,11	0,40	Fructose-bisphosphate aldolase
ANXA5	28,19	35,39	29,95	44,99	31,78	27,41	1,27	1,18	1,07	1,27	0,40	Annexin A5
PSMA4	7,78	4,54	3,99	3,21	4,38	2,94	-1,02	-1,71	1,68	1,71	0,40	Proteasome subunit alpha type-4
EEF1A1	30,13	26,31	26,96	23,56	38,36	27,41	-1,30	-1,12	-1,17	1,30	0,41	Elongation factor 1-alpha 1
ATP1A1	112,76	89,83	117,82	102,83	61,37	113,55	1,26	1,09	1,16	1,26	0,41	Isoform Long of Sodium/potassium-transporting ATPase subunit alpha-1
TAGLN	0,97	4,54	4,99	26,78	2,19	26,43	1,11	5,77	-5,20	5,77	0,41	Transgelin
DNAJC6	2,92	3,63	3,00	0,00	3,29	0,00	-1,10	-2,19	1,99	2,19	0,41	Isoform 2 of Putative tyrosine-protein phosphatase auxilin
MGLL	5,83	9,07	9,98	0,00	0,00	7,83	1,28	-1,49	1,90	1,90	0,41	monoglyceride lipase isoform 1
ARHGEF7	0,97	2,72	0,00	1,07	0,00	3,92	-3,66	-3,45	-1,06	3,66	0,41	Isoform 2 of Rho guanine nucleotide exchange factor 7
NUTF2	2,92	6,35	2,00	3,21	2,19	2,94	1,02	-1,78	1,81	1,81	0,42	Nuclear transport factor 2
AHSA1	5,83	3,63	1,00	4,28	3,29	1,96	1,01	-1,79	1,80	1,80	0,42	Activator of 90 kDa heat shock protein ATPase homolog 1
CRYL1	3,89	5,44	3,00	2,14	3,29	1,96	-1,02	-1,82	1,78	1,82	0,42	Isoform 1 of Lambda-crystallin homolog
NDUFB3	1,94	1,81	1,00	0,00	1,10	1,96	-3,06	-3,76	1,23	3,76	0,42	NADH dehydrogenase [ubiquinone] 1 beta subcomplex subunit 3
SET	0,97	2,72	2,00	1,07	0,00	0,98	3,13	-1,20	3,77	3,77	0,42	Isoform 2 of Protein SET
SNTA1	0,97	2,72	1,00	2,14	1,10	0,00	2,87	-1,18	3,37	3,37	0,42	Alpha-1-syntrophin
MAP2K2	4,86	0,91	1,00	1,07	2,19	1,96	-2,01	-2,79	1,39	2,79	0,42	Dual specificity mitogen-activated protein kinase kinase 2
NECAP1	2,92	2,72	2,00	2,14	1,10	0,98	1,99	-1,36	2,72	2,72	0,42	Isoform 1 of Adaptin ear-binding coat-associated protein 1
DBNL	1,94	3,63	3,00	1,07	0,00	1,96	2,08	-1,37	2,85	2,85	0,42	Isoform 3 of Drebrin-like protein
HSPA1B/HSPA1A	54,44	78,04	53,92	97,47	52,61	55,80	1,40	1,14	1,22	1,40	0,42	Heat shock 70 kDa protein 1
PRELP	0,00	0,91	1,00	15,00	0,00	7,83	2,04	17,63	-8,63	17,63	0,42	Prolargin
GDA	13,61	29,94	14,98	13,92	31,78	15,66	-1,64	-1,51	-1,09	1,64	0,42	Guanine aminohydrolase
USO1	0,97	0,91	1,00	3,21	1,10	3,92	-1,19	2,24	-2,67	2,67	0,42	Putative uncharacterized protein DKFZp451D234
DTD1	0,97	0,91	2,00	2,14	3,29	1,96	-1,27	2,20	-2,79	2,79	0,42	D-tyrosyl-tRNA(Tyr) deacylase 1
ASRGL1	5,83	5,44	3,99	2,14	2,19	4,89	-1,15	-1,84	1,59	1,84	0,42	Isoform 1 of L-asparaginase
TRIM2	2,92	1,81	1,00	4,28	5,48	4,89	-1,96	-1,41	-1,39	1,96	0,43	Tripartite motif-containing protein 2
H1F0	2,92	4,54	3,00	7,50	3,29	1,96	2,00	1,41	1,42	2,00	0,43	Histone H1.0
TPP1	6,80	7,26	7,99	12,85	10,96	9,79	1,00	1,48	-1,48	1,48	0,43	Putative uncharacterized protein TPP1
ACTN4	16,53	10,89	13,98	22,49	6,58	17,62	1,51	1,33	1,13	1,51	0,43	Alpha-actinin-4
SSBP1	7,78	8,17	5,99	4,28	5,48	4,89	-1,01	-1,55	1,54	1,55	0,43	Single-stranded DNA-binding protein, mitochondrial
WASF3	0,97	2,72	1,00	0,00	0,00	1,96	-1,96	-3,70	1,89	3,70	0,43	Wiskott-Aldrich syndrome protein family member 3
SRP9/SRP9L1	1,94	1,81	1,00	0,00	1,10	0,98	-2,08	-3,76	1,81	3,76	0,43	Signal recognition particle 9 kDa protein
CAPG	0,97	2,72	0,00	1,07	2,19	0,00	-2,05	-3,45	1,69	3,45	0,43	Macrophage-capping protein
NDUFS5	2,92	2,72	3,99	2,14	3,29	6,85	-1,65	1,09	-1,80	1,80	0,43	NADH dehydrogenase [ubiquinone] iron-sulfur protein 5
S100A11	1,94	1,81	2,00	0,00	0,00	0,98	2,04	-1,88	3,84	3,84	0,43	Protein S100-A11
NDUFB2	1,94	1,81	1,00	1,07	0,00	0,98	2,11	-1,82	3,84	3,84	0,43	NDUFB2 protein
RUVBL1	1,94	1,81	1,00	1,07	1,10	0,00	1,89	-1,82	3,43	3,43	0,43	Isoform 1 of RuvB-like 1

Gene Symbol	AD1 nc	AD2 nc	capCAA1 nc	capCAA2 nc	C1 nc	C2 nc	fc.cap-CAA/C	fc.capCAA/AD	fc. AD/C	fc. max	pvalues	Protein name
-	2,92	0,91	1,00	1,07	1,10	0,00	1,89	-1,85	3,49	3,49	0,43	cDNA FLJ51067, highly similar to DNA damage-binding protein 1
DLG1	0,97	2,72	0,00	2,14	0,00	0,98	2,19	-1,72	3,77	3,77	0,43	Isoform 1 of Disks large homolog 1
SNAP25	41,80	39,02	45,93	35,35	47,13	48,94	-1,18	1,01	-1,19	1,19	0,43	Isoform SNAP-25b of Synaptosomal-associated protein 25
HIST2H2BE	17,50	23,59	13,98	19,28	14,25	16,64	1,08	-1,24	1,33	1,33	0,43	Histone H2B type 2-E
CNTNAP1	40,83	21,78	26,96	22,49	48,22	26,43	-1,51	-1,27	-1,19	1,51	0,43	Contactin-associated protein 1
STX1A	17,50	16,33	22,96	13,92	15,34	11,75	1,36	1,09	1,25	1,36	0,43	Isoform 1 of Syntaxin-1A
ACTC1	10,69	13,61	13,98	66,41	10,96	35,24	1,74	3,31	-1,90	3,31	0,43	Actin, alpha cardiac muscle 1
NQO2	3,89	1,81	3,00	4,28	1,10	1,96	2,38	1,28	1,87	2,38	0,43	Ribosyldihydronicotinamide dehydrogenase [quinone]
NME3	1,94	0,00	2,00	1,07	2,19	2,94	-1,67	1,58	-2,64	2,64	0,44	Nucleoside diphosphate kinase 3
CUL4B	1,94	0,00	3,00	2,14	2,19	0,98	1,62	2,64	-1,63	2,64	0,44	Isoform 1 of Cullin-4B
TKT	44,72	41,74	35,95	55,70	41,65	33,28	1,22	1,06	1,15	1,22	0,44	cDNA FLJ54957, highly similar to Transketolase
GSR	4,86	3,63	2,00	3,21	8,77	1,96	-2,06	-1,63	-1,26	2,06	0,44	Isoform Mitochondrial of Glutathione reductase, mitochondrial
C3	1,94	2,72	0,00	7,50	7,67	3,92	-1,55	1,61	-2,48	2,48	0,44	Complement C3 (Fragment)
PDIA6	2,92	1,81	2,00	6,43	1,10	2,94	2,09	1,78	1,17	2,09	0,44	Isoform 2 of Protein disulfide-isomerase A6
SEC23A	0,97	0,91	1,00	0,00	0,00	3,92	-3,92	-1,88	-2,08	3,92	0,44	Protein transport protein Sec23A
BPNT1	1,94	0,91	2,00	1,07	4,38	1,96	-2,07	1,08	-2,22	2,22	0,44	Isoform 1 of 3'(2'),5'-bisphosphate nucleotidase 1
FASN	29,16	10,89	19,97	7,50	23,01	20,56	-1,59	-1,46	-1,09	1,59	0,44	Fatty acid synthase
SLC30A3	0,97	0,00	1,00	0,00	2,19	0,98	-3,18	1,03	-3,26	3,26	0,44	Zinc transporter 3
GPS1	0,97	0,00	1,00	0,00	2,19	0,98	-3,18	1,03	-3,26	3,26	0,44	Isoform 1 of COP9 signalosome complex subunit 1
RPS6KA2	0,97	0,00	0,00	1,07	2,19	0,98	-2,96	1,10	-3,26	3,26	0,44	Isoform 2 of Ribosomal protein S6 kinase alpha-2
PFDN6	0,00	0,91	0,00	1,07	2,19	0,98	-2,96	1,18	-3,49	3,49	0,44	Prefoldin subunit 6
TBC1D24	0,00	1,81	3,99	0,00	2,19	2,94	-1,28	2,20	-2,83	2,83	0,44	Isoform 1 of TBC1 domain family member 24
PTPNA	8,75	2,72	4,99	1,07	3,29	2,94	-1,03	-1,89	1,84	1,89	0,44	Phosphatidylinositol transfer protein alpha isoform
CAPZA2	12,64	15,43	13,98	11,78	12,06	7,83	1,30	-1,09	1,41	1,41	0,44	F-actin-capping protein subunit alpha-2
YWHAQ	28,19	23,59	27,96	31,06	39,45	26,43	-1,12	1,14	-1,27	1,27	0,45	14-3-3 protein theta
CYCS	13,61	16,33	15,98	17,14	15,34	24,47	-1,20	1,11	-1,33	1,33	0,45	Cytochrome c
SOD1	13,61	15,43	10,98	11,78	5,48	14,68	1,13	-1,28	1,44	1,44	0,45	Superoxide dismutase [Cu-Zn]
VPS29	0,97	0,00	2,00	1,07	1,10	1,96	1,00	3,16	-3,14	3,16	0,45	Isoform 1 of Vacuolar protein sorting-associated protein 29
PMVK	0,00	0,91	2,00	1,07	1,10	1,96	1,00	3,38	-3,37	3,38	0,45	Phosphomevalonate kinase
WARS	0,00	0,91	1,00	2,14	2,19	0,98	-1,01	3,46	-3,49	3,49	0,45	Tryptophanyl-tRNA synthetase, cytoplasmic
CFL1	27,22	41,74	31,95	27,85	30,69	25,45	1,07	-1,15	1,23	1,23	0,45	Cofilin-1
CCT3	12,64	12,70	13,98	19,28	23,01	11,75	-1,05	1,31	-1,37	1,37	0,45	chaperonin containing TCP1, subunit 3 isoform b
MT-ND5	3,89	0,91	5,99	3,21	2,19	4,89	1,30	1,92	-1,48	1,92	0,45	NADH-ubiquinone oxidoreductase chain 5
DNM1	127,34	118,87	111,83	110,32	110,69	134,11	-1,10	-1,11	1,01	1,11	0,45	Isoform 5 of Dynamin-1
TCP1	11,66	4,54	9,98	9,64	14,25	9,79	-1,22	1,21	-1,48	1,48	0,45	T-complex protein 1 subunit alpha
COL6A3	0,97	0,91	6,99	28,92	0,00	49,92	-1,39	19,11	-26,56	26,56	0,45	alpha 3 type VI collagen isoform 4 precursor
ACOT7	25,27	24,50	21,97	18,21	30,69	21,54	-1,30	-1,24	-1,05	1,30	0,46	Isoform 1 of Cytosolic acyl coenzyme A thioester hydrolase
ATP5H	17,50	12,70	16,97	19,28	17,54	22,51	-1,10	1,20	-1,33	1,33	0,46	Isoform 1 of ATP synthase subunit d, mitochondrial
HIST1H1E	9,72	15,43	6,99	12,85	9,86	7,83	1,12	-1,27	1,42	1,42	0,46	Histone H1.4
EEF1A2	18,47	11,80	13,98	15,00	9,86	11,75	1,34	-1,04	1,40	1,40	0,46	Elongation factor 1-alpha 2
C10orf58	6,80	3,63	7,99	6,43	7,67	8,81	-1,14	1,38	-1,58	1,58	0,46	Uncharacterized protein C10orf58
-	114,70	58,07	88,86	161,74	117,27	65,58	1,37	1,45	-1,06	1,45	0,46	NEFM protein
PSMA6	7,78	6,35	5,99	5,36	4,38	3,92	1,37	-1,25	1,70	1,70	0,46	Proteasome subunit alpha type-6

Gene Symbol	AD1 nc	AD2 nc	capCAA1 nc	capCAA2 nc	C1 nc	C2 nc	fc.cap-CAA/C	fc.capCAA/AD	fc. AD/C	fc. max	pvalues	Protein name
SV2B	11,66	9,07	11,98	2,14	5,48	7,83	1,06	-1,47	1,56	1,56	0,46	Synaptic vesicle glycoprotein 2B
DPP10	1,94	4,54	6,99	4,28	4,38	2,94	1,54	1,74	-1,13	1,74	0,46	DPPY splice variant c
LMNA	5,83	7,26	4,99	13,92	3,29	7,83	1,70	1,44	1,18	1,70	0,46	Progerin
NDUFV1	20,41	13,61	23,96	22,49	13,15	29,37	1,09	1,37	-1,25	1,37	0,46	Isoform 1 of NADH dehydrogenase [ubiquinone] flavoprotein 1, mitochondrial
CAP2	7,78	7,26	8,99	6,43	9,86	11,75	-1,40	1,03	-1,44	1,44	0,47	Adenylyl cyclase-associated protein 2
TPD52L2	3,89	4,54	3,99	2,14	1,10	2,94	1,52	-1,37	2,09	2,09	0,47	Isoform 2 of Tumor protein D54
RAB1A	27,22	22,68	22,96	21,42	19,73	18,60	1,16	-1,12	1,30	1,30	0,47	Isoform 1 of Ras-related protein Rab-1A
GNA11	1,94	2,72	3,00	2,14	1,10	0,98	2,48	1,10	2,25	2,48	0,47	Guanine nucleotide-binding protein subunit alpha-11
NEFH	42,77	24,50	27,96	73,91	30,69	29,37	1,70	1,51	1,12	1,70	0,47	Isoform 1 of Neurofilament heavy polypeptide
MAOB	12,64	24,50	14,98	16,07	31,78	15,66	-1,53	-1,20	-1,28	1,53	0,47	Amine oxidase [flavin-containing] B
AP3B2	6,80	2,72	11,98	3,21	7,67	7,83	-1,02	1,60	-1,63	1,63	0,47	AP-3 complex subunit beta-2
NDUFA9	16,53	11,80	19,97	15,00	7,67	17,62	1,38	1,23	1,12	1,38	0,47	NADH dehydrogenase [ubiquinone] 1 alpha subcomplex subunit 9, mitochondrial
ARF1	14,58	16,33	15,98	13,92	19,73	19,58	-1,31	-1,03	-1,27	1,31	0,47	ADP-ribosylation factor 1
AP2S1	2,92	1,81	1,00	1,07	0,00	1,96	1,06	-2,29	2,42	2,42	0,47	Isoform 1 of AP-2 complex subunit sigma-1
PSMC6	2,92	1,81	1,00	1,07	2,19	0,00	-1,06	-2,29	2,16	2,29	0,47	26S protease regulatory subunit S10B
NDRG2	14,58	19,96	20,97	19,28	19,73	25,45	-1,12	1,17	-1,31	1,31	0,48	Isoform 1 of Protein NDRG2
EIF4H	3,89	2,72	4,99	1,07	1,10	1,96	1,99	-1,09	2,16	2,16	0,48	Isoform Long of Eukaryotic translation initiation factor 4H
HSPD1	67,07	84,39	78,88	91,04	81,10	90,06	-1,01	1,12	-1,13	1,13	0,48	60 kDa heat shock protein, mitochondrial
EPDR1	13,61	8,17	7,99	11,78	3,29	10,77	1,41	-1,10	1,55	1,55	0,48	Isoform 1 of Mammalian ependymin-related protein 1
MTCH1	3,89	2,72	5,99	1,07	3,29	7,83	-1,57	1,07	-1,68	1,68	0,48	Isoform 1 of Mitochondrial carrier homolog 1
SLC8A1	0,97	1,81	2,00	0,00	3,29	1,96	-2,63	-1,40	-1,88	2,63	0,48	Isoform 1 of Sodium/calcium exchanger 1
RAB4A	1,94	0,91	3,00	2,14	1,10	0,98	2,48	1,80	1,37	2,48	0,48	RAB4A, member RAS oncogene family variant
SELENBP1	8,75	14,52	7,99	9,64	24,11	7,83	-1,81	-1,32	-1,37	1,81	0,48	cDNA FLJ55757, highly similar to Selenium-binding protein 1
HSPG2	0,00	0,91	0,00	11,78	1,10	8,81	1,19	12,98	-10,92	12,98	0,48	Basement membrane-specific heparan sulfate proteoglycan core protein
CAP1	8,75	10,89	12,98	10,71	16,44	11,75	-1,19	1,21	-1,44	1,44	0,48	Isoform 1 of Adenylyl cyclase-associated protein 1
GNAI1	10,69	9,07	11,98	11,78	15,34	12,73	-1,18	1,20	-1,42	1,42	0,48	Guanine nucleotide-binding protein G(i), alpha-1 subunit
PPP1R7	5,83	6,35	8,99	7,50	12,06	6,85	-1,15	1,35	-1,55	1,55	0,49	Isoform 1 of Protein phosphatase 1 regulatory subunit 7
EPB41L3	74,85	35,39	58,91	41,77	18,63	55,80	1,35	-1,09	1,48	1,48	0,49	Isoform A of Band 4.1-like protein 3
RAC1	16,53	17,24	11,98	13,92	19,73	14,68	-1,33	-1,30	-1,02	1,33	0,49	Isoform A of Ras-related C3 botulinum toxin substrate 1
ABAT	34,02	37,20	41,94	42,84	32,88	39,15	1,18	1,19	-1,01	1,19	0,49	cDNA FLJ56034, highly similar to 4-aminobutyrate aminotransferase, mitochondrial
LOC284889;MIF	9,72	9,98	6,99	6,43	7,67	6,85	-1,08	-1,47	1,36	1,47	0,49	Macrophage migration inhibitory factor
FABP7	6,80	9,07	6,99	4,28	4,38	5,87	1,10	-1,41	1,55	1,55	0,49	Fatty acid-binding protein, brain
BASP1	41,80	40,83	39,94	48,20	52,61	46,01	-1,12	1,07	-1,19	1,19	0,49	Brain acid soluble protein 1
NAPB	36,94	43,55	34,95	35,35	42,74	42,09	-1,21	-1,15	-1,05	1,21	0,49	cDNA FLJ52546, highly similar to Beta-soluble NSF attachment protein
SYNGR3	9,72	12,70	14,98	3,21	13,15	13,70	-1,48	-1,23	-1,20	1,48	0,49	Synaptogyrin-3
LRRC57	1,94	0,91	3,00	2,14	4,38	1,96	-1,23	1,80	-2,22	2,22	0,49	Leucine-rich repeat-containing protein 57
THY1	18,47	15,43	22,96	19,28	17,54	15,66	1,27	1,25	1,02	1,27	0,50	Thy-1 membrane glycoprotein
GNAQ	18,47	15,43	12,98	16,07	15,34	9,79	1,16	-1,17	1,35	1,35	0,50	Guanine nucleotide binding protein (G protein), q polypeptide, isoform CRA_c
TLN2	11,66	18,15	20,97	16,07	14,25	24,47	-1,05	1,24	-1,30	1,30	0,50	Talin-2
NEFL	129,28	91,65	104,84	191,73	134,80	95,93	1,29	1,34	-1,04	1,34	0,50	Neurofilament light polypeptide
ENO2	108,87	116,15	104,84	126,39	103,02	103,76	1,12	1,03	1,09	1,12	0,50	Gamma-enolase
CNTN2	7,78	5,44	8,99	8,57	3,29	7,83	1,58	1,33	1,19	1,58	0,50	Contactin-2
FIS1	1,94	4,54	2,00	2,14	3,29	4,89	-1,98	-1,57	-1,26	1,98	0,50	Mitochondrial fission 1 protein

Gene Symbol	AD1 nc	AD2 nc	capCAA1 nc	capCAA2 nc	C1 nc	C2 nc	fc.capCAA/C	fc.capCAA/AD	fc.AD/C	fc.max	pvalues	Protein name
KHSRP	0,00	0,91	3,99	0,00	0,00	0,98	4,08	4,40	-1,08	4,40	0,50	KH-type splicing regulatory protein
OCIAD1	3,89	2,72	3,00	0,00	1,10	2,94	-1,35	-2,21	1,64	2,21	0,50	Isoform 1 of OCIA domain-containing protein 1
RAB7A	17,50	14,52	16,97	12,85	21,92	17,62	-1,33	-1,07	-1,23	1,33	0,50	Ras-related protein Rab-7a
PROSC	3,89	2,72	2,00	2,14	1,10	1,96	1,36	-1,60	2,16	2,16	0,50	Proline synthetase co-transcribed bacterial homolog protein
HNRNPH3	2,92	3,63	3,00	1,07	1,10	1,96	1,33	-1,61	2,14	2,14	0,50	Isoform 1 of Heterogeneous nuclear ribonucleoprotein H3
NDUFV2	6,80	5,44	9,98	5,36	6,58	11,75	-1,19	1,25	-1,50	1,50	0,50	NADH dehydrogenase [ubiquinone] flavoprotein 2, mitochondrial
PDE2A	0,00	1,81	3,99	0,00	6,58	0,98	-1,89	2,20	-4,16	4,16	0,50	cGMP-dependent 3',5'-cyclic phosphodiesterase
CHCHD6	1,94	1,81	3,99	3,21	2,19	1,96	1,74	1,92	-1,10	1,92	0,51	Coiled-coil-helix-coiled-coil-helix domain-containing protein 6
CTNNA2	11,66	27,22	21,97	21,42	10,96	19,58	1,42	1,12	1,27	1,42	0,51	cDNA FLJ59799, highly similar to Alpha-2 catenin
CADM1	0,00	2,72	2,00	2,14	4,38	1,96	-1,53	1,52	-2,33	2,33	0,51	Isoform 1 of Cell adhesion molecule 1
PCCB	1,94	0,91	4,99	1,07	1,10	2,94	1,50	2,13	-1,41	2,13	0,51	Propionyl-CoA carboxylase beta chain, mitochondrial
USP14	1,94	4,54	5,99	3,21	7,67	3,92	-1,26	1,42	-1,79	1,79	0,51	Ubiquitin carboxyl-terminal hydrolase 14
HIST2H2AB	15,55	23,59	15,98	13,92	16,44	19,58	-1,20	-1,31	1,09	1,31	0,51	Histone H2A type 2-B
CEND1	10,69	9,07	7,99	10,71	4,38	8,81	1,42	-1,06	1,50	1,50	0,51	Cell cycle exit and neuronal differentiation protein 1
AHCY	13,61	10,89	7,99	9,64	14,25	9,79	-1,36	-1,39	1,02	1,39	0,51	Adenosylhomocysteinase
PRKACA	2,92	0,91	2,00	0,00	2,19	2,94	-2,57	-1,91	-1,34	2,57	0,51	Isoform 2 of cAMP-dependent protein kinase catalytic subunit alpha
NDUFA2	0,97	2,72	2,00	0,00	1,10	3,92	-2,51	-1,85	-1,36	2,51	0,51	NADH dehydrogenase [ubiquinone] 1 alpha subcomplex subunit 2
YARS	1,94	1,81	2,00	0,00	3,29	1,96	-2,63	-1,88	-1,40	2,63	0,51	Tyrosyl-tRNA synthetase, cytoplasmic
RPS21	0,97	2,72	1,00	1,07	2,19	2,94	-2,48	-1,79	-1,39	2,48	0,51	40S ribosomal protein S21
CPNE6	7,78	7,26	7,99	9,64	18,63	5,87	-1,39	1,17	-1,63	1,63	0,51	cDNA FLJ55997, highly similar to Copine-6
TPM4	9,72	9,07	4,99	7,50	7,67	7,83	-1,24	-1,50	1,21	1,50	0,51	Isoform 1 of Tropomyosin alpha-4 chain
ACAD9	0,97	0,00	1,00	0,00	0,00	2,94	-2,94	1,03	-3,02	3,02	0,52	Acyl-CoA dehydrogenase family member 9, mitochondrial
ETFB	3,89	4,54	4,99	7,50	6,58	6,85	-1,08	1,48	-1,59	1,59	0,52	Isoform 1 of Electron transfer flavoprotein subunit beta
RALA	9,72	6,35	8,99	8,57	15,34	7,83	-1,32	1,09	-1,44	1,44	0,52	Ras-related protein Ral-A
DECR1	6,80	8,17	9,98	7,50	4,38	6,85	1,56	1,17	1,33	1,56	0,52	2,4-dienoyl-CoA reductase, mitochondrial
MDH1	69,02	78,04	64,90	69,62	62,47	66,56	1,04	-1,09	1,14	1,14	0,52	Malate dehydrogenase, cytoplasmic
TMX4	0,97	0,00	3,00	0,00	0,00	0,98	3,06	3,08	-1,01	3,08	0,52	Thioredoxin domain-containing protein 13
RHOA	19,44	17,24	12,98	17,14	21,92	17,62	-1,31	-1,22	-1,08	1,31	0,52	Transforming protein RhoA
PIN1	9,72	10,89	6,99	8,57	8,77	5,87	1,06	-1,32	1,41	1,41	0,52	Peptidyl-prolyl cis-trans isomerase NIMA-interacting 1
VIM	30,13	76,78	55,91	94,26	36,17	85,16	1,24	1,49	-1,20	1,49	0,52	Vimentin
DCTN2	5,83	9,98	5,99	4,28	8,77	5,87	-1,42	-1,54	1,08	1,54	0,52	dynactin 2
-	2,92	3,63	2,00	1,07	2,19	2,94	-1,67	-2,13	1,28	2,13	0,52	14 kDa protein
RABC	4,86	3,63	3,00	2,14	5,48	3,92	-1,83	-1,65	-1,11	1,83	0,52	Ras-related protein Rab-3C
MAG	12,64	11,80	7,99	20,35	14,25	3,92	1,56	1,16	1,35	1,56	0,52	Myelin-associated glycoprotein
NDUFB7	0,97	0,00	0,00	1,07	0,00	2,94	-2,74	1,10	-3,02	3,02	0,53	NADH dehydrogenase [ubiquinone] 1 beta subcomplex subunit 7
KRT5	8,75	1,81	4,99	0,00	5,48	2,94	-1,69	-2,12	1,26	2,12	0,53	Keratin, type II cytoskeletal 5
CRMP1	39,85	40,83	49,92	29,99	65,76	37,20	-1,29	-1,01	-1,28	1,29	0,53	collapsin response mediator protein 1 isoform 1
TOMM70A	18,47	11,80	17,97	21,42	16,44	18,60	1,12	1,30	-1,16	1,30	0,53	Mitochondrial import receptor subunit TOM70
HYOU1	2,92	4,54	5,99	6,43	4,38	5,87	1,21	1,67	-1,38	1,67	0,53	Hypoxia up-regulated protein 1
AP2A2	22,36	29,94	29,95	22,49	28,49	34,26	-1,20	1,00	-1,20	1,20	0,53	Isoform 1 of AP-2 complex subunit alpha-2
GPR158	0,97	0,00	2,00	0,00	1,10	1,96	-1,53	2,05	-3,14	3,14	0,53	Probable G-protein coupled receptor 158
SACM1L	0,00	0,91	1,00	1,07	1,10	1,96	-1,48	2,28	-3,37	3,37	0,53	Phosphatidylinositide phosphatase SAC1
RPL7A	0,97	0,00	2,00	0,00	1,10	1,96	-1,53	2,05	-3,14	3,14	0,53	60S ribosomal protein L7a

Gene Symbol	AD1 nc	AD2 nc	capCAA1 nc	capCAA2 nc	C1 nc	C2 nc	fc.cap-CAA/C	fc.capCAA/AD	fc. AD/C	fc. max	pvalues	Protein name
LAMA5	0.97	0.00	1.00	1.07	0.00	2.94	-1.42	2.13	-3.02	3.02	0.53	Laminin subunit alpha-5
TMEM126A	0.97	0.00	1.00	1.07	0.00	2.94	-1.42	2.13	-3.02	3.02	0.53	Transmembrane protein 126A
IPO7	0.97	0.00	1.00	1.07	2.19	0.98	-1.53	2.13	-3.26	3.26	0.53	Importin-7
KPNA6	0.00	0.91	1.00	1.07	2.19	0.98	-1.53	2.28	-3.49	3.49	0.53	cDNA FLJ53229, highly similar to Importin alpha-7 subunit
NPC2	0.97	0.00	1.00	1.07	2.19	0.98	-1.53	2.13	-3.26	3.26	0.53	cDNA FLJ59142, highly similar to Epididymal secretory protein E1
C21orf33	6.80	8.17	10.98	10.71	5.48	12.73	1.19	1.45	-1.22	1.45	0.53	Isoform Long of ES1 protein homolog, mitochondrial
CAPZB	18.47	19.06	15.98	12.85	15.34	15.66	-1.08	-1.30	1.21	1.30	0.54	cDNA, FLJ93598, highly similar to Homo sapiens capping protein (actin filament) muscle Z-line, beta (CAPZB), mRNA
LASP1	5.83	5.44	4.99	2.14	1.10	5.87	1.02	-1.58	1.62	1.62	0.54	Isoform 1 of LIM and SH3 domain protein 1
C1orf123	0.97	1.81	0.00	1.07	1.10	0.00	-1.02	-2.60	2.54	2.60	0.54	UPF0587 protein C1orf123
FKBP1B	1.94	0.91	1.00	0.00	0.00	0.98	1.02	-2.86	2.91	2.91	0.54	Isoform 1 of Peptidyl-prolyl cis-trans isomerase FKBP1B
CDC37	1.94	0.91	1.00	0.00	1.10	0.00	-1.10	-2.86	2.60	2.86	0.54	Hsp90 co-chaperone Cdc37
DPP3	1.94	0.91	1.00	0.00	1.10	0.00	-1.10	-2.86	2.60	2.86	0.54	Isoform 1 of Dipeptidyl-peptidase 3
RPS3	9.72	4.54	10.98	4.28	1.10	7.83	1.71	1.07	1.60	1.71	0.54	40S ribosomal protein S3
ACO2	87.49	90.74	82.87	101.75	83.29	122.36	-1.11	1.04	-1.15	1.15	0.54	Aconitate hydratase, mitochondrial
MAPRE2	4.86	5.44	3.00	5.36	8.77	4.89	-1.64	-1.23	-1.33	1.64	0.54	Isoform 1 of Microtubule-associated protein RP/EB family member 2
CYB5R2	0.97	0.00	1.00	1.07	3.29	0.00	-1.59	2.13	-3.38	3.38	0.54	Isoform 1 of NADH-cytochrome b5 reductase 2
LAMC1	0.00	2.72	1.00	5.36	2.19	1.96	1.53	2.33	-1.52	2.33	0.54	Laminin subunit gamma-1
RPL13	2.92	0.91	3.99	2.14	2.19	4.89	-1.15	1.60	-1.85	1.85	0.54	60S ribosomal protein L13
DYNLRB1	0.97	1.81	1.00	0.00	1.10	1.96	-3.06	-2.79	-1.10	3.06	0.55	Dynein, light chain, roadblock-type 1
MTAP	0.97	1.81	0.00	1.07	1.10	1.96	-2.85	-2.60	-1.10	2.85	0.55	cDNA FLJ59758, highly similar to S-methyl-5-thioadenosine phosphorylase
-	2.92	0.00	2.00	1.07	0.00	0.98	3.13	1.05	2.98	3.13	0.55	cDNA FLJ59764, highly similar to Apolipoprotein-L2
OSBPL1A	0.97	1.81	2.00	1.07	0.00	0.98	3.13	2.13	2.85	3.13	0.55	Isoform B of Oxysterol-binding protein-related protein 1
CCBL2	1.94	0.91	3.00	0.00	0.00	0.98	3.06	2.33	2.91	3.06	0.55	kynurenine aminotransferase III isoform 3
PCBP1	9.72	9.98	14.98	9.64	13.15	13.70	-1.09	1.60	-1.36	1.36	0.55	Poly(rC)-binding protein 1
CNRIP1	1.94	4.54	3.00	2.14	4.38	4.89	-1.81	1.25	-1.43	1.81	0.55	Isoform 1 of CB1 cannabinoid receptor-interacting protein 1
TPM1	1.94	4.54	3.00	2.14	5.48	3.92	-1.83	-1.26	-1.45	1.83	0.55	tropomyosin 1 alpha chain isoform 7
PAFAH1B1	7.78	3.63	6.99	1.07	5.48	7.83	-1.65	-1.42	-1.17	1.65	0.55	Isoform 1 of Platelet-activating factor acetylhydrolase IB subunit alpha
STK39	1.94	0.91	0.00	3.21	1.10	0.00	2.93	1.13	2.60	2.93	0.55	STE20/SPS1-related proline-alanine-rich protein kinase
NME1-NME2	18.47	21.78	19.97	24.64	24.11	26.43	-1.13	1.11	-1.26	1.26	0.55	Nucleoside diphosphate kinase
ETFA	14.58	12.70	11.98	20.35	8.77	14.68	1.38	1.19	1.16	1.38	0.55	Electron transfer flavoprotein subunit alpha, mitochondrial
KRT2	46.66	23.59	33.95	16.07	28.49	28.39	-1.14	-1.40	1.24	1.40	0.55	Keratin, type II cytoskeletal 2 epidermal
ATP6V1E1	26.25	25.41	26.96	26.78	21.92	21.54	1.24	1.04	1.19	1.24	0.55	V-type proton ATPase subunit E 1
SULT4A1	1.94	2.72	3.99	4.28	3.29	1.96	1.58	1.77	-1.12	1.77	0.55	Isoform 1 of Sulfotransferase 4A1
ECHDC1	3.89	3.63	3.00	4.28	2.19	1.96	1.75	-1.03	1.81	1.81	0.55	Isoform 1 of Enoyl-CoA hydratase domain -containing protein 1
ATP5L	17.50	11.80	12.98	8.57	7.67	15.66	-1.08	-1.36	1.26	1.36	0.55	ATP synthase subunit g, mitochondrial
SEPT8	11.66	14.52	10.98	8.57	15.34	10.77	-1.34	-1.34	1.00	1.34	0.55	Isoform 2 of Septin-8
NCAN	17.50	11.80	11.98	11.78	10.96	10.77	1.09	-1.23	1.35	1.35	0.56	Neurocan core protein
SLC25A4	7.78	9.98	10.98	13.92	8.77	11.75	1.21	1.40	-1.16	1.40	0.56	ADP/ATP translocase 1
TUFM	17.50	14.52	16.97	13.92	14.25	24.47	-1.25	-1.04	-1.21	1.25	0.56	Tu translation elongation factor, mitochondrial precursor
PREP	2.92	0.00	3.99	1.07	0.00	1.96	2.59	1.74	1.49	2.59	0.56	Prolyl endopeptidase
DDX3X	5.83	0.91	2.00	1.07	1.10	2.94	-1.31	-2.20	1.67	2.20	0.56	ATP-dependent RNA helicase DDX3X
STX12	3.89	0.91	5.99	2.14	1.10	3.92	1.62	1.70	-1.04	1.70	0.56	Syntaxin-12
ACAT2	5.83	4.54	3.00	3.21	5.48	1.96	-1.20	-1.67	1.39	1.67	0.56	cDNA FLJ53975, highly similar to Acetyl-CoA acetyltransferase, cytosolic

Gene Symbol	AD1 nc	AD2 nc	capCAA1 nc	capCAA2 nc	C1 nc	C2 nc	fc.cap-CAA/C	fc.capCAA/AD	fc. AD/C	fc. max	pvalues	Protein name
TUBA8	4,86	2,72	6,99	4,28	1,10	5,87	1,62	1,49	1,09	1,62	0,56	Tubulin alpha-8 chain
PEBP1	50,55	45,37	44,93	40,70	55,89	45,03	-1,18	-1,12	-1,05	1,18	0,56	Phosphatidylethanolamine-binding protein 1
NDUFB8	1,94	1,81	2,00	3,21	4,38	2,94	-1,40	1,39	-1,95	1,95	0,56	NADH dehydrogenase [ubiquinone] 1 beta subcomplex subunit 8, mitochondrial
GUK1	0,97	2,72	2,00	1,07	2,19	3,92	-1,99	-1,20	-1,65	1,99	0,56	Guanylate kinase
BAIAP2	1,94	1,81	2,00	1,07	4,38	1,96	-2,07	-1,23	-1,69	2,07	0,56	Isoform 5 of Brain-specific angiogenesis inhibitor 1-associated protein 2
UBE2L3	0,97	2,72	4,99	2,14	2,19	2,94	1,39	1,93	-1,39	1,93	0,56	Ubiquitin-conjugating enzyme E2 L3
PCYOX1	1,94	1,81	2,00	5,36	2,19	2,94	1,43	1,96	-1,36	1,96	0,56	Prenylcysteine oxidase 1
MAPRE3	9,72	6,35	7,99	5,36	9,86	9,79	-1,47	-1,20	-1,22	1,47	0,56	Isoform 1 of Microtubule-associated protein RP/EB family member 3
UBE2K	1,94	1,81	3,99	2,14	2,19	0,98	1,94	1,63	1,19	1,94	0,56	Isoform 1 of Ubiquitin-conjugating enzyme E2 K
VCL	1,94	4,54	2,00	15,00	4,38	7,83	1,39	2,62	-1,88	2,62	0,56	Isoform 1 of Vinculin
ATP6V1G2	11,66	12,70	7,99	9,64	9,86	11,75	-1,23	-1,38	1,13	1,38	0,57	V-type proton ATPase subunit G 2
PGRMC2	1,94	2,72	2,00	0,00	2,19	1,96	-2,08	-2,34	1,12	2,34	0,57	Membrane-associated progesterone receptor component 2
CRKL	2,92	1,81	2,00	2,14	1,10	0,98	1,99	-1,14	2,28	2,28	0,57	Crk-like protein
HSPE1	5,83	8,17	3,00	6,43	5,48	7,83	-1,41	-1,49	1,05	1,49	0,57	10 kDa heat shock protein, mitochondrial
SLC25A11	24,30	17,24	22,96	18,21	17,54	33,28	-1,23	-1,01	-1,22	1,23	0,57	Mitochondrial 2-oxoglutarate/malate carrier protein
SLC2A3	7,78	4,54	11,98	5,36	9,86	6,85	1,04	1,41	-1,36	1,41	0,57	Solute carrier family 2, facilitated glucose transporter member 3
EEF2	21,39	16,33	18,97	9,64	12,06	20,56	-1,14	-1,32	1,16	1,32	0,57	Elongation factor 2
HSD17B12	5,83	3,63	5,99	8,57	5,48	5,87	1,28	1,54	-1,20	1,54	0,57	Estradiol 17-beta-dehydrogenase 12
ATP6V1B2	63,18	62,61	73,89	62,12	71,24	71,46	-1,05	1,08	-1,13	1,13	0,57	V-type proton ATPase subunit B, brain isoform
LDHB	85,54	98,00	85,87	95,33	89,87	76,35	1,09	-1,01	1,10	1,10	0,57	L-lactate dehydrogenase B chain
RPL23	4,86	5,44	3,99	2,14	3,29	5,87	-1,49	-1,68	1,12	1,68	0,57	60S ribosomal protein L23
CTSD	28,19	27,22	18,97	26,78	24,11	29,37	-1,17	-1,21	1,04	1,21	0,57	Cathepsin D
TPD52	10,69	8,17	7,99	10,71	6,58	6,85	1,39	-1,01	1,40	1,40	0,57	Isoform 1 of Tumor protein D52
NDUFA13	6,80	5,44	3,99	5,36	5,48	8,81	-1,53	-1,31	-1,17	1,53	0,58	NADH dehydrogenase (ubiquinone) 1 alpha subcomplex, 13
PCMT1	17,50	16,33	11,98	13,92	17,54	11,75	-1,13	-1,31	1,16	1,31	0,58	Isoform 2 of Protein-L-isoaspartate(D-aspartate) O-methyltransferase
ENO1	120,54	137,02	124,81	128,53	135,90	100,82	1,07	-1,02	1,09	1,09	0,58	Isoform alpha-enolase of Alpha-enolase
ATP6V1G1	0,97	0,91	2,00	0,00	3,29	0,98	-2,14	2,16	-2,27	2,27	0,58	V-type proton ATPase subunit G 1
MLF2	1,94	0,00	2,00	0,00	1,10	2,94	-2,02	1,03	-2,07	2,07	0,58	Myeloid leukemia factor 2
ACO1	0,97	0,91	2,00	0,00	2,19	1,96	-2,08	1,06	-2,21	2,21	0,58	Cytoplasmic aconitate hydratase
VPS26A	0,97	0,91	2,00	0,00	2,19	1,96	-2,08	1,06	-2,21	2,21	0,58	Vacuolar protein sorting-associated protein 26A
CYB5R1	0,97	0,91	1,00	1,07	3,29	0,98	-2,06	1,10	-2,27	2,27	0,58	NADH-cytochrome b5 reductase 1
GABRB2	5,83	1,81	7,99	1,07	0,00	3,92	2,31	1,18	1,95	2,31	0,58	Isoform Short of Gamma-aminobutyric acid receptor subunit beta-2
TBCA	0,97	0,91	3,00	1,07	1,10	0,98	1,96	2,16	-1,10	2,16	0,58	Tubulin-specific chaperone A
PIP4K2A	7,78	6,35	2,00	10,71	6,58	1,96	1,49	-1,11	1,66	1,66	0,58	Phosphatidylinositol-5-phosphate 4-kinase type-2 alpha
BRP44	1,94	2,72	6,99	1,07	3,29	3,92	1,12	1,73	-1,54	1,73	0,58	Brain protein 44
HPCA	2,92	1,81	2,00	0,00	2,19	0,98	-1,59	-2,37	1,49	2,37	0,58	Neuron-specific calcium-binding protein hippocalcin
NEDD8	2,92	1,81	0,00	2,14	1,10	1,96	-1,43	-2,21	1,55	2,21	0,58	NEDD8
DNAJB6	2,92	1,81	1,00	1,07	1,10	1,96	-1,48	-2,29	1,55	2,29	0,58	Isoform A of DnaJ homolog subfamily B member 6
SRP14	2,92	1,81	1,00	1,07	1,10	1,96	-1,48	-2,29	1,55	2,29	0,58	Signal recognition particle 14 kDa protein
PSMA3	3,89	0,91	0,00	2,14	2,19	0,98	1,57	-2,24	2,42	2,24	0,58	Isoform 2 of Proteasome subunit alpha type-3
RPS9	2,92	1,81	2,00	1,07	0,00	1,96	1,40	-1,54	2,42	2,42	0,58	40S ribosomal protein S9
PSMD13	3,89	0,91	2,00	1,07	2,19	0,00	1,40	-1,56	2,19	2,19	0,58	proteasome 26S non-ATPase subunit 13 isoform 2
SLC25A3	36,94	24,50	32,95	27,85	30,69	40,13	-1,16	-1,01	-1,15	1,16	0,58	Isoform B of Phosphate carrier protein, mitochondrial

Gene Symbol	AD1 nc	AD2 nc	capCAA1 nc	capCAA2 nc	C1 nc	C2 nc	fc.cap-CAA/C	fc.capCAA/AD	fc.AD/C	fc. max	pvalues	Protein name
ARL8B	3,89	3,63	6,99	4,28	4,38	6,85	1,00	1,50	-1,49	1,50	0,58	cDNA FLJ56285, highly similar to ADP-ribosylation factor-like protein 8B
CSTB	2,92	4,54	1,00	3,21	3,29	1,96	-1,25	-1,77	1,42	1,77	0,59	Cystatin-B
GLUL	47,63	33,57	38,94	26,78	15,34	46,99	1,05	-1,24	1,30	1,30	0,59	Glutamine synthetase
MAP2K1	7,78	9,98	11,98	8,57	9,86	4,89	1,39	1,16	1,20	1,39	0,59	Dual specificity mitogen-activated protein kinase kinase 1
STX7	2,92	2,72	3,99	2,14	7,67	1,96	-1,57	1,09	-1,71	1,71	0,59	Isoform 1 of Syntaxin-7
THEM2	3,89	1,81	3,00	3,21	4,38	4,89	-1,49	1,09	-1,63	1,63	0,59	Thioesterase superfamily member 2
GAP43	16,53	22,68	14,98	20,35	26,30	18,60	-1,27	-1,11	-1,15	1,27	0,59	Neuromodulin
COL1A1	0,00	0,91	1,00	3,21	0,00	11,75	-2,79	4,64	-12,95	12,95	0,59	Collagen alpha-1(I) chain
FARSA	0,97	0,91	1,00	0,00	0,00	2,94	-2,94	-1,88	-1,56	2,94	0,59	Phenylalanyl-tRNA synthetase alpha chain
C14orf156	1,94	0,00	1,00	0,00	1,10	1,96	-3,06	-1,95	-1,57	3,06	0,59	SRA stem-loop-interacting RNA-binding protein, mitochondrial
SVIP	0,00	1,81	0,00	1,07	1,10	1,96	-2,85	-1,69	-1,68	2,85	0,59	Small VCP/p97-interacting protein
GLRX5	1,94	0,00	1,00	0,00	2,19	0,98	-3,18	-1,95	-1,63	3,18	0,59	Glutaredoxin-related protein 5
ATP1A3	268,29	238,64	265,59	258,13	247,68	288,77	-1,02	1,03	-1,06	1,06	0,59	Sodium/potassium-transporting ATPase subunit alpha-3
CIRBP	0,97	0,91	3,00	0,00	0,00	0,98	3,06	1,59	1,92	3,06	0,59	Cold-inducible RNA-binding protein
SLC6A7	0,97	0,91	3,00	0,00	1,10	0,00	2,73	1,59	1,71	2,73	0,59	Sodium-dependent proline transporter
HNRNPA0	1,94	0,00	2,00	1,07	0,00	0,98	3,13	1,58	1,99	3,13	0,59	Heterogeneous nuclear ribonucleoprotein A0
HGS	1,94	0,00	1,00	2,14	0,00	0,98	3,21	1,62	1,99	3,21	0,59	Isoform 1 of Hepatocyte growth factor-regulated tyrosine kinase substrate
PPP3R1	9,72	8,17	9,98	6,43	6,58	5,87	1,32	-1,09	1,44	1,44	0,59	Calcineurin subunit B type 1
MGST3	12,64	9,07	9,98	7,50	7,67	7,83	1,13	-1,24	1,40	1,40	0,59	Microsomal glutathione S-transferase 3
SLC2A13	0,97	0,91	0,00	0,00	3,29	0,00	-3,29	-1,88	-1,75	3,29	0,59	solute carrier family 2 (facilitated glucose transporter), member 13
ACAA1	2,92	2,72	2,00	1,07	0,00	2,94	1,04	-1,84	1,92	1,92	0,59	3-ketoacyl-CoA thiolase, peroxisomal
NINJ2	0,97	0,91	0,00	1,07	5,48	0,00	-5,12	-1,75	-2,92	5,12	0,59	Ninjurin-2
TMEM205	0,97	0,91	3,99	0,00	1,10	0,98	1,92	2,13	-1,10	2,13	0,59	Transmembrane protein 205
FAM49B	20,41	14,52	14,98	15,00	14,25	12,73	1,11	-1,17	1,30	1,30	0,60	Protein FAM49B
RAP2A	6,80	6,35	9,98	4,28	9,86	8,81	-1,31	1,08	-1,42	1,42	0,60	Ras-related protein Rap-2a
HBA2;HBA1	106,93	126,13	64,90	118,89	76,72	194,79	-1,48	-1,27	-1,17	1,48	0,60	Hemoglobin subunit alpha
GNAS	5,83	5,44	7,99	8,57	6,58	6,85	1,23	1,47	-1,19	1,47	0,60	Isoform XLas-1 of Guanine nucleotide-binding protein G(s) subunit alpha isoforms XLas
PRKAR2B	15,55	14,52	16,97	9,64	8,77	13,70	1,18	-1,13	1,34	1,34	0,60	cAMP-dependent protein kinase type II-beta regulatory subunit
TUBB2B	67,07	75,31	77,88	72,83	105,21	64,61	-1,13	1,06	-1,19	1,19	0,60	Tubulin beta-2B chain
RPS28	2,92	1,81	3,00	0,00	3,29	2,94	-2,08	-1,58	-1,32	2,08	0,60	40S ribosomal protein S28
TST	2,92	1,81	3,00	0,00	3,29	2,94	-2,08	-1,58	-1,32	2,08	0,60	Thiosulfate sulfurtransferase
GMFB	1,94	2,72	1,00	2,14	2,19	3,92	-1,94	-1,49	-1,31	1,94	0,60	Glia maturation factor, beta
ATP6V1H	18,47	17,24	24,96	19,28	20,82	17,62	1,15	1,24	-1,08	1,24	0,60	Isoform 1 of V-type proton ATPase subunit H
ISCU	3,89	0,91	3,99	2,14	0,00	2,94	2,09	1,28	1,63	2,09	0,60	Isoform 1 of Iron-sulfur cluster assembly enzyme ISCU, mitochondrial
CCT8	14,58	18,15	15,98	22,49	27,40	14,68	-1,09	1,18	-1,29	1,29	0,60	T-complex protein 1 subunit theta
PHB2	15,55	13,61	15,98	17,14	14,25	22,51	-1,11	1,14	-1,26	1,26	0,60	Prohibitin-2
ACYP2	5,83	2,72	3,00	3,21	7,67	2,94	-1,71	-1,38	-1,24	1,71	0,60	Acylphosphatase-2
ADD1	36,94	46,28	33,95	38,56	36,17	37,20	-1,01	-1,15	1,13	1,15	0,60	Adducin 1
SH3BGRL	5,83	8,17	4,99	4,28	6,58	5,87	-1,34	-1,51	1,12	1,51	0,60	SH3 domain-binding glutamic acid-rich-like protein
SEPT4	8,75	4,54	3,99	6,43	8,77	6,85	-1,50	-1,27	-1,18	1,50	0,60	cDNA FLJ55761, highly similar to Septin-4
COX4I1	16,53	16,33	13,98	11,78	15,34	11,75	-1,05	-1,28	1,21	1,28	0,60	Cytochrome c oxidase subunit 4 isoform 1, mitochondrial
ATP5J	3,89	3,63	3,99	2,14	0,00	3,92	1,57	-1,23	1,92	1,92	0,60	ATP synthase, H+ transporting, mitochondrial F0 complex, subunit E
CAMK2B	27,22	29,04	24,96	21,42	24,11	29,37	-1,15	-1,21	1,05	1,21	0,60	calcium/calmodulin-dependent protein kinase II beta isoform 1

Gene Symbol	AD1 nc	AD2 nc	capCAA1 nc	capCAA2 nc	C1 nc	C2 nc	fc.cap-CAA/C	fc.capCAA/AD	fc. AD/C	fc. max	pvalues	Protein name
STX1B	59,30	51,72	51,92	44,99	43,84	55,80	-1,03	-1,15	1,11	1,15	0,60	Syntaxin-1B
HBB	164,28	188,74	138,79	188,51	150,14	251,27	-1,23	-1,08	-1,14	1,23	0,61	Hemoglobin subunit beta
ATP5O	23,33	18,15	24,96	24,64	14,25	26,43	1,22	1,20	1,02	1,22	0,61	ATP synthase subunit O, mitochondrial
LMNB2	8,75	4,54	7,99	1,07	2,19	5,87	1,12	-1,47	1,65	1,65	0,61	Lamin-B2
ATP2B3	12,64	10,89	12,98	5,36	5,48	11,75	1,06	-1,28	1,37	1,37	0,61	Isoform XB of Plasma membrane calcium-transporting ATPase 3
BDH1	5,83	6,35	6,99	7,50	6,58	10,77	-1,20	1,19	-1,42	1,42	0,61	D-beta-hydroxybutyrate dehydrogenase, mitochondrial
GSN	28,19	29,94	29,95	48,20	51,51	23,49	1,04	1,34	-1,29	1,34	0,61	Isoform 1 of Gelsolin
STIP1	7,78	9,98	3,99	8,57	9,86	5,87	-1,25	-1,41	1,13	1,41	0,61	Stress-induced-phosphoprotein 1
ATP6V0A1	41,80	50,81	48,93	29,99	38,36	51,88	-1,14	-1,17	1,03	1,17	0,61	Isoform 2 of V-type proton ATPase 116 kDa subunit a isoform 1
PVALB	4,86	0,00	1,00	1,07	0,00	0,98	2,11	-2,35	4,97	4,97	0,61	Parvalbumin alpha
SLC25A12	60,27	50,81	65,90	69,62	30,69	82,23	1,20	1,22	-1,02	1,22	0,61	Calcium-binding mitochondrial carrier protein Aralar1
RPS4X	5,83	5,44	4,99	2,14	3,29	4,89	-1,15	-1,58	1,38	1,58	0,61	40S ribosomal protein S4, X isoform
PCBP2	4,86	6,35	3,99	3,21	5,48	2,94	-1,17	-1,56	1,33	1,56	0,61	poly(rC) binding protein 2 isoform b
SARS	3,89	4,54	3,00	2,14	5,48	2,94	-1,64	-1,64	1,00	1,64	0,61	Seryl-tRNA synthetase, cytoplasmic
HADH	6,80	3,63	2,00	5,36	5,48	5,87	-1,54	-1,42	-1,09	1,54	0,62	Isoform 1 of Hydroxyacyl-coenzyme A dehydrogenase, mitochondrial
CPLX2	6,80	3,63	4,99	2,14	4,38	6,85	-1,57	-1,46	-1,08	1,57	0,62	Complexin-2
GNAO1	123,45	144,27	137,79	134,96	140,28	112,57	1,08	1,02	1,06	1,08	0,62	Isoform Alpha-1 of Guanine nucleotide-binding protein G(o) subunit alpha
NAPA	13,61	11,80	17,97	13,92	12,06	13,70	1,24	1,26	-1,01	1,26	0,62	Alpha-soluble NSF attachment protein
FBXO2	11,66	9,07	12,98	13,92	17,54	8,81	1,02	1,30	-1,27	1,30	0,62	F-box only protein 2
SYN1	90,40	123,40	107,84	100,68	113,98	115,51	-1,10	-1,03	-1,07	1,10	0,62	Isoform 1A of Synapsin-1
GABARAPL2	6,80	4,54	4,99	2,14	6,58	3,92	-1,47	-1,59	1,08	1,59	0,62	Gamma-aminobutyric acid receptor-associated protein-like 2
MBOAT7	2,92	1,81	3,00	1,07	4,38	2,94	-1,80	-1,16	-1,55	1,80	0,62	Putative uncharacterized protein MBOAT7
GABBR2	1,94	2,72	3,00	1,07	2,19	4,89	-1,74	-1,15	-1,52	1,74	0,62	Gamma-aminobutyric acid type B receptor subunit 2
ARPC1A	2,92	1,81	3,99	0,00	4,38	2,94	-1,83	-1,18	-1,55	1,83	0,62	Actin-related protein 2/3 complex subunit 1A
KRT10	88,46	46,28	71,89	28,92	76,72	48,94	-1,25	-1,34	1,07	1,34	0,62	Keratin, type I cytoskeletal 10
AP1G1	1,94	2,72	2,00	5,36	1,10	2,94	1,82	1,58	1,16	1,82	0,62	adaptor-related protein complex 1, gamma 1 subunit isoform a
CS	31,11	36,30	39,94	39,63	27,40	50,90	1,02	1,18	-1,16	1,18	0,62	Citrate synthase, mitochondrial
INA	64,16	36,30	53,92	70,69	72,33	42,09	1,09	1,24	-1,14	1,24	0,62	Alpha-internexin
GRIA3	0,00	0,91	2,00	0,00	0,00	2,94	-1,47	2,20	-3,24	3,24	0,62	Isoform Flop of Glutamate receptor 3
GBAS	9,72	8,17	5,99	7,50	6,58	11,75	-1,36	-1,33	-1,02	1,36	0,62	Protein NipSnap homolog 2
GPM6B	9,72	6,35	10,98	6,43	8,77	12,73	-1,23	1,08	-1,34	1,34	0,62	glycoprotein M6B isoform 1
RAB27B	0,97	0,91	1,00	1,07	4,38	0,00	-2,12	1,10	-2,33	2,33	0,62	Ras-related protein Rab-27B
GSTT1	2,92	0,00	1,00	0,00	0,00	0,98	1,02	-2,92	2,98	2,98	0,62	Glutathione S-transferase theta-1
NDUFS8	8,75	5,44	9,98	6,43	7,67	11,75	-1,18	1,16	-1,37	1,37	0,62	NADH dehydrogenase [ubiquinone] iron-sulfur protein 8, mitochondrial
SYNCRIP	1,94	0,91	2,00	3,21	2,19	2,94	1,02	1,83	-1,80	1,83	0,62	Isoform 1 of Heterogeneous nuclear ribonucleoprotein Q
NCSTN	1,94	0,91	1,00	4,28	3,29	1,96	1,01	1,85	-1,84	1,85	0,62	Isoform 1 of Nicastrin
HK1	105,96	122,50	116,82	138,17	104,11	141,94	1,04	1,12	-1,08	1,12	0,63	Isoform 1 of Hexokinase-1
NEGR1	6,80	12,70	7,99	7,50	6,58	7,83	1,07	-1,26	1,35	1,35	0,63	Neuronal growth regulator 1
OXCT1	25,27	26,31	31,95	28,92	19,73	32,30	1,17	1,18	-1,01	1,18	0,63	Succinyl-CoA:3-ketoacid-coenzyme A transferase 1, mitochondrial
BRI3BP	3,89	0,00	3,99	0,00	3,29	2,94	-1,56	1,03	-1,60	1,60	0,63	BRI3-binding protein
CTBP1	7,78	8,17	6,99	4,28	6,58	8,81	-1,36	-1,41	1,04	1,41	0,63	C-terminal-binding protein 1
CCT6A	7,78	7,26	7,99	9,64	13,15	7,83	-1,19	1,17	-1,40	1,40	0,63	T-complex protein 1 subunit zeta
SUCLG1	7,78	3,63	8,99	6,43	7,67	7,83	-1,01	1,35	-1,36	1,36	0,63	Succinyl-CoA ligase [GDP-forming] subunit alpha, mitochondrial

Gene Symbol	AD1 nc	AD2 nc	capCAA1 nc	capCAA2 nc	C1 nc	C2 nc	fc.cap-CAA/C	fc.capCAA/AD	fc. AD/C	fc. max	pvalues	Protein name
RPH3A	13,61	0,00	15,98	1,07	2,19	22,51	-1,45	1,25	-1,82	1,82	0,64	Isoform 1 of Rabphilin-3A
PHYHIPL	12,64	6,35	8,99	4,28	6,58	9,79	-1,23	-1,43	1,16	1,43	0,64	Isoform 1 of Phytanoyl-CoA hydroxylase-interacting protein-like
SCG2	0,97	0,91	1,00	0,00	6,58	0,00	-6,59	-1,88	-3,50	6,59	0,64	Secretogranin-2
NCAM1	71,93	90,74	80,88	76,05	78,91	68,52	1,06	-1,04	1,10	1,10	0,64	Isoform 2 of Neural cell adhesion molecule 1
PURA	12,64	8,17	10,98	12,85	7,67	9,79	1,37	1,15	1,19	1,37	0,64	Transcriptional activator protein Pur-alpha
CST3	2,92	4,54	3,99	4,28	4,38	6,85	-1,36	-1,56	-1,51	1,51	0,64	Cystatin-C
GPX1	5,83	5,44	3,99	3,21	5,48	3,92	-1,30	1,20	1,20	1,56	0,64	glutathione peroxidase 1 isoform 1
UBA1	53,46	60,79	54,92	69,62	62,47	47,96	1,13	1,09	1,03	1,13	0,64	Ubiquitin-like modifier-activating enzyme 1
AGL	0,97	0,91	3,00	0,00	1,10	2,94	-1,35	1,59	-2,15	2,15	0,64	Isoform 5 of Glycogen debranching enzyme
ARL2.5NX15	1,94	0,00	2,00	1,07	2,19	1,96	-1,35	1,58	-2,13	2,13	0,64	ADP-ribosylation factor-like protein 2
NIT1	0,97	0,91	2,00	1,07	2,19	1,96	-1,35	1,63	-2,21	2,21	0,64	Isoform 2 of Nitrilase homolog 1
RPS13	0,97	0,91	2,00	1,07	1,10	2,94	-1,31	1,63	-2,15	2,15	0,64	40S ribosomal protein S13
SYT1	64,16	87,11	75,88	61,05	63,56	73,42	-1,00	-1,10	1,10	1,10	0,64	Synaptotagmin-1
LRRC47	1,94	0,00	3,00	1,07	2,19	0,98	1,28	2,09	-1,63	2,09	0,64	Leucine-rich repeat-containing protein 47
NDUFB11	0,97	0,91	3,00	1,07	2,19	0,98	1,28	2,16	-1,69	2,16	0,64	Neuronal protein
PSAP	7,78	7,26	7,99	4,28	5,48	4,89	1,18	-1,23	1,45	1,45	0,64	Isoform Sap-mu-0 of Proactivator polypeptide
DSTN	5,83	5,44	7,99	7,50	4,38	6,85	1,38	1,37	1,00	1,38	0,64	Destrin
SYP	12,64	16,33	16,97	10,71	10,96	11,75	1,22	-1,05	1,28	1,28	0,65	Synaptophysin
PEX11B	1,94	0,91	1,00	0,00	0,00	1,96	-1,96	-2,86	1,46	2,86	0,65	Peroxisomal membrane protein 11B
RAB39B	0,97	1,81	1,00	0,00	1,10	0,98	-2,08	-2,79	1,34	2,79	0,65	Ras-related protein Rab-39B
GLRX	0,97	1,81	0,00	1,07	1,10	0,98	-1,94	-2,60	1,34	2,60	0,65	Glutaredoxin-1
SNX4	0,97	5,44	0,00	1,07	1,10	0,98	-1,94	-2,60	1,34	2,60	0,65	Sorting nexin-4
ATPIF1	1,94	0,91	1,00	0,00	2,19	0,00	-2,20	-2,86	1,30	2,86	0,65	ATPase inhibitory factor 1 isoform 3 precursor
CLIC4	4,86	4,54	4,99	7,50	4,38	3,92	1,50	1,33	1,13	1,50	0,65	Chloride intracellular channel protein 4
HNRNPR	5,83	3,63	6,99	5,36	3,29	4,89	1,51	1,30	1,16	1,51	0,65	Heterogeneous nuclear ribonucleoprotein R
CISD2	0,97	1,81	1,00	1,07	1,10	0,00	1,89	-1,35	2,54	2,54	0,65	CDGSH iron sulfur domain-containing protein 2
HIST1H2AH	0,97	1,81	1,00	1,07	1,10	0,00	1,89	-1,35	2,54	2,54	0,65	Histone H2A type I-H
COQ9	1,94	0,91	2,00	0,00	0,00	0,98	2,04	-1,43	2,91	2,91	0,65	Isoform 1 of Ubiquinone biosynthesis protein COQ9, mitochondrial
PSMC1	1,94	0,91	2,00	0,00	0,00	0,98	2,04	-1,43	2,91	2,91	0,65	26S protease regulatory subunit 4
MYO5A	45,69	29,04	44,93	15,00	33,97	35,24	-1,15	-1,25	1,08	1,25	0,65	myosin VA isoform 2
ACSL6	7,78	2,72	6,99	1,07	1,10	10,77	-1,70	-1,50	-1,13	1,70	0,65	acyl-CoA synthetase long-chain family member 6 isoform b
ATP1B1	51,52	37,20	40,94	40,70	38,35	38,18	1,07	-1,09	1,16	1,16	0,65	Isoform 1 of Sodium/potassium-transporting ATPase subunit beta-1
PEPD	5,83	2,72	2,00	3,21	3,29	2,94	-1,19	-1,64	1,37	1,64	0,65	Xaa-Pro dipeptidase
EZR	15,55	18,15	13,98	12,85	20,82	11,75	-1,21	-1,26	1,03	1,26	0,65	Ezrin
FKBP3	5,83	2,72	4,99	1,07	2,19	2,94	1,18	-1,41	1,67	1,67	0,65	FK506-binding protein 3
PRKCB	12,64	12,70	12,98	7,50	6,58	12,73	1,06	-1,24	1,31	1,31	0,65	Isoform Beta-II of Protein kinase C beta type
CAB39	0,97	1,81	2,00	1,07	2,19	2,94	-1,67	1,10	-1,84	1,84	0,65	Calcium-binding protein 39
RHOG	0,97	1,81	1,00	2,14	3,29	1,96	-1,67	1,13	-1,88	1,88	0,65	Rho-related GTP-binding protein RhoG
AK5	1,94	0,91	1,00	2,14	2,19	2,94	-1,63	1,10	-1,80	1,80	0,65	Putative uncharacterized protein
TUBB3	45,69	49,91	44,93	48,20	58,08	47,96	-1,14	-1,03	-1,11	1,14	0,66	Tubulin beta-3 chain
NIF3L1	1,94	0,91	3,00	2,14	2,19	0,98	1,62	1,80	-1,11	1,80	0,66	NIF3L1 isoform gamma
PTGR1	0,97	1,81	3,00	2,14	2,19	0,98	1,62	1,84	-1,14	1,84	0,66	Prostaglandin reductase 1
TARDBP	1,94	0,91	3,99	1,07	0,00	2,94	1,72	1,78	-1,03	1,78	0,66	TDP43

Gene Symbol	AD1 nc	AD2 nc	capCAA1 nc	capCAA2 nc	C1 nc	C2 nc	fc.cap-CAA/C	fc.capCAA/AD	fc.AD/C	fc.max	pvalues	Protein name
DDAHI	37,91	46,28	37,94	35,35	43,84	38,18	-1,12	-1,15	1,03	1,15	0,66	N(G),N(G)-dimethylarginine dimethylaminohydrolase 1
CORO1A	4,86	6,35	9,98	3,21	4,38	12,73	-1,30	1,18	-1,53	1,53	0,66	Coronin-1A
NDUFA10	10,69	10,89	14,98	12,85	8,77	14,68	1,19	1,29	-1,09	1,29	0,66	NADH dehydrogenase [ubiquinone] 1 alpha subcomplex subunit 10, mitochondrial
ATP6V1F	2,92	2,72	3,99	1,07	5,48	2,94	-1,66	-1,11	-1,49	1,66	0,66	V-type proton ATPase subunit F
MAOA	1,94	3,63	3,99	0,00	5,48	1,96	-1,86	-1,40	-1,33	1,86	0,66	Amine oxidase [flavin-containing] A
HIBCH	3,89	1,81	2,00	2,14	4,38	2,94	-1,77	-1,38	-1,28	1,77	0,66	Isoform 1 of 3-hydroxyisobutyryl-CoA hydrolase, mitochondrial
LOC440926;H3F3B;H3F3A	0,97	4,54	3,00	5,36	2,19	2,94	1,63	1,52	1,07	1,63	0,66	Histone H3.3
TMED10	2,92	2,72	2,00	1,07	2,19	2,94	-1,67	-1,84	1,10	1,84	0,66	Transmembrane emp24 domain-containing protein 10
SNX12	2,92	2,72	2,00	1,07	2,19	2,94	-1,67	-1,84	1,10	1,84	0,66	Isoform 1 of Sorting nexin-12
RPS14	2,92	2,72	1,00	2,14	2,19	2,94	-1,63	-1,80	1,10	1,80	0,66	40S ribosomal protein S14
ELAVL4	2,92	2,72	3,00	2,14	0,00	2,94	1,75	-1,10	1,92	1,92	0,66	Isoform 2 of ELAV-like protein 4
IGHG2	1,94	3,63	1,00	4,28	2,19	0,98	1,67	-1,06	1,76	1,76	0,66	Putative uncharacterized protein DKFZp686I04196 (Fragment)
IMPA1	14,58	9,98	7,99	12,85	7,67	10,77	1,13	-1,18	1,33	1,33	0,66	Inositol monophosphatase
APBD1	1,94	1,81	3,99	2,14	2,19	3,92	1,00	1,63	-1,62	1,63	0,66	Isoform 1 of AP-3 complex subunit delta-1
PSMB2	3,89	4,54	4,99	2,14	3,29	1,96	1,36	-1,18	1,61	1,61	0,67	Proteasome subunit beta type-2
CKAP5	2,92	0,00	2,00	1,07	4,38	0,98	-1,75	1,05	-1,84	1,84	0,67	Isoform 1 of Cytoskeleton-associated protein 5
KRT14	5,83	0,91	3,00	0,00	4,38	0,98	-1,79	-1,10	1,26	2,25	0,67	Keratin, type I cytoskeletal 14
SNCA	18,47	15,43	14,98	11,78	14,25	16,64	-1,15	-1,27	1,10	1,27	0,67	Isoform 1 of Alpha-synuclein
SEPT7	49,58	68,96	49,92	56,77	51,51	57,75	-1,02	-1,11	1,08	1,11	0,67	Isoform 1 of Septin-7
MT-CO2	19,44	19,96	17,97	19,28	12,06	19,58	1,18	-1,06	1,25	1,25	0,67	Cytochrome c oxidase subunit 2
PTGES3	4,86	5,44	6,99	6,43	4,38	4,89	1,45	1,30	1,11	1,45	0,67	Prostaglandin E synthase 3
NCDN	43,74	49,00	41,94	42,84	38,36	43,07	1,04	-1,09	1,14	1,14	0,67	Isoform 1 of Neurochondrin
HNRNPA3	7,78	2,72	7,99	3,21	1,10	5,87	1,61	1,07	1,51	1,61	0,67	Isoform 1 of Heterogeneous nuclear ribonucleoprotein A3
PYGM	12,64	11,80	13,98	7,50	4,38	13,70	1,19	-1,14	1,35	1,35	0,67	Glycogen phosphorylase, muscle form
ATP2B2	4,86	2,72	5,99	2,14	0,00	4,89	1,66	1,07	1,55	1,66	0,67	Isoform 1 of Plasma membrane calcium-transporting ATPase 2
ASNA1	2,92	3,63	2,00	2,14	1,10	2,94	1,03	-1,58	1,62	1,62	0,68	Arsenical pump-driving ATPase
EPN1	2,92	3,63	1,00	3,21	2,19	1,96	1,01	-1,55	1,58	1,58	0,68	Isoform 2 of Epsin-1
ATP5G1	17,50	16,33	18,97	21,42	16,44	23,49	1,01	1,19	-1,18	1,19	0,68	Isoform Liver of ATP synthase subunit gamma, mitochondrial
BCAM	0,00	0,91	0,00	3,21	0,00	1,96	1,64	3,54	-2,16	3,54	0,68	Lutheran blood group glycoprotein
COL18A1	0,00	0,91	0,00	3,21	0,00	1,96	1,64	3,54	-2,16	3,54	0,68	Isoform 2 of Collagen alpha-1(XVIII) chain
CD9	10,69	13,61	7,99	11,78	15,34	3,92	1,03	-1,23	1,26	1,26	0,68	CD9 antigen
YWHAE	79,71	88,02	76,88	77,12	84,39	71,46	-1,01	-1,09	1,08	1,09	0,68	14-3-3 protein epsilon
GLTP	1,94	2,72	2,00	6,43	6,58	0,98	1,12	1,81	-1,62	1,81	0,68	Glycolipid transfer protein
HNRNPC	13,61	8,17	9,98	6,43	6,58	10,77	-1,06	-1,33	1,26	1,33	0,68	Isoform C1 of Heterogeneous nuclear ribonucleoproteins C1/C2
RHEB	2,92	0,91	2,00	0,00	1,10	2,94	-2,02	-1,91	-1,05	2,02	0,68	GTP-binding protein Rheb
ITGAV	1,94	1,81	1,00	1,07	2,19	1,96	-2,01	-1,82	-1,10	2,01	0,68	Isoform 1 of Integrin alpha-V
COPS3	2,92	0,91	2,00	2,14	1,10	0,98	1,99	1,08	1,84	1,99	0,68	COP9 signalosome complex subunit 3
Magmas	1,94	1,81	2,00	2,14	1,10	0,98	1,99	1,10	1,81	1,99	0,68	Mitochondrial import inner membrane translocase subunit Tim16
HSPC159	2,92	0,91	3,00	1,07	2,19	0,00	1,86	1,06	1,74	1,86	0,68	Galectin-related protein
SCP2	1,94	1,81	2,00	2,14	0,00	1,96	2,11	1,10	1,92	2,11	0,68	Isoform SCPx of Non-specific lipid-transfer protein
DCTN3	2,92	2,72	2,00	1,07	1,10	2,94	-1,31	-1,84	1,40	1,84	0,68	Isoform 1 of Dynactin subunit 3
XPO1	3,89	1,81	2,00	1,07	2,19	1,96	-1,35	-1,86	1,37	1,86	0,68	Exportin-1
RPLP2	2,92	2,72	2,00	1,07	2,19	1,96	-1,35	-1,84	1,36	1,84	0,68	60S acidic ribosomal protein P2

Gene Symbol	AD1 nc	AD2 nc	capCAA1 nc	capCAA2 nc	C1 nc	C2 nc	fc.cap-CAA/C	fc.capCAA/AD	fc. AD/C	fc. max	pvalues	Protein name
BLVRA	3,89	1,81	2,00	2,14	2,19	0,98	1,31	-1,38	1,80	1,80	0,68	Biliverdin reductase A
YWHAZ	50,55	68,96	53,92	55,70	69,04	53,84	-1,12	-1,09	-1,03	1,12	0,68	14-3-3 protein zeta/delta
CYFIP2	15,55	19,06	15,98	11,78	13,15	17,62	-1,11	-1,25	1,12	1,25	0,68	Isoform 2 of Cytoplasmic FMR1-interacting protein 2
PLXNA4	2,92	0,00	3,99	0,00	3,29	1,96	-1,31	1,37	-1,80	1,80	0,69	Isoform 1 of Plexin-A4
CCT5	3,89	7,26	5,99	8,57	9,86	5,87	-1,08	1,31	-1,41	1,41	0,69	T-complex protein 1 subunit epsilon
RAB2A	10,69	10,89	9,98	6,43	10,96	9,79	-1,26	-1,32	1,04	1,32	0,69	Ras-related protein Rab-2A
PPIA	55,41	50,81	44,93	50,34	51,51	45,03	-1,01	-1,11	1,10	1,11	0,69	Peptidyl-prolyl cis-trans isomerase A
PRSS3	8,75	1,81	4,99	3,21	7,67	4,89	-1,53	-1,29	-1,19	1,53	0,69	Isoform C of Trypsin-3
PYGB	52,49	68,96	57,91	65,34	72,33	62,65	-1,10	1,01	-1,11	1,11	0,69	Glycogen phosphorylase, brain form
MAPK1	16,53	26,31	13,98	22,49	46,03	13,70	-1,64	-1,17	-1,39	1,64	0,69	Mitogen-activated protein kinase 1
ARF4	1,94	2,72	4,99	2,14	5,48	1,96	-1,04	1,53	-1,59	1,59	0,69	ADP-ribosylation factor 4
CRIP2	1,94	2,72	3,99	3,21	3,29	3,92	1,00	1,54	-1,54	1,54	0,69	Cysteine-rich protein 2
BDH2	1,94	2,72	3,99	3,21	4,38	2,94	-1,02	1,54	-1,57	1,57	0,69	Isoform 2 of 3-hydroxybutyrate dehydrogenase type 2
CDS2	2,92	3,63	4,99	4,28	4,38	1,96	1,46	1,42	1,03	1,46	0,69	Isoform 1 of Phosphatidate cytidylyltransferase 2
SLC17A7	10,69	15,43	16,97	6,43	5,48	13,70	1,22	-1,12	1,36	1,36	0,69	Vesicular glutamate transporter 1
SCN2A	7,78	3,63	10,98	0,00	7,67	4,89	-1,14	-1,04	-1,10	1,14	0,69	Isoform 2 of Sodium channel protein type 2 subunit alpha
CRYZ	6,80	4,54	4,99	7,50	9,86	5,87	-1,26	1,10	-1,39	1,39	0,69	Quinone oxidoreductase
MSN	3,89	7,26	7,99	7,50	7,67	4,89	-1,27	1,12	-1,42	1,42	0,69	Moesin
RTN3	4,86	6,35	7,99	4,28	7,67	7,83	-1,26	1,09	-1,38	1,38	0,69	Isoform 2 of Reticulon-3
SYNPO	0,97	0,91	2,00	0,00	0,00	4,89	-2,45	1,06	-2,60	2,60	0,70	Isoform 1 of Synaptopodin
RPSAP12	7,78	3,63	8,99	6,43	4,38	7,83	1,26	1,35	-1,07	1,35	0,70	similar to 40S ribosomal protein SA (p40) (34/67 kDa laminin receptor) (Colon carcinoma laminin-binding protein) (NEM/1CHD4) (Multidrug resistance-associated protein MGr1-Ag) isoform 1
CSNK2A1	1,94	0,91	2,00	2,14	3,29	1,96	-1,27	1,45	-1,84	1,84	0,70	CSNK2A1 protein
FAHD2A	1,94	0,91	3,00	1,07	3,29	1,96	-1,29	1,43	-1,84	1,84	0,70	Fumarylacetoacetate hydrolase domain-containing protein 2A
GNPDA1	0,97	1,81	3,00	1,07	3,29	1,96	-1,29	1,46	-1,88	1,88	0,70	Glucosamine-6-phosphate isomerase 1
PLEKHB1	0,97	1,81	1,00	3,21	4,38	0,98	-1,27	1,51	-1,92	1,92	0,70	Isoform 2 of Pleckstrin homology domain-containing family B member 1
AADACL1	7,78	5,44	7,99	2,14	4,38	4,89	1,09	-1,31	1,42	1,42	0,70	arylacetamide deacetylase-like 1 isoform b
CDH13	0,97	1,81	3,00	2,14	3,29	0,98	1,20	1,84	-1,53	1,84	0,70	cDNA FLJ52398, highly similar to Cadherin-13
LOC389842	1,94	0,91	2,00	3,21	2,19	1,96	1,26	1,83	-1,46	1,83	0,70	similar to RanBP1
HSPA2	11,66	11,80	3,00	12,85	31,78	3,92	-2,25	-1,48	-1,52	2,25	0,70	Heat shock-related 70 kDa protein 2
LOC442975;SLC3A2	25,27	23,59	25,96	25,71	19,73	23,49	1,20	1,06	1,13	1,20	0,70	4F2 cell-surface antigen heavy chain
DPYSL4	10,69	4,54	8,99	5,36	14,25	5,87	-1,40	-1,06	-1,32	1,40	0,70	Dihydropyrimidinase-related protein 4
AUH	2,92	0,91	2,00	2,14	4,38	1,96	-1,53	1,08	-1,66	1,66	0,70	Isoform 1 of Methylglutaconyl-CoA hydratase, mitochondrial
SLC12A2	2,92	0,91	2,00	2,14	5,48	0,98	-1,56	1,08	-1,69	1,69	0,70	Isoform 1 of Solute carrier family 12 member 2
NUDT3	1,94	1,81	3,00	3,21	3,29	0,98	1,46	1,65	-1,14	1,65	0,70	Diphosphoinositol polyphosphate phosphohydrolase 1
PIP5K1C	1,94	1,81	3,00	3,21	1,10	2,94	1,54	1,65	-1,07	1,65	0,70	Phosphatidylinositol-4-phosphate 5-kinase type-1 gamma
IGK@	13,61	10,89	13,98	16,07	9,86	14,68	1,22	1,23	-1,00	1,23	0,70	IGK@ protein
HNRNPK	22,36	24,50	23,96	20,35	12,06	26,43	1,15	-1,06	1,22	1,22	0,70	Isoform 1 of Heterogeneous nuclear ribonucleoprotein K
SEPT9	16,53	14,52	16,97	9,64	6,58	17,62	1,10	-1,17	1,28	1,28	0,70	septin 9 isoform a
BCAP31	4,86	1,81	2,00	3,21	3,29	4,89	-1,57	-1,28	-1,23	1,57	0,70	B-cell receptor-associated protein 31
ATP1A2	2,92	3,63	3,00	2,14	4,38	3,92	-1,62	-1,27	-1,27	1,62	0,70	cDNA FLJ42590 fis, clone BRACE3009708, highly similar to Sodium/potassium-transporting ATPase alpha-2 chain
ANXA7	6,80	9,98	9,98	11,78	9,86	7,83	1,23	1,30	-1,05	1,30	0,70	Putative uncharacterized protein ANXA7
S100A8	1,94	1,81	1,00	1,07	0,00	1,96	1,06	-1,82	1,92	1,92	0,70	Protein S100-A8

Gene Symbol	AD1 nc	AD2 nc	capCAA1 nc	capCAA2 nc	C1 nc	C2 nc	fc.cap-CAA/C	fc.capCAA/AD	fc.AD/C	fc.max	pvalues	Protein name
UQCRH	2,92	0,91	1,00	1,07	1,10	0,98	-1,00	-1,85	1,84	1,85	0,70	Cytochrome b-c1 complex subunit 6, mitochondrial
PSMB4	2,92	0,91	1,00	1,07	1,10	0,98	-1,00	-1,85	1,84	1,85	0,70	Proteasome subunit beta type-4
CPE	0,97	2,72	1,00	1,07	2,19	0,00	-1,06	-1,79	1,69	1,79	0,70	Carboxypeptidase E precursor
ACYP1	1,94	1,81	1,00	1,07	1,10	0,98	-1,00	-1,82	1,81	1,82	0,70	Acylphosphatase-1
ERMN	1,94	1,81	0,00	2,14	2,19	0,00	-1,02	-1,75	1,71	1,75	0,70	Isoform 1 of Ermin
DCUN1D1	1,94	1,81	2,00	0,00	2,19	0,00	-1,10	-1,88	1,71	1,88	0,70	DCN1-like protein 1
ELAVL1	2,92	0,91	2,00	0,00	0,00	1,96	1,02	-1,91	1,95	1,95	0,70	cDNA FLJ60076, highly similar to ELAV-like protein 1
TPPP3	2,92	1,81	3,99	2,14	10,96	0,98	-1,95	1,30	-2,52	2,52	0,70	Tubulin polymerization-promoting protein family member 3
PDHB	32,08	19,96	33,95	26,78	21,92	38,18	1,01	1,17	-1,15	1,17	0,70	Isoform 1 of Pyruvate dehydrogenase E1 component subunit beta, mitochondrial
RAP2B	0,97	1,81	1,00	1,07	2,19	1,96	-2,01	-1,35	-1,49	2,01	0,70	Ras-related protein Rap-2b
PCYT2	1,94	0,91	1,00	1,07	3,29	0,98	-2,06	-1,38	-1,50	2,06	0,70	Ethanolamine-phosphate cytidylyltransferase
SLC9A6	1,94	0,91	2,00	0,00	2,19	1,96	-2,08	-1,43	-1,46	2,08	0,70	solute carrier family 9 (sodium/hydrogen exchanger), member 6 isoform a
SERPINB1	0,97	1,81	2,00	0,00	3,29	0,98	-2,14	-1,40	-1,53	2,14	0,70	Leukocyte elastase inhibitor
LTA4H	2,92	0,00	2,00	0,00	2,19	1,96	-2,08	-1,46	-1,42	2,08	0,70	Isoform 1 of Leukotriene A-4 hydrolase
ATP9A	3,89	2,72	4,99	3,21	3,29	1,96	1,56	1,24	1,26	1,56	0,70	Isoform Long of Probable phospholipid-transporting ATPase IIA
PFDN1	1,94	0,91	2,00	2,14	2,19	0,00	1,89	1,45	1,30	1,89	0,71	Prefoldin subunit 1
SPR	0,97	1,81	2,00	2,14	1,10	0,98	1,99	1,49	1,34	1,99	0,71	Sepiapterin reductase
TTR	1,94	0,91	2,00	2,14	0,00	1,96	2,11	1,45	1,46	2,11	0,71	Transthyretin
NDUFA8	7,78	9,98	7,99	6,43	5,48	7,83	1,08	-1,23	1,33	1,33	0,71	NADH dehydrogenase [ubiquinone] 1 alpha subcomplex subunit 8
ANK2	69,99	71,68	83,87	52,48	56,99	68,52	1,09	-1,04	1,13	1,13	0,71	Isoform 4 of Ankyrin-2
CYC1	17,50	15,43	14,98	17,14	8,77	17,62	1,22	-1,03	1,25	1,25	0,71	Cytochrome c1, heme protein, mitochondrial
CALB2	1,94	6,35	3,00	1,07	21,92	0,98	-5,63	-2,04	-2,76	5,63	0,71	Calretinin
OPCML	10,69	9,07	7,99	13,92	7,67	8,81	1,33	1,11	1,20	1,33	0,71	OPCML protein
PKM2	3,89	7,26	7,99	7,50	8,77	4,89	1,13	1,39	-1,23	1,39	0,71	Isoform M2 of Pyruvate kinase isozymes M1/M2
ST13	4,86	6,35	5,99	9,64	6,58	6,85	1,16	1,39	-1,20	1,39	0,71	Hsc70-interacting protein
RAB3A	34,99	41,74	37,94	28,92	28,49	44,05	-1,08	-1,15	1,06	1,15	0,71	Ras-related protein Rab-3A
PFN1	8,75	8,17	8,99	11,78	12,06	9,79	-1,05	1,23	-1,29	1,29	0,71	Profilin-1
CISD1	9,72	9,07	8,99	7,50	12,06	9,79	-1,33	-1,14	-1,16	1,33	0,71	CDGSH iron sulfur domain-containing protein 1
MAP1B	119,56	89,83	128,80	98,54	98,63	109,63	1,09	1,09	1,01	1,09	0,71	Microtubule-associated protein 1B
PSAT1	10,69	26,31	10,98	20,35	26,30	15,66	-1,34	-1,18	-1,13	1,34	0,71	Phosphoserine aminotransferase
PTGDS	12,64	14,52	16,97	13,92	14,25	10,77	1,24	1,14	1,09	1,24	0,71	Prostaglandin-H2 D-isomerase
UQCRC2	39,85	27,22	35,95	40,70	20,82	44,05	1,18	1,14	1,03	1,18	0,71	Cytochrome b-c1 complex subunit 2, mitochondrial
TUBA1A	304,26	320,31	321,51	322,40	421,94	280,94	-1,09	1,03	-1,13	1,13	0,71	Tubulin alpha-1A chain
RHOB	3,89	5,44	3,00	3,21	5,48	2,94	-1,36	-1,50	1,11	1,50	0,71	Rho-related GTP-binding protein RhoB
FKBP1A	4,86	4,54	3,99	2,14	5,48	2,94	-1,37	-1,53	1,12	1,53	0,71	FKBP1A protein
PFN2	7,78	8,17	8,99	3,21	9,86	6,85	-1,37	-1,31	-1,05	1,37	0,71	Isoform IIa of Profilin-2
DPYSL5	8,75	6,35	3,00	9,64	18,63	3,92	-1,78	-1,20	-1,49	1,78	0,71	Dihydropyrimidinase-related protein 5
NRGN	3,89	5,44	3,99	4,28	2,19	3,92	1,36	-1,13	1,53	1,53	0,71	Neurogranin
SOD2	11,66	8,17	12,98	10,71	12,06	12,73	-1,05	1,19	-1,25	1,25	0,71	Superoxide dismutase [Mn], mitochondrial
CAMKV	8,75	13,61	13,98	4,28	8,77	8,81	1,04	-1,22	1,27	1,27	0,71	Isoform 2 of CaM kinase-like vesicle-associated protein
CACYBP	8,75	7,26	4,99	11,78	6,58	5,87	1,35	1,05	1,29	1,35	0,71	Isoform 1 of Calcyclin-binding protein
CMPK1	7,78	5,44	4,99	4,28	4,38	6,85	-1,21	-1,43	1,18	1,43	0,72	cytidine monophosphate (UMP-CMP) kinase 1, cytosolic isoform a
HNRNPA1	8,75	4,54	7,99	3,21	2,19	6,85	1,24	-1,19	1,47	1,47	0,72	Isoform A1-B of Heterogeneous nuclear ribonucleoprotein A1

Gene Symbol	AD1 nc	AD2 nc	capCAA1 nc	capCAA2 nc	C1 nc	C2 nc	fc.cap-CAA/C	fc.capCAA/AD	fc. AD/C	fc. max	pvalues	Protein name
GOT2	60.27	62.61	62.90	70.69	52.61	85.16	-1.03	1.09	-1.12	1.12	0.72	Aspartate aminotransferase, mitochondrial
AKR7A2	5.83	7.26	8.99	7.50	9.86	2.94	1.29	1.26	1.02	1.29	0.72	Aflatoxin B1 aldehyde reductase member 2
ESD	9.72	9.07	8.99	13.92	14.25	3.92	1.26	1.22	1.03	1.26	0.72	S-formylglutathione hydrolase
CD81	14.58	16.33	15.98	16.07	20.82	16.64	-1.17	1.04	-1.21	1.21	0.72	CD81 antigen
PLEC1	171.08	167.87	207.68	126.39	158.91	142.91	1.11	-1.01	1.12	1.12	0.72	Isoform 1 of Plectin-1
VPS35	10.69	10.89	9.98	10.71	17.54	8.81	-1.27	-1.04	-1.22	1.27	0.72	Vacuolar protein sorting-associated protein 35
ROCK2	7.78	0.91	3.00	1.07	4.38	1.96	-1.56	-2.14	1.37	2.14	0.72	Rho-associated protein kinase 2
PFKM	48.60	35.39	47.93	42.84	37.26	43.07	1.13	1.08	1.05	1.13	0.73	Isoform 1 of 6-phosphofructokinase, muscle type
ATP5J2	13.61	9.07	8.99	10.71	3.29	13.70	1.16	-1.15	1.33	1.33	0.73	Isoform 2 of ATP synthase subunit f, mitochondrial
AFG3L2	4.86	1.81	3.99	5.36	4.38	4.89	1.01	1.40	-1.39	1.40	0.73	AFG3-like protein 2
ATP1A2	71.93	67.15	78.88	68.55	53.70	79.29	1.11	1.06	1.05	1.11	0.73	Sodium/potassium-transporting ATPase subunit alpha-2
HINT2	2.92	3.63	3.00	1.07	3.29	2.94	-1.53	-1.61	1.05	1.61	0.73	Histidine triad nucleotide-binding protein 2
GSTT2;GSTT2B	0.97	0.91	2.00	1.07	6.58	0.00	-2.14	1.63	-3.50	3.50	0.73	Glutathione S-transferase theta-2
SPTBN2	26.25	12.70	33.95	13.92	7.67	26.43	1.40	1.23	1.14	1.40	0.73	Isoform 1 of Spectrin beta chain, brain 2
SLC25A5	14.58	9.98	19.97	8.57	8.77	13.70	1.27	1.16	1.09	1.27	0.73	ADP/ATP translocase 2
KRT1	116.65	78.04	103.84	76.05	108.50	94.95	-1.13	-1.08	-1.05	1.13	0.73	Keratin, type II cytoskeletal 1
RAB35	6.80	7.26	6.99	3.21	4.38	6.85	-1.10	-1.38	1.25	1.38	0.73	Ras-related protein Rab-35
RPS3A	8.75	5.44	6.99	4.28	4.38	5.87	1.10	-1.26	1.38	1.38	0.73	40S ribosomal protein S3a
NCAM2	19.44	19.06	12.98	19.28	19.73	14.68	-1.07	-1.19	1.12	1.19	0.73	Neural cell adhesion molecule 2
GSTM2	4.86	8.17	4.99	6.43	6.58	8.81	-1.35	-1.14	-1.18	1.35	0.73	Glutathione S-transferase Mu 2
PCCA	3.89	0.91	3.00	2.14	2.19	4.89	-1.38	1.07	-1.48	1.48	0.73	propionyl-Coenzyme A carboxylase, alpha polypeptide isoform a precursor
TPT1	1.94	2.72	2.00	3.21	4.38	2.94	-1.40	1.12	-1.57	1.57	0.73	Tumor protein, translationally-controlled 1
UQCRC1	38.88	39.93	36.94	43.91	31.78	59.71	-1.13	1.03	-1.16	1.16	0.73	Cytochrome b-c1 complex subunit 1, mitochondrial
ANK3	6.80	1.81	3.99	4.28	6.58	4.89	-1.39	-1.04	-1.33	1.39	0.73	Isoform 2 of Ankyrin-3
TNC	1.94	0.91	0.00	1.07	20.82	0.00	-19.44	-2.66	-7.30	19.44	0.73	Isoform 1 of Tenascin
TMOD2	10.69	9.98	13.98	9.64	8.77	9.79	1.27	1.14	1.11	1.27	0.73	Tropomodulin-2
SORT1	2.92	1.81	3.00	4.28	2.19	2.94	1.42	1.54	-1.08	1.54	0.73	Sortilin
TUBB4	46.66	60.79	45.93	54.63	50.41	46.99	1.03	-1.07	1.10	1.10	0.74	Tubulin beta-4 chain
PSMB3	2.92	4.54	2.00	4.28	4.38	4.89	-1.48	-1.19	-1.24	1.48	0.74	Proteasome subunit beta type-3
DMXL2	11.66	5.44	15.98	4.28	2.19	10.77	1.56	1.18	1.32	1.56	0.74	DMXL2 protein
COX7A2	2.92	4.54	3.99	1.07	2.19	2.94	-1.01	-1.47	1.45	1.47	0.74	Cytochrome c oxidase polypeptide 7A2, mitochondrial
MBLAC2	3.89	3.63	2.00	3.21	3.29	1.96	-1.01	-1.44	1.43	1.44	0.74	Isoform 1 of Beta-lactamase-like protein FLJ75971
VSNL1	41.80	43.55	37.94	39.63	31.78	44.05	1.02	-1.10	1.13	1.13	0.74	Visinin-like protein 1
ENPP6	5.83	2.72	0.00	7.50	9.86	0.98	-1.45	-1.14	-1.27	1.45	0.74	Ectonucleotide pyrophosphatase/phosphodiesterase family member 6
ATP2B1	22.36	21.78	30.95	10.71	7.67	27.41	1.19	-1.06	1.26	1.26	0.74	Isoform D of Plasma membrane calcium-transporting ATPase 1
GRHPR	11.66	9.07	9.98	10.71	10.96	5.87	1.23	-1.00	1.23	1.23	0.74	Glyoxylate reductase/hydroxypyruvate reductase
ATP8A1	9.72	14.52	16.97	6.43	24.11	8.81	-1.41	-1.04	-1.36	1.41	0.74	Isoform Long of Probable phospholipid-transporting ATPase IA
ATP2B4	31.11	39.93	48.93	18.21	44.93	34.26	-1.18	-1.44	-1.11	1.18	0.74	Isoform XA of Plasma membrane calcium-transporting ATPase 4
HSPA5	15.55	21.78	12.98	28.92	14.25	18.60	1.28	1.12	1.14	1.28	0.75	HSPA5 protein
ARF5	20.41	20.87	17.97	17.14	18.63	17.62	-1.03	-1.18	1.14	1.18	0.75	ADP-ribosylation factor 5
CAMK2A	63.18	71.68	78.88	48.20	60.28	60.69	1.05	-1.06	1.11	1.11	0.75	Isoform A of Calcium/calmodulin-dependent protein kinase type II alpha chain
HBD	15.55	9.07	11.98	15.00	12.06	17.62	-1.10	1.10	-1.20	1.20	0.75	Hemoglobin subunit delta
RAB5B	8.75	5.44	5.99	6.43	8.77	7.83	-1.34	-1.14	-1.17	1.34	0.75	Ras-related protein Rab-5B

Gene Symbol	AD1 nc	AD2 nc	capCAA1 nc	capCAA2 nc	C1 nc	C2 nc	fc.cap-CAA/C	fc.capCAA/AD	fc.AD/C	fc.max	pvalues	Protein name
LGALS1	10,69	12,70	7,99	10,71	13,15	8,81	-1,17	-1,25	1,07	1,25	0,75	Galectin-1
RAB21	6,80	3,63	3,99	3,21	5,48	2,94	-1,17	-1,45	1,24	1,45	0,75	Ras-related protein Rab-21
PDIA3	13,61	21,78	15,98	13,92	16,44	14,68	-1,04	-1,18	1,14	1,18	0,75	Protein disulfide-isomerase A3
ARPC5L	5,83	4,54	4,99	3,21	3,29	3,92	1,14	-1,26	1,44	1,44	0,75	Actin-related protein 2/3 complex subunit 5-like protein
ARL3	4,86	4,54	3,99	5,36	6,58	5,87	-1,33	-1,01	-1,32	1,33	0,75	ADP-ribosylation factor-like protein 3
DDAH2	4,86	3,63	2,00	3,21	7,67	0,00	-1,47	-1,63	1,11	1,63	0,75	N(G),N(G)-dimethylarginine dimethylaminohydrolase 2
GSTO1	7,78	8,17	9,98	9,64	8,77	6,85	1,26	1,23	1,02	1,26	0,75	Glutathione S-transferase omega-1
AGPAT3	0,97	0,00	2,00	0,00	1,10	0,98	-1,04	2,05	-2,13	2,13	0,75	1-acyl-sn-glycerol-3-phosphate acyltransferase gamma
RPL18A	0,97	0,00	1,00	1,07	0,00	1,96	1,06	2,13	-2,01	2,13	0,75	60S ribosomal protein L18a
PCBD2	0,97	0,00	2,00	0,00	0,00	1,96	1,02	2,05	-2,01	2,05	0,75	pterin-4-alpha-carbinolamine dehydratase 2
CAND1	27,22	29,94	27,96	34,28	31,78	22,51	1,15	1,09	1,05	1,15	0,75	Isoform 1 of Cullin-associated NEDD8-dissociated protein 1
PSMB6	2,92	3,63	2,00	2,14	2,19	2,94	-1,24	-1,58	1,28	1,58	0,75	Proteasome subunit beta type-6
FKBP2	2,92	3,63	3,00	1,07	1,10	3,92	-1,23	-1,61	1,31	1,61	0,75	FK506-binding protein 2
RPS17	2,92	3,63	3,00	2,14	2,19	1,96	1,24	-1,27	1,58	1,58	0,75	40S ribosomal protein S17
CRYM	36,94	27,22	32,95	33,20	28,49	29,37	1,14	1,03	1,11	1,14	0,75	Mu-crystallin homolog
CBR1	31,11	36,30	26,96	40,70	32,88	27,41	1,12	1,00	1,12	1,12	0,75	Carbonyl reductase [NADPH] 1
PRDX2	18,47	16,33	15,98	17,14	19,73	19,58	-1,19	-1,05	-1,13	1,19	0,76	Peroxiredoxin-2
C1orf128	2,92	2,72	3,99	4,28	3,29	2,94	1,33	1,47	-1,10	1,47	0,76	Isoform 1 of UPF0424 protein C1orf128
CDC42	1,94	3,63	4,99	3,21	2,19	3,92	1,34	1,47	-1,10	1,47	0,76	Isoform 1 of Cell division control protein 42 homolog
PPIB	1,94	3,63	3,99	4,28	3,29	2,94	1,33	1,49	-1,12	1,49	0,76	Peptidyl-prolyl cis-trans isomerase B
NP	1,94	2,72	2,00	1,07	1,10	3,92	-1,63	-1,52	-1,07	1,63	0,76	cDNA FLJ25678 fis, clone TST04067, highly similar to PURINE NUCLEOSIDE PHOSPHORYLASE
MAL2	1,94	2,72	3,00	0,00	1,10	3,92	-1,67	-1,56	-1,07	1,67	0,76	Protein MAL2
TCEB1	1,94	2,72	2,00	1,07	3,29	1,96	-1,71	-1,52	-1,12	1,71	0,76	Transcription elongation factor B polypeptide 1
LAMP2	0,97	3,63	1,00	2,14	4,38	0,98	-1,71	-1,47	-1,17	1,71	0,76	Isoform LAMP-2A of Lysosome-associated membrane glycoprotein 2
CADM2	12,64	16,33	12,98	12,85	10,96	12,73	1,09	-1,12	1,22	1,22	0,76	Isoform 3 of Cell adhesion molecule 2
USMG5	2,92	1,81	3,99	1,07	1,10	1,96	1,66	1,07	1,55	1,66	0,76	Up-regulated during skeletal muscle growth protein 5
C9orf5	2,92	1,81	3,99	1,07	1,10	1,96	1,66	1,07	1,55	1,66	0,76	Protein of unknown function UPF0118 family protein
ARPC5	1,94	2,72	2,00	3,21	2,19	0,98	1,64	1,12	1,47	1,64	0,76	Isoform 1 of Actin-related protein 2/3 complex subunit 5
ATP6AP1	1,94	2,72	3,00	2,14	1,10	1,96	1,68	1,10	1,53	1,68	0,76	V-type proton ATPase subunit S1
CALB1	0,00	1,81	1,00	0,00	4,38	0,00	-4,39	-1,82	-2,42	4,39	0,76	Calbindin
CAPNS1	5,83	6,35	3,99	5,36	5,48	3,92	-1,00	-1,30	1,30	1,30	0,76	Calpain small subunit 1
ACTR2	6,80	3,63	6,99	3,21	7,67	5,87	-1,33	-1,02	-1,30	1,33	0,76	Actin-related protein 2
ARHGAP26	0,97	0,00	1,00	0,00	0,00	1,96	-1,96	1,03	-2,01	2,01	0,76	Isoform 1 of Rho GTPase-activating protein 26
XPO7	0,00	0,91	2,00	0,00	0,00	0,98	2,04	1,03	-1,08	2,20	0,76	Exportin-7
RAPGEF2	0,00	0,91	2,00	0,00	0,00	0,98	2,04	2,20	-1,08	2,20	0,76	Rap guanine nucleotide exchange factor 2
C9orf126	0,97	0,00	2,00	0,00	0,00	0,98	2,04	2,05	-1,01	2,05	0,76	Isoform 2 of UPF0682 protein C9orf126
LGI3	0,97	0,00	0,00	2,14	0,00	0,98	2,19	2,20	-1,01	2,20	0,76	Leucine-rich repeat LGI family member 3
CACNG2	0,97	0,00	2,00	0,00	0,00	0,98	2,04	2,05	-1,01	2,05	0,76	Voltage-dependent calcium channel gamma-2 subunit
SLC9A1	0,97	0,00	2,00	0,00	0,00	0,98	2,04	2,05	-1,01	2,05	0,76	Isoform 1 of Sodium/hydrogen exchanger 1
RAB2B	0,97	0,00	2,00	0,00	0,00	0,98	2,04	2,05	-1,01	2,05	0,76	Ras-related protein Rab-2B
BAT3	0,97	0,00	2,00	0,00	1,10	0,00	1,82	2,05	-1,13	2,05	0,76	Isoform 1 of Large proline-rich protein BAT3
COPB2	0,97	0,00	2,00	0,00	1,10	0,00	1,82	2,05	-1,13	2,05	0,76	Coatomer subunit beta'
ALAD	4,86	7,26	3,99	5,36	9,86	2,94	-1,37	-1,30	-1,06	1,37	0,76	Delta-aminolevulinic acid dehydratase

Gene Symbol	AD1 nc	AD2 nc	capCAA1 nc	capCAA2 nc	C1 nc	C2 nc	fc.cap-CAA/C	fc.capCAA/AD	fc. AD/C	fc. max	pvalues	Protein name
GPD1L	4,86	3,63	5,99	4,28	3,29	3,92	1,43	1,21	1,18	1,43	0,76	Glycerol-3-phosphate dehydrogenase 1-like protein
CASKIN1	3,89	0,91	3,99	1,07	0,00	2,94	1,72	1,06	1,63	1,72	0,76	Caskin-1
SYN3	0,00	0,91	3,00	0,00	0,00	5,87	-1,96	3,30	-6,47	6,47	0,76	Synapsin-3
MPP2	2,92	0,00	1,00	0,00	0,00	1,96	-1,96	-2,92	1,49	2,92	0,76	cDNA FLJ56090, highly similar to MAGUK p55 subfamily member 2
COPA	2,92	0,00	1,00	0,00	0,00	1,96	-1,96	-2,92	1,49	2,92	0,76	Isoform 1 of Coatomer subunit alpha
ATP5A1	117,62	137,92	122,81	152,10	119,46	153,68	1,01	1,08	-1,07	1,08	0,76	ATP synthase subunit alpha, mitochondrial
GJA1	3,89	5,44	7,99	1,07	8,77	3,92	-1,40	-1,03	-1,36	1,40	0,77	Gap junction alpha-1 protein
ADH5	2,92	0,91	2,00	1,07	3,29	1,96	-1,71	-1,25	-1,37	1,71	0,77	Alcohol dehydrogenase class-3
NFS1	2,92	0,91	1,00	2,14	2,19	2,94	-1,63	-1,22	-1,34	1,63	0,77	Isoform Mitochondrial of Cysteine desulfurase, mitochondrial
CDC42	11,66	12,70	10,98	11,78	12,06	7,83	1,14	-1,07	1,23	1,23	0,77	Isoform 2 of Cell division control protein 42 homolog
MYL6,MYL6B	5,83	7,26	6,99	9,64	7,67	8,81	1,01	1,27	-1,26	1,27	0,77	Isoform Non-muscle of Myosin light polypeptide 6
F3	1,94	1,81	3,00	2,14	1,10	1,96	1,68	1,37	1,23	1,68	0,77	Tissue factor
SLC12A5	20,41	23,59	27,96	13,92	13,15	23,49	1,14	-1,05	1,20	1,20	0,77	Isoform 2 of Solute carrier family 12 member 5
PMP2	6,80	0,00	0,00	4,28	6,58	0,98	-1,76	-1,59	-1,11	1,76	0,77	Myelin P2 protein
NDUFA6	2,92	2,72	3,99	3,21	2,19	5,87	-1,12	1,28	-1,43	1,43	0,77	NADH dehydrogenase (ubiquinone) 1 alpha subcomplex, 6, 14kDa
RPL7	2,92	2,72	3,00	4,28	2,19	5,87	-1,11	1,29	-1,43	1,43	0,77	60S ribosomal protein L7
SCN1A	2,92	0,00	2,00	0,00	0,00	0,98	2,04	-1,46	2,98	2,98	0,77	Isoform 1 of Sodium channel protein type 1 subunit alpha
KBTBD11	7,78	7,26	9,98	8,57	6,58	11,75	1,01	1,23	-1,22	1,23	0,77	Kelch repeat and BTB domain-containing protein 11
SLC8A2	8,75	7,26	8,99	3,21	8,77	6,85	-1,28	-1,31	1,02	1,31	0,77	Sodium/calcium exchanger 2
COL1A2	0,00	0,91	0,00	2,14	0,00	8,81	-4,11	2,36	-9,71	9,71	0,77	Collagen alpha-2(I) chain
NLGN2	0,00	2,72	0,00	1,07	0,00	2,94	-2,74	-2,54	-1,08	2,74	0,77	Neuroligin-2
DNM3	12,64	7,26	11,98	7,50	8,77	14,68	-1,20	-1,02	-1,18	1,20	0,77	Putative uncharacterized protein DNM3
TUBA4A	38,88	45,37	39,94	39,63	40,55	35,24	1,05	-1,06	1,11	1,11	0,77	Tubulin alpha-4A chain
TSN	2,92	3,63	5,99	3,21	2,19	4,89	1,30	1,41	-1,08	1,41	0,77	Translin
ACTR3B	1,94	0,00	1,00	0,00	3,29	0,00	-3,29	-1,95	-1,69	3,29	0,77	Isoform 1 of Actin-related protein 3B
GFAP	177,89	296,72	247,62	184,23	272,89	219,27	-1,14	-1,10	-1,04	1,14	0,77	Isoform 1 of Glial fibrillary acidic protein
PAK1	2,92	4,54	3,99	1,07	3,29	3,92	-1,42	-1,47	1,03	1,47	0,78	Isoform 1 of Serine/threonine-protein kinase PAK 1
SCARB2	2,92	4,54	2,00	3,21	3,29	3,92	-1,38	-1,43	1,03	1,43	0,78	Lysosome membrane protein 2
TPI1	73,88	74,41	71,89	76,05	75,62	62,65	1,07	-1,00	1,07	1,07	0,78	triosephosphate isomerase 1 isoform 2
ATP5D	2,92	4,54	2,00	5,36	2,19	2,94	1,43	1,45	1,45	1,45	0,78	ATP synthase subunit delta, mitochondrial
HPCAL1	3,89	3,63	5,99	1,07	3,29	1,96	1,35	-1,06	1,43	1,43	0,78	Hippocalcin-like protein 1
HOMER1	1,94	1,81	2,00	0,00	0,00	2,94	-1,47	-1,88	1,28	1,88	0,78	Isoform 1 of Homer protein homolog 1
RPL23A	1,94	1,81	1,00	1,07	2,19	0,98	-1,53	-1,82	1,19	1,82	0,78	60S ribosomal protein L23a
RAN	11,66	9,07	11,98	8,57	13,15	11,75	-1,21	-1,01	-1,20	1,21	0,78	GTP-binding nuclear protein Ran
PRKCSH	1,94	1,81	2,00	1,07	2,19	0,00	1,40	-1,23	1,71	1,71	0,78	cDNA FLJ59211, highly similar to Glucosidase 2 subunit beta
DYNC1LI2	2,92	0,91	2,00	1,07	1,10	0,98	1,48	-1,25	1,84	1,84	0,78	Cytoplasmic dynein 1 light intermediate chain 2
HAGH	9,72	7,26	8,99	9,64	9,86	4,89	1,26	1,10	1,15	1,26	0,78	Hydroxyacylglutathione hydrolase
HSPA4L	10,69	6,35	6,99	13,92	4,38	11,75	1,30	1,23	1,06	1,30	0,78	Heat shock 70 kDa protein 4L
BCAN	24,30	29,94	25,96	23,56	25,21	22,51	1,04	-1,10	1,14	1,14	0,78	Isoform 1 of Brevican core protein
SNX1	1,94	0,00	0,00	3,21	1,10	0,00	2,93	1,65	1,77	2,93	0,78	sorting nexin 1 isoform c
SDHA	2,92	3,63	3,99	4,28	2,19	6,85	-1,09	1,26	-1,38	1,38	0,78	cDNA FLJ61478, highly similar to Succinate dehydrogenase (ubiquinone) flavoprotein subunit, mitochondrial
EIF5A	3,89	2,72	5,99	2,14	5,48	3,92	-1,16	1,23	-1,42	1,42	0,78	Isoform 2 of Eukaryotic translation initiation factor 5A-1
SAR1A	3,89	2,72	3,99	5,36	4,38	3,92	1,13	1,41	-1,26	1,41	0,78	GTP-binding protein SAR1a

Gene Symbol	AD1 nc	AD2 nc	capCAA1 nc	capCAA2 nc	C1 nc	C2 nc	fc.cap-CAA/C	fc.capCAA/AD	fc. AD/C	fc. max	pvalues	Protein name
PRPS1	3,89	2,72	3,99	5,36	5,48	2,94	1,11	1,41	-1,27	1,41	0,78	Ribose-phosphate pyrophosphokinase 1
COX5A	15,55	11,80	12,98	13,92	12,06	10,77	1,18	-1,02	1,20	1,20	0,78	Cytochrome c oxidase subunit 5A, mitochondrial
COX6B1	3,89	4,54	3,00	3,21	1,10	4,89	1,04	-1,36	1,41	1,41	0,79	Cytochrome c oxidase subunit 6B1
BAT1	5,83	2,72	3,99	2,14	2,19	3,92	1,00	-1,39	1,40	1,40	0,79	Isoform 2 of Spliceosome RNA helicase BAT1
FGA	8,75	4,54	0,00	18,21	8,77	1,96	1,70	1,37	1,24	1,70	0,79	Isoform 1 of Fibrinogen alpha chain
PPT1	5,83	7,26	8,99	4,28	5,48	4,89	1,28	1,01	1,26	1,28	0,79	Palmitoyl-protein thioesterase 1
CLDN11	15,55	19,06	7,99	18,21	28,49	4,89	-1,27	-1,32	1,04	1,32	0,79	Claudin-11
C22orf28	2,92	0,91	0,00	3,21	2,19	0,00	1,47	-1,19	1,74	1,74	0,79	UPF0027 protein C22orf28
SPTAN1	394,66	476,38	460,30	411,30	413,17	423,85	1,04	1,00	1,04	1,04	0,79	Isoform 2 of Spectrin alpha chain, brain
NCALD	9,72	4,54	7,99	6,43	7,67	9,79	-1,21	1,01	-1,22	1,22	0,79	Neurocalcin-delta
MARCKS	11,66	15,43	14,98	12,85	20,82	11,75	-1,17	1,03	-1,20	1,20	0,79	Myristoylated alanine-rich C-kinase substrate
RAB6B	4,86	3,63	3,99	5,36	6,58	4,89	-1,23	1,10	-1,35	1,35	0,79	Ras-related protein Rab-6B
APOA1BP	4,86	3,63	3,00	6,43	6,58	4,89	-1,22	1,11	-1,35	1,35	0,79	cDNA FLJ56357, highly similar to Homo sapiens apolipoprotein A-I binding protein (APOA1BP), mRNA
AP2M1	15,55	18,15	21,97	7,50	16,44	18,60	-1,19	-1,14	-1,04	1,19	0,79	Isoform 1 of AP-2 complex subunit mu-1
SH3BGRL2	2,92	1,81	3,00	0,00	1,10	1,96	-1,02	-1,58	1,55	1,58	0,79	SH3 domain-binding glutamic acid-rich-like protein 2
PFDN2	2,92	1,81	3,00	0,00	2,19	0,98	-1,06	-1,58	1,49	1,58	0,79	Prefoldin subunit 2
PSMD11	2,92	1,81	2,00	1,07	1,10	1,96	1,00	-1,54	1,55	1,55	0,79	Proteasome 26S non-ATPase subunit 11 variant (Fragment)
RPL11	2,92	1,81	2,00	1,07	1,10	1,96	1,00	-1,54	1,55	1,55	0,79	Isoform 1 of 60S ribosomal protein L11
-	3,89	5,44	7,99	5,36	14,25	1,96	-1,21	1,43	-1,74	1,74	0,80	Dihydropyrimidinase-like 2 long form (Fragment)
PACS	3,89	6,35	2,00	7,50	8,77	3,92	-1,34	-1,08	-1,24	1,34	0,80	Multifunctional protein ADE2
GNAI2	14,58	15,43	13,98	12,85	18,63	13,70	-1,21	-1,12	-1,08	1,21	0,80	Isoform 2 of Guanine nucleotide-binding protein G(i), alpha-2 subunit
PRKCG	0,00	0,91	1,00	0,00	14,25	0,00	-14,27	1,10	-15,70	15,70	0,80	cDNA FLJ60619, highly similar to Protein kinase C gamma type
SFRS7	2,92	0,00	3,00	0,00	0,00	0,98	3,06	1,03	2,98	3,06	0,80	Isoform 1 of Splicing factor, arginine/serine-rich 7
ATP6V1A	94,29	98,00	85,87	94,26	103,02	86,14	-1,05	-1,07	1,02	1,07	0,80	V-type proton ATPase catalytic subunit A
PSMB1	3,89	3,63	2,00	3,21	4,38	1,96	-1,22	-1,44	1,19	1,44	0,80	Proteasome subunit beta type-1
HNRNPH1	3,89	3,63	2,00	4,28	0,00	4,89	1,28	-1,20	1,54	1,54	0,80	Heterogeneous nuclear ribonucleoprotein H
AK3L2;AK3L1	4,86	2,72	3,00	3,21	1,10	3,92	1,24	-1,22	1,51	1,51	0,80	Adenylate kinase isoenzyme 4, mitochondrial
STOML2	4,86	2,72	3,00	3,21	2,19	2,94	1,21	-1,22	1,48	1,48	0,80	Stomatin-like protein 2
RDX	2,92	1,81	0,00	3,21	4,38	0,00	1,21	-1,47	1,08	1,47	0,80	Radixin, isoform CRA_a
C20orf3	4,86	4,54	5,99	6,43	5,48	4,89	-1,36	1,32	-1,10	1,32	0,80	Isoform 1 of Adipocyte plasma membrane-associated protein
PHB	18,47	17,24	20,97	20,35	17,54	21,54	1,20	1,16	1,08	1,16	0,80	Prohibitin
SH3GLB2	5,83	9,98	8,99	10,71	7,67	8,81	1,06	1,25	-1,09	1,25	0,80	SH3-domain GRB2-like endophilin B2
OLA1	8,75	7,26	7,99	11,78	12,06	4,89	1,17	1,24	-1,04	1,24	0,80	Isoform 1 of Obg-like ATPase 1
SERPINB6	4,86	6,35	5,99	6,43	6,58	2,94	1,31	1,11	1,18	1,31	0,80	Putative uncharacterized protein DKFZp686J0422
NIT2	6,80	4,54	6,99	5,36	5,48	3,92	1,31	1,09	1,21	1,31	0,80	Nitrilase homolog 2
CAMK1D	2,92	0,00	0,00	1,07	0,00	2,94	-2,74	-2,72	-1,01	2,74	0,80	Isoform 1 of Calcium/calmodulin-dependent protein kinase type 1D
POTEE	9,72	13,61	12,98	15,00	14,25	12,73	1,04	1,20	-1,16	1,20	0,81	Isoform 1 of POTE ankyrin domain family member E
RPS6	2,92	1,81	4,99	1,07	2,19	1,96	1,46	1,28	1,14	1,46	0,81	40S ribosomal protein S6
CDH2	1,94	2,72	3,00	3,21	2,19	1,96	1,50	1,33	1,12	1,50	0,81	Cadherin-2
CNDP2	27,22	30,85	23,96	27,85	35,07	22,51	-1,11	-1,12	1,01	1,12	0,81	Cytosolic non-specific dipeptidase
LANCL2	5,83	5,44	5,99	7,50	7,67	6,85	-1,08	1,20	-1,29	1,29	0,81	LanC-like protein 2
EEF1B2	3,89	1,81	3,00	3,21	3,29	0,98	1,46	1,09	1,34	1,46	0,81	Elongation factor 1-beta
SNRPD2	3,89	1,81	3,99	2,14	2,19	1,96	1,48	1,08	1,37	1,48	0,81	Small nuclear ribonucleoprotein Sm D2

Gene Symbol	AD1 nc	AD2 nc	capCAA1 nc	capCAA2 nc	C1 nc	C2 nc	fc.cap-CAA/C	fc.capCAA/AD	fc. AD/C	fc. max	pvalues	Protein name
VDAC1	55,41	69,87	58,91	56,77	55,89	63,63	-1,03	-1,08	1,05	1,08	0,81	Voltage-dependent anion-selective channel protein 1
TUBA1C	14,58	22,68	18,97	19,28	18,63	14,68	1,15	1,03	1,12	1,15	0,81	Tubulin alpha-1C chain
RAP1B	4,86	7,26	5,99	8,57	6,58	8,81	-1,06	1,20	-1,27	1,27	0,81	Ras-related protein Rap-1b
GSTM3	20,41	14,52	20,97	18,21	19,73	14,68	1,14	1,12	1,02	1,14	0,81	Glutathione S-transferase Mu 3
HMGB1	2,92	8,17	6,99	1,07	5,48	3,92	-1,17	-1,37	1,18	1,37	0,81	High mobility group protein B1
ATP6V1D	8,75	4,54	8,99	6,43	8,77	7,83	-1,08	1,16	-1,25	1,25	0,81	V-type proton ATPase subunit D
DPYSL3	9,72	9,98	7,99	16,07	28,49	5,87	-1,43	1,22	-1,74	1,74	0,81	Dihydropyrimidinase-related protein 3
PDXP	8,75	8,17	9,98	9,64	13,15	7,83	-1,07	1,16	-1,24	1,24	0,81	Pyridoxal phosphate phosphatase
PLP1	97,21	85,29	52,92	114,61	130,42	67,54	-1,18	-1,09	-1,08	1,18	0,81	Isoform 1 of Myelin proteolipid protein
HSD17B4	4,86	1,81	6,99	1,07	1,10	3,92	1,61	1,21	1,33	1,61	0,81	Peroxisomal multifunctional enzyme type 2
CLTA	5,83	2,72	3,00	3,21	3,29	4,89	-1,32	-1,38	1,05	1,38	0,81	Isoform Brain of Clathrin light chain A
FAM49A	3,89	4,54	4,99	3,21	2,19	3,92	1,34	-1,03	1,38	1,38	0,81	Protein FAM49A
KRT6A	12,64	0,00	2,00	0,00	2,19	0,98	-1,59	-6,33	3,99	6,33	0,81	Keratin, type II cytoskeletal 6A
KRT16	10,69	0,00	3,99	0,00	2,19	2,94	-1,28	-2,68	2,08	2,68	0,81	Keratin, type I cytoskeletal 16
IDH3B	13,61	9,07	10,98	12,85	13,15	13,70	-1,13	1,05	-1,18	1,18	0,81	Isocitrate dehydrogenase 3, beta subunit isoform a precursor
TIPRL	1,94	0,00	2,00	1,07	2,19	0,98	-1,03	1,58	-1,63	1,63	0,81	Isoform 2 of TIP41-like protein
SLC25A27	0,97	0,91	2,00	1,07	1,10	1,96	1,00	1,63	-1,62	1,63	0,82	Mitochondrial uncoupling protein 4
VBP1	0,97	0,91	2,00	1,07	2,19	0,98	-1,03	1,63	-1,69	1,69	0,82	Von Hippel-Lindau binding protein 1
CRAT	0,97	0,91	2,00	1,07	2,19	0,98	-1,03	1,63	-1,69	1,69	0,82	Isoform 1 of Carnitine O-acetyltransferase
GNB2L1	6,80	5,44	7,99	5,36	7,67	7,83	-1,16	1,09	-1,27	1,27	0,82	38 kDa protein
VDAC3	25,27	27,22	28,96	29,99	21,92	31,32	1,11	1,12	-1,01	1,12	0,82	Isoform 2 of Voltage-dependent anion-selective channel protein 3
ABHD10	6,80	5,44	10,98	4,28	5,48	7,83	1,15	1,25	-1,09	1,25	0,82	Abhydrolase domain-containing protein 10, mitochondrial
MTCH2	8,75	3,63	9,98	5,36	5,48	7,83	1,15	1,24	-1,08	1,24	0,82	Mitochondrial carrier homolog 2
COX5B	13,61	10,89	17,97	7,50	10,96	17,62	-1,12	1,04	-1,17	1,17	0,82	Cytochrome c oxidase subunit 5B, mitochondrial
SFXN3	7,78	5,44	10,98	3,21	6,58	9,79	-1,15	1,07	-1,24	1,24	0,82	sideroflexin 3
ECHS1	20,41	17,24	21,97	20,35	17,54	24,47	1,01	1,12	-1,12	1,12	0,82	Enoyl-CoA hydratase, mitochondrial
CLTB	7,78	6,35	4,99	6,43	5,48	5,87	1,01	-1,24	1,24	1,24	0,82	Isoform Brain of Clathrin light chain B
CLTC	265,37	303,97	311,52	283,84	229,05	329,88	1,07	1,05	1,02	1,07	0,82	Isoform 1 of Clathrin heavy chain 1
ATP6V0D1	30,13	40,83	36,94	26,78	31,78	36,22	-1,07	-1,11	1,04	1,11	0,82	V-type proton ATPase subunit d 1
A2M	19,44	8,17	9,98	12,85	13,15	11,75	-1,09	-1,21	1,11	1,21	0,82	Alpha-2-macroglobulin
AP2B1	54,44	54,44	62,90	53,55	51,51	64,61	1,00	1,07	-1,07	1,07	0,83	Isoform 1 of AP-2 complex subunit beta-1
ACBD7	0,97	0,91	1,00	0,00	0,00	1,96	-1,96	-1,88	-1,04	1,96	0,83	Acyl-CoA-binding domain-containing protein 7
HMGCL	0,97	0,91	1,00	0,00	0,00	1,96	-1,96	-1,88	-1,04	1,96	0,83	Hydroxymethylglutaryl-CoA lyase, mitochondrial
TOMM22	1,94	0,00	1,00	0,00	0,00	1,96	-1,96	-1,95	-1,01	1,96	0,83	Mitochondrial import receptor subunit TOM22 homolog
RAP1GAP	1,94	0,00	1,00	0,00	2,19	0,00	-2,20	-1,95	-1,13	2,20	0,83	RAP1 GTPase activating protein
DYNC1I1	1,94	0,00	1,00	0,00	2,19	0,00	-2,20	-1,95	-1,13	2,20	0,83	Isoform 2 of Cytoplasmic dynein 1 intermediate chain 1
ME1	0,97	0,91	0,00	2,14	0,00	0,98	2,19	1,14	1,92	2,19	0,83	NADP-dependent malic enzyme
GRM5	0,97	0,91	2,00	0,00	0,00	0,98	2,04	1,06	1,92	2,04	0,83	Isoform 2 of Metabotropic glutamate receptor 5
PGAM5	1,94	0,00	1,00	1,07	1,10	0,98	1,89	1,06	1,77	1,89	0,83	Isoform 2 of Phosphoglycerate mutase family member 5
DNAJA1	0,00	1,81	0,00	2,14	1,10	0,00	1,95	1,18	1,66	1,95	0,83	DnaJ homolog subfamily A member 1
WDR37	0,00	1,81	2,00	0,00	1,10	0,00	1,82	1,10	1,66	1,82	0,83	cDNA FLJ76685, highly similar to Homo sapiens WD repeat domain 37 (WDR37), mRNA
GGCT	2,92	2,72	3,00	2,14	4,38	2,94	-1,42	-1,10	-1,30	1,42	0,83	Isoform 1 of Gamma-glutamylcyclotransferase
DNAJA2	3,89	1,81	3,00	2,14	3,29	3,92	-1,40	-1,11	-1,26	1,40	0,83	DnaJ homolog subfamily A member 2

Gene Symbol	AD1 nc	AD2 nc	capCAA1 nc	capCAA2 nc	C1 nc	C2 nc	fc.cap-CAA/C	fc.capCAA/AD	fc. AD/C	fc. max	pvalues	Protein name
PPP2R1A	37,91	36,30	39,94	40,70	42,74	38,18	-1,00	-1,09	-1,09	1,09	0,83	Serine/threonine-protein phosphatase 2A 65 kDa regulatory subunit A alpha isoform
RAB14	14,58	9,07	10,98	9,64	8,77	10,77	1,06	-1,15	1,21	1,21	0,83	Ras-related protein Rab-14
PPP2CB	14,58	12,70	10,98	12,85	14,25	13,70	-1,17	-1,14	-1,02	1,17	0,83	Serine/threonine-protein phosphatase 2A catalytic subunit beta isoform
VAMP2	15,55	19,96	15,98	15,00	16,44	15,66	-1,04	-1,15	1,11	1,15	0,83	Vesicle-associated membrane protein 2
APOA1	5,83	3,63	3,00	4,28	1,10	9,79	-1,50	-1,30	-1,15	1,50	0,83	Apolipoprotein A-I
PRKT2	18,47	16,33	18,97	13,92	9,86	19,58	1,12	-1,06	1,18	1,18	0,84	Isoform 2 of Proline-rich transmembrane protein 2
SYNJ1	37,91	25,41	31,95	24,64	31,78	30,34	-1,10	-1,12	1,02	1,12	0,84	Isoform 1 of Synaptojanin-1
OAT	1,94	0,00	1,00	1,07	1,10	1,96	-1,48	1,06	-1,57	1,57	0,84	Ornithine aminotransferase, mitochondrial
MGEA5	0,00	1,81	1,00	1,07	1,10	1,96	-1,48	1,14	-1,68	1,68	0,84	meningioma expressed antigen 5 (hyaluronidase) isoform b
PABPC1	1,94	0,00	2,00	0,00	1,10	1,96	-1,53	1,03	-1,57	1,57	0,84	Isoform 1 of Polyadenylate-binding protein 1
TIMM8A	0,00	1,81	2,00	0,00	1,10	1,96	-1,53	1,10	-1,68	1,68	0,84	Mitochondrial import inner membrane translocase subunit Tim8 A
DNAJC19	0,97	0,91	1,00	1,07	1,10	1,96	-1,48	1,10	-1,62	1,62	0,84	Mitochondrial import inner membrane translocase subunit TIM14
PPIF	0,97	0,91	1,00	1,07	1,10	1,96	-1,48	1,10	-1,62	1,62	0,84	Peptidyl-prolyl cis-trans isomerase, mitochondrial
ISOC1	0,97	0,91	1,00	1,07	2,19	0,98	-1,53	1,10	-1,69	1,69	0,84	Isochorismatase domain-containing protein 1
NSFL1C	0,97	0,91	1,00	1,07	2,19	0,98	-1,53	1,10	-1,69	1,69	0,84	Isoform 1 of NSFL1 cofactor p47
CPPED1	0,97	0,91	1,00	1,07	2,19	0,98	-1,53	1,10	-1,69	1,69	0,84	Isoform 1 of Calcineurin-like phosphoesterase domain-containing protein 1
SEPT3	8,75	14,52	9,98	11,78	9,86	15,66	-1,17	-1,07	-1,10	1,17	0,84	Isoform 1 of Neuronal-specific septin-3
DEFA1|LOC728358	0,00	1,81	1,00	2,14	1,10	0,98	1,51	1,73	-1,14	1,73	0,84	Neutrophil defensin 1
MRPS36	0,97	0,91	2,00	1,07	0,00	1,96	1,57	1,63	-1,04	1,63	0,84	28S ribosomal protein S36, mitochondrial
CHMP6	0,97	0,91	2,00	1,07	2,19	0,00	1,40	1,63	-1,17	1,63	0,84	Charged multivesicular body protein 6
APRT	0,97	0,91	2,00	1,07	1,10	0,98	1,48	1,63	-1,10	1,63	0,84	Adenine phosphoribosyltransferase
EIF4E	0,97	0,91	2,00	1,07	1,10	0,98	1,48	1,63	-1,10	1,63	0,84	Eukaryotic translation initiation factor 4E
ABHD11	0,97	0,91	2,00	1,07	1,10	0,98	1,48	1,63	-1,10	1,63	0,84	Isoform 4 of Abhydrolase domain-containing protein 11
PGP	0,97	0,91	2,00	1,07	1,10	0,98	1,48	1,63	-1,10	1,63	0,84	Phosphoglycolate phosphatase
TPM3	0,97	0,91	2,00	1,07	1,10	0,98	1,48	1,63	-1,10	1,63	0,84	tropomyosin 3 isoform 1
CARKD	5,83	2,72	3,00	3,21	4,38	2,94	-1,18	-1,38	1,17	1,38	0,84	Isoform 1 of Carbohydrate kinase domain-containing protein
TPP2	1,94	0,00	1,00	0,00	0,00	0,98	1,02	-1,95	1,99	1,99	0,84	Tripeptidyl-peptidase 2
C1orf31	0,00	1,81	0,00	1,07	0,00	0,98	1,09	-1,69	1,85	1,85	0,84	Isoform 1 of Uncharacterized protein C1orf31
GNG4	0,00	1,81	1,00	0,00	1,10	0,00	-1,10	-1,82	1,66	1,82	0,84	Guanine nucleotide-binding protein G(I)/G(S)/G(O) subunit gamma-4
PPFIA3	1,94	0,00	1,00	0,00	1,10	0,00	-1,10	-1,95	1,77	1,95	0,84	Isoform 1 of Liprin-alpha-3
COPS6	1,94	0,00	0,00	0,00	1,10	0,00	-1,10	-1,95	1,77	1,95	0,84	COP9 signalosome complex subunit 6
AP1B1	4,86	1,81	3,00	2,14	5,48	1,96	-1,45	-1,30	-1,11	1,45	0,84	Isoform A of AP-1 complex subunit beta-1
SEPT6	3,89	4,54	4,99	2,14	2,19	3,92	1,17	-1,18	1,38	1,38	0,84	Isoform 1 of Septin-6
ERLIN2	4,86	3,63	3,00	4,28	4,38	1,96	1,15	-1,17	1,34	1,34	0,84	Isoform 1 of Erlin-2
RAB4B	4,86	3,63	3,99	3,21	3,29	2,94	1,16	-1,18	1,36	1,36	0,84	Isoform 2 of Ras-related protein Rab-4B
DIRAS2	4,86	1,81	4,99	2,14	2,19	2,94	1,39	1,07	1,30	1,39	0,84	GTP-binding protein Di-Ras2
SNX3	2,92	3,63	3,99	3,21	2,19	2,94	1,41	1,10	1,28	1,41	0,84	Isoform 1 of Sorting nexin-3
GDI2	26,25	20,87	19,97	22,49	28,49	19,58	-1,13	-1,11	-1,02	1,13	0,84	cDNA FLJ60299, highly similar to Rab GDP dissociation inhibitor beta
FGB	5,83	5,44	3,00	22,49	14,25	2,94	1,48	2,26	-1,52	2,26	0,84	Fibrinogen beta chain
UBE2N	5,83	9,07	6,99	5,36	7,67	4,89	-1,02	-1,21	1,19	1,21	0,84	Ubiquitin-conjugating enzyme E2 N
SNAP91	36,94	36,30	38,94	37,49	31,78	37,20	1,11	1,04	1,06	1,11	0,84	Isoform 1 of Clathrin coat assembly protein AP180
REEP5	14,58	9,07	11,98	7,50	10,96	10,77	-1,12	-1,21	1,09	1,21	0,84	Receptor expression-enhancing protein 5
SEPT2	16,53	20,87	16,97	20,35	16,44	16,64	1,13	-1,00	1,13	1,13	0,84	Septin-2

Gene Symbol	AD1 nc	AD2 nc	capCAA1 nc	capCAA2 nc	C1 nc	C2 nc	fc.cap-CAA/C	fc.capCAA/AD	fc.AD/C	fc.max	pvalues	Protein name
L1CAM	7,78	16,33	11,98	10,71	16,44	10,77	-1,20	-1,06	-1,13	1,20	0,84	Isoform 1 of Neural cell adhesion molecule L1
TPRG1L	0,00	2,72	3,00	1,07	1,10	2,94	1,01	1,49	-1,48	1,49	0,84	Isoform 1 of Tumor protein p63-regulated gene 1-like protein
CD200	0,97	1,81	2,00	2,14	1,10	2,94	1,03	1,49	-1,45	1,49	0,84	Isoform 1 of OX-2 membrane glycoprotein
FAM62A	2,92	0,00	3,00	1,07	2,19	1,96	-1,02	1,39	-1,42	1,42	0,84	Isoform 1 of Extended synaptotagmin-1
COPG	1,94	0,91	2,00	2,14	2,19	1,96	-1,00	1,45	-1,46	1,46	0,84	Coatomer subunit gamma
IAH1	1,94	0,91	2,00	2,14	2,19	1,96	-1,00	1,45	-1,46	1,46	0,84	Isoamyl acetate-hydrolyzing esterase 1 homolog
PLCB1	21,39	14,52	22,96	7,50	10,96	21,54	-1,07	-1,18	1,10	1,18	0,84	Isoform A of 1-phosphatidylinositol-4,5-bisphosphate phosphodiesterase beta-1
TCEB2	2,92	1,81	3,00	0,00	2,19	1,96	-1,39	-1,58	1,14	1,58	0,84	Transcription elongation factor B polypeptide 2
COMT	2,92	1,81	2,00	2,14	2,19	0,98	1,31	-1,14	1,49	1,49	0,85	Isoform Membrane-bound of Catechol O-methyltransferase
LY6G5B;CSNK2B	1,94	2,72	2,00	2,14	2,19	0,98	1,31	-1,13	1,47	1,47	0,85	Casein kinase II subunit beta
NHP2L1	2,92	1,81	2,00	2,14	1,10	1,96	1,36	-1,14	1,55	1,55	0,85	NHP2-like protein 1
PLCXD3	2,92	1,81	1,00	3,21	3,29	0,00	1,28	-1,12	1,44	1,44	0,85	cDNA FLJ45199 fis, clone BRCAN2003814, highly similar to Homo sapiens phosphatidylinositol-specific phospholipase C, X domain containing 3 (PLCXD3), mRNA
NCL	6,80	1,81	4,99	1,07	1,10	4,89	1,01	-1,42	1,44	1,44	0,85	cDNA FLJ45706 fis, clone FEBRA2028457, highly similar to Nucleolin
PGAM1	39,85	35,39	33,95	37,49	32,88	35,24	1,05	-1,05	1,10	1,10	0,85	Phosphoglycerate mutase 1
CPLX1	3,89	0,91	3,99	0,00	0,00	2,94	1,36	-1,20	1,63	1,63	0,85	Complexin-1
TOM1	2,92	3,63	3,99	4,28	2,19	3,92	1,36	1,26	1,07	1,36	0,85	cDNA FLJ54710, highly similar to Target of Myb protein 1
NDUFS3	21,39	15,43	19,97	21,42	15,34	24,47	1,04	1,12	-1,08	1,12	0,85	NADH dehydrogenase [ubiquinone] iron-sulfur protein 3, mitochondrial
GNAZ	14,58	8,17	18,97	7,50	14,25	11,75	1,02	1,16	-1,14	1,16	0,85	Guanine nucleotide-binding protein G(z) subunit alpha
CNP	163,31	162,42	99,85	211,01	213,71	83,20	1,05	-1,05	1,10	1,10	0,85	Isoform CNPI of 2',3'-cyclic-nucleotide 3'-phosphodiesterase
CNTN1	95,26	117,05	117,82	82,47	109,59	90,06	1,00	-1,06	1,06	1,06	0,85	Isoform 1 of Contactin-1
NDUFA3	3,89	1,81	2,00	2,14	2,19	1,96	-1,00	-1,38	1,37	1,38	0,85	NADH dehydrogenase [ubiquinone] 1 alpha subcomplex subunit 3
RNH1	22,36	14,52	14,98	27,85	24,11	13,70	1,13	1,16	-1,03	1,16	0,85	Ribonuclease inhibitor
SV2A	22,36	26,31	25,96	20,35	20,82	22,51	1,07	-1,05	1,12	1,12	0,85	Isoform 1 of Synaptic vesicle glycoprotein 2A
-	4,86	5,44	2,00	6,43	4,38	3,92	1,01	-1,22	1,24	1,24	0,85	cDNA FLJ39243 fis, clone OCBBF2008283, highly similar to Protein NDRG1
NNT	28,19	20,87	32,95	18,21	23,01	31,32	-1,06	1,04	-1,11	1,11	0,85	NAD(P) transhydrogenase, mitochondrial
BGN	0,00	0,91	0,00	18,21	0,00	9,79	1,86	20,07	-10,79	20,07	0,86	Biglycan
FABP5;FABP5L7	7,78	6,35	5,99	7,50	5,48	5,87	1,19	-1,05	1,24	1,24	0,86	Fatty acid-binding protein, epidermal
OTUB1	11,66	10,89	12,98	12,85	16,44	9,79	-1,02	1,15	-1,16	1,16	0,86	cDNA FLJ56307, highly similar to Ubiquitin thioesterase protein OTUB1
ADD2	17,50	21,78	21,97	17,14	13,15	21,54	1,13	-1,00	1,13	1,13	0,86	Isoform 1 of Beta-adducin
HSPA8	173,03	177,85	165,75	200,29	192,89	170,32	1,01	1,04	-1,04	1,04	0,86	Isoform 1 of Heat shock cognate 71 kDa protein
EEA1	2,92	0,91	3,00	2,14	4,38	0,98	-1,04	1,34	-1,40	1,40	0,86	Early endosome antigen 1
DST	2,92	0,91	3,99	1,07	3,29	1,96	-1,04	1,32	-1,37	1,37	0,86	Dystonin
PBXIP1	1,94	1,81	2,00	3,21	4,38	0,98	-1,03	1,39	-1,43	1,43	0,86	Isoform 3 of Pre-B-cell leukemia transcription factor-interacting protein 1
TMEM109	1,94	1,81	3,00	2,14	3,29	1,96	-1,02	1,37	-1,40	1,40	0,86	Transmembrane protein 109
DCLK1	7,78	9,98	8,99	6,43	10,96	7,83	-1,22	-1,15	-1,06	1,22	0,86	Isoform 2 of Serine/threonine-protein kinase DCLK1
AQP4	15,55	21,78	20,97	11,78	18,63	17,62	-1,11	-1,14	1,03	1,14	0,86	Isoform 2 of Aquaporin-4
NDUFB4	5,83	4,54	5,99	2,14	3,29	6,85	-1,25	-1,27	1,02	1,27	0,86	NADH dehydrogenase [ubiquinone] 1 beta subcomplex subunit 4
VAT1	2,92	7,26	3,99	7,50	19,73	1,96	-1,89	1,13	-2,13	2,13	0,86	Synaptic vesicle membrane protein VAT-1 homolog
ACAT1	15,55	19,96	17,97	22,49	16,44	20,56	1,09	1,14	-1,04	1,14	0,86	Acetyl-CoA acetyltransferase, mitochondrial
SRI	19,44	18,15	18,97	17,14	12,06	20,56	1,11	-1,04	1,15	1,15	0,86	Sorcin
SLC4A10	4,86	0,91	6,99	0,00	0,00	3,92	1,79	1,21	1,47	1,79	0,86	Isoform 1 of Sodium-driven chloride bicarbonate exchanger
VDAC2	48,60	45,37	44,93	47,13	41,65	56,77	-1,07	-1,02	-1,05	1,07	0,86	Isoform 3 of Voltage-dependent anion-selective channel protein 2

Gene Symbol	AD1 nc	AD2 nc	capCAA1 nc	capCAA2 nc	C1 nc	C2 nc	fc.cap-CAA/C	fc.capCAA/AD	fc.AD/C	fc.max	pvalues	Protein name
SIRT2	18,47	17,24	13,98	35,35	36,17	7,83	1,12	1,38	-1,23	1,38	0,86	Isoform 1 of NAD-dependent deacetylase sirtuin-2
NDUFS7	4,86	2,72	5,99	1,07	2,19	6,85	-1,28	-1,07	-1,19	1,28	0,87	NADH dehydrogenase [ubiquinone] iron-sulfur protein 7, mitochondrial
OPALIN	4,86	4,54	2,00	6,43	6,58	0,98	1,12	-1,12	1,24	1,24	0,87	Opalin
WDR7	9,72	1,81	6,99	1,07	3,29	3,92	1,12	-1,43	1,60	1,60	0,87	Isoform 1 of WD repeat-containing protein 7
TSPAN7	7,78	4,54	9,98	1,07	6,58	6,85	-1,21	-1,11	-1,09	1,21	0,87	cDNA FLJ58051, highly similar to Tetraspanin-7
PTGES2	5,83	3,63	4,99	2,14	3,29	4,89	-1,15	-1,33	1,16	1,33	0,87	Prostaglandin E synthase 2
TUBB	25,27	25,41	24,96	24,64	31,78	23,49	-1,11	-1,02	-1,09	1,11	0,87	Tubulin beta chain
COPS5	2,92	0,00	2,00	1,07	3,29	0,98	-1,39	1,05	-1,46	1,46	0,87	COP9 signalosome complex subunit 5
BSCL2	1,94	0,91	2,00	1,07	2,19	1,96	-1,35	1,08	-1,46	1,46	0,87	Seipin
MRAS	1,94	0,91	1,00	2,14	2,19	1,96	-1,32	1,10	-1,46	1,46	0,87	Ras-related protein M-Ras
DLG2	1,94	0,91	2,00	1,07	2,19	1,96	-1,35	1,08	-1,46	1,46	0,87	Isoform 1 of Disks large homolog 2
PDDC1	1,94	0,91	2,00	1,07	2,19	1,96	-1,35	1,08	-1,46	1,46	0,87	Isoform 3 of Parkinson disease 7 domain-containing protein 1
CORO2B	0,00	2,72	2,00	1,07	1,10	2,94	-1,31	1,13	-1,48	1,48	0,87	coronin, actin binding protein, 2B
ROGDI	2,92	0,00	1,00	1,07	1,10	2,94	-1,31	1,05	-1,38	1,38	0,87	Protein rogdi homolog
C14orf159	2,92	0,00	1,00	3,21	1,10	1,96	1,38	1,44	-1,05	1,44	0,87	Isoform 3 of UPF0317 protein C14orf159, mitochondrial
IGHM	0,97	1,81	2,00	2,14	2,19	0,98	1,31	1,49	-1,14	1,49	0,87	FLJ00385 protein (Fragment)
HINT3	0,97	1,81	1,00	2,14	4,38	0,00	-1,40	1,13	-1,57	1,57	0,87	Histidine triad nucleotide-binding protein 3
C14orf166	5,83	2,72	4,99	5,36	3,29	4,89	1,26	1,21	1,05	1,26	0,87	UPF0568 protein C14orf166
BSN	8,75	8,17	15,98	3,21	1,10	16,64	1,08	1,13	-1,05	1,13	0,87	Protein bassoon
GLUD1	66,10	107,98	82,87	78,19	86,58	73,42	1,01	-1,08	1,09	1,09	0,87	Glutamate dehydrogenase 1, mitochondrial
SPTBN1	304,26	363,86	357,45	319,19	333,17	322,05	1,03	1,01	1,02	1,03	0,87	Isoform Long of Spectrin beta chain, brain 1
SNCG	14,58	12,70	15,98	10,71	14,25	9,79	1,11	-1,02	1,14	1,14	0,87	Gamma-synuclein
PARK7	25,27	28,13	29,95	26,78	30,69	28,39	-1,04	1,06	-1,11	1,11	0,87	Protein DJ-1
STMN1	12,64	9,98	7,99	11,78	12,06	7,83	-1,01	-1,14	1,14	1,14	0,87	Stathmin
CANX	15,55	17,24	13,98	22,49	16,44	15,66	1,14	1,11	1,02	1,14	0,87	cDNA FLJ55574, highly similar to Calnexin
QDPR	40,83	34,48	26,96	49,27	40,55	28,39	1,11	1,01	1,09	1,11	0,87	Dihydropteridine reductase
DYNC1H1	172,06	117,96	160,75	102,83	165,49	117,46	-1,07	-1,10	1,02	1,10	0,87	Cytoplasmic dynein 1 heavy chain 1
HAPLN2	24,30	5,44	5,99	21,42	19,73	2,94	1,21	-1,09	1,31	1,31	0,88	Hyaluronan and proteoglycan link protein 2
KRAS	4,86	4,54	4,99	4,28	6,58	4,89	-1,24	-1,01	-1,22	1,24	0,88	Isoform 2B of GTPase KRas
AKR1A1	5,83	3,63	6,99	4,28	4,38	4,89	1,22	1,19	1,02	1,22	0,88	Alcohol dehydrogenase [NADP+]
NDUFB10	8,75	9,07	8,99	7,50	6,58	12,73	-1,17	-1,08	-1,08	1,17	0,88	NADH dehydrogenase [ubiquinone] 1 beta subcomplex subunit 10
GDAP1	9,72	8,17	8,99	7,50	9,86	9,79	-1,19	-1,09	-1,10	1,19	0,88	Ganglioside-induced differentiation-associated protein 1
MTX2	4,86	2,72	4,99	4,28	3,29	5,87	1,01	1,22	-1,21	1,22	0,88	Metaxin-2
FLOT1	3,89	6,35	7,99	4,28	7,67	4,89	-1,02	1,20	-1,23	1,23	0,88	Flotillin-1
C1QBP	7,78	7,26	6,99	6,43	5,48	6,85	1,09	-1,12	1,22	1,22	0,88	Complement component 1 Q subcomponent-binding protein, mitochondrial
ACTR1A	8,75	6,35	6,99	6,43	7,67	4,89	1,07	-1,13	1,20	1,20	0,88	Alpha-centractin
SCAMP5	7,78	7,26	6,99	6,43	6,58	5,87	1,08	-1,12	1,21	1,21	0,88	Isoform 1 of Secretory carrier-associated membrane protein 5
OMG	12,64	11,80	12,98	15,00	15,34	11,75	1,03	1,14	-1,11	1,14	0,88	Oligodendrocyte-myelin glycoprotein
ECH1	5,83	5,44	3,99	7,50	3,29	5,87	1,25	1,02	1,23	1,25	0,88	Delta(3,5)-Delta(2,4)-dienoyl-CoA isomerase, mitochondrial
SDHA	18,47	14,52	13,98	15,00	12,06	18,60	-1,06	-1,14	1,08	1,14	0,88	57 kDa protein
HPR	10,69	9,07	3,99	23,56	16,44	9,79	1,05	1,39	-1,33	1,39	0,88	47 kDa protein
ICAM5	3,89	14,52	11,98	2,14	4,38	11,75	-1,14	-1,30	1,14	1,30	0,88	intercellular adhesion molecule 5 precursor
YWHAH	16,53	22,68	17,97	17,14	19,73	17,62	-1,06	-1,12	1,05	1,12	0,88	14-3-3 protein eta

Gene Symbol	AD1 nc	AD2 nc	capCAA1 nc	capCAA2 nc	C1 nc	C2 nc	fc.cap-CAA/C	fc.capCAA/AD	fc. AD/C	fc. max	pvalues	Protein name
FSCN1	30,13	26,31	27,96	24,64	31,78	26,43	-1,11	-1,07	-1,03	1,11	0,88	Fascin
GOT1	59,30	62,61	56,91	66,41	53,70	61,67	1,07	1,01	1,06	1,07	0,88	Aspartate aminotransferase, cytoplasmic
TNR	68,04	63,52	66,90	56,77	69,04	61,67	-1,06	-1,06	1,01	1,06	0,88	Isoform 1 of Tenascin-R
LAP3	3,89	7,26	4,99	6,43	7,67	5,87	-1,19	1,02	-1,22	1,22	0,89	Isoform 1 of Cytosol aminopeptidase
NDUFB5	2,92	0,91	3,00	1,07	1,10	3,92	-1,23	1,06	-1,31	1,31	0,89	NADH dehydrogenase [ubiquinone] 1 beta subcomplex subunit 5, mitochondrial
UBE2V1;TMEM189-UBE2V1	2,92	2,72	2,00	2,14	2,19	2,94	-1,24	-1,36	1,10	1,36	0,89	Isoform 1 of Ubiquitin-conjugating enzyme E2 variant 1
NME1	2,92	2,72	1,00	3,21	2,19	2,94	-1,22	-1,34	1,10	1,34	0,89	Isoform 1 of Nucleoside diphosphate kinase A
CYB5B	1,94	1,81	3,00	2,14	2,19	1,96	1,24	1,37	-1,10	1,37	0,89	cytochrome b5 outer mitochondrial membrane precursor
PEF1	1,94	1,81	3,00	2,14	2,19	1,96	1,24	1,37	-1,10	1,37	0,89	Peflin
RDH11	2,92	0,91	3,00	2,14	3,29	0,98	1,20	1,34	-1,12	1,34	0,89	Isoform 1 of Retinol dehydrogenase 11
RPS2	2,92	0,91	3,99	1,07	3,29	0,98	1,19	1,32	-1,12	1,32	0,89	40S ribosomal protein S2
NDUFB6	0,97	2,72	3,99	1,07	1,10	2,94	1,26	1,37	-1,09	1,37	0,89	NADH dehydrogenase [ubiquinone] 1 beta subcomplex subunit 6
RPS18;LOC100130553	4,86	6,35	7,99	5,36	3,29	7,83	1,20	1,19	1,01	1,20	0,89	40S ribosomal protein S18
ADAM22	5,83	0,91	3,99	4,28	1,10	5,87	1,19	1,23	-1,03	1,23	0,89	Isoform 1 of Disintegrin and metalloproteinase domain-containing protein 22
GPR37L1	1,94	3,63	3,00	2,14	1,10	2,94	1,27	-1,08	1,38	1,38	0,89	Endothelin B receptor-like protein 2
EEF1D	3,89	1,81	3,00	2,14	4,38	0,00	1,17	-1,11	1,30	1,30	0,89	Elongation factor 1-delta
KPNB1	10,69	10,89	10,98	13,92	14,25	9,79	1,04	1,15	-1,11	1,15	0,89	Importin subunit beta-1
CCT4;ILK-2	15,55	11,80	11,98	11,78	14,25	11,75	-1,09	-1,15	1,05	1,15	0,89	T-complex protein 1 subunit delta
HNRNPU	10,69	4,54	13,98	4,28	4,38	9,79	1,29	1,20	1,07	1,29	0,89	Isoform Short of Heterogeneous nuclear ribonucleoprotein U
SDHB	13,61	8,17	8,99	9,64	6,58	13,70	-1,09	-1,17	1,07	1,17	0,89	Succinate dehydrogenase [ubiquinone] iron-sulfur subunit, mitochondrial
NIPSNAP1	11,66	8,17	11,98	9,64	13,15	9,79	-1,06	1,09	-1,16	1,16	0,89	Protein NipSnap homolog 1
NDUFA12	5,83	4,54	5,99	3,21	2,19	5,87	1,14	-1,13	1,29	1,29	0,89	13kDa differentiation-associated protein variant (Fragment)
STX8P1	223,58	207,79	231,65	212,08	197,27	234,93	1,03	1,03	-1,00	1,03	0,89	Isoform 1 of Syntaxin-binding protein 1
AARS	23,33	9,07	16,97	10,71	14,25	17,62	-1,15	-1,17	1,02	1,17	0,89	Alanyl-tRNA synthetase, cytoplasmic
-	8,75	6,35	8,99	6,43	6,58	10,77	-1,13	1,02	-1,15	1,15	0,89	22 kDa protein
EPB41L2	7,78	6,35	5,99	11,78	9,86	4,89	1,13	1,18	-1,04	1,18	0,89	Band 4.1-like protein 2
ASAH1	7,78	7,26	5,99	11,78	8,77	6,85	1,14	1,18	-1,04	1,18	0,89	Acid ceramidase
SERPINA3	3,89	5,44	2,00	6,43	5,48	4,89	-1,23	-1,11	-1,11	1,23	0,89	cDNA FLJ35730fis, clone TESTI2003131, highly similar to ALPHA-1-ANTICHYMOTRYPSIN
FAHD1	5,83	3,63	3,99	4,28	3,29	6,85	-1,22	-1,14	-1,07	1,22	0,89	Isoform 2 of Fumarylacetoacetate hydrolase domain-containing protein 1
RAB10	7,78	8,17	8,99	5,36	7,67	5,87	1,06	-1,11	1,18	1,18	0,90	Ras-related protein Rab-10
KIF2A	3,89	0,91	3,99	1,07	3,29	2,94	-1,23	1,06	-1,30	1,30	0,90	Isoform 1 of Kinesin-like protein KIF2A
MAP1LC3B2	2,92	1,81	2,00	1,07	3,29	2,94	-1,23	1,07	-1,32	1,32	0,90	Microtubule-associated proteins 1A/1B light chain 3 beta 2
CUTA	0,97	3,63	2,00	3,21	3,29	2,94	-1,19	1,13	-1,35	1,35	0,90	Isoform A of Protein CutA
HP1BP3	1,94	2,72	2,00	3,21	4,38	1,96	-1,22	1,12	-1,36	1,36	0,90	Heterochromatin protein 1, binding protein 3
ARF6	2,92	1,81	3,99	2,14	1,10	3,92	1,22	1,30	-1,06	1,30	0,90	ADP-ribosylation factor 6
RTN4	24,30	16,33	19,97	19,28	23,01	20,56	-1,11	-1,04	-1,07	1,11	0,90	Isoform 1 of Reticulon-4
PRKAR2A	1,94	0,91	2,00	0,00	3,29	0,00	-1,65	-1,43	-1,15	1,65	0,90	Protein kinase, cAMP-dependent, regulatory, type II, alpha, isoform CRA_b
B2M	1,94	0,91	0,00	2,14	1,10	1,96	-1,43	-1,33	-1,07	1,43	0,90	Beta-2-microglobulin
BCL2L13	1,94	0,91	2,00	0,00	1,10	1,96	-1,53	-1,43	-1,07	1,53	0,90	Isoform 2 of Bcl-2-like protein 13
PREPL	2,92	0,00	2,00	1,07	1,10	0,98	1,48	1,05	1,41	1,48	0,90	Isoform 1 of Prolyl endopeptidase-like
RPL31	1,94	0,91	2,00	1,07	1,10	0,98	1,48	1,08	1,37	1,48	0,90	60S ribosomal protein L31
SAMM50	2,92	0,00	1,00	2,14	1,10	0,98	1,51	1,08	1,41	1,51	0,90	Sorting and assembly machinery component 50 homolog
PPP1CC	1,94	0,91	3,00	0,00	0,00	1,96	1,53	1,05	1,46	1,53	0,90	Isoform Gamma-1 of Serine/threonine-protein phosphatase PP1 gamma catalytic subunit

Gene Symbol	AD1 nc	AD2 nc	capCAA1 nc	capCAA2 nc	C1 nc	C2 nc	fc.cap-CAA/C	fc.capCAA/AD	fc. AD/C	fc. max	pvalues	Protein name
JAM2	0.97	1.81	1.00	2.14	0.00	1.96	1.60	1.13	1.42	1.60	0.90	Junctional adhesion molecule B
UQCRFS1	17.50	17.24	14.98	16.07	14.25	18.60	-1.06	-1.12	1.06	1.12	0.90	Cytochrome-b-c1 complex subunit Rieske, mitochondrial
NTM	6.80	5.44	4.99	5.36	5.48	4.89	-1.00	-1.18	1.18	1.18	0.90	neurotrimin isoform 3
PDXK	14.58	9.07	12.98	12.85	16.44	6.85	1.11	1.09	1.02	1.11	0.90	Isoform 1 of Pyridoxal kinase
RAB18	2.92	2.72	3.99	2.14	3.29	3.92	-1.17	1.09	-1.28	1.28	0.90	Ras-related protein Rab-18
RAB5A	2.92	2.72	3.99	2.14	4.38	2.94	-1.19	1.09	-1.30	1.30	0.90	Ras-related protein Rab-5A
RPS7	3.89	1.81	3.99	2.14	4.38	2.94	-1.19	1.08	-1.28	1.28	0.90	40S ribosomal protein S7
ACADVL	3.89	1.81	3.00	3.21	2.19	4.89	-1.14	1.09	-1.24	1.24	0.90	cDNA FLJ56425, highly similar to Very-long-chain specific acyl-CoA dehydrogenase, mitochondrial
CCT2	14.58	14.52	12.98	12.85	14.25	12.73	-1.04	-1.13	1.08	1.13	0.90	T-complex protein 1 subunit beta
ALB	151.64	156.98	112.83	216.36	151.24	185.99	-1.02	1.07	-1.09	1.09	0.90	Isoform 1 of Serum albumin
METTL7A	3.89	6.35	4.99	4.28	4.38	6.85	-1.21	-1.10	-1.10	1.21	0.90	Methyltransferase-like protein 7A
DUSP3	4.86	5.44	3.00	6.43	5.48	5.87	-1.20	-1.09	-1.10	1.20	0.90	Dual specificity protein phosphatase 3
GRB2	2.92	3.63	3.99	3.21	3.29	4.89	-1.14	1.10	-1.25	1.25	0.90	Isoform 1 of Growth factor receptor-bound protein 2
GNB2	18.47	25.41	17.97	23.56	26.30	19.58	-1.10	-1.06	-1.05	1.10	0.90	Guanine nucleotide-binding protein G(I)/G(S)/G(T) subunit beta-2
ISOC2	3.89	2.72	3.99	4.28	2.19	4.89	1.17	1.25	-1.07	1.25	0.91	Isoform 2 of Isochorismatase domain-containing protein 2, mitochondrial
NFASC	2.92	3.63	3.99	4.28	3.29	3.92	1.15	1.26	-1.10	1.26	0.91	Isoform 9 of Neurofascin
EEF1G	6.80	5.44	4.99	8.57	7.67	6.85	-1.07	1.11	-1.19	1.19	0.91	cDNA FLJ56389, highly similar to Elongation factor 1-gamma
NDUFA4	6.80	6.35	5.99	5.36	6.58	6.85	-1.18	-1.16	-1.02	1.18	0.91	NADH dehydrogenase [ubiquinone] 1 alpha subcomplex subunit 4
TXN	2.92	4.54	4.99	4.28	3.29	4.89	1.13	1.24	-1.10	1.24	0.91	Thioredoxin
KIF5C	9.72	9.07	8.99	7.50	10.96	5.87	-1.02	-1.14	1.12	1.14	0.91	Isoform 1 of Kinesin heavy chain isoform 5C
FXYD6	6.80	6.35	7.99	5.36	6.58	4.89	1.16	1.01	1.15	1.16	0.91	FXYD domain-containing ion transport regulator 6
IGL@	4.86	4.54	5.99	4.28	5.48	5.87	-1.10	1.09	-1.21	1.21	0.91	IGL@ protein
TUBB2C	308.14	352.97	320.51	354.53	408.78	292.68	-1.04	1.02	-1.06	1.06	0.91	Tubulin beta-2C chain
SCCPDH	4.86	4.54	6.99	4.28	4.38	5.87	1.10	1.20	-1.09	1.20	0.91	Probable saccharopine dehydrogenase
ACTB	229.41	269.49	232.64	273.13	266.31	222.20	1.04	1.01	1.02	1.04	0.91	Actin, cytoplasmic 1
LOC100133623;CKMT1A;CKMT1B	35.97	31.76	33.95	28.92	26.30	40.13	-1.06	-1.08	-1.06	1.08	0.91	Creatine kinase, ubiquitous mitochondrial
HSPH1	24.30	19.06	18.97	26.78	27.40	14.68	1.09	1.06	1.03	1.09	0.91	Isoform Beta of Heat shock protein 105 kDa
CAT	0.00	2.72	0.00	2.14	0.00	4.89	-2.28	-1.27	-1.80	2.28	0.91	Catalase
PGLS	4.86	6.35	4.99	5.36	5.48	3.92	1.10	-1.08	1.19	1.19	0.91	6-phosphogluconolactonase
NPEPPS	36.94	31.76	33.95	29.99	41.65	27.41	-1.08	-1.07	-1.01	1.08	0.91	Puromycin-sensitive aminopeptidase
PRKCA	5.83	5.44	7.99	2.14	5.48	6.85	-1.22	-1.11	-1.09	1.22	0.91	Protein kinase C alpha type
EIF4A2	19.44	8.17	14.98	12.85	7.67	16.64	1.14	1.01	1.14	1.14	0.91	Isoform 1 of Eukaryotic initiation factor 4A-II
ACP1	4.86	6.35	5.99	6.43	4.38	5.87	1.21	1.11	1.09	1.21	0.91	Isoform 1 of Low molecular weight phosphotyrosine protein phosphatase
PNPO	3.89	2.72	3.00	2.14	3.29	2.94	-1.21	-1.29	1.06	1.29	0.91	Pyridoxine-5'-phosphate oxidase
RPS19	4.86	1.81	3.00	3.21	1.10	3.92	1.24	-1.08	1.33	1.33	0.91	40S ribosomal protein S19
GNA13	2.92	3.63	3.00	3.21	3.29	1.96	1.18	-1.05	1.25	1.25	0.91	Guanine nucleotide-binding protein subunit alpha-13
RYR2	4.86	1.81	5.99	0.00	1.10	4.89	1.00	-1.11	1.11	1.11	0.92	cardiac muscle ryanodine receptor
ILE2	4.86	2.72	3.00	3.21	3.29	2.94	-1.00	-1.22	1.22	1.22	0.92	Interleukin enhancer-binding factor 2
COX7A2L	3.89	3.63	4.99	1.07	3.29	2.94	-1.03	-1.24	1.21	1.24	0.92	Cytochrome c oxidase subunit 7A-related protein, mitochondrial
SLC6A1	4.86	7.26	8.99	4.28	3.29	7.83	1.19	1.09	1.09	1.19	0.92	Sodium- and chloride-dependent GABA transporter 1
SYNGR1	8.75	9.07	9.98	6.43	5.48	9.79	1.07	-1.09	1.17	1.17	0.92	cDNA FLJ76992, highly similar to Homo sapiens synaptogyrin 1a
CLASP2	0.00	2.72	1.00	1.07	1.10	0.98	-1.00	-1.32	1.31	1.32	0.92	CLIP-associating protein 2
RPS11	1.94	0.91	1.00	1.07	0.00	1.96	1.06	-1.38	1.46	1.46	0.92	40S ribosomal protein S11

Gene Symbol	AD1 nc	AD2 nc	capCAA1 nc	capCAA2 nc	C1 nc	C2 nc	fc.cap-CAA/C	fc.capCAA/AD	fc. AD/C	fc. max	pvalues	Protein name
PSME1	0,97	1,81	2,00	0,00	2,19	0,00	-1,10	-1,40	1,27	1,40	0,92	Proteasome activator complex subunit 1
TFAM	1,94	0,91	1,00	1,07	1,10	0,98	-1,00	-1,38	1,37	1,38	0,92	Transcription factor A, mitochondrial
PI4K2C	0,97	1,81	1,00	1,07	0,00	1,96	1,06	-1,35	1,42	1,42	0,92	Phosphatidylinositol-5-phosphate 4-kinase type-2 gamma
PITPNB	0,97	1,81	1,00	1,07	1,10	0,98	-1,00	-1,35	1,34	1,35	0,92	Isoform 1 of Phosphatidylinositol transfer protein beta isoform
UBQLN2	0,97	1,81	1,00	1,07	1,10	0,98	-1,00	-1,35	1,34	1,35	0,92	Ubiquilin-2
TPM3	6,80	5,44	5,99	4,28	7,67	3,92	-1,13	-1,19	1,06	1,19	0,92	Isoform 2 of Tropomyosin alpha-3 chain
LETM1	8,75	10,89	8,99	8,57	6,58	12,73	-1,10	-1,12	1,02	1,12	0,92	LETM1 and EF-hand domain-containing protein 1, mitochondrial
SKP1	5,83	8,17	7,99	5,36	7,67	7,83	-1,16	-1,05	-1,11	1,16	0,93	Isoform 1 of S-phase kinase-associated protein 1
MBP	128,31	121,59	65,90	174,59	177,54	72,44	-1,04	-1,04	-1,00	1,04	0,93	Isoform 1 of Myelin basic protein
HPRT1	15,55	20,87	16,97	17,14	17,54	19,58	-1,09	-1,07	-1,02	1,09	0,93	Hypoxanthine-guanine phosphoribosyltransferase
TXNL1	2,92	0,91	2,00	1,07	3,29	0,98	-1,39	-1,25	-1,12	1,39	0,93	Thioredoxin-like protein 1
EIF3A	1,94	1,81	2,00	1,07	2,19	1,96	-1,35	-1,23	-1,10	1,35	0,93	Eukaryotic translation initiation factor 3 subunit A
MAT2B	1,94	1,81	2,00	1,07	2,19	1,96	-1,35	-1,23	-1,10	1,35	0,93	Isoform 1 of Methionine adenosyltransferase 2 subunit beta
VCP	31,11	45,37	31,95	43,91	39,45	33,28	1,04	-1,01	1,05	1,05	0,93	Transitional endoplasmic reticulum ATPase
MYH10	16,53	19,96	24,96	8,57	18,63	15,66	-1,02	-1,09	1,06	1,09	0,93	Isoform 3 of Myosin-10
HNRNPL	2,92	0,91	3,00	1,07	0,00	2,94	1,38	1,06	1,30	1,38	0,93	Heterogeneous nuclear ribonucleoprotein L
GNG12	1,94	1,81	2,00	2,14	1,10	1,96	1,36	1,10	1,23	1,36	0,93	Guanine nucleotide-binding protein G(I)/G(S)/G(O) subunit gamma-12
PNKD	1,94	1,81	2,00	2,14	2,19	0,98	1,31	1,10	1,19	1,31	0,93	Isoform 2 of Probable hydrolase PNKD
NTRK2	2,92	0,91	1,00	3,21	1,10	1,96	1,38	1,10	1,25	1,38	0,93	Isoform TrkB of BDNF/NT-3 growth factors receptor
S100A1	0,97	2,72	2,00	2,14	2,19	0,98	1,31	1,12	1,17	1,31	0,93	S100 calcium binding protein A1, isoform CRA_a
XPNPEP1	2,92	0,91	3,00	1,07	2,19	0,98	1,28	1,06	1,21	1,28	0,93	X-prolyl aminopeptidase (Aminopeptidase P) 1, soluble
HSP90AB1	44,72	58,07	39,94	71,76	50,41	51,88	1,09	1,09	1,00	1,09	0,93	Heat shock protein HSP 90-beta
PACSIN1	28,19	31,76	35,95	26,78	38,36	26,43	-1,03	1,05	-1,08	1,08	0,93	Protein kinase C and casein kinase substrate in neurons protein 1
FABP3	6,80	9,07	5,99	8,57	8,77	7,83	-1,14	-1,09	-1,05	1,14	0,93	Fatty acid-binding protein, heart
UBE2V2	7,78	7,26	9,98	6,43	7,67	6,85	1,13	1,09	1,04	1,13	0,93	Ubiquitin-conjugating enzyme E2 variant 2
HSP90AA1	122,48	139,74	104,84	157,45	130,42	120,40	1,05	1,00	1,05	1,05	0,93	heat shock 90kDa protein 1, alpha isoform 1
SCRN1	33,05	36,30	29,95	37,49	38,36	27,41	1,03	-1,03	1,05	1,05	0,93	Secernin-1
IDH3A	33,05	29,04	26,96	39,63	30,69	33,28	1,04	1,07	-1,03	1,07	0,93	Isoform 1 of Isocitrate dehydrogenase [NAD] subunit alpha, mitochondrial
NAGK	1,94	5,44	2,00	4,28	8,77	0,00	-1,40	-1,18	-1,19	1,40	0,93	N-acetylglucosamine kinase
FAM162A	3,89	3,63	3,00	3,21	2,19	4,89	-1,14	-1,21	1,06	1,21	0,93	UPF0389 protein FAM162A
MYADM	5,83	1,81	3,00	3,21	5,48	1,96	-1,20	-1,23	1,03	1,23	0,93	Myeloid-associated differentiation marker
BCAS1	0,97	3,63	0,00	5,36	6,58	0,00	-1,23	1,16	-1,43	1,43	0,93	Isoform 2 of Breast carcinoma-amplified sequence 1
TOLLIP	2,92	4,54	3,99	3,21	3,29	2,94	1,16	-1,03	1,20	1,20	0,93	Toll-interacting protein
PSMA7	3,89	3,63	3,99	3,21	4,38	1,96	1,14	-1,04	1,19	1,19	0,93	Isoform 1 of Proteasome subunit alpha type-7
RPL18	4,86	2,72	4,99	2,14	4,38	1,96	1,13	-1,06	1,20	1,20	0,93	60S ribosomal protein L18
DNM1L	19,44	20,87	16,97	20,35	16,44	21,54	-1,02	-1,08	1,06	1,08	0,93	cDNA FLJ55044, highly similar to Dynamin-1-like protein
DNAJC5	8,75	9,98	9,98	8,57	9,86	10,77	-1,11	-1,01	-1,10	1,11	0,94	Isoform 1 of DnaJ homolog subfamily C member 5
RPLP0	10,69	10,89	11,98	11,78	8,77	12,73	1,11	1,10	1,00	1,11	0,94	60S acidic ribosomal protein P0
PAFAH1B2	5,83	2,72	3,00	4,28	4,38	2,94	-1,01	-1,18	1,17	1,18	0,94	Platelet-activating factor acetylhydrolase IB subunit beta
DLST	13,61	11,80	10,98	16,07	9,86	17,62	-1,02	1,06	-1,08	1,08	0,94	Dihydrolipoyllysine-residue succinyltransferase component of 2-oxoglutarate dehydrogenase complex, mitochondrial
SYT2	1,94	0,91	0,00	5,36	0,00	2,94	1,82	1,88	-1,03	1,88	0,94	Synaptotagmin-2
UQCRB	11,66	8,17	7,99	9,64	9,86	8,81	-1,06	-1,13	1,06	1,13	0,94	Cytochrome b-c1 complex subunit 7
ATPA2	32,08	27,22	45,93	16,07	18,63	35,24	1,15	1,05	1,10	1,15	0,94	Isoform SERCA2B of Sarcoplasmic/endoplasmic reticulum calcium ATPase 2

Gene Symbol	AD1 nc	AD2 nc	capCAA1 nc	capCAA2 nc	C1 nc	C2 nc	fc.cap-CAA/C	fc.capCAA/AD	fc. AD/C	fc. max	pvalues	Protein name
ALDH7A1	14,58	26,31	19,97	23,56	23,01	21,54	-1,02	1,06	-1,09	1,09	0,94	aldehyde dehydrogenase 7 family, member A1
CRYAB	15,55	24,50	12,98	25,71	19,73	17,62	1,04	-1,04	1,07	1,07	0,94	Alpha-crystallin B chain
NPTN	8,75	13,61	10,98	11,78	10,96	9,79	1,10	1,02	1,08	1,10	0,94	Isoform 2 of Neuroplastin
RPS12	2,92	1,81	2,00	2,14	1,10	3,92	-1,21	-1,14	-1,06	1,21	0,95	40S ribosomal protein S12
MAT2A	2,92	1,81	2,00	2,14	3,29	1,96	-1,27	-1,14	-1,11	1,27	0,95	S-adenosylmethionine synthetase isoform type-2
FN3K	2,92	1,81	1,00	3,21	3,29	1,96	-1,25	-1,12	-1,11	1,25	0,95	Fructosamine-3-kinase
GPX4	2,92	1,81	2,00	3,21	2,19	1,96	1,26	1,10	1,14	1,26	0,95	Isoform Mitochondrial of Phospholipid hydroperoxide glutathione peroxidase, mitochondrial
RAB6A	9,72	10,89	7,99	10,71	9,86	9,79	-1,05	-1,10	1,05	1,10	0,95	Isoform 2 of Ras-related protein Rab-6A
TBC1B	3,89	4,54	2,00	6,43	3,29	3,92	1,17	-1,00	1,17	1,17	0,95	Tubulin folding cofactor B
APOO	5,83	2,72	3,00	5,36	3,29	3,92	1,16	-1,02	1,19	1,19	0,95	Isoform 1 of Apolipoprotein O
P4HB	3,89	4,54	3,00	5,36	4,38	2,94	1,14	-1,01	1,15	1,15	0,95	Protein disulfide-isomerase
CDK5	5,83	2,72	4,99	3,21	4,38	2,94	1,12	-1,04	1,17	1,17	0,95	Cell division protein kinase 5
ALDH2	31,11	50,81	42,93	40,70	38,36	41,11	1,05	1,02	1,03	1,05	0,95	Aldehyde dehydrogenase, mitochondrial
LSAMP	8,75	10,89	8,99	11,78	9,86	8,81	1,11	1,06	1,05	1,11	0,95	Limbic system-associated membrane protein
HIBADH	7,78	7,26	7,99	8,57	6,58	9,79	1,01	1,10	-1,09	1,10	0,95	3-hydroxyisobutyrate dehydrogenase, mitochondrial
NDUFA7	9,72	6,35	6,99	7,50	6,58	7,83	1,01	-1,11	1,12	1,12	0,95	NADH dehydrogenase [ubiquinone] 1 alpha subcomplex subunit 7
SDR39U1	2,92	0,91	3,00	1,07	0,00	4,89	-1,20	1,06	-1,28	1,28	0,95	Isoform 2 of Epimerase family protein SDR39U1
SLC25A22	12,64	8,17	10,98	8,57	5,48	15,66	-1,08	-1,06	-1,02	1,08	0,95	Mitochondrial glutamate carrier 1
SLC2A1	5,83	3,63	6,99	1,07	4,38	3,92	-1,03	-1,17	1,14	1,17	0,95	Solute carrier family 2, facilitated glucose transporter member 1
NFASC	46,66	42,65	36,94	50,34	50,41	41,11	-1,05	-1,02	-1,02	1,05	0,95	Isoform 6 of Neurofascin
DCTN1	11,66	11,80	13,98	7,50	9,86	11,75	-1,01	-1,09	1,09	1,09	0,95	Isoform p150 of Dynactin subunit 1
RAB5C	11,66	9,98	9,98	9,64	7,67	12,73	-1,04	-1,10	1,06	1,10	0,95	Ras-related protein Rab-5C
NUDC	3,89	1,81	3,00	2,14	2,19	3,92	-1,19	-1,11	-1,07	1,19	0,96	Nuclear migration protein nudC
DCI	2,92	2,72	2,00	3,21	2,19	3,92	-1,17	-1,08	-1,08	1,17	0,96	Isoform 1 of 3,2-trans-enoyl-CoA isomerase, mitochondrial
NDUFA5	6,80	8,17	5,99	7,50	5,48	8,81	-1,06	-1,11	1,05	1,11	0,96	Putative uncharacterized protein DKFZp781K1356
PRNP	10,69	12,70	11,98	10,71	13,15	11,75	-1,10	-1,03	-1,06	1,10	0,96	Major prion protein
ARPC3	1,94	3,63	3,99	2,14	2,19	2,94	1,20	1,10	1,09	1,20	0,96	Actin-related protein 2/3 complex subunit 3
TAGLN3	17,50	19,06	19,97	15,00	19,73	14,68	1,02	-1,05	1,06	1,06	0,96	Neuronal protein NP25
KRT9	68,04	58,98	74,89	52,48	73,43	58,73	-1,04	1,00	-1,04	1,04	0,96	Keratin, type I cytoskeletal 9
HAPLN4	2,92	0,91	2,00	1,07	0,00	2,94	1,04	-1,25	1,30	1,30	0,96	Hyaluronan and proteoglycan link protein 4
CHMP4B	1,94	1,81	2,00	1,07	3,29	0,00	-1,07	-1,23	1,14	1,23	0,96	Charged multivesicular body protein 4b
RPS15A	2,92	0,91	2,00	1,07	1,10	1,96	1,00	-1,25	1,25	1,25	0,96	40S ribosomal protein S15a
KGHM	1,94	1,81	1,00	2,14	1,10	1,96	1,03	-1,20	1,23	1,23	0,96	Full-length cDNA clone CS0DD006Y02 of Neuroblastoma of Homo sapiens
DDX17	2,92	0,91	2,00	1,07	1,10	1,96	1,00	-1,25	1,25	1,25	0,96	Isoform 1 of Probable ATP-dependent RNA helicase DDX17
RPS20	2,92	0,91	1,00	2,14	2,19	0,98	-1,01	-1,22	1,21	1,22	0,96	40S ribosomal protein S20
RPS5	0,97	2,72	2,00	1,07	1,10	1,96	1,00	-1,20	1,21	1,21	0,96	40S ribosomal protein S5
AK1	18,47	19,96	20,97	15,00	17,54	20,56	-1,06	-1,07	1,01	1,07	0,96	Adenylate kinase isozyme 1
HRSP12	3,89	5,44	4,99	4,28	4,38	3,92	1,12	-1,01	1,12	1,12	0,96	Ribonuclease UK114
SNCB	6,80	2,72	5,99	3,21	3,29	4,89	1,12	-1,04	1,16	1,16	0,96	Beta-synuclein
PRAF2	4,86	1,81	4,99	1,07	4,38	2,94	-1,21	-1,10	-1,10	1,21	0,96	PRA1 family protein 2
FKBP4	3,89	2,72	3,00	3,21	2,19	4,89	-1,14	-1,06	-1,07	1,14	0,96	FK506-binding protein 4
RPL12	3,89	2,72	3,99	2,14	3,29	3,92	-1,17	-1,08	-1,09	1,17	0,96	Isoform 1 of 60S ribosomal protein L12
DPYSL2	250,79	274,03	237,64	279,56	280,56	242,76	-1,01	-1,01	1,00	1,01	0,96	Dihydropyrimidinase-related protein 2

Gene Symbol	AD1 nc	AD2 nc	capCAA1 nc	capCAA2 nc	C1 nc	C2 nc	fc.cap-CAA/C	fc.capCAA/AD	fc.AD/C	fc.max	pvalues	Protein name
GNB5	2,92	3,63	5,99	1,07	1,10	4,89	1,18	1,08	1,09	1,18	0,96	Isoform 1 of Guanine nucleotide-binding protein subunit beta-5
PPME1	4,86	1,81	3,00	4,28	3,29	2,94	1,17	1,09	1,07	1,17	0,96	Isoform 1 of Protein phosphatase methylesterase 1
SEC22B	3,89	2,72	3,99	3,21	3,29	2,94	1,16	1,09	1,06	1,16	0,96	Vesicle-trafficking protein SEC22b
SFXN1	14,58	13,61	15,98	13,92	13,15	16,64	1,00	1,06	-1,06	1,06	0,96	Sideroflexin-1
NAPG	6,80	9,07	6,99	7,50	12,06	3,92	-1,10	-1,10	-1,01	1,10	0,96	Gamma-soluble NSF attachment protein
CD47	7,78	8,17	7,99	7,50	6,58	7,83	1,07	-1,03	1,11	1,11	0,96	Isoform OA3-323 of Leukocyte surface antigen CD47
SLC4A4	8,75	2,72	7,99	4,28	4,38	7,83	1,00	1,07	-1,06	1,07	0,96	Isoform 1 of Electrogenic sodium bicarbonate cotransporter 1
AK3	4,86	5,44	3,99	5,36	4,38	4,89	1,01	-1,10	1,11	1,11	0,96	GTP:AMP phosphotransferase mitochondrial
PHGDH	12,64	23,59	12,98	20,35	30,69	9,79	-1,21	-1,09	-1,12	1,21	0,96	D-3-phosphoglycerate dehydrogenase
SCAMP1	5,83	1,81	5,99	2,14	2,19	4,89	1,15	1,06	1,08	1,15	0,96	Isoform 1 of Secretory carrier-associated membrane protein 1
SLC1A4	2,92	4,54	3,99	4,28	4,38	2,94	1,13	1,11	1,02	1,13	0,96	Neutral amino acid transporter A
HSP90B1	12,64	18,15	10,98	21,42	19,73	13,70	-1,03	1,05	-1,09	1,09	0,97	Endoplasmin
TTLL3,ARPC4	3,89	6,35	4,99	4,28	5,48	4,89	-1,12	-1,10	-1,01	1,12	0,97	Actin-related protein 2/3 complex subunit 4
FGG	5,83	3,63	1,00	23,56	8,77	2,94	2,10	2,60	-1,24	2,60	0,97	Isoform Gamma-B of Fibrinogen gamma chain
ERP29	4,86	5,44	4,99	5,36	4,38	4,89	1,12	1,00	1,11	1,12	0,97	Endoplasmic reticulum protein ERp29
NDUFS4	5,83	4,54	5,99	4,28	3,29	5,87	1,12	-1,01	1,13	1,13	0,97	NADH dehydrogenase [ubiquinone] iron-sulfur protein 4, mitochondrial
IPO5	3,89	8,17	4,99	7,50	5,48	7,83	-1,07	1,04	-1,10	1,10	0,97	importin 5
GDI1	115,68	133,39	114,82	133,89	136,99	108,65	1,01	-1,00	1,01	1,01	0,97	Rab GDP dissociation inhibitor alpha
NDUFB9	4,86	4,54	5,99	3,21	4,38	5,87	-1,11	-1,02	-1,09	1,11	0,97	NADH dehydrogenase [ubiquinone] 1 beta subcomplex subunit 9
KHA1	4,86	4,54	5,99	3,21	3,29	6,85	-1,10	-1,02	-1,08	1,10	0,97	cDNA FLJ90170 fis, clone MAMMA1000370, highly similar to Ig alpha-1 chain C region
HERP1	5,83	3,63	3,99	6,43	4,38	3,92	1,12	1,10	1,02	1,12	0,97	Heme-binding protein 1
DLG4	14,58	12,70	17,97	11,78	6,58	22,51	1,02	1,09	-1,07	1,09	0,97	Isoform 2 of Disks large homolog 4
TWF2	2,92	0,00	2,00	0,00	0,00	1,96	1,02	-1,46	1,49	1,49	0,97	Twinfilin-2
GPSN2	2,92	0,00	3,00	0,00	0,00	1,96	1,53	1,03	1,49	1,53	0,97	Isoform 1 of Synaptic glycoprotein SC2
BIN1	7,78	16,33	7,99	18,21	16,44	9,79	-1,00	1,09	-1,09	1,09	0,97	Isoform IIA of Myc-box-dependent-interacting protein 1
MYL12B	4,86	6,35	3,99	6,43	6,58	3,92	-1,01	-1,08	1,07	1,08	0,97	Myosin regulatory light chain MRLC2
PHYHIP	12,64	5,44	10,98	6,43	5,48	10,77	1,07	-1,04	1,11	1,11	0,97	Phytanoyl-CoA hydroxylase-interacting protein
CHCHD3	3,89	3,63	5,99	2,14	4,38	3,92	-1,02	1,08	-1,10	1,10	0,98	Coiled-coil-helix-coiled-coil-helix domain-containing protein 3, mitochondrial
XRCC6	5,83	1,81	4,99	3,21	2,19	5,87	1,02	1,07	-1,05	1,07	0,98	ATP-dependent DNA helicase 2 subunit 1
CFL2	4,86	2,72	3,99	4,28	4,38	3,92	-1,00	1,09	-1,09	1,09	0,98	Cofilin-2
GARS	7,78	4,54	5,99	5,36	5,48	6,85	-1,09	-1,09	-1,00	1,09	0,98	Glycyl-tRNA synthetase
PDCD6	2,92	1,81	2,00	2,14	2,19	1,96	-1,00	-1,14	1,14	1,14	0,98	Programmed cell death protein 6
COP9S7A	3,89	0,91	2,00	2,14	2,19	1,96	-1,00	-1,16	1,16	1,16	0,98	COP9 signalosome complex subunit 7a
SFRS1	3,89	0,91	3,00	1,07	1,10	2,94	1,01	-1,18	1,19	1,19	0,98	Isoform ASF-1 of Splicing factor, arginine/serine-rich 1
GSTK1	2,92	1,81	2,00	2,14	1,10	2,94	1,03	-1,14	1,17	1,17	0,98	Glutathione S-transferase kappa 1
PSMD1	1,94	2,72	2,00	2,14	1,10	2,94	1,03	-1,13	1,16	1,16	0,98	Isoform 1 of 26S proteasome non-ATPase regulatory subunit 1
AGAP3	2,92	1,81	3,00	1,07	2,19	1,96	-1,02	-1,16	1,14	1,16	0,98	centaurin, gamma 3 isoform a
NARS	2,92	0,00	2,00	0,00	2,19	0,00	-1,10	-1,46	1,33	1,46	0,98	Asparaginyl-tRNA synthetase, cytoplasmic
PRKACB	8,75	3,63	6,99	5,36	3,29	7,83	1,11	-1,00	1,11	1,11	0,98	Isoform 2 of cAMP-dependent protein kinase catalytic subunit beta
ALDOA	107,90	112,52	99,85	119,96	118,36	98,87	1,01	-1,00	1,01	1,01	0,98	Fructose-bisphosphate aldolase A
CSRP1	18,47	15,43	15,98	17,14	15,34	16,64	1,04	-1,02	1,06	1,06	0,98	Cysteine and glycine-rich protein 1
ATP6V1C1	13,61	5,44	9,98	8,57	8,77	8,81	1,06	-1,03	1,08	1,08	0,98	V-type proton ATPase subunit C 1
RTN1	8,75	9,98	8,99	9,64	9,86	7,83	1,05	-1,01	1,06	1,06	0,98	Isoform RTN1-C of Reticulon-1

Gene Symbol	AD1 nc	AD2 nc	capCAA1 nc	capCAA2 nc	C1 nc	C2 nc	fc.cap-CAA/C	fc.capCAA/AD	fc. AD/C	fc. max	pvalues	Protein name
COTL1	3,89	2,72	3,00	4,28	3,29	3,92	1,01	1,10	-1,09	1,10	0,98	Coactosin-like protein
PSMA5	6,80	6,35	5,99	6,43	6,58	6,85	-1,08	-1,06	-1,02	1,08	0,98	Proteasome subunit alpha type-5
PPP2R4	8,75	5,44	4,99	8,57	6,58	7,83	-1,06	-1,05	-1,02	1,06	0,98	Isoform 3 of Serine/threonine-protein phosphatase 2A regulatory subunit B'
SH3GL3	2,92	2,72	3,99	2,14	5,48	0,98	-1,05	1,09	-1,15	1,15	0,98	Isoform 1 of Endophilin-A3
GLO1	5,83	8,17	8,99	5,36	5,48	7,83	1,08	1,02	1,05	1,08	0,98	Lactoylglutathione lyase
AKR1B1	6,80	9,07	6,99	9,64	6,58	8,81	1,08	1,05	1,03	1,08	0,98	Aldose reductase
TXNDC17	1,94	2,72	2,00	3,21	2,19	2,94	1,02	1,12	-1,10	1,12	0,98	Thioredoxin domain-containing protein 17
FTH1	21,39	16,33	11,98	24,64	20,82	16,64	-1,02	-1,03	1,01	1,03	0,99	Ferritin heavy chain
PSMA2	2,92	2,72	3,00	2,14	2,19	2,94	1,00	-1,10	1,10	1,10	0,99	Proteasome subunit alpha type-2
RAB1B	3,89	1,81	3,00	2,14	2,19	2,94	1,00	-1,11	1,11	1,11	0,99	Ras-related protein Rab-1B
COPS8	1,94	3,63	2,00	3,21	3,29	1,96	-1,01	-1,07	1,06	1,07	0,99	COP9 signalosome complex subunit 8
UBE2M	0,97	2,72	2,00	2,14	4,38	0,00	-1,06	1,12	-1,19	1,19	0,99	NEDD8-conjugating enzyme Ubc12
C10orf35	2,92	0,91	3,00	1,07	2,19	1,96	-1,02	1,06	-1,09	1,09	0,99	Uncharacterized protein C10orf35
MARCKSL1	1,94	1,81	2,00	2,14	2,19	1,96	-1,00	1,10	-1,10	1,10	0,99	MARCKS-related protein
SUCLA2	17,50	13,61	17,97	13,92	12,06	18,60	1,04	1,03	1,01	1,04	0,99	Isoform 2 of Succinyl-CoA ligase [ADP-forming] subunit beta, mitochondrial
ALDH6A1	16,53	25,41	24,96	18,21	18,63	24,47	1,00	1,03	-1,03	1,03	0,99	Methylmalonate-semialdehyde dehydrogenase [acylating], mitochondrial
SEPT5	16,53	14,52	18,97	11,78	10,96	18,60	1,04	-1,01	1,05	1,05	0,99	Septin-5
TALDO1	13,61	9,07	11,98	9,64	15,34	6,85	-1,03	-1,05	1,02	1,05	0,99	Transaldolase
RAB11B	10,69	11,80	10,98	10,71	9,86	11,75	1,00	-1,04	1,04	1,04	0,99	Ras-related protein Rab-11B
HNRNPD	7,78	6,35	8,99	4,28	5,48	7,83	-1,00	-1,06	1,06	1,06	0,99	Isoform 1 of Heterogeneous nuclear ribonucleoprotein D0
RPS16	1,94	0,91	2,00	1,07	1,10	1,96	1,00	1,08	-1,07	1,08	0,99	40S ribosomal protein S16
DIABLO	1,94	0,91	2,00	1,07	1,10	1,96	1,00	1,08	-1,07	1,08	0,99	Diablo homolog, mitochondrial precursor
GLIPR2	1,94	0,91	0,00	3,21	2,19	0,98	1,01	1,13	-1,11	1,13	0,99	Golgi-associated plant pathogenesis-related protein 1
RAP1A	1,94	0,91	1,00	2,14	2,19	0,98	-1,01	1,10	-1,11	1,11	0,99	Ras-related protein Rap-1A
ANXA4	0,97	1,81	2,00	1,07	2,19	0,98	-1,03	1,10	-1,14	1,14	0,99	annexin IV
FMN2	1,94	0,91	0,00	6,43	8,77	0,00	-1,36	2,25	-3,07	3,07	0,99	Isoform 3 of Formin-like protein 2
GRIA2	8,75	5,44	12,98	3,21	3,29	11,75	1,08	1,14	-1,06	1,14	0,99	Isoform Flop of Glutamate receptor 2
CTNND2	2,92	3,63	3,99	2,14	3,29	2,94	-1,01	-1,07	1,05	1,07	0,99	Isoform 2 of Catenin delta-2
DNAJB2	3,89	2,72	2,00	4,28	4,38	1,96	-1,01	-1,05	1,04	1,05	0,99	Isoform 3 of DnaJ homolog subfamily B member 2
CD59	9,72	6,35	7,99	8,57	7,67	8,81	1,00	1,03	-1,03	1,03	0,99	CD59 glycoprotein
SLC6A17	6,80	8,17	8,99	5,36	5,48	8,81	1,00	-1,04	1,05	1,05	0,99	Orphan sodium- and chloride-dependent neurotransmitter transporter NTT4
SLC16A1	0,97	0,91	2,00	0,00	1,10	0,98	-1,04	1,06	-1,10	1,10	0,99	Monocarboxylate transporter 1
MT-CO1	0,97	0,91	1,00	1,07	0,00	1,96	1,06	1,10	-1,04	1,10	0,99	Cytochrome c oxidase subunit 1
MFF	0,97	0,91	1,00	1,07	0,00	1,96	1,06	1,10	-1,04	1,10	0,99	Isoform 2 of Mitochondrial fission factor
PPP3CB	0,97	0,91	1,00	1,07	2,19	0,00	-1,06	1,10	-1,17	1,17	0,99	protein phosphatase 3 (formerly 2B), catalytic subunit, beta isoform isoform a
RPL36	0,97	0,91	1,00	1,07	2,19	0,00	-1,06	1,10	-1,17	1,17	0,99	60S ribosomal protein L36
GUCY1B3	1,94	0,00	1,00	1,07	0,00	0,00	-1,06	1,02	-1,13	1,13	0,99	Isoform HSGC-2 of Guanylate cyclase soluble subunit beta-1
YWHAB	25,27	24,50	24,96	25,71	27,40	22,51	1,02	1,06	-1,00	1,02	0,99	Isoform Long of 14-3-3 protein beta/alpha
SCAMP3	1,94	0,00	2,00	0,00	2,19	0,00	-1,10	1,03	-1,13	1,13	0,99	Isoform 1 of Secretory carrier-associated membrane protein 3
ACTR1B	6,80	7,26	6,99	7,50	7,67	6,85	-1,00	1,03	-1,03	1,03	1,00	Beta-centractin
C5orf33	3,89	3,63	4,99	2,14	3,29	3,92	-1,01	-1,05	1,04	1,05	1,00	Isoform 1 of UPF0465 protein C5orf33
GABRA1	4,86	1,81	5,99	1,07	1,10	5,87	1,01	1,06	-1,04	1,06	1,00	Gamma-aminobutyric acid receptor subunit alpha-1
PDCD6IP	11,66	5,44	7,99	8,57	9,86	6,85	-1,01	-1,03	1,02	1,03	1,00	PDCD6IP protein

Gene Symbol	AD1 nc	AD2 nc	capCAA1 nc	capCAA2 nc	C1 nc	C2 nc	fc.cap-CAA/C	fc.capCAA/AD	fc. AD/C	fc. max	pvalues	Protein name
ENOPH1	3,89	4,54	4,99	3,21	4,38	3,92	-1,01	-1,03	1,02	1,03	1,00	Isoform 1 of Enolase-phosphatase E1
MOG	32,08	22,68	18,97	37,49	48,22	13,70	-1,10	1,03	-1,13	1,13	1,00	Isoform 1 of Myelin-oligodendrocyte glycoprotein
SYNGAP1	1,94	0,91	5,99	0,00	0,00	5,87	1,02	2,10	-2,06	2,10	1,00	Isoform 1 of Ras GTPase-activating protein SynGAP
NDUFS6	4,86	4,54	4,99	4,28	1,10	7,83	1,04	-1,01	1,05	1,05	1,00	NADH dehydrogenase [ubiquinone] iron-sulfur protein 6, mitochondrial
RTN1	16,53	14,52	20,97	9,61	14,25	16,64	-1,01	-1,01	1,01	1,01	1,00	Isoform RTN1-A of Reticulon-1

GO code	Biological process	pvalues	Corrected pvalues	Cluster frequency	Total frequency	Proteins
18149	peptide cross-linking	1,91E-06	1,34E-03	3/14 21.4%	26/14305 0.1%	BGN F13A1 ANXA1
9611	response to wounding	1,14E-04	2,39E-02	5/14 35.7%	541/14305 3.7%	APOE F13A1 CLU ANXA1 SERPINA1
43691	reverse cholesterol transport	1,20E-04	2,39E-02	2/14 14.2%	17/14305 0.1%	APOE CLU
6869	lipid transport	3,02E-04	2,39E-02	3/14 21.4%	139/14305 0.9%	APOE CLU ANXA1
43066	negative regulation of apoptosis	3,81E-04	2,39E-02	4/14 28.5%	376/14305 2.6%	APOE CLU ANXA1 CAT
10876	lipid localization	3,85E-04	2,39E-02	3/14 21.4%	151/14305 1.0%	APOE CLU ANXA1
43069	negative regulation of programmed cell death	4,01E-04	2,39E-02	4/14 28.5%	381/14305 2.6%	APOE CLU ANXA1 CAT
60548	negative regulation of cell death	4,34E-04	2,39E-02	4/14 28.5%	389/14305 2.7%	APOE CLU ANXA1 CAT
15918	sterol transport	6,46E-04	2,39E-02	2/14 14.2%	39/14305 0.2%	APOE CLU
30301	cholesterol transport	6,46E-04	2,39E-02	2/14 14.2%	39/14305 0.2%	APOE CLU
6979	response to oxidative stress	6,87E-04	2,39E-02	3/14 21.4%	184/14305 1.2%	APOE CLU CAT
6950	response to stress	6,89E-04	2,39E-02	7/14 50.0%	1773/14305 12.3%	PENK APOE F13A1 CLU ANXA1 SERPINA1 CAT
6641	triglyceride metabolic process	7,49E-04	2,39E-02	2/14 14.2%	42/14305 0.2%	APOE CAT
48812	neuron projection morphogenesis	8,62E-04	2,39E-02	3/14 21.4%	199/14305 1.3%	APP APOE CLU
6916	anti-apoptosis	8,62E-04	2,39E-02	3/14 21.4%	199/14305 1.3%	APOE CLU ANXA1
42981	regulation of apoptosis	9,44E-04	2,39E-02	5/14 35.7%	852/14305 5.9%	APP APOE CLU ANXA1 CAT
6639	acylglycerol metabolic process	9,78E-04	2,39E-02	2/14 14.2%	48/14305 0.3%	APOE CAT
46687	response to chromate	9,79E-04	2,39E-02	1/14 7.1%	1/14305 0.0%	SERPINA1
48668	collateral sprouting	9,79E-04	2,39E-02	1/14 7.1%	1/14305 0.0%	APP
48669	collateral sprouting in the absence of injury	9,79E-04	2,39E-02	1/14 7.1%	1/14305 0.0%	APP
32805	positive regulation of low-density lipoprotein receptor catabolic process	9,79E-04	2,39E-02	1/14 7.1%	1/14305 0.0%	APOE
33986	response to methanol	9,79E-04	2,39E-02	1/14 7.1%	1/14305 0.0%	SERPINA1
34014	response to triglyceride	9,79E-04	2,39E-02	1/14 7.1%	1/14305 0.0%	SERPINA1
32462	regulation of protein homooligomerization	9,79E-04	2,39E-02	1/14 7.1%	1/14305 0.0%	CLU
32463	negative regulation of protein homooligomerization	9,79E-04	2,39E-02	1/14 7.1%	1/14305 0.0%	CLU
32460	negative regulation of protein oligomerization	9,79E-04	2,39E-02	1/14 7.1%	1/14305 0.0%	CLU
51124	synaptic growth at neuromuscular junction	9,79E-04	2,39E-02	1/14 7.1%	1/14305 0.0%	APP
43067	regulation of programmed cell death	9,84E-04	2,39E-02	5/14 35.7%	860/14305 6.0%	APP APOE CLU ANXA1 CAT
6638	neutral lipid metabolic process	1,02E-03	2,39E-02	2/14 14.2%	49/14305 0.3%	APOE CAT
10941	regulation of cell death	1,02E-03	2,39E-02	5/14 35.7%	867/14305 6.0%	APP APOE CLU ANXA1 CAT
51436	negative regulation of ubiquitin-protein ligase activity involved in mitotic cell cycle	8,13E-04	3,15E-02	2/10 20.0%	62/14304 0.4%	PSMC6 PSMA3
31145	anaphase-promoting complex-dependent proteasomal ubiquitin-dependent protein catabolic process	8,40E-04	3,15E-02	2/10 20.0%	63/14304 0.4%	PSMC6 PSMA3
51437	positive regulation of ubiquitin-protein ligase activity involved in mitotic cell cycle	8,67E-04	3,15E-02	2/10 20.0%	64/14304 0.4%	PSMC6 PSMA3
51352	negative regulation of ligase activity	9,21E-04	3,15E-02	2/10 20.0%	66/14304 0.4%	PSMC6 PSMA3

GO code	Biological process	pvalues	Corrected pvalues	Cluster frequency	Total frequency	Proteins
31589	cell-substrate adhesion	8,28E-12	2,72E-09	6/9 66.6%	100/14305 0.6%	LAMB2 CD44 LAMA5 ITGAV LAMC1 ITGB1
34446	substrate adhesion-dependent cell spreading	2,83E-08	4,65E-06	3/9 33.3%	11/14305 0.0%	LAMB2 LAMA5 LAMC1
31663	lipopolysaccharide-mediated signaling pathway	6,59E-06	9,26E-04	2/6 33.3%	10/14305 0.0%	MAPK3 STAT1
43330	response to exogenous dsRNA	8,05E-06	9,26E-04	2/6 33.3%	11/14305 0.0%	MAPK3 STAT1
71222	cellular response to lipopolysaccharide	1,99E-05	1,52E-03	2/6 33.3%	17/14305 0.1%	MAPK3 STAT1
71219	cellular response to molecule of bacterial origin	2,78E-05	1,60E-03	2/6 33.3%	20/14305 0.1%	MAPK3 STAT1
43331	response to dsRNA	5,12E-05	2,35E-03	2/6 33.3%	27/14305 0.1%	MAPK3 STAT1
6468	protein amino acid phosphorylation	6,14E-05	2,35E-03	4/6 66.6%	657/14305 4.5%	MAPK3 CAMK2D STAT1 CAMK1D
16310	phosphorylation	1,24E-04	4,08E-03	4/6 66.6%	786/14305 5.4%	MAPK3 CAMK2D STAT1 CAMK1D
6936	muscle contraction	8,06E-10	9,38E-08	5/6 83.3%	154/14306 1.0%	ACTC1 DES ACTN2 TPM2 VCL
3012	muscle system process	1,25E-09	9,38E-08	5/6 83.3%	168/14306 1.1%	ACTC1 DES ACTN2 TPM2 VCL
3008	system process	7,04E-05	3,52E-03	5/6 83.3%	1506/14306 10.5%	ACTC1 DES ACTN2 TPM2 VCL
15992	proton transport	5,00E-05	1,58E-03	2/3 66.6%	59/14306 0.4%	ATP6V1G1 ATP5J
6818	hydrogen transport	5,35E-05	1,58E-03	2/3 66.6%	61/14306 0.4%	ATP6V1G1 ATP5J
71344	diphosphate metabolic process	4,19E-04	8,25E-03	1/3 33.3%	2/14306 0.0%	PPA1
42136	neurotransmitter biosynthetic process	8,21E-07	6,16E-05	2/3 66.6%	8/14306 0.0%	GAD2 ALDH9A1
42133	neurotransmitter metabolic process	6,15E-06	2,31E-04	2/3 66.6%	21/14306 0.1%	GAD2 ALDH9A1
6644	phospholipid metabolic process	5,61E-04	1,13E-02	2/3 66.6%	197/14306 1.3%	PLCD1 PIP4K2B
19637	organophosphate metabolic process	6,25E-04	1,13E-02	2/3 66.6%	208/14306 1.4%	PLCD1 PIP4K2B
10824	regulation of centrosome duplication	1,47E-03	1,81E-02	1/3 33.3%	7/14306 0.0%	ROCK2
45039	protein import into mitochondrial inner membrane	1,47E-07	5,57E-06	2/2 100.0%	6/14306 0.0%	TIMM9 TIMM13
7007	inner mitochondrial membrane organization	3,52E-07	6,68E-06	2/2 100.0%	9/14306 0.0%	TIMM9 TIMM13
6914	autophagy	8,82E-06	6,27E-04	2/2 100.0%	43/14306 0.3%	MAP1LC3A ATG7
45	autophagic vacuole assembly	2,24E-03	4,50E-02	1/2 50.0%	16/14306 0.1%	MAP1LC3A
10257	NADH dehydrogenase complex assembly	4,40E-07	3,66E-06	2/2 100.0%	10/14306 0.0%	NDUFAF4 NDUFAF3

3

part

BBB alterations in capCAA and AD

4.1

chapter

Amyloid Beta Induces Oxidative Stress-Mediated Blood-Brain Barrier Changes in Capillary Amyloid Angiopathy

Anna Carrano, Jeroen J. Hoozemans, Saskia M. van der Vies, Annemieke J.M. Rozemuller, Jack van Horssen and Helga E. de Vries

Amyloid Beta Induces Oxidative Stress-Mediated Blood–Brain Barrier Changes in Capillary Amyloid Angiopathy

Anna Carrano [1], Jeroen J.M. Hoozemans [1], Saskia M. van der Vies [1], Annemieke J.M. Rozemuller [1], Jack van Horssen [2*], and Helga E. de Vries [2*].

[*] These authors contributed equally to this work.

[1] Departments of Pathology and [2] Molecular Cell Biology and Immunology (MCBI), VU University Medical Center, Amsterdam, The Netherlands.

Abstract

Cerebral amyloid angiopathy (CAA) is frequently observed in Alzheimer's disease (AD) and is characterized by deposition of amyloid beta (Aβ) in leptomeningeal and cortical brain vasculature. In 40% of AD cases, Aβ mainly accumulates in cortical capillaries, a phenomenon referred to as capillary CAA (capCAA). The aim of this study was to investigate blood–brain barrier (BBB) alterations in CAA-affected capillaries with the emphasis on tight junction (TJ) changes. First, capCAA brain tissue was analyzed for the distribution of TJs. Here, we show for the first time a dramatic loss of occludin, claudin-5, and ZO-1 in Aβ-laden capillaries surrounded by NADPH oxidase-2 (NOX-2)-positive activated microglia. Importantly, we observed abundant vascular expression of the Aβ transporter receptor for advanced glycation endproducts (RAGE). To unravel the underlying mechanism, a human brain endothelial cell line was stimulated with Aβ1-42 to analyze the effects of Aβ. We observed a dose-dependent cytotoxicity and increased ROS generation, which interestingly was reversed by administration of exogenous antioxidants, NOX-2 inhibitors, and by blocking RAGE. Taken together, our data evidently show that Aβ is toxic to brain endothelial cells via binding to RAGE and induction of ROS production, which ultimately leads to disruption of TJs and loss of BBB integrity.

Introduction

Alzheimer's disease (AD) is the most common neurological disorder affecting elderly and is clinically characterized by a progressive cognitive decline associated with extracellular accumulation of neurotoxic amyloid β (Aβ) and hyperphosphorylated tau-positive neurofibrillary tangles (Deane and Zlokovic, 2007; Jeynes and Provias, 2006). Senile plaques predominantly consist of Aβ deposits and can be observed throughout the cerebral cortex in advanced stages of the disease. Alternatively, Aβ is able to accumulate in the cerebrovasculature, which is referred to as cerebral amyloid angiopathy (CAA). CAA is a common finding in the elderly, with an incidence up to 50% of the population (Rensink, et al., 2003). There is a strong association between AD and CAA as CAA occurs in 80%–100% of AD cases. CAA can be widespread and is usually observed in larger vessels, including leptomeningeal vessels and cortical arteries and arterioles. Remarkably, Aβ depositions are also observed in cortical capillaries (Attems, 2005). Several groups support the distinction between CAA present in larger vessels (CAA type II) and Aβ accumulation in both larger vessels and capillaries (CAA type I or capillary CAA (capCAA) (Thal, et al., 2002). CAA is a major cause of hemorrhagic and ischemic strokes in elderly patients, probably also involved in microbleeds (Attems, et al., 2005; van Horssen, et al., 2005), and may play a role in AD progression. Relatively little is known on the impact of capCAA in AD pathogenesis, although it is tempting to speculate that Aβ accumulation in capillaries may affect blood–brain barrier (BBB) integrity. Notably, BBB dysfunction has been reported in various neurological conditions, including multiple sclerosis, cerebral ischemia, and AD (Coisne and Engelhardt, 2011; Hawkins and Davis, 2005; Zipser, et al., 2007; Zlokovic, 2008).

The BBB is a tight sealed barrier between the circulating blood and the central nervous system (CNS), consisting of brain microvascular endothelial cells that are surrounded by basement membranes, astrocytic endfeet, and pericytes. The brain microvascular endothelium is characterized by the presence of tight junctions (TJs) and lack of fenestrae, thereby limiting the entry of plasma components, red blood cells, and leukocytes into the CNS, and confer the low paracellular permeability and high electrical resistance of the BBB (Hawkins and Davis, 2005; Zlokovic, 2008). TJs are complex structures located at the apical region between endothelial cells and are composed of connecting transmembrane proteins (occludin and claudins) that form the primary seal linked via accessory cytoplasmic proteins (zona occludens family

members) to the actin cytoskeleton (Hawkins and Davis, 2005).

Occludin is a phosphoprotein with four transmembrane domains and intracellular amino and the carboxyl termini (Blasig, et al., 2011). Occludin expression is associated with increased electrical resistance and decreased paracellular transport. Claudins comprise a multigene family consisting of more than 20 members and contain two extracellular loops and four transmembrane domains and interact in both a homophilic and heterophilic way with claudins of adjacent cells. Claudin-5 is a critical component of the BBB as it prevents the passage of molecules larger than 800 Da (Overgaard, et al., 2011). Carboxyterminal parts of both occludin and claudins interact with membrane-associated recruiting proteins of the zona occludens (ZO) protein family. ZO proteins are reported to link transmembrane proteins to the actin cytoskeleton and have signaling potential (Gonzalez-Mariscal, et al., 2011).

Leakage of the BBB in AD has been suggested by the detection of plasma proteins associated with amyloid plaques (Akiyama, et al., 1992; Kalaria, 1992; Wisniewski, et al., 1997) and within AD brain parenchyma (Kalaria, 1992; Wisniewski, et al., 1997; Zipser, et al., 2007). Likewise, in CAA, an impaired barrier function was detected associated with cerebrovascular Aβ deposits (Wisniewski, et al., 1997). Opening of the BBB and concomitant altered TJ expression or localization has been attributed to vascular Aβ aggregates (Blanc, et al., 1997; Gonzalez-Velasquez, et al., 2008; Marco and Skaper, 2006; Tai, et al., 2009), which in turn are able to induce reactive oxygen species (ROS) production, mainly generated by NADPH oxidase (NOX), in neuronal and non-neuronal cell cultures (Babior, 2000; Li, et al., 2008; Zhou, et al., 2008). Both endogenous and exogenous ROS induce loss of endothelial cell–cell interactions (van Wetering, et al., 2002) and are able to modulate BBB integrity and disrupt TJs (Lehner, et al., 2011; Schreibelt, et al., 2007). However, to date, the link between Aβ, ROS production and TJs alterations remains elusive.

The involvement of RAGE appears to be very important in the development of the AD and CAA pathology, since RAGE mediates the influx of Aβ into the brain parenchyma and consequently in an unbalanced situation enhances Aβ accumulation. RAGE is also known to be critical regarding the effects exerted by Aβ through its binding to the transporter. Aβ/RAGE interaction has been reported to activate NOX and a cascade of effects such as NF-kB-mediated endothelial activation resulting in secretion of proinflammatory cytokines, the expression of adhesion molecules and suppression of cerebral blood flow (Zlokovic, 2008).

In this study, we combine neuropathological findings in unique brain samples of capCAA

patients and show a dramatic loss of TJ proteins in Aβ-laden capillaries. Interestingly, cap-CAA-affected vessels are surrounded by NOX2-immunopositive activated microglia. We next investigated the link between Aβ toxicity and TJ changes using a human cerebral microvascular endothelial cell line and demonstrated that cytotoxic Aβ via production of ROS, decreased TJ proteins expression which could be rescued by exogenous antioxidants, NOX-2 inhibition, and RAGE blocking antibody.

Materials and methods

Postmortem tissue

Six patients with extensive capCAA and two age-matched non-demented controls were selected. Human brain specimens were obtained at autopsy with a short postmortem interval (The Netherlands Brain Bank, Amsterdam, The Netherlands and University Medical Centre in Utrecht, The Netherlands). Neuropathological evaluation was performed on frozen tissue and formalin-fixed, paraffin-embedded tissue from occipital pole cortex. CapCAA score was defined as follow: severe (+++), moderate (++), and mild (+). Staging of AD was evaluated according to Braak and colleagues (Braak and Braak, 1991). Age, gender, postmortem delay (PMD), Braak, CERAD, and CAA scores and cause of death of all cases used in this study are listed in Table1.

Immunohistochemistry

For immunohistochemical staining, 5-μm cryosections were air-dried and fixed in acetone for 10 min. Next, sections were preincubated with normal goat serum 1:10, diluted in phosphate buffered saline (PBS) containing 1% bovine serum albumin (Roche Diagnostics, Mannheim, Germany) for 10 min. Sections were incubated O/N with primary antibodies: anti-occludin (mouse, Zymed), anti-ZO1 (rabbit, Zymed) (Table2) diluted in PBS containing 1% bovine serum albumin. Subsequently, sections were incubated with EnVision goat-anti-mouse horseradish peroxidase (HRP) or EnVision goat-anti-rabbit HRP (Dako, Glostrup, Denmark) for 60 min. Peroxidase labeling was visualized by EnVision 3,3-diaminobenzidine 1:50 (EV-DAB; Dako). Sections were counterstained with hematoxylin. Finally, tissue sections were rinsed with 70% ethanol prior to a 20 min incubation with 50 ml saturated NaCl

solution (0.5 *M* NaCl in 80% ethanol) which was supplemented with 0.5 ml 1% NaOH solution. Then sections were transferred to saturated Congo Red (VWR internationaal, Leuven, the Netherlands) solution supplemented with 0.5 ml 1% NaOH solution for 20 min. Congo Red staining was used to visualize Aβ fibrils. Between all incubation steps, sections were extensively washed with PBS (pH 7.4). PBS served as negative control.

Paraffin sections (5 μm) were mounted on coated glass slides (Menzel Gläzer super frost PLUS, Brainschweig, Germany) and dried O/N at 37°C. Sections were deparaffinized and rehydrated by xylene and a sloping concentration of ethanol (100%, 96%, and 70%). Endogenous peroxidase was blocked by incubating the sections in methanol+0.3% H_2O_2 for 30 min. Antigen retrieval was established by boiling the sections in 1 m*M* EDTA buffer for 10 min. Then, sections were O/N incubated with anti-claudin-5 (mouse, Zymed) or anti-NOX2 (mouse) (see Table 2) diluted in PBS supplemented with 1% BSA. Then the sections were incubated for 30 min with EnVision anti-rabbit/anti-mouse HRP. Peroxidase labeling was visualized by EVDAB 1:50. Sections were counterstained with hematoxylin. The sections were stained with Congo Red as described above. Finally sections were rinsed twice with 100% ethanol, put in xylene and covered with DePeX mounting medium (Gurr, Germany). Between all incubation steps, sections were extensively washed with PBS (pH 7.4). PBS served as negative control.

Table 1. Summary of Patient Details

Patient #	Age	Gender	PMD	Braak	CERAD	CAA	cause of death
1	75	F	6	V	0	+++	dehydration
2	65	M	7	V	C	++/+++	pneumonia
3	83	F	5	III	B	++/+++	cachexia by dementia syndrome
4	71	F	< 24	IV	B	+++	pneumonia
5	86	M	> 24	VI	B	+	pneumonia
6	78	F	-	IV	A	+++	pneumonia

Immunofluorescence

For co-localization studies, cryosections were incubated in thioflavin S solution (100 mg/ml) for 5 min to stain Aβ fibrils and washed subsequently three times in ethanol 70%. Sections were preincubated with normal goat serum 1:10 for 10 min and incubated O/N with a

mix of primary antibodies: anti occludin/claudin-5 and anti factor VIII or anti ZO-1/RAGE and anti CD31 diluted in PBS containing 1% bovine serum albumin. Sections were then incubated with secondary antibodies: Cy5 labeled goat-anti-rabbit 1:100, diluted in EnVision goat-anti-mouse HRP (Dako) for 30 min. Peroxidase labeling was visualized by reaction with rhodamine-tyramide (1:3000) in presence of 0.01% of H_2O_2 for 5 min. After washing, slides were covered with Vectashield (Vector laboratories, Burlington, ON, Canada). Between all incubation steps, sections were extensively washed with PBS (pH 7.4). Fluorescent analysis was performed with a Leica TCS SP2 AOBS confocal laser-scanning microscope (Leica Microsystem, Heidelberg, Germany). Quantification of TJ protein-expressing vessel was also performed normal vessels versus Aβ-laden vessels. Four fields per slides were counted and a ratio was calculated (magnification X10).

Table 2. Primary Antibodies Used in this Study

Primary Antibody	species raised in	dilution	method	ARS	source
Occludin	mouse	1:200	EnVision	EDTA	Zymed (Invitrogen)
Claudin-5	mouse	1:200	EnVision	Na-citrate	Zymed (Invitrogen)
ZO-1	rabbit	1:100	ABC	-	Zymed (Invitrogen)
NOX-2	mouse	1:100	EnVision	Na-citrate	Gift of D. Roos
RAGE	goat	1:500	ABC	-	Biochem
Factor VIII	rabbit	1:250	ABC	-	DAKO
CD31	mouse	1:10	ABC	-	DAKO

Cell culture

A human cerebral microvascular endothelial cell line (hCMEC/D3) (Weksler, et al., 2005) was maintained in EBM-2 medium (Clonetics, Cambrex BioScience, Wokingham, UK) supplemented with VEGF, IGF-1, EGF, basic FGF, hydrocortisone, ascorbate, gentamycin, and 2.5% fetal bovine serum (FBS) 40. T75 flasks, 96-well plates and 24-well plates were coated with type 1 collagen (Gibco HBSS, Invitrogen, Carlsbad, CA). hCMECs were detached at 37°C with 2 ml trypsin/EDTA in PBS. Cultures were grown to confluence at 37°C in 5% CO_2 until the formation of monolayers.

Aβ1-42 preincubation

Synthetic Aβ1-42 (Bachem, Bubendorf, Switzerland) was dissolved in 0.1% ammonium hydroxide and stored in 50 μl, 1 mM aliquots at−80°C. 40 μM Aβ1-42 was preincubated in EBM-2 medium without FBS for 3 days in order to form aggregates. Then Aβ1-42 was further diluted in cell medium to obtain appropriate concentrations.

Electron microscopy

Pre-aggregated Aβ1-42 was applied to formvar carbon-coated copper grids (Stork Veco BV, Eerbeek, The Netherlands) and dried for 10 min. Grids were negatively stained with uranyl acetate for 5 min and examined with a Zeiss EM109 electron microscope to visualize the formation of fibrils.

MTT assay

The cytotoxicity of synthetic Aβ1-42 preparations was assessed by the 3-(4,5-dimethylthiazol-2-yl)-2,5-diphenyltetrazolium bromide (MTT; Sigma Aldrich, Germany) assay. hCMECs were cultured in 96-well plates until they reached 100% confluence. Cells were incubated for 24 h with different concentrations of Aβ1-42 (1 nM, 10 nM, 100 nM, 1 μM, 10 μM). Antioxidants and blocking antibody anti-RAGE were applied 2 h prior Aβ incubation and were still present during the entire treatment. Then cells were incubated with MTT (1 mg/ml) for 3 h at 37°C. The formazan-salt generated by mitochondria of viable cells as a result of conversion of MTT was dissolved in glycin/DMSO (ratio 1:6) and the absorbance was measured at 540 nm.

Live/dead assay

Using the LIVE/DEAD Viability/Cytotoxicity Assay Kit (Molecular Probes Inc, Eugene, OR) living and dead cells can be distinguished from each other. hCMECs were cultured in 96-well plates until they reached 100% confluence. Cells were incubated for 24 h with different concentrations of Aβ1-42 (1 μM, 10 μM, 20 μM). Cells were washed gently with warm PBS. Then 1 μl calcein AM and 1.5 μl ethidium homodimer 1 were added to warm EBM-2 medium and 100 μl of this mixture was added per well for 20 minutes. The cell permeable calcein AM is converted into the green fluorescent calcein by intracellular esterase activity (excitation ~495 nm; emission ~515 nm). Ethidium homodimer 1 is able to enter cells with damaged membranes. It undergoes a 40-fold enhancement of fluorescence upon binding to nucleic acids and produces a red fluorescent signal in dead cells (excitation ~495 nm, emission ~

635nm). Four 10 times magnified fields were counted and a ratio was calculated for live and dead cells.

Amplex Red assay

hCMECs were cultured in 96-well plates until they reached 100% confluence. Cells were treated with different concentrations of Aβ1-42 (1 nM, 10 nM, 100 nM, 1 μM, and 10 μM) for 24 h. After incubation, Aβ was removed and H_2O_2 production was detected using the Amplex red fluorescent dye (Molecular Probes, Breda, the Netherlands) which reacts 1:1 with H_2O_2 in the presence of horseradish peroxidase, producing highly fluorescent resorufin. Fluorescence was detected at 37°C in a fluorimeter (Galaxy-Fluostar, BMG, Offenburg, Germany). The excitation and emission fluorescent wavelengths were 550 and 590 nm, respectively. The calibration signal was produced by addition of known amounts of H_2O_2 added to the reaction mix. The velocity whereby H_2O_2 was produced was calculated using non-linear regression.

mRNA isolation and real-time quantitative PCR

To investigate mRNA expression of TJ proteins cells were grown on a 24-well plate until they reached 100% confluency. Cells were incubated with different concentrations of Aβ1-42 (10 nM, 100 nM, 1 μM) for 24 h. mRNA was isolated by using the mRNA capture kit (Roche Applied Science, Almere, the Netherlands) following the manufacturer's protocol. mRNA was reverse transcribed using the Reverse transcription system kit (Promega, Madison, WI) according to the manufacturer's instructions using GeneAmp PCR system 9700 (Applied Biosystems, Foster City, CA). cDNA was diluted three times and quantified for mRNA levels of occludin/claudin-5/ZO-1 relative to the housekeeping gene GAPDH. The accumulation of PCR product is measured using Sybergreen II (Applied Biosystems). Primers were developed using the program Primer Express 2.0 (Applied Biosystems). The sequences of primers are as follows: human occludin: sense 5'-CCCGTTTGGATAAAGAATTGG-3', antisense 5'-TCAAACAACTTGGCATCAGA-3'; human ZO-1: sense 5'-CCCGAAGGAGTTGAG-CAGGAAATC-3', antisense 5'-CCACAGGCTTCAGGAACTTGAGG-3'. The PCR amplification was performed in triplicate in a 7900 HT Fast Real-Time PCRSystem (Applied Biosystems). Relative expression levels of TJ proteins in relation to the reference GAPDH were calculated using the mathematical model: ΔΔCT. The formula is 2-ΔΔCT where ΔCT=CTtarget - CTreference and ΔΔCT=ΔCTsample - ΔCTcalibrator.

Data were analyzed statistically by Student's *t*-test or analysis of variance (ANOVA) followed by post hoc analysis with Bonferroni's method (*$P<0.05$, **$P<0.01$, ***$P<0.001$).

Results

Reduced tight junction protein expression in CapCAA-affected vessels

Using Congo Red, we observed extensive Aβ deposits throughout the occipital cortex in capillaries and larger vessels. No Aβ was detected in brain vessels of control brains. To investigate the expression of TJ proteins, postmortem tissue of 6 capCAA patients and 2 non-neurological controls was stained for occludin, claudin-5, and ZO-1. We observed a normal vascular expression pattern of TJ proteins in control tissue capillaries and in vessels not affected by Aβ deposition in samples from capCAA patients (Figs.1A, 1C, and 1E). Interestingly, we observed a marked reduction or even complete loss of occludin, claudin-5 and ZO-1 staining in CAA-affected capillaries (Figs.1B, 1D, and 1F). Quantification based on triple fluorescent staining for Aβ, TJs and an endothelium marker confirmed significant loss of TJ proteins expression in Aβ-laden capillaries compared to non-affected capillaries (Figs. 2d–2f).

Aβ-laden capillaries are surrounded by NOX-2-positive activated microglia

Aβ is known to induce ROS-generating enzymes, including NOX-2 in microglia. NOX-2 is constitutively expressed by microglial cells and under physiological conditions NOX-2 activity is low. However, NOX-2 is strikingly upregulated in response to acute and chronic stimuli, including Aβ (Li and Shah, 2003; Park, et al., 2005). We show that NOX-2 is expressed in microglial cells in control brain tissue (Fig. 3A), however NOX-2 is abundantly and widely expressed in microglia throughout capCAA-affected tissue. Cells stained positive for NOX-2 were recognized as microglia based on their morphology (*e.g.,* characteristic long branching processes and a small cellular body). Particularly, Aβ-positive capillaries are engulfed by NOX2-immunoreactive microglia (Fig. 3B), strongly suggesting increased ROS production in close vicinity of Aβ-laden capillaries with TJ changes.

Aβ induces occludin and ZO-1 mRNA downregulation

Immunohistopathological findings showed reduced TJ expression in Aβ-laden capillaries. To

investigate the direct effects of Aβ on mRNA expression of TJ proteins, we examined the effects of Aβ1-42 on occludin, claudin-5, and ZO-1, using a human cerebral microvascular endothelial cell line (hCMEC/D3) (Weksler, et al., 2005). Endothelial cells treated for 24h with increasing concentration of Aβ fibrils (Fig. 4C)showed a dose-dependent significant reduction of occludin and ZO-1 transcripts (max reduction of 55% and 45%, respectively) (Figs. 4A and 4B). Remarkably, no changes in claudin-5 mRNA were detected (data not shown). These results are in line with the loss of occludin and ZO-1 in capCAA tissue, and suggest
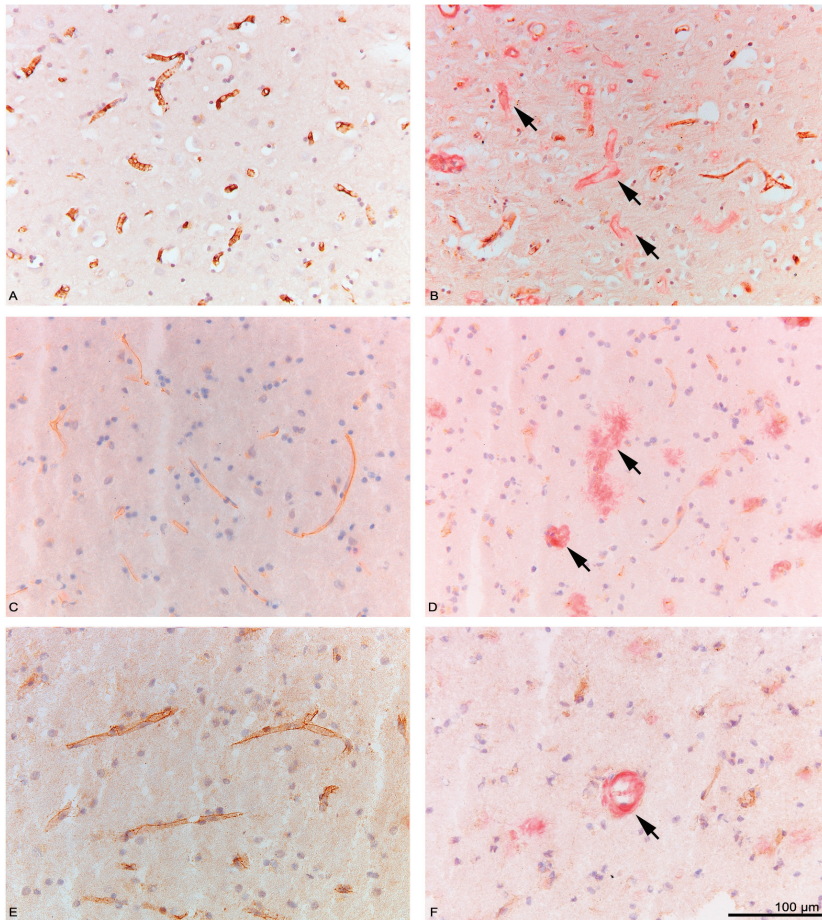
Figure 1. Loss of TJ proteins in capCAA. TJ proteins (brown) are normally expressed in endothelial cells of capillaries. Claudin-5 immunoreactivity was localized virtually in all the vasculature in control and unaffected tissue (A). Loss of endothelial claudin-5 was observed in Aβ-laden capillaries (Congo red) (arrows) (B). Occludin immunoreactivity was localized virtually in all the vasculature in control and unaffected tissue (C). Loss of occludin in endothelial cells was observed in Aβ-laden capillaries indicated by the arrows (D). ZO1 expression was detected in the vasculature of control and unaffected tissue (E). Loss of ZO1 in endothelial cells was observed in Aβ-laden capillaries indicated by the arrow (F).

that reduced TJ protein expression might be caused by Aβ deposits in the microvasculature.

Aβ is toxic to brain endothelial cells via enhanced ROS production

In order to test which concentration of Aβ is lethal to brain endothelial cells, we performed a live/dead assay. Hereto, cells were incubated for 4 h and 24 h with different concentrations of Aβ1-42. Cells treated for 4 h with Aβ1-42 did not show any sign of cell death (data not shown), however after 24 h of Aβ treatment, we observed cell death using Aβ concentration of 10 μ*M* and higher. No significant cytotoxicity was detected upon 1 μ*M* Aβ treatment when compared to vehicle-treated cells (Fig. 5A).

To evaluate the cytotoxic effect of Aβ on hCMECs, we assessed the effect on mitochondrial function as a measure of cell viability. We showed a dose-dependent decrease in brain endothelial cell viability after 24 and 48 h of Aβ1-42 treatment. After 24 h, a dose-dependent effect of Aβ on mitochondrial function was observed with a maximum effect at 1 μ*M* Aβ1-42 with a decline of mitochondrial function around 50% (Fig. 5B). Dose-dependent toxicity was also present at 48 h (data not shown).

We observed cell death and impaired mitochondrial function, which can both be related to ROS production (Hsu, et al., 2010; Turrens, 2003). In order to investigate whether Aβ1-42 induces production of ROS, hCMECs were treated with Aβ1-42 for 24 h. Using an Amplex Red assay, we showed that Aβ1-42 induced a dose-dependent increase in H_2O_2 production compared to vehicle-treated cells (Fig. 5C).

Antioxidants/ROS scavengers rescue endothelial cells from Aβ1-42 toxicity

Since we detected hydrogen peroxide production in response to Aβ incubation, we further elucidated the involvement of NADPH oxidase and xanthine oxidase in Aβ-mediated ROS production using specific inhibitors such as diphenylene iodonium (DPI) and allopurinol. Alpha-lipoic acid (alpha-LA) was used as general ROS scavenger. Endothelial cells preincubated with DPI, allopurinol, and alpha-LA for 2 h were then treated with different concentrations of Aβ1-42 (10 n*M* and 100 n*M*) in presence of the different compounds for 24 h. Cell viability was measured by MTT assay. DPI, allopurinol, and LA were all able to rescue hCMECs from Aβ-mediated toxicity (Fig. 6), indicating that Aβ-mediated cytotoxicity is mainly due to Aβ-induced ROS production.
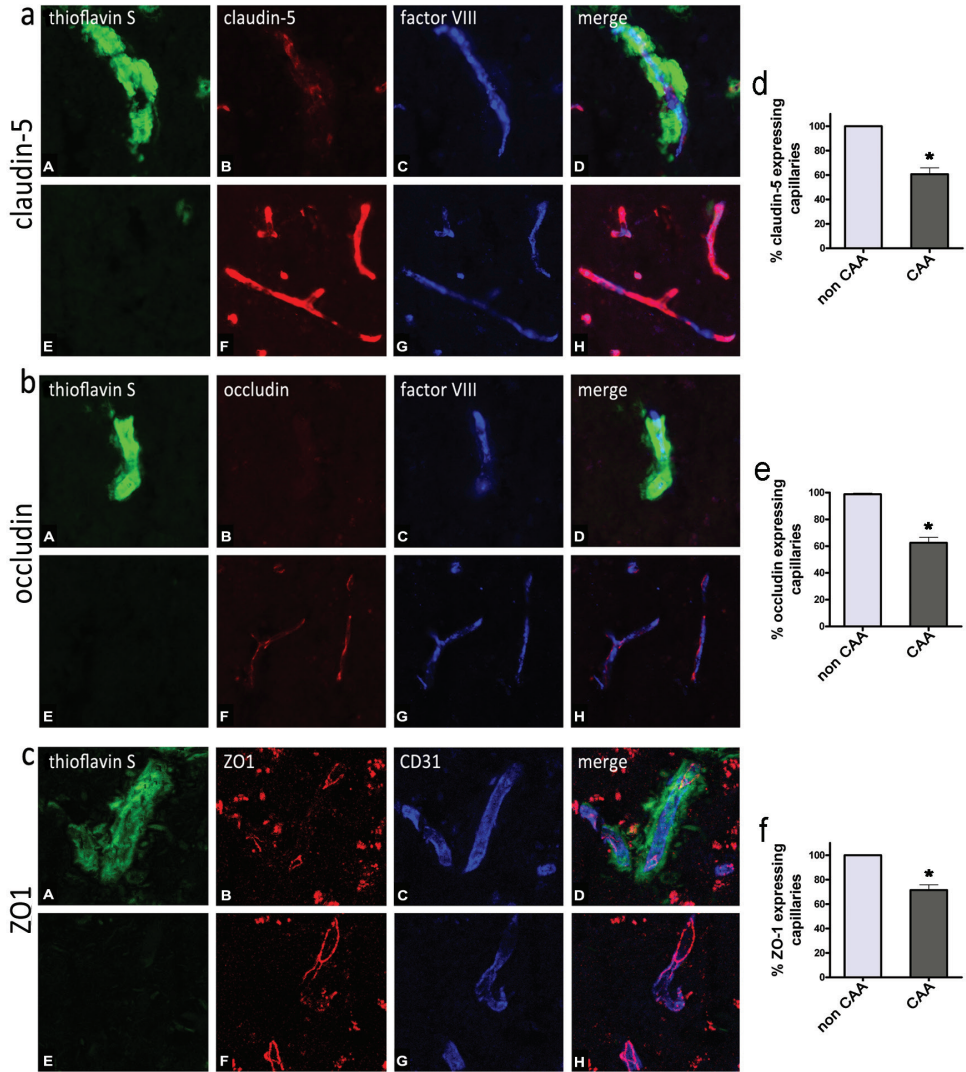
Figure 2. Loss of TJ proteins in capCAA: co-localization study. Triple immunofluorescence analysis confirmed loss of TJs in endothelial cells affected by Aβ deposition; (a), (b), and (c) represent respectively analysis for TJ proteins claudin-5, occludin, and ZO1. Aβ was detected by Thioflavin S (green). Claudin-5, occludin, and ZO1 (red) were downregulated in capillaries detected by endothelial markers factor VIII and CD31 (blue). (A, B, C, D) Aβ-laden capillaries; (E, F, G, H) normal capillaries. Quantification of claudin-5 (d), occludin (e), and ZO-1 (f) expressing capillaries in CAA and non-CAA microvasculature is shown in the graphs. *p < 0.05, by Student t test.

Antioxidants rescue Aβ-dependent downregulation of TJ proteins

We proved that Aβ1-42 fibrils induce ROS generation in our cell system and it has been previously shown that ROS can affect TJs integrity (Schreibelt, et al., 2007; van Wetering, et al., 2002). We hypothesized that the downregulation of TJ proteins observed upon Aβ1-42 fibrils treatment is due to the Aβ-dependent ROS production. To elucidate the link between Aβ, ROS, and TJs expression changes, we incubated hCMEC with allopurinol for 2 h prior to Aβ treatment; we then measured the expression of occludin and ZO-1 mRNA levels. As allopurinol was able to rescue cells from Aβ-mediated cytotoxicity, it was also capable of restoring TJ mRNA levels, confirming that indeed Aβ-driven ROS production is responsible for major TJ alterations (Fig. 7).

Upregulation of RAGE in capCAA

RAGE is the most important influx transporter for Aβ across the BBB and is expressed at relatively low levels in the microvasculature under physiological conditions. We show by means
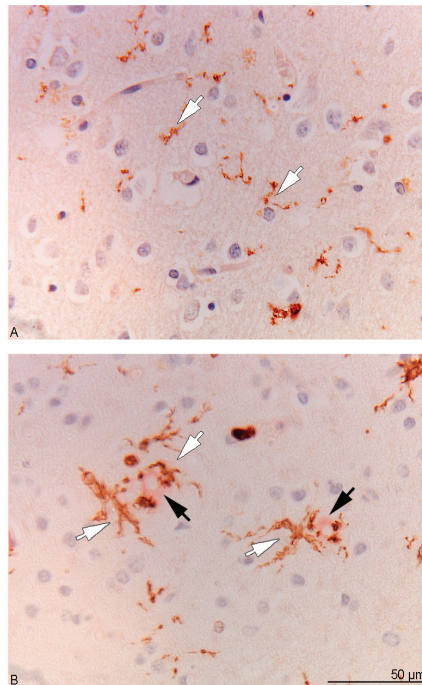
Figure 3. NOX2 expression in capCAA. NOX2 is normally detected in microglia of control brains (A, white arrows). No immunoreactivity is detected in endothelial cells. In capCAA tissue, NOX2 immunoreactivity is increased in microglia (white arrows) and endothelial cells of Aβ-laden vasculature (black arrows) (B).

of immunohistochemical analysis a striking increase in RAGE expression in capCAA-affected capillaries compared to control and nonaffected capillaries. These results confirm, as previously reported (Donahue, et al., 2006), that Aβ induces a local upregulation of RAGE (Fig. 8).

RAGE mediates Aβ-induced cytotoxicity

In order to determine the involvement of RAGE in the Aβ cytotoxic effects, we treated hCMEC with a blocking antibody against RAGE. Cells were treated with the blocking antibody for 2 h and for 24 h together with Aβ1-42 fibrils. MTT assay showed that blocking RAGE rescued cells from Aβ-induced toxicity, demonstrating that Aβ effects on endothelial cells are exerted at least partially by its binding to RAGE (Fig. 9).
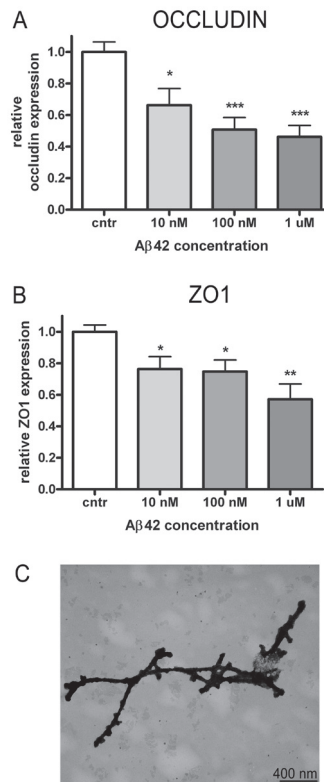
Figure 4. Aβ induces downregulation of TJ proteins. Occludin (A) and ZO1 (B) mRNA expression was assessed by q-PCR on hCMEC upon 24 h Aβ treatment. Cells were treated with increasing concentration of Aβ 1-42 (10 nM, 100 nM, 1 lM). TJs expression was normalized to the expression of housekeeping gene GAPDH. Data were represented as the mean ± SEM; n = at least three experiments with triplicate samples. *p < 0.05, ***p < 0.001 by Student t test. Aβ fibrils were characterized by electron microscopy. (C) shows electron micrographs of Aβ 1-42 incubated 3 days at 37 °C prior to being added to the cell cultures.
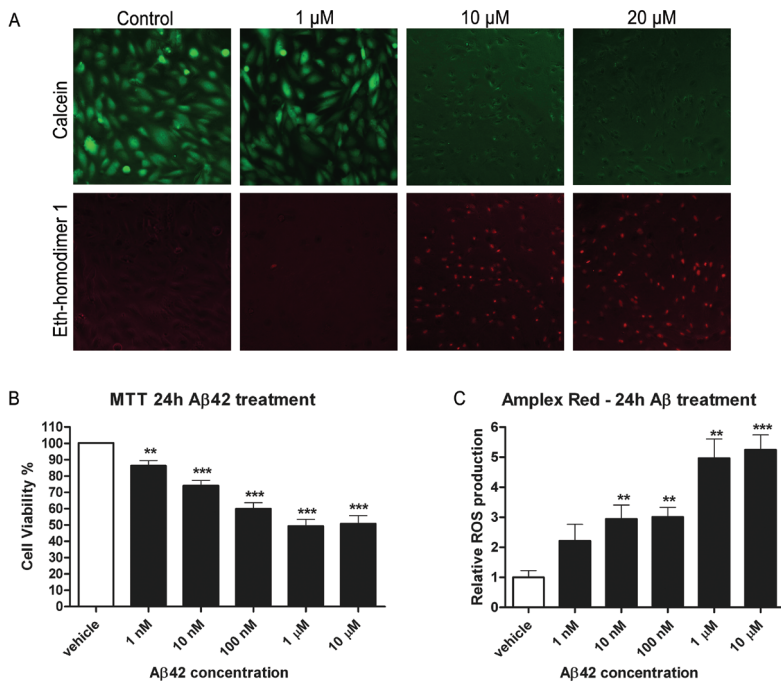
Figure 5. Aβ cytoxicity and ROS production. HCMEC/D3 were incubated with increasing concentrations of Aβ 1-42. Cells incubated for 24 h with 1 μM Aβ 1-42 or less looked morphologically normal and appeared fluorescently green at the live/ dead assay, no significant cells death was detected. At 10 μM or higher concentration, Aβ 1-42 was toxic to hCMEC, dead red fluorescent cells were detected respect to control (A). After 24 h incubation with Aβ 42, there was a cell viability response in a dose-dependent manner with a maximum effect of 1 μM Aβ 42 and a maximum decline of mitochondrial function around 50% measured by MTT assay (B). The same treatment induced ROS production, here measured as production of H2O2. A dosedependent H2O2 was observed after 24 h of treatment (C). Data were represented as the mean – SEM; n = at least three experiments with triplicate samples. **p < 0.01, ***p < 0.001 by Student t test.
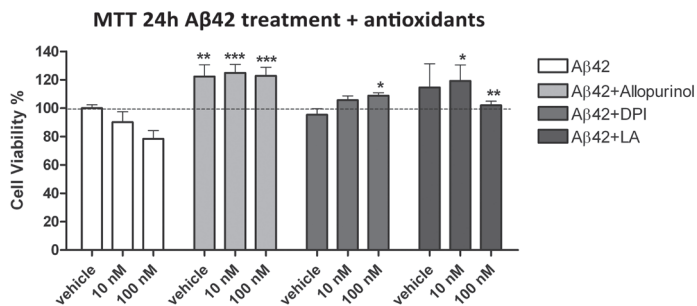
Figure 6. Antioxidants rescue hCMEC from Aβ toxicity. HCMEC were preincubated for 2 h with antioxidants, allopurinol, DPI, and lipoic acid, before Aβ treatment. After preincubation, cells were treated with 10 nM, 100 nM, or vehicle in presence of the antioxidants. Antioxidants could reverse the toxic effect of Aβ 1-42 on endothelial cells. Data were represented as the mean ± SEM; n = at least three. *p < 0.05, **p < 0.01, ***p < 0.001 by two-way ANOVA, followed by post hoc Bonferroni test.

Discussion

For the first time, we show in this study a dramatic loss of TJ proteins in Aβ-laden capillaries, which are surrounded by NOX2-positive activated microglia. We demonstrated in an *in vitro* BBB system that Aβ is able to induce ROS formation and decrease TJ mRNA levels, which could be rescued upon pretreatment with NOX inhibitors and lipoic acid. We further demonstrate that blocking RAGE is a way to rescue cells from Aβ-induced toxicity.

Using our unique postmortem tissue, we here provide evidence on the loss of expression of TJ proteins in capCAA. So far, histopathological studies have demonstrated that microvascular alterations can be extensive in AD patients (Claudio, 1996; Farkas and Luiten, 2001). These alterations have been shown associated with vascular Aβ deposition as degeneration of perivascular cells, including pericytes and smooth muscle cells, swollen astrocytic end feet (Higuchi, et al., 1987; Yamashita, et al., 1991), reduced expression of brain endothelial glucose transporter-1 protein, increased pinocytotic vesicles, and decreased numbers of mitochondria. In addition, prominent thickening and local disruption of vascular basement membranes was reported by several research groups analyzing either biopsy tissue or postmortem AD material (Claudio, 1996; Mancardi, et al., 1980; Perlmutter and Chui, 1990). Vascular abnormalities that are associated with local amyloid accumulation suggest that impaired vascular function and thus impaired BBB integrity represents a common phenomenon in AD pathology. Although there are several studies demonstrating BBB alterations in CAA type II, comprehensive immunohistochemical studies on BBB abnormalities in Aβ-laden capillaries (CAA type I) are limited. *In vitro* studies support the idea that Aβ deposition affects BBB integrity since different Aβ peptides are able to increase endothelial permeability (Blanc, et al., 1997; Tai, et al., 2009) and induce altered expression and translocation of TJs proteins in human and animal ECs (Gonzalez-Velasquez, et al., 2008; Marco and Skaper, 2006). Remarkably, data on putative TJ alterations and the underlying mechanisms in CAA-affected capillaries are lacking.

To provide novel data on the BBB integrity during CAA, we selected a unique cohort of patients with abundant Aβ deposits in cortical capillaries. We observed a striking loss of occludin, claudin-5, and ZO-1 immunostaining in Aβ-laden capillaries, whereas unaffected capillaries showed a normal expression pattern, indicating that loss of TJ expression was predominantly related to microvascular Aβ deposition. Importantly, endothelial cells of cap-
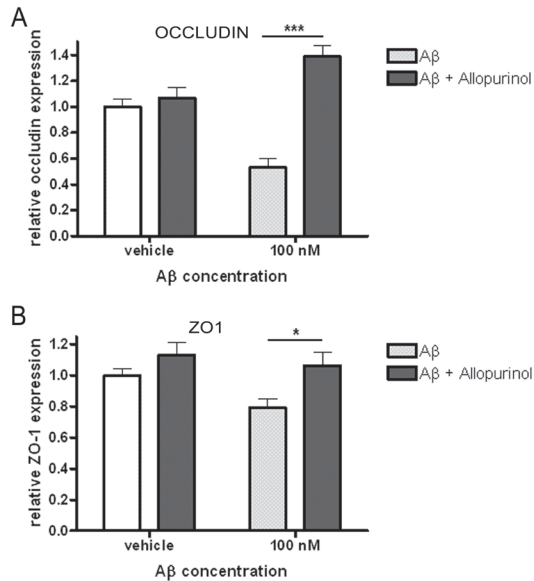
Figure 7. Antioxidants rescue Aβ-dependent downregulation of TJ proteins. Occludin (A) and ZO-1 (B) mRNA expression was assessed by q-PCR on hCMEC upon 24 h 100 μM Aβ treatment in the presence of allopurinol. TJs expression was normalized to the expression of house-keeping gene GAPDH. Co-treatment with allopurinol was able to restore normal levels of TJ transcripts. Data were represented as the mean ± SEM, n = at least three. *p < 0.05, ***p < 0.001 by two-way ANOVA followed by post hoc Bonferroni test.

CAA-affected vessels still express endothelial markers, including factor VIII and CD31, excluding brain endothelial cell death as a potential reason for the lack of TJ protein expression. Although leakage of the BBB has been supported by elevated plasma proteins associated with Aβ deposits, we here for the first time provide direct evidence of TJ proteins loss in AD brains linked to Aβ accumulation. The subsequent breakdown of the BBB may in turn disrupt normal transport of nutrients, vitamins, and electrolytes across the BBB, which are essential for proper neuronal functioning.

Interestingly, we detected enhanced expression of the ROS-generating enzyme NADPH oxidase-2 (NOX-2) in microglia surrounding Aβ-laden vessels. Previous data from our group demonstrated that deposition of Aβ throughout the brain parenchyma, especially extravascular deposition of Aβ that from the vessel wall radiates into the neuropil (named dyshoric changes), is able to induce an inflammatory response, consisting in activation of microglia and astrocytes (Richard, et al., 2010; Rozemuller, et al., 1989). Upon phagocytosis or recognition of Aβ by microglia cells, a series of responses may occur that includes the release of
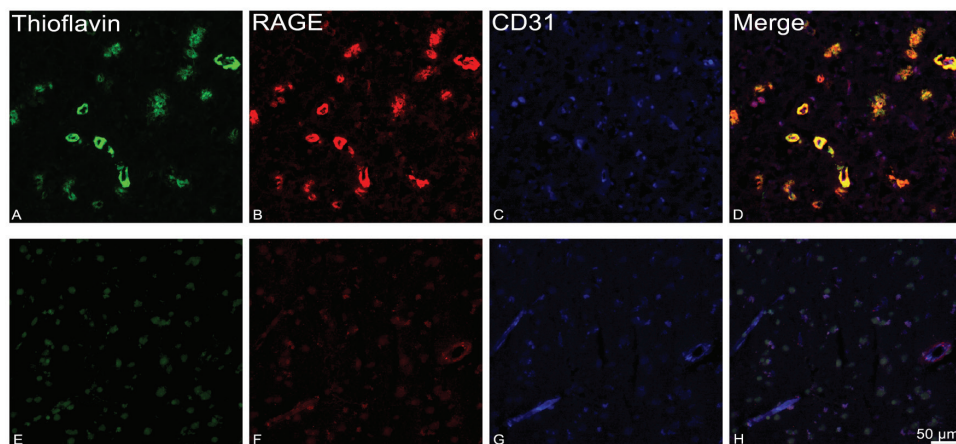
Figure 8. RAGE expression in capCAA brain tissue. Expression of RAGE was detected by triple immunofluorescence analysis. Aβ was detected by Thioflavin S (green, A and E). No Aβ was detected in control tissue. RAGE (red) is strongly higher expressed in Aβ-laden capillaries (B) with respect to control (F). Capillaries were stained with endothelial marker CD31 (C, G). Merge show co-localization of Aβ and RAGE at capillary level in cap CAA (D), but no co-localization in control tissue (H).
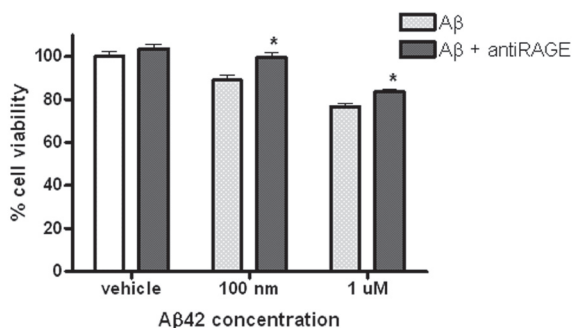
Figure 9. Blocking RAGE rescue cell from Aβ cytotoxic effects. HCMEC were preincubated for 2 h with blocking antibody anti-RAGE (40 μg/ml) prior to Aβ 1-42 treatment. Anti-RAGE was always present during treatment. Blocking RAGE could reverse the toxic effect of Aβ 1-42 on endothelial cells. Data were represented as the mean – SEM; n = at least three. $*p < 0.05$, by Student t test.

proinflammatory cytokines and ROS. One of the main sources of ROS under neuropathological conditions is enhanced NOX activity, together with the mitochondrial respiratory chain. In particular, NOX-2 is a well-known NADPH oxidase expressed in microglia where it is normally expressed at low levels. However, under pathological conditions, NOX-2 is upregulated and associated with a wide variety of vascular pathologies such as hypertension, diabetes, and hyperlipidemia (35). Enhanced expression of NOX-2 leads to increased ROS levels, partic-

ularly superoxide, and induces oxidative stress. In material derived from non-neurological controls, NOX-2 expression is mainly limited to microglia. Notably, the expression pattern of NOX-2 in capCAA tissue was strikingly different; revealing a stronger microglial expression, especially around capCAA-affected vessels, and NOX-2 was clearly expressed in perivascular macrophages associated with Aβ-laden capillaries. From these findings we conclude that Aβ deposition within and surrounding capillaries induces microglial activation and subsequent upregulation of NOX-2 protein expression in activated microglial cells and perivascular macrophages. These results support the idea of increased production of ROS in close proximity of capCAA-affected vessels and are in line with the observation that protein and DNA oxidative damage are increased in AD brains (Lyras, et al., 1997; Wang, et al., 2005).

To unravel pathways involved in BBB damage and Aβ-induced oxidative stress in brain endothelial cells, an *in vitro* approach was taken using the validated human brain endothelial cell line hCMEC/D3. We first assessed the cytotoxic effects of Aβ1-42, one of the predominant Aβ isoforms accumulating in Aβ-laden capillaries. Aβ1-40 is the predominant form of Aβ in larger CAA-affected vessels, such as arterioles and leptomeningeal vessels. However, the Aβ1-40/Aβ1-42 ratio of capillary Aβ is significantly lower than that of affected arteries and veins but equals that found in senile plaques (Richard, et al., 2010), indicating that Aβ1-42 is a common Aβ isoforms in microvascular CAA. Furthermore, Aβ1-42 is known to be the most toxic form of Aβ to endothelial cells (Eisenhauer, et al., 2000). Hence, we used the Aβ1-42 isoform for our *in vitro* studies. We treated endothelial cells with pre-aggregated Aβ peptide as aggregates were reported to be more toxic to ECs (5). At standardized conditions we could observe cells death after 24 h incubation at concentrations higher than 10 μ*M*. Subtoxic concentrations of Aβ1-42 were then used to assess the effects of amyloid on TJ expression *in vitro*. Using this set-up, we showed a significant dose-dependent downregulation of TJ proteins occludin and ZO-1 mRNA levels upon Aβ1-42 incubation, but no changes in claudin-5 mRNA level, as also reported by Tai *et al.* (Tai, et al., 2009), which was in contrast to our postmortem findings. Reduced expression of occludin after 48 h of Aβ1-40 incubation has been previously described in hCMEC, but no changes in claudin-5 or ZO-1 (Gonzalez-Velasquez, et al., 2008). Aβ1-42 has been reported to reduce expression of claudin-5 and occludin in primary rat brain endothelial cells albeit at higher concentrations than the concentration used in this study (Marco and Skaper, 2006). Our results, together with the previous findings, confirm the

significant loss of occludin and ZO-1 in capCAA tissue and directly related these observations to Aβ deposit in the microvasculature. We speculate that claudin-5 protein expression may be altered by Aβ, as our immunohistochemical results strongly suggested. It is conceivable that prolonged exposure to Aβ is needed to decrease claudin-5 expression, as occurs in the patient material, or that loss of claudin-5 reported in capCAA tissue is not due to altered expression at transcriptional level but to a post-translational modification or degradation of the protein.

Our *in vitro* results showed dose-dependent decrease of mitochondrial function and increased production of ROS upon Aβ1-42 stimulation of hCMEC. One consequence of impaired mitochondrial function is enhanced generation of ROS, and since dysfunctional mitochondria will produce more ROS, a feed-forward loop is set up, resulting in a vicious cycle (Wang, et al., 2007; Zhu, et al., 2006). Aβ is also known to increase ROS production in different cerebral cell types and we showed that both NOX inhibition and exogenous antioxidants were able to counteract the toxic effect of Aβ1-42, confirming that reduced cell viability was indeed caused by ROS.

The cytotoxic effects of vascular Aβ might be caused by Aβ binding to RAGE. We observed for the first time a striking increase of RAGE expression in Aβ-laden capillaries. RAGE is a major influx transporter for Aβ across the BBB and its expression is upregulated in AD and transgenic models of amyloidosis in the affected cerebral vessels, microglia, and neurons (Zlokovic, 2008). RAGE not only imports Aβ into the brain, increasing Aβ accumulation in the cerebral parenchyma, but when bound to its ligands also induces ROS production through NADPH oxidase activation (Wautier, et al., 2001). Importantly, we showed that blocking RAGE prevents Aβ-induced decrease of cell viability.

Conclusion

Taken together, we show the occurrence of severe TJ alterations in Aβ-laden capillaries. Interestingly, affected capillaries were surrounded by NOX2-positive activated microglia. *In vitro* experiments confirmed that Aβ was able to decrease TJ mRNA levels and that both exogenous antioxidants as well as NOX inhibitors limit Aβ-mediated cellular toxicity. We further demonstrated that RAGE is the mediator of the Aβ-cytotoxic effects on endothelial cells. We speculate that due to increased local Aβ-driven ROS production, TJ protein expression is altered in the microvasculature of capCAA brains. It is plausible that extensive microvascular

Aβ depositions, enhanced microvascular expression of RAGE, and concomitant loss of TJ protein expression impair BBB function and consequently leads to inefficient transport of nutrients into the brain. Collectively, these pathological processes might hamper Aβ clearance from the brain and thereby contribute to neuronal damage.

References

Akiyama, H., Ikeda, K., Kondo, H., McGeer, P.L. 1992. Thrombin accumulation in brains of patients with Alzheimer's disease. *Neurosci Lett* 146(2), 152-4.

Attems, J. 2005. Sporadic cerebral amyloid angiopathy: pathology, clinical implications, and possible pathomechanisms. *Acta Neuropathol* 110(4), 345-59.

Attems, J., Jellinger, K.A., Lintner, F. 2005. Alzheimer's disease pathology influences severity and topographical distribution of cerebral amyloid angiopathy. *Acta Neuropathol* 110(3), 222-31.

Babior, B.M. 2000. The NADPH oxidase of endothelial cells. *IUBMB Life* 50(4-5), 267-9.

Blanc, E.M., Toborek, M., Mark, R.J., Hennig, B., Mattson, M.P. 1997. Amyloid beta-peptide induces cell monolayer albumin permeability, impairs glucose transport, and induces apoptosis in vascular endothelial cells. *J Neurochem* 68(5), 1870-81.

Blasig, I.E., Bellmann, C., Cording, J., Del Vecchio, G., Zwanziger, D., Huber, O., Haseloff, R.F. 2011. Occludin protein family: oxidative stress and reducing conditions. *Antioxid Redox Signal* 15(5), 1195-219.

Braak, H., Braak, E. 1991. Neuropathological stageing of Alzheimer-related changes. *Acta Neuropathol* 82(4), 239-59.

Claudio, L. 1996. Ultrastructural features of the blood-brain barrier in biopsy tissue from Alzheimer's disease patients. *Acta Neuropathol* 91(1), 6-14.

Coisne, C., Engelhardt, B. 2011. Tight junctions in brain barriers during central nervous system inflammation. *Antioxid Redox Signal* 15(5), 1285-303.

Deane, R., Zlokovic, B.V. 2007. Role of the blood-brain barrier in the pathogenesis of Alzheimer's disease. *Curr Alzheimer Res* 4(2), 191-7.

Donahue, J.E., Flaherty, S.L., Johanson, C.E., Duncan, J.A., 3rd, Silverberg, G.D., Miller, M.C., Tavares, R., Yang, W., Wu, Q., Sabo, E., Hovanesian, V., Stopa, E.G. 2006. RAGE, LRP-1, and amyloid-beta protein in Alzheimer's disease. *Acta Neuropathol* 112(4), 405-15.

Eisenhauer, P.B., Johnson, R.J., Wells, J.M., Davies, T.A., Fine, R.E. 2000. Toxicity of various amyloid beta peptide species in cultured human blood-brain barrier endothelial cells: increased toxicity of dutch-type mutant. *J Neurosci Res* 60(6), 804-10.

Farkas, E., Luiten, P.G. 2001. Cerebral microvascular pathology in aging and Alzheimer's disease. *Prog Neurobiol* 64(6), 575-611.

Gonzalez-Mariscal, L., Quiros, M., Diaz-Coranguez, M. 2011. ZO proteins and redox-dependent processes. *Antioxid Redox Signal* 15(5), 1235-53.

Gonzalez-Velasquez, F.J., Kotarek, J.A., Moss, M.A. 2008. Soluble aggregates of the amyloid-beta protein selectively stimulate permeability in human brain microvascular endothelial monolayers. *J Neurochem* 107(2), 466-77.

Hawkins, B.T., Davis, T.P. 2005. The blood-brain barrier/neurovascular unit in health and disease. *Pharmacol Rev* 57(2), 173-85.

Higuchi, Y., Miyakawa, T., Shimoji, A., Katsuragi, S. 1987. Ultrastructural changes of blood vessels in the cerebral cortex in Alzheimer's disease. *Jpn J Psychiatry Neurol* 41(2), 283-90.

Hsu, M.J., Sheu, J.R., Lin, C.H., Shen, M.Y., Hsu, C.Y. 2010. Mitochondrial mechanisms in amyloid beta peptide-induced cerebrovascular degeneration. *Biochim Biophys Acta* 1800(3), 290-6.

Jeynes, B., Provias, J. 2006. The possible role of capillary cerebral amyloid angiopathy in Alzheimer lesion development: a regional comparison. *Acta Neuropathol* 112(4), 417-27.

Kalaria, R.N. 1992. The blood-brain barrier and cerebral microcirculation in Alzheimer disease. *Cerebrovasc Brain Metab Rev* 4(3), 226-60.

Lehner, C., Gehwolf, R., Tempfer, H., Krizbai, I., Hennig, B., Bauer, H.C., Bauer, H. 2011. Oxidative stress and blood-brain barrier dysfunction under particular consideration of matrix metalloproteinases. *Antioxid Redox Signal* 15(5), 1305-23.

Li, G., Ma, R., Huang, C., Tang, Q., Fu, Q., Liu, H., Hu, B., Xiang, J. 2008. Protective effect of erythropoietin on beta-amyloid-induced PC12 cell death through antioxidant mechanisms. *Neurosci Lett* 442(2), 143-7.

Li, J.M., Shah, A.M. 2003. ROS generation by nonphagocytic NADPH oxidase: potential relevance in diabetic nephropathy. *J Am Soc Nephrol* 14(8 Suppl 3), S221-6.

Lyras, L., Cairns, N.J., Jenner, A., Jenner, P., Halliwell, B. 1997. An assessment of oxidative damage to proteins, lipids, and DNA in brain from patients with Alzheimer's disease. *J Neurochem* 68(5), 2061-9.

Mancardi, G.L., Perdelli, F., Rivano, C., Leonardi, A., Bugiani, O. 1980. Thickening of the basement membrane of cortical capillaries in Alzheimer's disease. *Acta Neuropathol* 49(1), 79-83.

Marco, S., Skaper, S.D. 2006. Amyloid beta-peptide1-42 alters tight junction protein distribution and expression in brain microvessel endothelial cells. *Neurosci Lett* 401(3), 219-24.

Overgaard, C.E., Daugherty, B.L., Mitchell, L.A., Koval, M. 2011. Claudins: control of barrier function and regulation in response to oxidant stress. *Antioxid Redox Signal* 15(5), 1179-93.

Park, L., Anrather, J., Zhou, P., Frys, K., Pitstick, R., Younkin, S., Carlson, G.A., Iadecola, C. 2005. NADPH-oxidase-derived reactive oxygen species mediate the cerebrovascular dysfunction induced by the amyloid beta peptide. *J Neurosci* 25(7), 1769-77.

Perlmutter, L.S., Chui, H.C. 1990. Microangiopathy, the vascular basement membrane and Alzheimer's disease: a review. *Brain Res Bull* 24(5), 677-86.

Rensink, A.A., de Waal, R.M., Kremer, B., Verbeek, M.M. 2003. Pathogenesis of cerebral amyloid angiopathy. *Brain Res Brain Res Rev* 43(2), 207-23.

Richard, E., Carrano, A., Hoozemans, J.J., van Horssen, J., van Haastert, E.S., Eurelings, L.S., de Vries, H.E., Thal, D.R., Eikelenboom, P., van Gool, W.A., Rozemuller, A.J. 2010. Characteristics of dyshoric capillary cerebral amyloid angiopathy. *J Neuropathol Exp Neurol* 69(11), 1158-67.

Rozemuller, J.M., Eikelenboom, P., Stam, F.C., Beyreuther, K., Masters, C.L. 1989. A4 protein in Alzheimer's disease: primary and secondary cellular events in extracellular amyloid deposition. *J Neuropathol Exp Neurol* 48(6), 674-91.

Schreibelt, G., Kooij, G., Reijerkerk, A., van Doorn, R., Gringhuis, S.I., van der Pol, S., Weksler, B.B., Romero, I.A., Couraud, P.O., Piontek, J., Blasig, I.E., Dijkstra, C.D., Ronken, E., de Vries, H.E. 2007. Reactive oxygen species alter brain endothelial tight junction dynamics via RhoA, PI3 kinase, and PKB signaling. *FASEB J* 21(13), 3666-76.

Tai, L.M., Holloway, K.A., Male, D.K., Loughlin, A.J., Romero, I.A. 2009. Amyloid-beta-induced occludin down-regulation and increased permeability in human brain endothelial cells is mediated by MAPK activation. *J Cell Mol Med*.

Thal, D.R., Ghebremedhin, E., Rub, U., Yamaguchi, H., Del Tredici, K., Braak, H. 2002. Two types of sporadic cerebral amyloid angiopathy. *J Neuropathol Exp Neurol* 61(3), 282-93.

Turrens, J.F. 2003. Mitochondrial formation of reactive oxygen species. *J Physiol* 552(Pt 2), 335-44.

van Horssen, J., de Jong, D., de Waal, R.M., Maass, C., Otte-Holler, I., Kremer, B., Verbeek, M.M., Wesseling, P. 2005. Cerebral amyloid angiopathy with severe secondary vas-

cular pathology: a histopathological study. *Dement Geriatr Cogn Disord* 20(5), 321-30.

van Wetering, S., van Buul, J.D., Quik, S., Mul, F.P., Anthony, E.C., ten Klooster, J.P., Collard, J.G., Hordijk, P.L. 2002. Reactive oxygen species mediate Rac-induced loss of cell-cell adhesion in primary human endothelial cells. *J Cell Sci* 115(Pt 9), 1837-46.

Wang, J., Xiong, S., Xie, C., Markesbery, W.R., Lovell, M.A. 2005. Increased oxidative damage in nuclear and mitochondrial DNA in Alzheimer's disease. *J Neurochem* 93(4), 953-62.

Wang, X., Su, B., Perry, G., Smith, M.A., Zhu, X. 2007. Insights into amyloid-beta-induced mitochondrial dysfunction in Alzheimer disease. *Free Radic Biol Med* 43(12), 1569-73.

Wautier, M.P., Chappey, O., Corda, S., Stern, D.M., Schmidt, A.M., Wautier, J.L. 2001. Activation of NADPH oxidase by AGE links oxidant stress to altered gene expression via RAGE. *Am J Physiol Endocrinol Metab* 280(5), E685-94.

Weksler, B.B., Subileau, E.A., Perriere, N., Charneau, P., Holloway, K., Leveque, M., Tricoire-Leignel, H., Nicotra, A., Bourdoulous, S., Turowski, P., Male, D.K., Roux, F., Greenwood, J., Romero, I.A., Couraud, P.O. 2005. Blood-brain barrier-specific properties of a human adult brain endothelial cell line. *FASEB J* 19(13), 1872-4.

Wisniewski, H.M., Vorbrodt, A.W., Wegiel, J. 1997. Amyloid angiopathy and blood-brain barrier changes in Alzheimer's disease. *Ann N Y Acad Sci* 826, 161-72.

Yamashita, K., Miyakawa, T., Katsuragi, S. 1991. Vascular changes in the brains with Alzheimer's disease. *Jpn J Psychiatry Neurol* 45(1), 79-84.

Zhou, J., Zhang, S., Zhao, X., Wei, T. 2008. Melatonin impairs NADPH oxidase assembly and decreases superoxide anion production in microglia exposed to amyloid-beta1-42. *J Pineal Res* 45(2), 157-65.

Zhu, X., Perry, G., Moreira, P.I., Aliev, G., Cash, A.D., Hirai, K., Smith, M.A. 2006. Mitochondrial abnormalities and oxidative imbalance in Alzheimer disease. *J Alzheimers Dis* 9(2), 147-53.

Zipser, B.D., Johanson, C.E., Gonzalez, L., Berzin, T.M., Tavares, R., Hulette, C.M., Vitek, M.P., Hovanesian, V., Stopa, E.G. 2007. Microvascular injury and blood-brain barrier leakage in Alzheimer's disease. *Neurobiol Aging* 28(7), 977-86.

Zlokovic, B.V. 2008. The blood-brain barrier in health and chronic neurodegenerative disorders. *Neuron* 57(2), 178-201.

4.2

chapter

Neuroinflammation and Blood-Brain Barrier Changes in Capillary
Amyloid Angiopathy

Anna Carrano, Jeroen J. Hoozemans, Saskia M. van der Vies, Jack van Horssen,
Helga E. de Vries and Annemieke J.M. Rozemuller

Neuroinflammation and Blood–Brain Barrier Changes in Capillary Amyloid Angiopathy

Anna Carrano[1], Jeroen J.M. Hoozemans[1], Saskia M. van der Vies[1], Jack van Horssen[2]*, Helga E. de Vries[2]*, Annemieke J.M.Rozemuller[1]

Departments of [1]Pathology and [2]Molecular Cell Biology and Immunology (MCBI), VU University Medical Center, Amsterdam, The Netherlands

* Both authors contributed equally

Abstract

Introduction: β-Amyloid (Aβ) accumulation in cortical capillaries is a variant of cerebral amyloid angiopathy (CAA) referred to as capillary CAA (capCAA). CapCAA is associated with a neuroinflammatory response. In vitro studies indicate that Aβ induces reactive oxygen species (ROS) production, mainly generated through NADPH oxidase (NOX), by activated microglia. ROS in turn can induce altered expression of tight junctions (TJ), which are eminent for blood brain barrier (BBB) function. Whether the function of the BBB is affected in the brains of Alheimer's disease (AD) patients with co-morbidity capCAA remains elusive. Interestingly cases with only capCAA exist making it possible to study the capCAA independent of the AD pathology

Aim: In this study we have investigated BBB alterations in capCAA and addressed the role of the neuroinflammatory response.

Methods: Human *post mortem* brain tissue with capCAA was analyzed by immunohistochemical staining.

Results: In this study we show for the first time a dramatic loss of TJ proteins claudin-5, occludin and ZO-1 in Aβ-laden capillaries. In addition, affected capillaries are associated with clusters of NOX-2-positive activated microglia. Disrupted BBB function was observed by increased presence of fibrinogen around the affected capillaries.

Conclusions: Our data provide support for early observation that the neuroinflammatory response is involved in the altered expression of TJs in endothelial cells and loss of BBB integrity in capCAA.

Key words: Alzheimer's disease, Cerebral Amyloid Angiopathy, neuroinflammation, blood-brain barrier.

Introduction

Cerebral amyloid angiopathy (CAA) is frequently observed in Alzheimer's disease (AD) and is characterized by deposition of β-amyloid (Aβ) in leptomeningeal and cortical brain vasculature. In 40% of AD cases, Aβ mainly accumulates in cortical capillaries, a phenomenon referred to as capillary CAA (capCAA) (Richard, et al., 2010). Relatively little is known about the impact of capCAA on AD pathogenesis. Previously, we have shown that a strong neuroinflammatory response, consisting of clusters of activated microglia and astrocytes, occurs specifically around capCAA vessels with dyshoric Aβ deposits, similar to the observed changes around Aβ plaques in the parenchyma (Akiyama, et al., 2000; Richard, et al., 2010). The inflammatory reaction associated with Aβ deposits is thought to play a role in the pathogenesis of AD and likely contributes to the symptoms of cognitive decline (Arends, et al., 2000; Rozemuller, et al., 2005). Concomitant to cognitive decline, the inflammatory reaction associated with Aβ deposits is thought to play a role in the pathogenesis of AD and likely contributes to the symptoms of cognitive decline (Arends, et al., 2000; Rozemuller, et al., 2005). Concomitant to cognitive decline, the inflammatory reaction associated with Aβ deposits around capillaries could impair the function of the blood-brain barrier (BBB).

Upon phagocytosis or recognition of Aβ by microglia cells, a series of responses may occur, which include the release of proinflammatory cytokines and reactive oxygen species (ROS). ROS are predominantly produced by activation of NADPH oxidase (NOX) and during mitochondrial respiration and ROS generation are significantly increased under neuropathological conditions. Microglia mainly express NOX-2 and we showed that activated microglia around Aβ-laden capillaries show an enhanced expression of the ROS-generating enzyme NOX-2 suggesting local ROS production (Carrano, et al., 2011).

In vitro studies have revealed that both endogenous and exogenous ROS induce loss of endothelial cell–cell interactions (van Wetering, et al., 2002) and are able to modulate BBB integrity and disrupt tight junctions (Schreibelt, et al., 2007). Tight junctions (TJs) are the main structures responsible for the barrier properties of the BBB and restrict the entry of circulating molecules and cells. These results support the idea of increased production of ROS in close proximity of capCAA-affected vessels and are in line with the observation that protein and DNA oxidative damage are increased in AD brains (Lyras, et al., 1997; Wang, et al., 2005). Opening of the BBB and concomitant altered TJs expression or localization has been attrib-

uted to vascular Aβ aggregates (Blanc, et al., 1997; Gonzalez-Velasquez, et al., 2008; Marco and Skaper, 2006; Tai, et al., 2009), however, comprehensive immunohistochemical studies on BBB abnormalities in Aβ-laden capillaries are limited. In line with previous *in vitro* data we hypothesize that the recruitment and activation of microglia due to Aβ deposition at the capillaries would generate ROS in proximity of the endothelium and consequently affect the expression of TJ proteins and BBB integrity.

Methods

We selected a cohort of patients with severe capCAA (n = 23). Human brain specimens were obtained at autopsy with a short postmortem interval (The Netherlands Brain Bank, Amsterdam, The Netherlands and University Medical Centre Utrecht, The Netherlands). Neuropathological evaluation was performed on frozen tissue and formalin-fixed, paraffin-embedded tissue from occipital pole cortex. Brain tissue was analyzed for expression of TJs, NOX-2, plasma proteins and Aβ by immunohistochemical staining.

Results

In our cohort of capCAA cases, abundant Aβ deposits are localized at the capillary level, as we previously described (Richard, et al., 2010). Immunohistochemical staining of brain tissue slices of capCAA cases showed a strong inflammatory response and typical intraneuronal accumulation of ubiquitin and hyperphosphorylated tau in dystrophic neurites, a sign of a severe neuronal dysfunction, localized around capCAA. Both glia activation and neuritic changes strictly correlated with the severity of microvascular Aβ load in the tissue. Microglia clustered around capCAA capillaries not only appeared morphologically activated but showed a strong expression of NOX-2 when compared to control situation, suggesting increased production of ROS and consequent oxidative stress around capCAA (Carrano, et al., 2011).

When analyzing TJ expression, we observed a partial loss (30–40%) of TJ proteins, occludin, claudin-5 and ZO-1 in Aβ-laden capillaries. Furthermore, immunohistochemical stainings revealed leakage of fibrinogen within the brain parenchyma in severe capCAA. In the cases analyzed (n = 8), fibrinogen was found as a diffuse staining within the parenchyma-surrounding vessels and in the majority of the cases (n = 7), we also found colocalization of fibrinogen with the most fibrillar capillary Aβ deposits. In the 3 most severe capCAA cases, the positivity for fibrinogen was virtually present around all Aβ-laden vessels, suggesting an ongoing dis-

ruption of BBB integrity. The measured changes (reduced TJ expression, glia activation and fibrinogen leakage) all correlated with severity of capCAA pathology.

Discussion and conclusion

In this study we showed that activated microglia express NOX-2 cluster around capCAA capillaries; this induces increased production of ROS that eventually affects TJs and BBB integrity leading to leaking of fibrinogen. The effects of vascular Aβ on endothelial cells and microglia are mediated, at least in part, by Aβ interaction with the receptor for advanced glycation end products (RAGE), which we and others found to be upregulated in capCAA, AD and transgenic mouse models of amyloidosis in the affected cerebral vessels, microglia, and neurons (Carrano, et al., 2011; Zlokovic, 2008). RAGE mediates transport of Aβ into the brain parenchyma. In addition, Aβ/RAGE interaction has been reported to activate NOX and a cascade of effects such as NF-κB-mediated endothelial activation. Overall Aβ/RAGE interaction results in increased secretion of prion flammatory cytokines, expression of adhesion molecules and suppression of cerebral blood flow (Zlokovic, 2008). Aβ/RAGE interaction is also able to activate microglia, and consequent inflammatory response, and is thought to be involved in the clustering of microglia around Aβ deposits (Fang, et al., 2010). Aβ accumulation in the brain is a gradual process that probably involves alteration of the physiological clearance of amyloid from the brain, either through Aβ transport across the BBB or along perivascular spaces. Aβ deposits trigger the recruitment of microglia around affected capillaries. Both activated microglia and endothelium release proinflammatory cytokines and ROS which compromise not only TJs but also neuronal function. The breakdown of the BBB may disrupt the normal transport of nutrients, vitamins and electrolytes across the BBB, which are essential for proper neuronal functioning and thus contribute to the neurodegenerative process. In addition, the abnormal production of proinflammatory cytokines, chemokines and the complement system, as well as ROS, by microglia, can disrupt nerve terminals causing dysfunction and loss of synapses, which correlates with memory decline (Hensley, 2010). It appears that impairment of the BBB and a chronic neuroinflammatory response both aggravate synaptic and neuronal dysfunction, and are therefore important players in the resulting neuronal loss and dementia associated with AD.
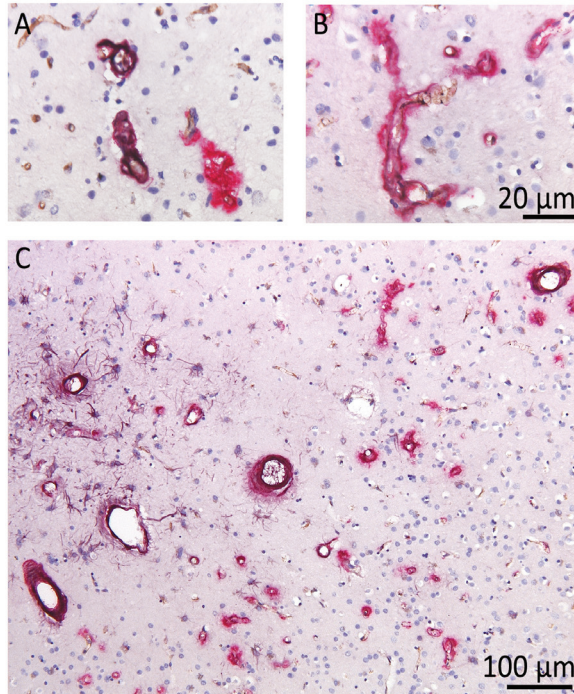
Figure 1. Fibrinogen leakage in capCAA. Post mortem tissue of capCAA brains shows fibrinogen staining (purple) surrounding Aβ (pink) laden vessels. A) depicts 2 microvessels affected by Aβ deposition. In the left one a strong staining for fibrinogen is also present colocalizing with Aβ. Non affected microvessels show expression of TJ protein claudin-5 (brown). B) magnification of an Aβ (pink) microvessel showing reduced expression of claudin-5 (brown) and deposition of fibrinogen (purple) along the vessel walls. C) On the left, a severe leakage of fibrinogen (purple) can be observed around Aβ (pink) laden vessels. Fibrinogen appears as a diffuse staining in the parenchyma surrounding the vasculature, and in some instances also colocalizes with vascular Aβ. In the most affected area, activated glia cells show fibrinogen positivity as well.

References

Akiyama, H., Barger, S., Barnum, S., Bradt, B., Bauer, J., Cole, G.M., Cooper, N.R., Eikelenboom, P., Emmerling, M., Fiebich, B.L., Finch, C.E., Frautschy, S., Griffin, W.S., Hampel, H., Hull, M., Landreth, G., Lue, L., Mrak, R., Mackenzie, I.R., McGeer, P.L., O'Banion, M.K., Pachter, J., Pasinetti, G., Plata-Salaman, C., Rogers, J., Rydel, R., Shen, Y., Streit, W., Strohmeyer, R., Tooyoma, I., Van Muiswinkel, F.L., Veerhuis, R., Walker, D., Webster, S., Wegrzyniak, B., Wenk, G., Wyss-Coray, T. 2000. Inflammation and Alzheimer's disease. *Neurobiol Aging* 21(3), 383-421.

Arends, Y.M., Duyckaerts, C., Rozemuller, J.M., Eikelenboom, P., Hauw, J.J. 2000. Microglia, amyloid and dementia in alzheimer disease. A correlative study. *Neurobiol Aging* 21(1), 39-47.

Blanc, E.M., Toborek, M., Mark, R.J., Hennig, B., Mattson, M.P. 1997. Amyloid beta-peptide induces cell monolayer albumin permeability, impairs glucose transport, and induces apoptosis in vascular endothelial cells. *J Neurochem* 68(5), 1870-81.

Carrano, A., Hoozemans, J.J., van der Vies, S.M., Rozemuller, A.J., van Horssen, J., de Vries, H.E. 2011. Amyloid beta Induces Oxidative Stress-Mediated Blood-Brain Barrier Changes in Capillary Amyloid Angiopathy. *Antioxid Redox Signal.*

Fang, F., Lue, L.F., Yan, S., Xu, H., Luddy, J.S., Chen, D., Walker, D.G., Stern, D.M., Schmidt, A.M., Chen, J.X., Yan, S.S. 2010. RAGE-dependent signaling in microglia contributes to neuroinflammation, Abeta accumulation, and impaired learning/memory in a mouse model of Alzheimer's disease. *FASEB J* 24(4), 1043-55.

Gonzalez-Velasquez, F.J., Kotarek, J.A., Moss, M.A. 2008. Soluble aggregates of the amyloid-beta protein selectively stimulate permeability in human brain microvascular endothelial monolayers. *J Neurochem* 107(2), 466-77.

Hensley, K. 2010. Neuroinflammation in Alzheimer's disease: mechanisms, pathologic consequences, and potential for therapeutic manipulation. *J Alzheimers Dis* 21(1), 1-14.

Lyras, L., Cairns, N.J., Jenner, A., Jenner, P., Halliwell, B. 1997. An assessment of oxidative damage to proteins, lipids, and DNA in brain from patients with Alzheimer's disease. *J Neurochem* 68(5), 2061-9.

Marco, S., Skaper, S.D. 2006. Amyloid beta-peptide1-42 alters tight junction protein distribution and expression in brain microvessel endothelial cells. *Neurosci Lett* 401(3), 219-24.

Richard, E., Carrano, A., Hoozemans, J.J., van Horssen, J., van Haastert, E.S., Eurelings, L.S., de Vries, H.E., Thal, D.R., Eikelenboom, P., van Gool, W.A., Rozemuller, A.J. 2010.

Characteristics of dyshoric capillary cerebral amyloid angiopathy. *J Neuropathol Exp Neurol* 69(11), 1158-67.

Rozemuller, A.J., van Gool, W.A., Eikelenboom, P. 2005. The neuroinflammatory response in plaques and amyloid angiopathy in Alzheimer's disease: therapeutic implications. *Curr Drug Targets CNS Neurol Disord* 4(3), 223-33.

Schreibelt, G., Kooij, G., Reijerkerk, A., van Doorn, R., Gringhuis, S.I., van der Pol, S., Weksler, B.B., Romero, I.A., Couraud, P.O., Piontek, J., Blasig, I.E., Dijkstra, C.D., Ronken, E., de Vries, H.E. 2007. Reactive oxygen species alter brain endothelial tight junction dynamics via RhoA, PI3 kinase, and PKB signaling. *FASEB J* 21(13), 3666-76.

Tai, L.M., Holloway, K.A., Male, D.K., Loughlin, A.J., Romero, I.A. 2009. Amyloid-beta-induced occludin down-regulation and increased permeability in human brain endothelial cells is mediated by MAPK activation. *J Cell Mol Med*.

van Wetering, S., van Buul, J.D., Quik, S., Mul, F.P., Anthony, E.C., ten Klooster, J.P., Collard, J.G., Hordijk, P.L. 2002. Reactive oxygen species mediate Rac-induced loss of cell-cell adhesion in primary human endothelial cells. *J Cell Sci* 115(Pt 9), 1837-46.

Wang, J., Xiong, S., Xie, C., Markesbery, W.R., Lovell, M.A. 2005. Increased oxidative damage in nuclear and mitochondrial DNA in Alzheimer's disease. *J Neurochem* 93(4), 953-62.

Zlokovic, B.V. 2008. The blood-brain barrier in health and chronic neurodegenerative disorders. *Neuron* 57(2), 178-201.

5

chapter

ABC transporters P-gp and BCRP are reduced in capillary cerebral amyloid angiopathy

Anna Carrano, Gijs Kooi, Susanne van der Pol, Jack van Horssen, Robert Veerhuis, Jeroen J. Hoozemans, Annemieke J.M. Rozemuller and Helga E. de Vries

ABC transporters P-gp and BCRP are reduced in capillary cerebral amyloid angiopathy

Anna Carrano[1], Gijs Kooij[2], Susanne van der Pol[2], Jack van Horssen[2], Robert Veerhuis[1,3], Jeroen Hoozemans[1], Annemieke Rozemuller[1], Helga de Vries[2]

Departments of [1]Pathology, [2]Molecular Cell Biology and Immunology (MCBI) and [3]Clinical Chemistry, VU University Medical Center, Amsterdam, The Netherlands.

Abstract

Alzheimer's disease (AD) is the most common form of dementia and marked by deposition of amyloid β (Aβ) within the brain. Alterations of Aβ transporters at the blood-brain barrier may have a role in the disease process. We investigated the expression of ABC transporters P-gp and BCRP in non-neurological controls, AD, and severe capillary cerebral amyloid angiopathy (capCAA) cases, which are characterized by deposition of Aβ within the structure of cerebral capillaries.

Our data show that P-gp and BCRP are profoundly downregulated in capCAA, but not in AD and control cases. *In vitro* P-gp, but not BCRP, was down-regulated in brain endothelial cells by exposure to oligomeric Aβ42, but not fibrillar Aβ42 or Aβ40. Co-incubating Aβ42 together with clusterin, an amyloid associated protein highly expressed in capCAA, strongly reduced levels of P-gp.

In conclusion, accumulation of Aβ, in combination with clusterin, within and around cerebral capillaries may further aggravate the disease process by affecting P-gp expression. Loss of P-gp expression or activity may serve as a selective biomarker for ongoing capCAA.

Introduction

Alzheimer's disease (AD) is the most common form of dementia and characterized by increased deposition of amyloid β (Aβ) within the brain. Accumulation of Aβ depends on a disequilibrium between production and clearance of Aβ. Several pathways for Aβ clearance have been described: (1) Aβ endocytosis by astrocytes and microglial cells; (2) Aβ enzymatic degradation (e.g., by neprilysin or the insulin-degrading enzyme; (3) Aβ transport across the BBB and/or (4) Aβ drainage along perivascular spaces (Thal, et al., 2008b; Weller, et al., 2008). If any of these mechanisms fail the result is an increased retention of Aβ within the brain and consequently Aβ aggregation and deposition.

The BBB plays a crucial role in maintaining the delicate homeostasis of the brain, including the active removal of Aβ. Through restrictive barrier properties and polarized expression of selective transporters, such as the ATP-binding cassette (ABC) transporters, the BBB effectively regulates movement of metabolites and nutrients between blood and brain parenchyma.

Previously, we have shown that the BBB is altered in cases with severe capillary cerebral amyloid angiopathy (capCAA) , a specific subtype of CAA characterized by Aβ protein accumulation in the walls of brain capillaries, which occurs in up to 51% of AD cases (Attems, 2005; Richard, et al., 2010; Thal, et al., 2002; Thal, et al., 2008b). Patients with capCAA can also present with rapidly progressive dementia disease (Eurelings, et al., 2010) or can have a diagnosis of vascular disease. In capCAA the deposition of Aβ occurs at the level of the BBB and it is therefore feasible that the mechanism principally altered in capCAA patients is Aβ transport across the BBB. It has been hypothesized that changes in protein expression at the BBB endothelial cells may increase the Aβ load in the brain leading to the Aβ accumulation as observed in AD and CAA (Zlokovic, 2011).

In recent years, the involvement of the ABC transporters in the pathogenesis of AD has been postulated. In particular, P-glycoprotein (P-gp) and breast cancer resistant protein (BCRP) are of interest in the disease process, since both transporters mediate Aβ clearance from the brain (Wolf, et al., 2012). Changes in expression and function of ABC transporters at the BBB may therefore be a primary cause of increased Aβ load in the brain, especially in the presence of capCAA.

In the brain, Aβ deposits often are associated with accumulation of other proteins, which can modulate the response of the cerebral cells to Aβ exposure (van Horssen, et al., 2005; Veerhuis, et al., 2005). Recently, genome-wide association studies showed that, in addition to ApoE genetic variants, single nucleotide polymorphisms in the clusterin gene may also confer risk to develop sporadic AD (Harold, et al., 2009; Lambert, et al., 2009). Therefore we hypothesized that clusterin, an amyloid associated protein (Kida, et al., 1995; McGeer, et al., 1994; Nuutinen, et al., 2009; Zhan, et al., 1994), might enhance the potential detrimental effects of Aβ on the brain endothelium. Clusterin also binds to and facilitates the transport of Aβ through the binding to LRP2 (low-density lipoprotein receptor-related protein 2) and it is actively involved in mechanisms that clear Aβ from the brain across the BBB (Calero, et al., 2000) (Bell, et al., 2007) (Zlokovic, 2008).

Because of the possible crucial role of P-gp and BCRP in maintaining a homeostatic level of Aβ and their localization at the brain capillaries, we set out to investigate the expression of the ABC transporters in AD cases, and we specifically selected cases that at the neuropathological examination presented with severe capCAA. Herein, we compared the expression profile of P-gp and BCRP to non-neurological control tissues and the differential incidence of transporter changes in AD and capCAA cases.

Accumulated Aβ itself can damage the BBB thereby altering the expression of several proteins, such as tight junctions (Carrano, et al., 2011b). Using an *in vitro* approach, we analysed the downstream effects of Aβ on the expression of P-gp and BCRP in a validated human endothelial BBB *in vitro* model accordingly to Aβ aggregation state (fibrillar or oligomeric) and isoform (Aβ40 or Aβ42).

We here describe that specifically in capCAA cases the expression of ABC transporters P-gp and BCRP is strongly reduced, in comparison with controls and AD without capCAA, and we demonstrated *in vitro* that Aβ reduces the expression of P-gp especially in combination with clusterin.

Material and Methods

Post-mortem tissue

Cases were selected on the basis of the neuropathological diagnosis and immunohistochemical characterisation of Aβ aggregates. Seven patients with neuropathologically diagnosed capCAA, 5 AD cases without capCAA and 4 age-matched non-demented controls were selected. Human brain specimens were obtained at autopsy with a short *post-mortem* interval (The Netherlands Brain Bank, Amsterdam, The Netherlands and University Medical Centre in Utrecht, The Netherlands). Neuropathological evaluation was performed on frozen tissue and formalin-fixed, paraffin-embedded tissue from occipital pole cortex. CapCAA score was defined as follow: severe (+++), moderate (++), mild (+). AD pathology was evaluated according to Braak (Braak, et al., 2006; Braak and Braak, 1991) and CERAD (Mirra, et al., 1991). Age, gender, *post-mortem* delay (PMD), Braak, CERAD and capCAA scores and cause of death of all cases used in this study are listed in Table 1.

Table1. Summary of Patient Details

Patient #	Age	Sex	PMD	Braak	CERAD	capCAA	cause of death
capCAA 1	76	M	< 24 h	IV	C	++/+++	peumonia
capCAA 2	78	F	< 24 h	IV	A	+++	pneumonia
capCAA 3	95	F	< 24 h	III	B	++	peritonitis
capCAA 4	75	M	22 h	III	0	+++	pneumonia
capCAA 5	65	M	7 h	V	C	++/+++	pneumonia
capCAA 6	75	F	6 h	V	C	+++	dehydration
capCAA 7	71	F	< 24 h	IV	B	+++	Pneumonia
AD 1	89	F	4:30 h	VI	C	-	pneumonia
AD 2	69	M	5 h	VI	C	-	pneumonia
AD 3	67	F	6 h	VI	C	-	pneumonia, dehydration
AD 4	81	F	6 h	VI	C	-	pneumonia
AD 5	91	F	5:45 h	VI	C	-	ruptured aneurysm
control 1	80	M	7 h	0	0	-	cachexia, dehydration
control 2	93	F	6 h	II	0	-	cachexia
control 3	84	M	7 h	I	0	-	Exacerbation of COPD
control 4	77	F	n.d.	I	A	-	cachexia

capCAA: capillary cerebral amyloid angiopathy; AD: Alzheimer's disease; PMD: post-mortem delay; M: male; F: female; COPD: chronic obstructive pulmonary disease

Immunohistochemistry

5 μm paraffin sections were mounted on coated glass slides (Menzel Gläzer super frost PLUS, Brainschweig, Germany) and dried O/N at 37 ° C. Sections were deparaffinized and rehydrated by xylene and a sloping concentration of ethanol (100%, 96% and 70%). Endogenous peroxidase was blocked by incubating the sections in methanol + 0.3% H_2O_2 for 30 minutes. Antigen retrieval was established by boiling the sections in 1 mM EDTA buffer for 10 minutes. Sections were O/N incubated with anti-P-gp or anti-BCRP antibodies (Table 2) diluted in PBS supplemented with 1% BSA. Next, sections were incubated for 1 h with relative secondary antibodies HRP-labelled. For P-gp HRP EnVision undiluted solution was used. For BCRP sections were incubated with goat anti-mouse IgG2a HRP-labelled. Peroxidase labelling was visualized by EVDAB 1:50. Sections were then stained for Aβ with anti-Aβ (mouse, DAKO) for 1h, after a further 15 minutes treatment with formic acid. After 60 minutes incubation with alkaline phosphatase conjugated goat anti-mouse IgG1, tissue sections were washed in 0.2 M Tris-HCl buffer, pH 8.5. Alkaline phosphatase was visualized by Liquid Permanent Red (LPR; Dako, Glostrup, Denmark). Finally, tissue sections were counterstained with haematoxylin. Slides were covered with aqueous mounting medium (Aquatex, Merck, Darmstadt, Germany). Between all incubation steps, sections were extensively washed with PBS (pH 7.4).

Table 2. Primary Antibodies Used in this Study

Primary Antibody	species raised in	Isotype	dilution	ARS	source
Pgp (clone 15D3)	mouse	IgG1	1:50	tris-EDTA	Dept of Pathology, VUmc Amsterdam; courtesy of G. Scheffer *
BCRP (clone BXP-21)	mouse	IgG2a	1:50	tris-EDTA	Dept of Pathology, VUmc Amsterdam; courtesy of G. Scheffer *
Factor VIII	rabbit	-	1:250	-	DAKO
Anti Aβ	mouse	IgG1	1:10	formic acid	DAKO
4G8	mouse	IgG2b	1:200	-	Covence
Clusterin (clone G7)	mouse	IgG1	1:100	-	Dept of Clinical Chemistry, Vumc Amsterdam; courtesy of prof. B Murphydr

ARS: antigen retrieval step
* Kooij G. et al. Brain. 2011 Feb;134(Pt 2):555-70

Immunofluorescence

For colocalization studies, cryosections were incubated in thioflavin S solution (100 mg/ml) for 5 minutes to stain Aβ fibrils and washed subsequently 3 times in ethanol (70% in water). Sections were incubated with normal goat serum 1:10 in PBS containing 1% bovine serum albumin for 10 minutes. For P-gp and BCRP staining sections were incubated O/N with a mix of primary antibodies: mouse-anti P-gp/BCRP and rabbit-anti factor VIII diluted in PBS containing 1% bovine serum albumin. Sections were then incubated with secondary antibodies: Cy5 labelled goat-anti-rabbit 1:100, diluted in EnVision goat-anti-mouse HRP (Dako, Glostrup, Denmark) for 30 minutes. For the immunohistochemical analysis of clusterin, sections were incubated O/N with a mix of primary antibodies: mouse-anti clusterin (IgG1) and mouse-anti Aβ 4G8 (IgG2b). Subsequently, sections were incubated with isotype-specific secondary antibodies: goat-anti-mouse IgG2b horseradish peroxidase (HRP) and biotinylated goat-anti-mouse IgG1. An incubation step of 1 h with Streptavidine-Alexa633 followed. For all stainings peroxidase labelling was visualized by reaction with rhodamine-tyramide (1:3000) in presence of 0.01% of H_2O_2 for 5 minutes. After washing, slides were covered with Vectashield (Vector laboratories, Burlington, CA, USA). Between all incubation steps, sections were extensively washed with PBS (pH 7.4). Fluorescent analysis was performed with a Leica TCS SP2 AOBS confocal laser-scanning microscope (Leica Microsystem, Heidelberg, Germany). Quantification of vessel expressing ABC transporters was performed by manually counting the percentage of positive vessels in four 100 times magnified fields per slide. Total amount of vessels in the field was counted based on factor VIII staining.

Cell culture

The human cerebral microvascular endothelial cell line (hCMECs) that expresses key BBB proteins were maintained in EBM-2 medium (Clonetics, Cambrex BioScience, Wokingham, UK) which was supplemented with VEGF, IGF-1, EGF, basic FGF, hydrocortisone, ascorbate, gentamycin and 2.5% fetal bovine serum (FBS) 40. T75 Flasks, 96 wells plates and 24 wells plates were coated with type 1 collagen (Gibco HBSS, Invitrogen, USA). hCMECs were detached at 37 °C with 2 ml trypsin/EDTA in PBS. Cultures were grown to confluence at 37 °C in 5% CO_2 until the formation of monolayers (Carrano, et al., 2011b; Weksler, et al., 2005).

Aβ preparations

Synthetic Aβ42 (Bachem, Bubendorf, Switzerland) and Aβ40 (Anaspec, USA) were dissolved in 0.1% ammonium hydroxide and stored in 50 µl, 1 mM aliquots at -80 °C. Aβ40 and Aβ42 preparations enriched in oligomers (O40, O42) and fibrils (F40, F42) were prepared essentially as described before (Chafekar, et al., 2008; Dahlgren, et al., 2002).

Fibrils were prepared as follows: 100 µM Aβ was prepared in 10% HCl sterile solution, diluting stock drop by drop on vortex, followed by 10 minutes sonication. Aβ was incubated for 24h at 37 ° C in order to form aggregates. The preparation was further diluted in culture medium to obtain appropriate concentrations prior to cell treatments. Oligomers were prepared as follows: 100 µM Aβ was prepared in FBS-free cell medium, diluting stock drop by drop on vortex, followed by 10 minutes sonication. Aβ was incubated for 24 h at 4 °C in order to form oligomers. The preparation was further diluted in culture medium to 100 nM prior to cell treatments and incubated at RT for 1 h alone or in combination with 10 nM clusterin (isolated from human plasma by affinity chromatography as previously described (Krijnen, et al., 2005; Mulder, et al., 2012; Murphy, et al., 1988).

Electron microscopy

Aβ aggregates were applied to formvar carbon-coated copper grids (Stork Veco BV, Eerbeek, The Netherlands) and dried for 10 min. Grids were negatively stained with uranyl acetate for 5 min and examined with a Zeiss EM109 electron microscope to characterize the Aβ preparations.

Viability assay

The cytotoxicity of synthetic Aβ preparations was assessed by the 3-(4,5-dimethylthiazol-2-yl)-2,5-diphenyltetrazolium bromide (MTT; Sigma Aldrich, Germany) assay. hCMECs were cultured in 96 well plates until they reached confluence. Cells were incubated for 24 hours with 100 nM of Aβ40 and Aβ42 fibrils or oligomers enriched preparations with or without 10 nM clusterin. Cells were incubated with MTT (1 mg/ml) for 3 hours at 37°C. The formazan-salt generated by mitochondria of viable cells as a result of conversion of MTT was dissolved in glycin/DMSO (ratio 1:6) and the absorbance was measured at 540 nm.

mRNA isolation and real-time quantitative PCR

To investigate mRNA expression of ABC transporters, hCMECs were grown on a 24 wells plate until they reached confluence. Cells were incubated for 24 hours with 100 nM of Aβ40

and Aβ42 fibrils or oligomers enriched preparations with or without 10 nM clusterin. mRNA was isolated by using the mRNA capture kit (Roche Applied Science, Almere, the Netherlands) following the manufacturer's protocol. mRNA was reverse transcribed using the reverse transcription system kit (Promega, Madison, USA) according to the manufacturer's instructions using GeneAmp PCR system 9700 (Applied Biosystems, Foster City, USA). cDNA was diluted 3 times and quantified for mRNA levels of P-gp and BCRP relative to the housekeeping gene GAPDH. The accumulation of PCR product is measured using Sybergreen II (Applied Biosystems, Foster City, USA). Primers were developed using the program Primer Express 2.0 (Applied Biosystems, Foster City, USA). The sequences of primers are as follows: human P-gp: sense 5'- GTCCCAGGAGCCCATCCT-3', antisense 5'-CCCGGCT-GTTGTCTCCATA-3'; human BCRP: sense 5'- AGATGGGTTTCCAAGCGTTCAT-3', antisense 5'-CCAGTCCCAGTACGACTGTGACA-3'. The PCR amplification was performed in triplicate in a 7900 HT Fast Real-Time PCRSystem (Applied Biosystems, Foster City, USA). Relative expression levels of the ABC transporters in relation to the reference GAPDH were calculated using the mathematical model: ΔΔCT. The formula is 2-ΔΔCT where ΔCT = CT-target - CTreference and ΔΔCT = ΔCTsample – ΔCTcalibrator.

Statistical analysis

Data were analyzed statistically by Student's t-test or analysis of variance (ANOVA) followed by post hoc analysis with Bonferroni's method ($*P<0.05$, $**P<0.01$, $***P<0.001$).

Results

P-gp and BCRP protein expression in capCAA and AD

To visualize the expression pattern of the ABC transporters P-gp and BCRP in AD and cap-CAA samples and correlate it to Aβ deposition, tissue sections from occipital cortex of AD with and without capCAA and non-demented controls were co-stained for Aβ and either P-gp or BCRP (Fig. 1). No Aβ deposits were observed in control cases. AD without capCAA showed Aβ accumulation in classical and diffuse plaques and occasionally in large vessels and leptomeningeal vessels. In capCAA cases, Aβ was mainly found to be deposited in capillaries and larger vessels, with few or no amyloid plaques (Fig. 1).

In our cohort of severe capCAA cases, 39.6±21.5% of microvessels was Aβ-positive.

In occipital cortex specimens of non-neurological control patients, homogeneous P-gp expression was observed in the cerebrovasculature and particularly in the microvasculature (Fig. 1a).

Interestingly, in capCAA most of the Aβ laden vessels showed profound loss of P-gp expression compared to controls (Fig. 1b). P-gp expression remained detectable in vessels not affect-
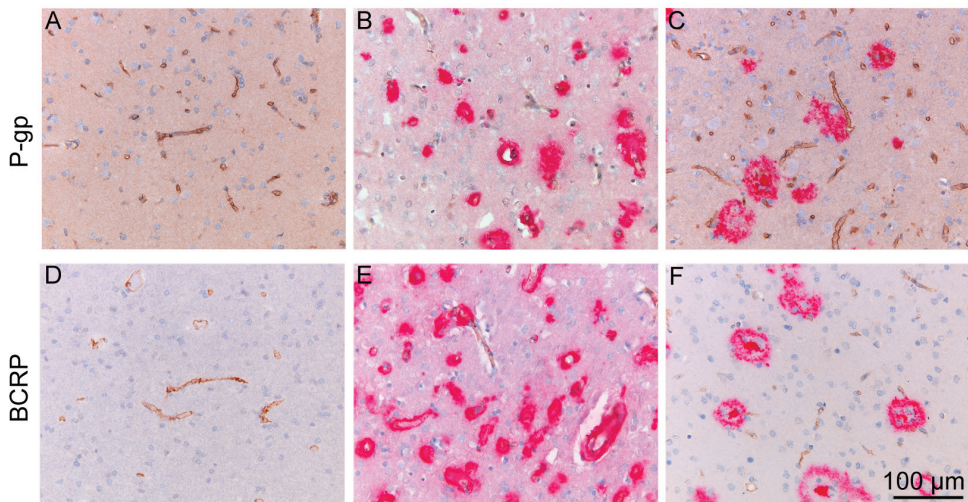
Figure 1. P-gp and BCRP expression in capCAA, AD and controls. Immunohistochemical detection of ABC transporter P-gp (a-c) and BCRP (d-f) in occipital cortex section from the brain of normal (a,d), AD (c, f) and capCAA case (b, e). ABC transporters (brown) are normally expressed in endothelial cells of capillaries as observed in control cases and in AD. Aβ (pink) is found deposited in parenchymal or vascular plaques, respectively in AD and capCAA cases. A severe loss of P-gp and BCRP is observable in Aβ-laden capillaries in capCAA cases compared to AD and controls.

ed by Aβ deposition. Expression of P-gp was occasionally detected in glial cells surrounding amyloid positive vessels, not in controls cases. In AD cases without capCAA the expression of P-gp in the capillary bed appeared unaltered (Fig. 1c), although we could observe some P-gp positive microglia in classical plaques.

BCRP showed a similar distribution pattern as P-gp in control cases, with strong immuno-reactivity in capillaries (Fig. 1d). We also observed a reduced expression of BCRP in capCAA cases, specifically in Aβ-laden vessels (Fig. 1e). No obvious changes were found in AD cases
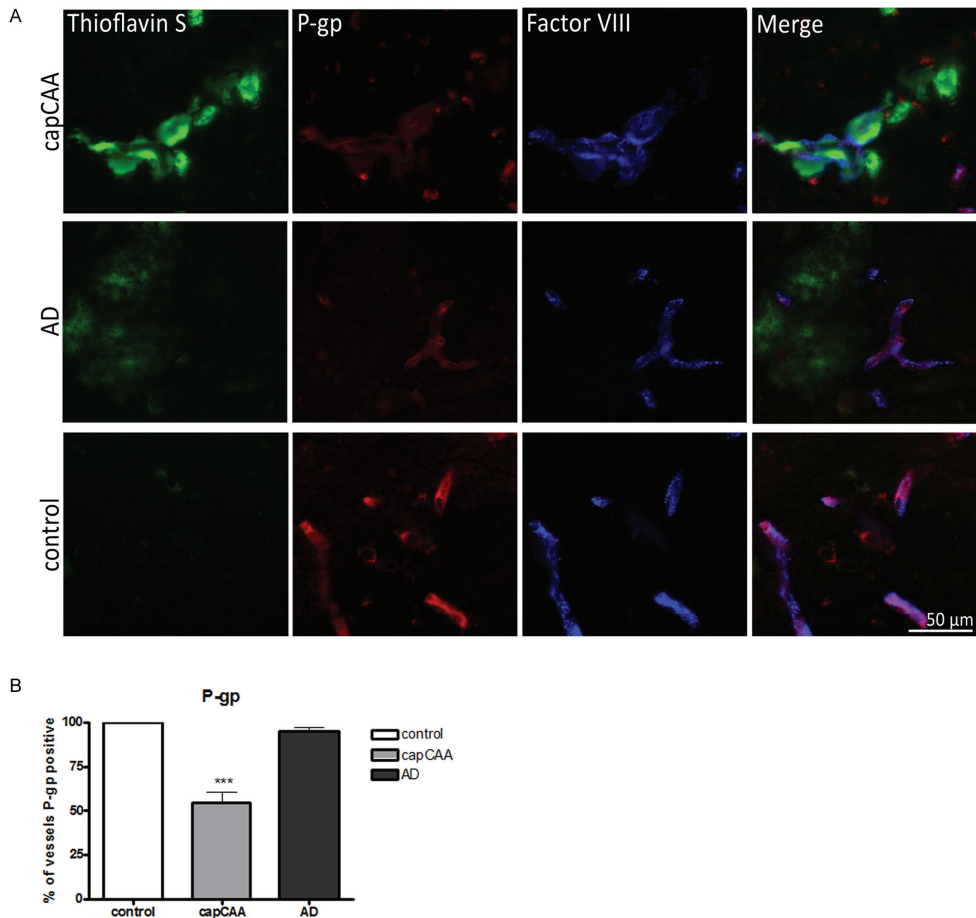
Figure 2. Loss of P-gp expression in capCAA: co-localization study and quantification. a) Triple immunofluorescence analysis confirmed loss of P-gp (red) in endothelial cells affected by Aβ deposition. Aβ was detected by Thioflavin S (green). Endothelial cells were detected by endothelial markers factor VIII-von Willebrand (blue). b) Quantification of P-gp expressing capillaries in capCAA, AD and control microvasculature is shown in the graph. Bars indicate the percentage of P-gp positive microvessels. ***p<0.001, by Student t test.

when compared to controls (Fig. 1f). No immunoreactivity for BCRP on glial cells could be detected.

To quantify the number of vessels positive for P-gp and BCRP, we performed a triple-staining for Aβ, P-gp/BCRP and the endothelial marker factor VIII (Fig. 2a and Fig. 3a). The total number of vessels per field was calculated based on the reactivity for factor VIII and did not significantly differ in the 3 groups.

The percentage of microvessels lacking P-gp expression was calculated showing that in the capCAA group 45.3±13.4% of the vessels lacked P-gp immunoreactivity (Fig. 2b). 75.3±17.7% of Aβ-positive microvessel lacked P-gp expression. P-gp negative microvessels all co-local-
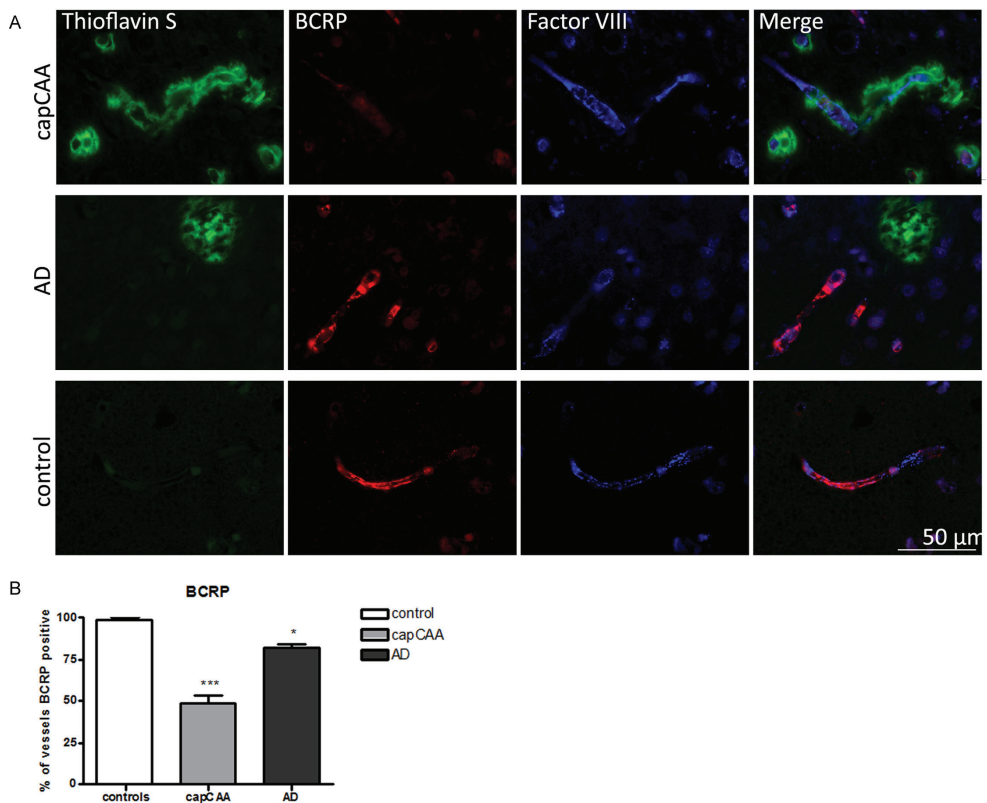
Figure 3. Loss of BCRP expression in capCAA and AD: co-localization study and quantification. a) Triple immunofluorescence analysis confirmed loss of BCRP (red) in endothelial cells affected by or in proximity of Aβ deposition. Aβ was detected by Thioflavin S (green). Endothelial cells were detected by endothelial markers factor VIII-von Willebrand (blue). b) Quantification of BCRP expressing microvessels in capCAA, AD and controls microvasculature is shown in the graph. Bars indicate the percentage of P-gp positive microvessels. *p<0.05, ***p<0.001, by Student t test.

ized with Aβ. In AD cases without capCAA P-gp staining of microvessels appeared to be of lower intensity, however no significant reduction was observed in the number of P-gp positive vessels in the AD group without capCAA compared to controls.

The number of BCRP-positive vessels was strongly reduced in capCAA cases, up to 50.8±12.9% of the total blood vessels, but no differences in staining intensity were observed. 77.4±15.5% of Aβ-positive microvessel lacked P-gp expression in capCAA cases. Upon quantification we could measure a reduction also in AD cases without capCAA, counting up to 18.1±6.1% BCRP negative vessels Fig. 3b).

Aβ effects on P-gp and BCRP gene expression

The observed reduction of P-gp and BCRP in the capillary endothelium of capCAA brain coincided with Aβ deposition, which suggests that Aβ may influence the expression of these transporters. To assess this, we analysed by means of quantitative real-time PCR, the expression of P-gp and BCRP by cultured human cerebral endothelial cells (hCMEC/D3) *in vitro* upon treatment (24 h) with either fibrils enriched or oligomers enriched Aβ40, or either fibril enriched or oligomer enriched Aβ42 preparations (100 nM). Of the 4 preparations tested, the oligomeric form of Aβ42 induced a significant downregulation (37.3±9.6%) in P-gp transcription levels (Fig. 4a) in line with the reduced expression observed by immunostaining in the human capCAA brains (Fig. 2b) . No changes in the transcription levels of BCRP mRNA could be observed in the brain endothelial cell culture after exposure to Aβ (Fig. 4b).

Clusterin alters Aβ effects on ABC transporters

The expression of clusterin is upregulated in AD brains and clusterin is also known as an amyloid associated protein localizing with Aβ plaques and CAA (McGeer, et al., 1994; Zhan, et al., 1994). We therefore studied the distribution of clusterin in the human AD brains with and without capCAA by immunostaining. Our immunohistological examination confirmed the high levels of clusterin in the AD and capCAA cases and the colocalization of clusterin with Aβ deposits, in parenchymal plaques as well as in areas with (capillary) CAA (Fig. 5).

Due to the strong interaction of clusterin and Aβ, we hypothesized that the first can modify the effects of the latter, especially when aggregated around the capillary endothelium. To test this, we exposed a monolayer of human brain endothelial cells to a mixture of Aβ and clusterin and measured the expression of P-gp and BCRP (Fig.6).
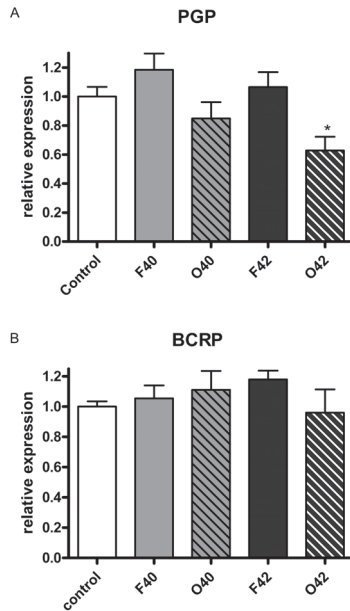
Figure 4. Aβ effects on P-gp and BCRP gene expression. P-gp (a) and BCRP (b) mRNA expression was assessed by q-PCR on hCMEC upon 24 h Aβ treatment. Cells were treated with fibrillar or oligomeric preparation of Aβ40 and Aβ42 at 100 nM. (F40: Fibrillar Aβ40; O40: oligomeric Aβ40; F42: fibrillar Aβ42; O42: oligomeric Aβ42). P-gp expression is reduced by Aβ42 oligomers. No effect on BCRP expression was observed. P-gp and BCRP expression was normalized to the expression of house-keeping gene GAPDH. Data were represented as the mean±SEM; n=at least three experiments with triplicate samples. *p<0.05, by Student t test.

Upon co-incubation with clusterin, Aβ fibrils and oligomers yielded similar results with respect to P-gp expression. Clusterin was found to predominantly affect the fibrillar Aβ preparations (of both Aβ40 and Aβ42) inducing a reduction in P-gp mRNA levels (36.8±0.12% and 46.8±0.14% respectively) when compared to Aβ treatment alone. On the other hand, the oligomeric Aβ-clusterin preparations did not significantly differ from oligomeric Aβ alone in their ability to affect P-gp expression.

In these conditions, a significant reduction in P-gp expression was observed when cells were treated with 100 nM fibrillar Aβ42 (41±0.5%) or oligomeric Aβ42 (37±0.7%) in the presence of 10 nM clusterin. Clusterin alone did not induce significant changes in P-gp mRNA levels (Fig. 6a). Importantly, using the same set-up, no changes were observed in BCRP mRNA expression levels (Fig. 6b). Used treatments did not affect the cell viability as determined by MTT assay (data not shown).
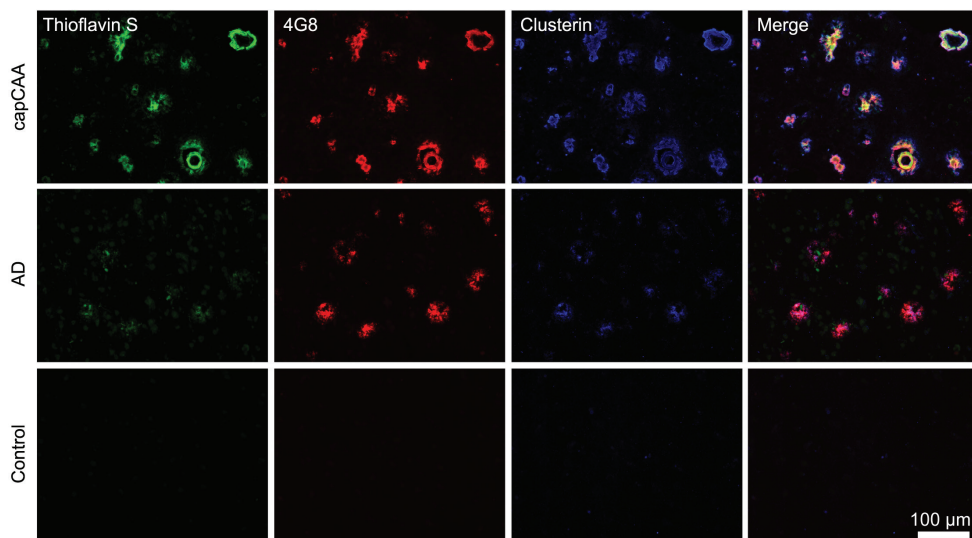
Figure 5. Clusterin expression in capCAA, AD and control brain tissue. Expression of clusterin was detected by triple immunofluorescence analysis. Aβ was detected by Thioflavin S (green) and anti- Aβ antibody 4G8 (red). No Aβ or clusterin was detected in control tissue. Clusterin (blue) is strongly expressed in and around Aβ-laden capillaries and Aβ plaques. Merge shows colocalization of Aβ and clusterin in capCAA and AD cases.

EM characterization of Aβ preparations

The characterization of the Aβ preparations by electron microscopy (EM) confirmed the difference in aggregation state between fibrils and oligomers (Fig. 7). Aβ fibrils clearly exhibited thread-like fibrillar structures whereas the oligomeric preparations showed smaller and amorphous aggregates of various sizes. There was no difference in appearance between Aβ40 and Aβ42, although Aβ40 fibrils seemed longer and less complex than Aβ42 fibrils.

Clusterin and clusterin-Aβ preparations were also analysed by EM. Clusterin appeared as electron dense globular aggregates associated in amorphous larger complexes. When co-incubated with clusterin, the appearance of Aβ preparations changed drastically, as the oligomeric and fibrillar preparation appeared identical to each other as judged by EM. There was no remnant of the fibrillar structure of neither the fibrils, nor the aggregates visible in the oligomeric preparations. Clusterin/Aβ complexes were large and homogeneously strongly electron dense, characterized by a somehow random organization of small compact globular units (Fig. 7).
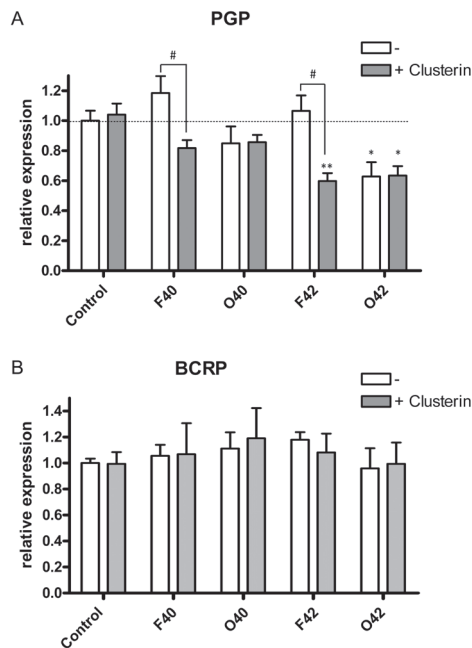
Figure 6. Clusterin alters Aβ effects on ABC transporters. P-gp (a) and Bcrp (b) mRNA expression was assessed by q-PCR on hCMEC upon 24 h 100 μM Aβ treatment in the presence of clusterin. Fibrillar and oligomeric preparations of Aβ40 and Aβ42 were incubated for 1h with 10 μM clusterin at room temperature prior to cell treatment. (F40: Fibrillar Aβ40; O40: oligomeric Aβ40; F42: fibrillar Aβ42; O42: oligomeric Aβ42). Transporter expression was normalized to the expression of house-keeping gene GAPDH. Clusterin altered the effects of the fibrillar, but not the oligomeric preparations, on P-gp expression. No effects on BCRP expression were detected. Data were represented as the mean±SEM, n=at least three. *$p < 0.05$, **$p < 0.005$ compared with vehicle treated endothelial cells; #$p < 0.05$ compared Aβ preparations with and without clusterin, by twoway ANOVA followed by post hoc Bonferroni test.
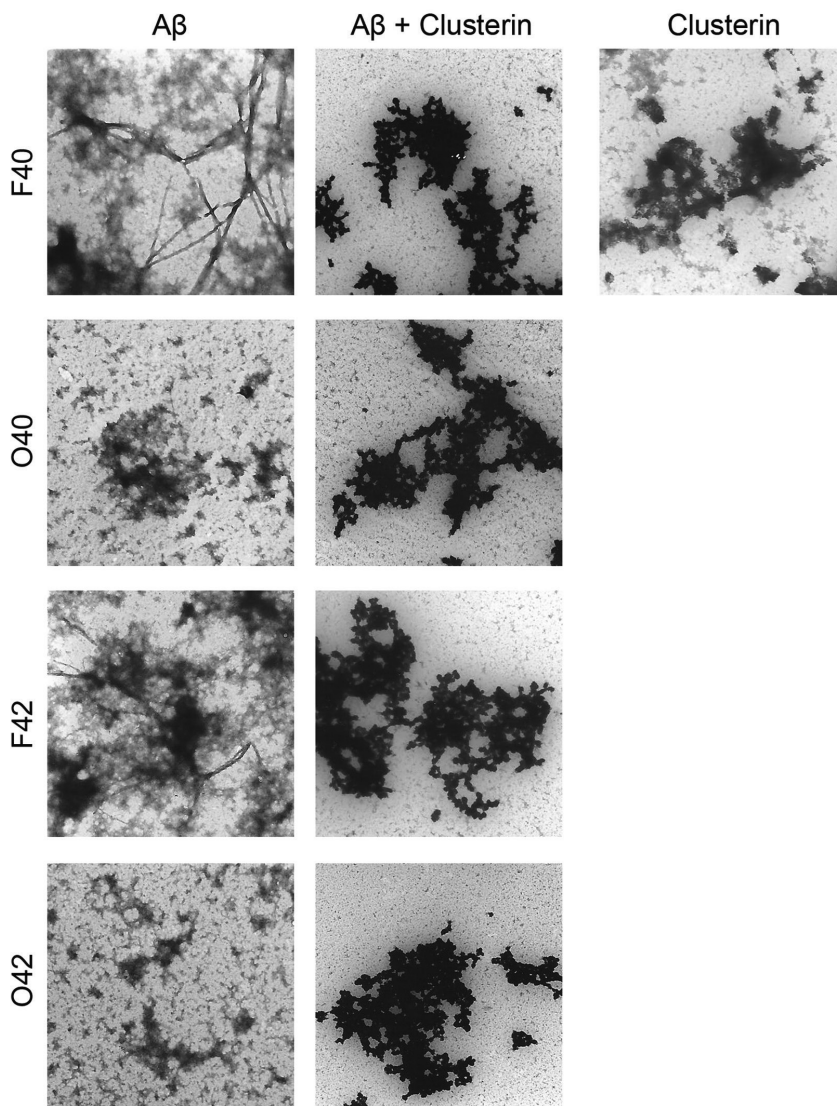
Figure 7. Electron microscopy characterization of Aβ preparations. Figure shows electron micrographs of fibrillar and oligomeric Aβ preparations individually or in combination with clusterin. Preparations were incubated 24 h followed by a further incubation of 1h with or without clusterin prior to being added to the cell cultures. (F40: Fibrillar Aβ40; O40: oligomeric Aβ40; F42: fibrillar Aβ42; O42: oligomeric Aβ42).

Discussion

In this study we have shown that the expression of ABC transporters P-gp and BCRP is severely decreased in capCAA cases compared to AD cases lacking microvascular amyloid deposits. *In vitro* treatment with the oligomeric form of Aβ42 specifically induces a reduction in P-gp expression, not BCRP expression, in cultured human brain endothelial cells. Furthermore, the presence of clusterin, which is highly expressed in capCAA affected vessels, strongly affects Aβ-mediated effects on P-gp, modifying the aggregation state of Aβ and inducing an oligomeric-like reduction in P-gp expression.

In our study we observed a selective loss of P-gp expression of in the microvasculature of cases with established capCAA compared to AD cases without amyloid-laden microvessels. P-gp, a transmembrane protein of 170 kDa, is thought to have a pivotal role in the clearance of Aβ from the brain and it has been shown to mediate the transport of Aβ in *in vitro* cell cultures (Kuhnke, et al., 2007; Lam, et al., 2001) and *in vivo* in AD mouse models (Cirrito, et al., 2005; Hartz, et al., 2010). We here are the first to report reduced expression of the ABC transporters P-gp and BCRP in cases with established capCAA using immunohistochemistry on *post-mortem* tissue. Several groups have analysed the expression of P-gp in models of AD. In hAPP mice, P-gp expression and function was profoundly reduced and re-instating its function restored the levels of amyloid in the brain of treated animals (Hartz, et al., 2010). Moreover, in a human cohort of non-demented elderly a reduced expression of P-gp was correlated with the extent of amyloid plaques (Vogelgesang, et al., 2002) and with vascular amyloid (Vogelgesang, et al., 2004). Diminished expression of P-gp has also been demonstrated in confirmed AD cases and correlated to vascular amyloid deposits (Jeynes and Provias, 2011; Wijesuriya, et al., 2010). In a recent *in vivo* study decreased P-gp function was measured in AD patients by positron emission tomography (PET) (van Assema, et al., 2012). Together, these data indicate that P-gp may have a role in the pathogenesis of AD. Our current findings confirm and extend this hypothesis that low capillary P-gp expression is specifically related to capCAA and not parenchymal Aβ deposition as we did not observe significant changes in P-gp expression in AD without microvascular amyloid deposits.

We show here a severe reduction in BCRP expression in Aβ-laden capillaries and we are the first to report a decrease in BCRP expression not only in capCAA, but also to a lesser extent

in AD without microvascular Aβ deposits. To date, there are conflicting reports in literature on the role of BCRP as an Aβ transporter and its involvement in AD pathogenesis is unclear. BCRP has been shown to transport Aβ40 in murine and human endothelial cell systems (Tai, et al., 2009; Xiong, et al., 2009) while others reported no effect on Aβ transport (Hartz, et al., 2010; Krohn, et al., 2011). It has been shown that the expression of BCRP is unaltered in AD cases (Wijesuriya 2010) or even upregulated (Xiong 2010). Such differences are probably due to different techniques. In the study of Xiong and coworkers BCRP expression was measured by microarray analysis using RNA extracted from brain tissue. This provides an assessment of BCRP levels in the brain, and in all the different brain cell populations, and not specifically in the microvasculature. Wijesuriya et al. analyzed BCRP expression in hippocampal blood vessels of AD by immunohistochemistry and did not observe any significant changes compared to controls. In our study we found a slight decrease in vascular BCRP expression in the occipital cortex of AD cases, and a more striking loss in capCAA. Therefore regional differences might exist in the brain expression of BCRP and the occipital area, which is also the preferential site for capCAA, could represent a hot spot in the brain particularly susceptible to vascular changes.

In our approach we have considered capCAA and AD without microvascular pathology as separate entities. Despite the overlap of the pathological conditions, half of AD cases do not show Aβ deposition at the capillaries (Thal, et al., 2008a) and it appears that the downstream effects on the function of the BBB differs. It is conceivable that the altered expression of the ABC transporters P-gp and BCRP that we have observed specifically in capCAA is secondary to amyloid deposition in affected capillaries. We here provide evidence that Aβ induces a downregulation of brain endothelial P-gp *in vitro*, although is it not excludible that an initial reduction in P-gp and/or BCRP is responsible for an initial impaired clearance of Aβ from the brain, which ultimately causes amyloid accumulation in microvasculature. In turn, impaired P-gp and BCRP expression may become more profound in later stages due to the amyloid deposition itself. This last hypothesis is supported by the fact that we observed a significantly lower expression of P-gp in capCAA cases, even in non-Aβ-affected vessels, compared to controls and AD. Whether reduced P-gp and BCRP expression in capCAA is a primary or secondary effect can, however, not be concluded from *post-mortem* immunohistochemical studies, as high cerebral concentrations of diffusible amyloid in the severe capCAA cases

might affect the status of the endothelium, even in the absence of local insoluble deposits.

Changes in P-gp and BCRP expression in capCAA can be attributed to the inflammatory processes around Aβ-laden vasculature. P-gp and BCRP are regulated by pro-inflammatory cytokines (IL-6, TNF-alpha, IL-1 beta) (Miller, 2010) or under inflammatory conditions (Kooij, et al., 2011). Activated glial cells, surrounding microvessels (Bruinsma, et al., 2012; Carrano, et al., 2011a; Carrano, et al., 2011c; Richard, et al., 2010), secrete high levels of pro-inflammatory cytokines when challenged with Aβ, especially in combination with clusterin (Mulder, et al., 2012; Nielsen, et al., 2011) and could have a detrimental effect on P-gp and BCRP expression.

Although we could mimic reduced expression of P-gp *in vitro* upon Aβ treatment in human cerebral microvascular endothelial cells (hcMEC), we did not observe changes in BCRP expression. This is probably due to the fact that Aβ does not trigger a massive release of cytokines in hcMEC at the conditions we tested (Poller, et al., 2010), which might be necessary to downregulate BCRP.

The observed P-gp decreased expression in our *in vitro* system might be associated with the induction of the NADPH oxidase complex by amyloid treatment (Carrano, et al., 2011b) as it has recently been shown that NADPH oxidase activation in endotoxin-activated microglia lower the function of P-gp (Matsumoto, et al., 2012). We previously demonstrated that pre-aggregated fibrillar Aβ induces NADPH oxidase-driven release of reactive oxygen species in hcMEC via binding to RAGE (Carrano, et al., 2011b) and we hypothesise that RAGE might be involved also in the downregulation of P-gp, but further investigation is needed in order to clarify this point.

We showed here that clusterin is present at high concentrations in capCAA brains and strictly colocalized with vascular amyloid deposits. Recent genome-wide association studies repeatedly identified clusterin as a genetic risk factor for sporadic AD (Harold, et al., 2009; Lambert, et al., 2009). Clusterin also binds to and facilitates the transport of Aβ across the BBB through binding to low-density lipoprotein receptor-related protein 2 (LRP2) (Calero, et al., 2000) (Bell, et al., 2007) (Zlokovic, 2008). When the ratio Aβ:clusterin is in favour of Aβ, as in the conditions we tested, clusterin is incorporated in the Aβ aggregates. *In vitro* we found that clusterin interaction with Aβ aggregates not only is able to change the aggregation state of the

amyloid species, but by doing so it also alters the effects of fibrillar Aβ42 on P-gp expression. In our system the binding of clusterin to Aβ fibrils changed the latter to complexes with *in vitro* effects similar to the oligomeric Aβ alone or oligomeric Aβ complexed with clusterin. On the other hand, no functional change was observed when we co-incubated Aβ oligomers with clusterin. Possibly this is due to the fact that clusterin disassembles Aβ fibrils into smaller particles with properties similar to the oligomers (Oda, et al., 1995). The effects evoked by clusterin might be either 1) conformational dependent: the binding to clusterin exposes one or multiple epitopes interacting with the endothelial cell surface; or 2) size dependent: the new generated small aggregates can be transported through the BBB. Both, either together or independently, might trigger a cascade of events leading to a change in P-gp expression.

In the light of our findings the reduced expression of the ABC transporters in AD and specifically in capCAA cases, might have relevant clinical implications. Several patient studies have suggested that humans with P-gp polymorphisms, or those receiving P-gp inhibitors, exhibit different pharmacological responses or even neurotoxicity in response to the administration of several drugs, such as loperamide, chemotherapeutics, antidepressants and antiepileptics when compared with control subjects (Greenberg, et al., 2005; Loscher, 2007; Sadeque, et al., 2000; Uhr, et al., 2008).

Vice versa, the selective loss of the function of P-gp may also have a beneficial effect by promoting the entry of therapeutics into brain. Some antiepileptics, most of which induce multidrug resistance, might be part of such a category, as very recently it has been found that the antiepileptic drug levetiracetam ameliorates memory performance in mild cognitive impairment cases and AD mouse model (Bakker, et al., 2012; Sanchez, et al., 2012).

Therefore assessing *in vivo* P-gp function by PET in AD and capCAA patients could be useful in the clinical practice as therapeutic intervention outcomes can differ in cases with altered BBB profile. Furthermore and most importantly, as we have shown that a significant difference exists in P-gp expression between capCAA and AD, P-gp function assessed by PET could therefore be used as a diagnostic biomarker to clinically discriminate capCAA from AD.

Similar implications may hold true for BCRP, although, to date no specific PET tracers are available to reliably determine BCRP function *in vivo* (Dorner, et al., 2011). Nonetheless,

BCRP remains an interesting target and the mechanisms involved in BCRP regulation and its role in the development of AD and capCAA need to be further elucidated.

Our data suggest that P-gp expression is the key ABC transporter affected in capCAA. We therefore hypothesize that alterations of P-gp at the cerebral capillaries are key to and specific for capCAA mediated disease progression and that loss of P-gp activity may serve as a selective marker for capCAA. The identification of underlying mechanisms of observed alterations of P-gp at the cerebral microvasculature in capCAA may hold the key for novel intervention strategies to limit Aβ accumulation within the brain thus preventing cognitive decline and concomitant neurodegeneration.

Disclosure Statement

There is no actual or potential conflict of interest for any author concerning this manuscript.

References

Attems, J. 2005. Sporadic cerebral amyloid angiopathy: pathology, clinical implications, and possible pathomechanisms. *Acta Neuropathol* 110(4), 345-59.

Bakker, A., Krauss, G.L., Albert, M.S., Speck, C.L., Jones, L.R., Stark, C.E., Yassa, M.A., Bassett, S.S., Shelton, A.L., Gallagher, M. 2012. Reduction of hippocampal hyperactivity improves cognition in amnestic mild cognitive impairment. *Neuron* 74(3), 467-74.

Bell, R.D., Sagare, A.P., Friedman, A.E., Bedi, G.S., Holtzman, D.M., Deane, R., Zlokovic, B.V. 2007. Transport pathways for clearance of human Alzheimer's amyloid beta-peptide and apolipoproteins E and J in the mouse central nervous system. *J Cereb Blood Flow Metab* 27(5), 909-18.

Braak, H., Alafuzoff, I., Arzberger, T., Kretzschmar, H., Del Tredici, K. 2006. Staging of Alzheimer disease-associated neurofibrillary pathology using paraffin sections and immunocytochemistry. *Acta Neuropathol* 112(4), 389-404.

Braak, H., Braak, E. 1991. Neuropathological stageing of Alzheimer-related changes. *Acta Neuropathol* 82(4), 239-59.

Bruinsma, I.B., de Jager, M., Carrano, A., Versleijen, A.A., Veerhuis, R., Boelens, W., Rozemuller, A.J., de Waal, R.M., Verbeek, M.M. 2012. Small heat shock proteins induce a cerebral inflammatory reaction. *J Neurosci* 31(33), 11992-2000.

Calero, M., Rostagno, A., Matsubara, E., Zlokovic, B., Frangione, B., Ghiso, J. 2000. Apolipoprotein J (clusterin) and Alzheimer's disease. *Microsc Res Tech* 50(4), 305-15.

Carrano, A., Hoozemans, J.J., van der Vies, S.M., Rozemuller, A.J., van Horssen, J., de Vries, H.E. 2011a. Amyloid Beta induces oxidative stress-mediated blood-brain barrier changes in capillary amyloid angiopathy. *Antioxid Redox Signal* 15(5), 1167-78.

Carrano, A., Hoozemans, J.J., van der Vies, S.M., Rozemuller, A.J., van Horssen, J., de Vries, H.E. 2011b. Amyloid beta Induces Oxidative Stress-Mediated Blood-Brain Barrier Changes in Capillary Amyloid Angiopathy. *Antioxid Redox Signal*.

Carrano, A., Hoozemans, J.J., van der Vies, S.M., van Horssen, J., de Vries, H.E., Rozemuller, A.J. 2011c. Neuroinflammation and Blood-Brain Barrier Changes in Capillary Amyloid Angiopathy. *Neurodegener Dis*.

Chafekar, S.M., Baas, F., Scheper, W. 2008. Oligomer-specific Abeta toxicity in cell models is mediated by selective uptake. *Biochim Biophys Acta* 1782(9), 523-31.

Cirrito, J.R., Deane, R., Fagan, A.M., Spinner, M.L., Parsadanian, M., Finn, M.B., Jiang, H.,

Prior, J.L., Sagare, A., Bales, K.R., Paul, S.M., Zlokovic, B.V., Piwnica-Worms, D., Holtzman, D.M. 2005. P-glycoprotein deficiency at the blood-brain barrier increases amyloid-beta deposition in an Alzheimer disease mouse model. *J Clin Invest* 115(11), 3285-90.

Dahlgren, K.N., Manelli, A.M., Stine, W.B., Jr., Baker, L.K., Krafft, G.A., LaDu, M.J. 2002. Oligomeric and fibrillar species of amyloid-beta peptides differentially affect neuronal viability. *J Biol Chem* 277(35), 32046-53.

Dorner, B., Kuntner, C., Bankstahl, J.P., Wanek, T., Bankstahl, M., Stanek, J., Mullauer, J., Bauer, F., Mairinger, S., Loscher, W., Miller, D.W., Chiba, P., Muller, M., Erker, T., Langer, O. 2011. Radiosynthesis and in vivo evaluation of 1-[18F]fluoroelacridar as a positron emission tomography tracer for P-glycoprotein and breast cancer resistance protein. *Bioorg Med Chem* 19(7), 2190-8.

Eurelings, L.S., Richard, E., Carrano, A., Eikelenboom, P., van Gool, W.A., Rozemuller, A.J. 2010. Dyshoric capillary cerebral amyloid angiopathy mimicking Creutzfeldt-Jakob disease. *J Neurol Sci* 295(1-2), 131-4.

Greenberg, M.L., Fisher, P.G., Freeman, C., Korones, D.N., Bernstein, M., Friedman, H., Blaney, S., Hershon, L., Zhou, T., Chen, Z., Kretschmar, C. 2005. Etoposide, vincristine, and cyclosporin A with standard-dose radiation therapy in newly diagnosed diffuse intrinsic brainstem gliomas: a pediatric oncology group phase I study. *Pediatr Blood Cancer* 45(5), 644-8.

Harold, D., Abraham, R., Hollingworth, P., Sims, R., Gerrish, A., Hamshere, M.L., Pahwa, J.S., Moskvina, V., Dowzell, K., Williams, A., Jones, N., Thomas, C., Stretton, A., Morgan, A.R., Lovestone, S., Powell, J., Proitsi, P., Lupton, M.K., Brayne, C., Rubinsztein, D.C., Gill, M., Lawlor, B., Lynch, A., Morgan, K., Brown, K.S., Passmore, P.A., Craig, D., McGuinness, B., Todd, S., Holmes, C., Mann, D., Smith, A.D., Love, S., Kehoe, P.G., Hardy, J., Mead, S., Fox, N., Rossor, M., Collinge, J., Maier, W., Jessen, F., Schurmann, B., van den Bussche, H., Heuser, I., Kornhuber, J., Wiltfang, J., Dichgans, M., Frolich, L., Hampel, H., Hull, M., Rujescu, D., Goate, A.M., Kauwe, J.S., Cruchaga, C., Nowotny, P., Morris, J.C., Mayo, K., Sleegers, K., Bettens, K., Engelborghs, S., De Deyn, P.P., Van Broeckhoven, C., Livingston, G., Bass, N.J., Gurling, H., McQuillin, A., Gwilliam, R., Deloukas, P., Al-Chalabi, A., Shaw, C.E., Tsolaki, M., Singleton, A.B., Guerreiro, R., Muhleisen, T.W., Nothen, M.M., Moebus, S., Jockel, K.H., Klopp, N., Wichmann, H.E., Carrasquillo, M.M., Pankratz, V.S., Younkin, S.G., Holmans, P.A., O'Donovan, M., Owen, M.J., Williams, J. 2009. Genome-wide association study identifies variants at CLU and PICALM associated with Alzheimer's disease. *Nat Genet* 41(10), 1088-93.

Hartz, A.M., Miller, D.S., Bauer, B. 2010. Restoring blood-brain barrier P-glycoprotein reduces brain amyloid-beta in a mouse model of Alzheimer's disease. *Mol Pharmacol*

77(5), 715-23.

Jeynes, B., Provias, J. 2011. An investigation into the role of P-glycoprotein in Alzheimer's disease lesion pathogenesis. *Neurosci Lett* 487(3), 389-93.

Kida, E., Choi-Miura, N.H., Wisniewski, K.E. 1995. Deposition of apolipoproteins E and J in senile plaques is topographically determined in both Alzheimer's disease and Down's syndrome brain. *Brain Res* 685(1-2), 211-6.

Kooij, G., Mizee, M.R., van Horssen, J., Reijerkerk, A., Witte, M.E., Drexhage, J.A., van der Pol, S.M., van Het Hof, B., Scheffer, G., Scheper, R., Dijkstra, C.D., van der Valk, P., de Vries, H.E. 2011. Adenosine triphosphate-binding cassette transporters mediate chemokine (C-C motif) ligand 2 secretion from reactive astrocytes: relevance to multiple sclerosis pathogenesis. *Brain* 134(Pt 2), 555-70.

Krijnen, P.A., Cillessen, S.A., Manoe, R., Muller, A., Visser, C.A., Meijer, C.J., Musters, R.J., Hack, C.E., Aarden, L.A., Niessen, H.W. 2005. Clusterin: a protective mediator for ischemic cardiomyocytes? *Am J Physiol Heart Circ Physiol* 289(5), H2193-202.

Krohn, M., Lange, C., Hofrichter, J., Scheffler, K., Stenzel, J., Steffen, J., Schumacher, T., Bruning, T., Plath, A.S., Alfen, F., Schmidt, A., Winter, F., Rateitschak, K., Wree, A., Gsponer, J., Walker, L.C., Pahnke, J. 2011. Cerebral amyloid-beta proteostasis is regulated by the membrane transport protein ABCC1 in mice. *J Clin Invest* 121(10), 3924-31.

Kuhnke, D., Jedlitschky, G., Grube, M., Krohn, M., Jucker, M., Mosyagin, I., Cascorbi, I., Walker, L.C., Kroemer, H.K., Warzok, R.W., Vogelgesang, S. 2007. MDR1-P-Glycoprotein (ABCB1) Mediates Transport of Alzheimer's amyloid-beta peptides--implications for the mechanisms of Abeta clearance at the blood-brain barrier. *Brain Pathol* 17(4), 347-53.

Lam, F.C., Liu, R., Lu, P., Shapiro, A.B., Renoir, J.M., Sharom, F.J., Reiner, P.B. 2001. beta-Amyloid efflux mediated by p-glycoprotein. *J Neurochem* 76(4), 1121-8.

Lambert, J.C., Heath, S., Even, G., Campion, D., Sleegers, K., Hiltunen, M., Combarros, O., Zelenika, D., Bullido, M.J., Tavernier, B., Letenneur, L., Bettens, K., Berr, C., Pasquier, F., Fievet, N., Barberger-Gateau, P., Engelborghs, S., De Deyn, P., Mateo, I., Franck, A., Helisalmi, S., Porcellini, E., Hanon, O., de Pancorbo, M.M., Lendon, C., Dufouil, C., Jaillard, C., Leveillard, T., Alvarez, V., Bosco, P., Mancuso, M., Panza, F., Nacmias, B., Bossu, P., Piccardi, P., Annoni, G., Seripa, D., Galimberti, D., Hannequin, D., Licastro, F., Soininen, H., Ritchie, K., Blanche, H., Dartigues, J.F., Tzourio, C., Gut, I., Van Broeckhoven, C., Alperovitch, A., Lathrop, M., Amouyel, P. 2009. Genome-wide association study identifies variants at CLU and CR1 associated with Alzheimer's disease. *Nat Genet* 41(10), 1094-9.

Loscher, W. 2007. Mechanisms of drug resistance in status epilepticus. *Epilepsia* 48 Suppl 8, 74-7.

Matsumoto, J., Dohgu, S., Takata, F., Nishioku, T., Sumi, N., Machida, T., Takahashi, H., Yamauchi, A., Kataoka, Y. 2012. Lipopolysaccharide-activated microglia lower P-glycoprotein function in brain microvascular endothelial cells. *Neurosci Lett* 524(1), 45-8.

McGeer, P.L., Klegeris, A., Walker, D.G., Yasuhara, O., McGeer, E.G. 1994. Pathological proteins in senile plaques. *Tohoku J Exp Med* 174(3), 269-77.

Miller, D.S. 2010. Regulation of P-glycoprotein and other ABC drug transporters at the blood-brain barrier. *Trends Pharmacol Sci* 31(6), 246-54.

Mirra, S.S., Heyman, A., McKeel, D., Sumi, S.M., Crain, B.J., Brownlee, L.M., Vogel, F.S., Hughes, J.P., van Belle, G., Berg, L. 1991. The Consortium to Establish a Registry for Alzheimer's Disease (CERAD). Part II. Standardization of the neuropathologic assessment of Alzheimer's disease. *Neurology* 41(4), 479-86.

Mulder, S.D., Veerhuis, R., Blankenstein, M.A., Nielsen, H.M. 2012. The effect of amyloid associated proteins on the expression of genes involved in amyloid-beta clearance by adult human astrocytes. *Exp Neurol* 233(1), 373-9.

Murphy, B.F., Kirszbaum, L., Walker, I.D., d'Apice, A.J. 1988. SP-40,40, a newly identified normal human serum protein found in the SC5b-9 complex of complement and in the immune deposits in glomerulonephritis. *J Clin Invest* 81(6), 1858-64.

Nielsen, H.M., Mulder, S.D., Belien, J.A., Musters, R.J., Eikelenboom, P., Veerhuis, R. 2011. Astrocytic A beta 1-42 uptake is determined by A beta-aggregation state and the presence of amyloid-associated proteins. *Glia* 58(10), 1235-46.

Nuutinen, T., Suuronen, T., Kauppinen, A., Salminen, A. 2009. Clusterin: a forgotten player in Alzheimer's disease. *Brain Res Rev* 61(2), 89-104.

Oda, T., Wals, P., Osterburg, H.H., Johnson, S.A., Pasinetti, G.M., Morgan, T.E., Rozovsky, I., Stine, W.B., Snyder, S.W., Holzman, T.F., et al. 1995. Clusterin (apoJ) alters the aggregation of amyloid beta-peptide (A beta 1-42) and forms slowly sedimenting A beta complexes that cause oxidative stress. *Exp Neurol* 136(1), 22-31.

Poller, B., Drewe, J., Krahenbuhl, S., Huwyler, J., Gutmann, H. 2010. Regulation of BCRP (ABCG2) and P-glycoprotein (ABCB1) by cytokines in a model of the human blood-brain barrier. *Cell Mol Neurobiol* 30(1), 63-70.

Richard, E., Carrano, A., Hoozemans, J.J., van Horssen, J., van Haastert, E.S., Eurelings, L.S., de Vries, H.E., Thal, D.R., Eikelenboom, P., van Gool, W.A., Rozemuller, A.J. 2010.

Characteristics of dyshoric capillary cerebral amyloid angiopathy. *J Neuropathol Exp Neurol* 69(11), 1158-67.

Sadeque, A.J., Wandel, C., He, H., Shah, S., Wood, A.J. 2000. Increased drug delivery to the brain by P-glycoprotein inhibition. *Clin Pharmacol Ther* 68(3), 231-7.

Sanchez, P.E., Zhu, L., Verret, L., Vossel, K.A., Orr, A.G., Cirrito, J.R., Devidze, N., Ho, K., Yu, G.Q., Palop, J.J., Mucke, L. 2012. Levetiracetam suppresses neuronal network dysfunction and reverses synaptic and cognitive deficits in an Alzheimer's disease model. *Proc Natl Acad Sci U S A* 109(42), E2895-903.

Tai, L.M., Loughlin, A.J., Male, D.K., Romero, I.A. 2009. P-glycoprotein and breast cancer resistance protein restrict apical-to-basolateral permeability of human brain endothelium to amyloid-beta. *J Cereb Blood Flow Metab* 29(6), 1079-83.

Thal, D.R., Ghebremedhin, E., Rub, U., Yamaguchi, H., Del Tredici, K., Braak, H. 2002. Two types of sporadic cerebral amyloid angiopathy. *J Neuropathol Exp Neurol* 61(3), 282-93.

Thal, D.R., Griffin, W.S., Braak, H. 2008a. Parenchymal and vascular Abeta-deposition and its effects on the degeneration of neurons and cognition in Alzheimer's disease. *J Cell Mol Med* 12(5B), 1848-62.

Thal, D.R., Griffin, W.S., de Vos, R.A., Ghebremedhin, E. 2008b. Cerebral amyloid angiopathy and its relationship to Alzheimer's disease. *Acta Neuropathol* 115(6), 599-609.

Uhr, M., Tontsch, A., Namendorf, C., Ripke, S., Lucae, S., Ising, M., Dose, T., Ebinger, M., Rosenhagen, M., Kohli, M., Kloiber, S., Salyakina, D., Bettecken, T., Specht, M., Putz, B., Binder, E.B., Muller-Myhsok, B., Holsboer, F. 2008. Polymorphisms in the drug transporter gene ABCB1 predict antidepressant treatment response in depression. *Neuron* 57(2), 203-9.

van Assema, D.M., Lubberink, M., Bauer, M., van der Flier, W.M., Schuit, R.C., Windhorst, A.D., Comans, E.F., Hoetjes, N.J., Tolboom, N., Langer, O., Muller, M., Scheltens, P., Lammertsma, A.A., van Berckel, B.N. 2012. Blood-brain barrier P-glycoprotein function in Alzheimer's disease. *Brain* 135(Pt 1), 181-9.

van Horssen, J., de Jong, D., de Waal, R.M., Maass, C., Otte-Holler, I., Kremer, B., Verbeek, M.M., Wesseling, P. 2005. Cerebral amyloid angiopathy with severe secondary vascular pathology: a histopathological study. *Dement Geriatr Cogn Disord* 20(5), 321-30.

Veerhuis, R., Boshuizen, R.S., Familian, A. 2005. Amyloid associated proteins in Alzheimer's and prion disease. *Curr Drug Targets CNS Neurol Disord* 4(3), 235-48.

Vogelgesang, S., Cascorbi, I., Schroeder, E., Pahnke, J., Kroemer, H.K., Siegmund, W., Kunert-Keil, C., Walker, L.C., Warzok, R.W. 2002. Deposition of Alzheimer's beta-amyloid is inversely correlated with P-glycoprotein expression in the brains of elderly non-demented humans. *Pharmacogenetics* 12(7), 535-41.

Vogelgesang, S., Warzok, R.W., Cascorbi, I., Kunert-Keil, C., Schroeder, E., Kroemer, H.K., Siegmund, W., Walker, L.C., Pahnke, J. 2004. The role of P-glycoprotein in cerebral amyloid angiopathy; implications for the early pathogenesis of Alzheimer's disease. *Curr Alzheimer Res* 1(2), 121-5.

Weksler, B.B., Subileau, E.A., Perriere, N., Charneau, P., Holloway, K., Leveque, M., Tricoire-Leignel, H., Nicotra, A., Bourdoulous, S., Turowski, P., Male, D.K., Roux, F., Greenwood, J., Romero, I.A., Couraud, P.O. 2005. Blood-brain barrier-specific properties of a human adult brain endothelial cell line. *FASEB J* 19(13), 1872-4.

Weller, R.O., Subash, M., Preston, S.D., Mazanti, I., Carare, R.O. 2008. Perivascular drainage of amyloid-beta peptides from the brain and its failure in cerebral amyloid angiopathy and Alzheimer's disease. *Brain Pathol* 18(2), 253-66.

Wijesuriya, H.C., Bullock, J.Y., Faull, R.L., Hladky, S.B., Barrand, M.A. 2010. ABC efflux transporters in brain vasculature of Alzheimer's subjects. *Brain Res* 1358, 228-38.

Wolf, A., Bauer, B., Hartz, A.M. 2012. ABC Transporters and the Alzheimer's Disease Enigma. *Front Psychiatry* 3, 54.

Xiong, H., Callaghan, D., Jones, A., Bai, J., Rasquinha, I., Smith, C., Pei, K., Walker, D., Lue, L.F., Stanimirovic, D., Zhang, W. 2009. ABCG2 is upregulated in Alzheimer's brain with cerebral amyloid angiopathy and may act as a gatekeeper at the blood-brain barrier for Abeta(1-40) peptides. *J Neurosci* 29(17), 5463-75.

Zhan, S.-S., Veerhuis, R., Janssen, I., Kamphorst, W., Eikelenboom, P. 1994. Immunohistochemical distribution of the inhibitors of the terminal complement complex in Alzheimer's disease. *Neurodegeneration* 3, 111-7.

Zlokovic, B.V. 2008. The blood-brain barrier in health and chronic neurodegenerative disorders. *Neuron* 57(2), 178-201.

Zlokovic, B.V. 2011. Neurovascular pathways to neurodegeneration in Alzheimer's disease and other disorders. *Nat Rev Neurosci* 12(12), 723-38.

4

part

General discussion

6

chapter

Discussion

Anna Carrano

Summary and discussion

capCAA and AD

Amyloid β protein deposition in the walls of capillaries is a subtype of cerebral amyloid angiopathy (CAA) referred to as capillary CAA (capCAA). CapCAA is a neuropathological feature present in 51% of AD cases (Thal, et al., 2008). Patients with capCAA can also present with rapidly progressive dementia disease or can have a diagnosis of vascular disease. We have selected cases with prominent capCAA pathology, in which vascular Aβ is the main form of amyloid deposition. The presence of extensive capCAA distinguishes a subgroup of AD cases showing few or no parenchymal plaques, the characteristics of which are studied and described in this thesis.

Identification of differentially expressed proteins in clinical cases that present capCAA pathology could reveal specific insight in the underlying molecular mechanism resulting in the disturbed clearance of Aβ across the BBB as well as specific biomarkers for capCAA.

For the aim of this thesis the following main goals were formulated:

- Describe the neuropathological characteristics of capCAA, common features and differences with classic AD.
- Assess BBB changes in capCAA and underlying pathological pathways.

Spatial localization of Aβ isoforms: Aβ40 and Aβ42

In chapter 2 we described the main histopathological features of capCAA comparing it with CAA in larger blood vessels (from now on referred to as CAA) and with the common hallmarks of AD (Richard, et al., 2010). Hereto, we histopathologically analyzed a unique cohort of severe capCAA cases. Interestingly, we observed major differences between capCAA and CAA. Firstly, capCAA is more often accompanied by dyshoric changes, i.e. extrusion of Aβ fibrils that radiate from the vessel wall into the brain parenchyma, compared to CAA. Such changes may occur in two distinct forms: bulb-like dense deposits sitting on the capillary walls and flame-like Aβ aggregates spreading from the capillaries into the neuropil. Upon studying the composition of the amyloid deposits in capCAA we could demonstrate that both

the main Aβ isoforms, Aβ40 and Aβ42, are present in capCAA. Specifically, we showed that Aβ42 is the main component of the dense bulb-like deposits adjacent to the capillary wall, while Aβ40 accumulation was predominantly found in the flame-like deposits. These features are significantly different from what has been observed in CAA-affected vessels in AD. In CAA the main isoform present is Aβ40, which is mostly localized within the vessel walls of arteries and leptomeningeal vessels. In CAA Aβ intercalates between smooth muscle cells and the tunica media and adventitia of small and mid-sized arteries. Capillaries lack such a structural organization (i.e. several concentric layers) in which Aβ can accumulate, therefore when the amyloid starts aggregating around the capillaries it cannot be trapped within the vessel walls and naturally spreads into the surrounding neuropil. The bulb-like deposits of Aβ42 that we described are likely to be the seeding focal points where Aβ aggregation starts, as it is known that Aβ42 is highly fibrillogenic and a seed of Aβ42 exponentially increases and speeds up fibril formation *in vitro* and *in vivo* (Lehner, et al., 2011). The peculiar deposition pattern seen in capCAA is also different from what is seen in the classical plaques of AD patients. The bulb-like and flame-like deposits remarkably resemble classical plaques, especially when they are combined and occur in the same location, with the dense bulb resembling the globular amyloid core of the plaque and the flames the halo of the plaque. In the absence of an isotype specific staining, capCAA with such characteristics can be easily mistaken for a plaque residing next to a capillary. Despite these morphological similarities, the core of classical plaques is mainly composed of Aβ40, versus the capCAA bulbs being Aβ42, and the diffuse halo is predominantly composed of Aβ42, versus the capCAA flames being Aβ40. This clearly shows that plaques and capCAA are two distinct phenomena, which are likely the result of different pathological pathways involved in Aβ aggregation and clearance. Importantly, the occurrence of plaques and capCAA are inversely correlated, meaning that areas of the brain densely affected by capCAA deposits show less plaque burden. This might implicate that the local microenvironment influences Aβ depositing either as plaque or capCAA, suggesting that capCAA occurs in those areas where Aβ flows toward the circulation in the attempt of being cleared from the brain. Amyloid driven pathogenesis/hypothesis of AD was first described by our own group with Masters and Beyreuther in 1989 (Rozemuller, et al., 1989), but what is the mechanism directing the aggregation of Aβ either toward the parenchymal compartment or the vascular one? It has been shown that in mouse models the ratio of Aβ40:Aβ42 is a critical factor that influences the formation of CAA or plaques. In the

presence of a high Aβ40:Aβ42 ratio, the formation of CAA is favored. Increasing the concentrations of both Aβ40 and Aβ42, maintaining the ratio in favor of Aβ40, induces the formation of both plaques and CAA. On the other hand, when Aβ42 is the main amyloid isoform, only plaques are formed (Oppenheim, 1909). It has also been demonstrated that the ApoE genotype can modify the ratio Aβ40:Aβ42 in transgenic AD mice. ApoE4, the most important risk factor for capCAA and AD, increases the ratio Aβ40:Aβ42 and, by doing so, switches the deposition of Aβ from the parenchyma to the vasculature compartment (Divry, 1927). ApoE is able to influence Aβ aggregation and alters both transport and clearance of soluble Aβ in the brain. ApoE isoforms do not differentially influence Aβ production *in vivo*; however, ApoE isoforms differentially affect Aβ clearance before Aβ deposition, with ApoE4 resulting in clearance that is slower than ApoE3 and ApoE2 (Glenner and Wong, 1984b).

In human capCAA cases the brain ratio Aβ40:Aβ42 is higher than in AD and the frequency of ApoE4 alleles is higher as well. It would be tempting to speculate that ApoE4 is the culprit, but it is not that simple. Although ApoE4 has a strong association with developing capCAA and also correlates with capCAA severity, having one or two ApoE4 alleles is neither sufficient nor necessary for developing capCAA. Other factors are likely being involved and contribute to the modulation of Aβ clearance and aggregation.
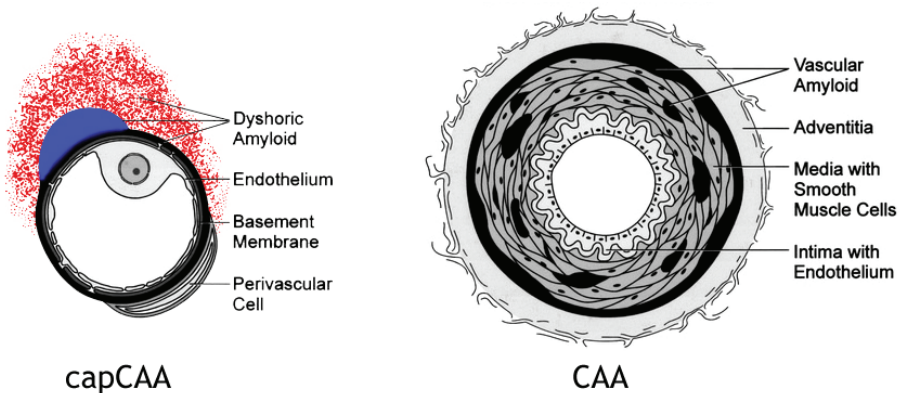
Figure 1. Schematic representation of Aβ deposition in capCAA and CAA. Dyshoric Aβ accumulates as dense bulb-like deposits (blue) and flame deposits (red) in capCAA microvessels. Flames and bulbs are often lacking in large vessels CAA, where Aβ (black) predominantly accumulates between smooth muscle cells layers and tunica media and adventitia.

Amyloid associated proteins

Next to Aβ and ApoE, virtually all vascular and parenchymal Aβ depositions contain several inflammation-related proteins (Akiyama, et al., 2000; Eikelenboom and Stam, 1982; Eikelenboom and Veerhuis, 1996). These so-called Aβ-associated proteins (AAP) include clusterin, complement proteins, serum amyloid P component (SAP), α1-antichymotrypsin (ACT), ICAM-1, α2-macroglobulin, small heat shock proteins (sHSP) and heparan sulphate proteoglycans. These proteins play a role in the transport, fibrillogenesis, deposition and toxicity of Aβ and they are also important for the sequestration of neurotoxic Aβ species in plaques or CAA. Normally most AAPs are produced at low levels in the brain, however their synthesis rate increases in AD, following Aβ deposition (Eikelenboom and Stam, 1982; Greenberg, et al., 2008). Due to the involvement of AAPs in determining Aβ aggregation and transport, we have investigated their expression in capCAA cases. We have specifically shown that clusterin, laminin, complement proteins and SAP expression are strongly increased in capCAA. This increased expression was more striking in capCAA-affected vessels compared to what we observed around senile plaques, and clusterin, laminin, complement proteins and SAP strictly colocalized with fibrillar capillary amyloid deposits (chapter 3).

Besides ApoE, recent genome-wide association studies repeatedly identified clusterin as a genetic risk factor for sporadic late-onset AD (Harold, et al., 2009; Lambert, et al., 2009). Clusterin is associated with amyloid plaques, but we showed in chapter 3 and chapter 5 that its expression is significantly higher in capCAA. Similar to ApoE, clusterin is a glycoprotein involved in the clearance of Aβ peptides and fibrils by binding to low-density lipoprotein receptor-related protein 2 (LRP2) (Bell, et al., 2007; Calero, et al., 2000; Zlokovic, 2008) and enhancing endocytosis of fibrils by glial cells. The binding of clusterin to Aβ should promote Aβ clearance and thus overexpression of clusterin could be a cellular defense mechanism aimed at reducing Aβ levels in the capCAA brain. On the other hand, it has been demonstrated that the presence of clusterin can alter the aggregation of the amyloid leading to the formation of slowly sedimenting, non fibrillar Aβ complexes that are toxic to neurons (Bibl, et al., 2008; Goos, et al., 2009) and endothelial cells (chapter 5). Furthermore, an AD mouse model crossed with clusterin knockouts deposits fewer Aβ fibrils and have healthier neurites than those with clusterin, suggesting the protein exacerbates pathology (DeMattos, et al., 2002). The effect of clusterin may depend on the relative ratio of the protein to Aβ; small

amounts of clusterin may stabilize oligomers, but not completely encase them, allowing the molecules to exert toxic effects.

Clusterin can also inhibit the activation of the complement system. This is an important property since several studies have demonstrated that protein aggregates, such as Aβ, can activate the complement system and provoke inflammatory responses in AD (Vinters, et al., 1996). Although clusterin is highly expressed in and around capCAA-affected vessels, it is apparently not able to regulate complement activation. Histochemical studies have revealed that in capCAA and CAA the complement system is activated and amyloid deposits contain several complement factors, e.g. C1q protein, and the membrane attack complex C5b-9 (chapter 3) (Eikelenboom and Stam, 1982; Eikelenboom and Veerhuis, 1996).

So it seems that the putative protective effects of clusterin fail in capCAA, where not only we observe a tremendous deposition of fibrillar Aβ, but also a severe inflammatory response, including activation of the complement system.

Inflammatory response in capCAA

Neuroinflammation seems to be a common response associated with capCAA and plaques as clusters of activated glial cells are observed in close proximity to capCAA-affected vessels and classic senile plaques. The inflammatory reaction associated with Aβ deposits is thought to play a role in the pathogenesis of AD and contributes to the symptoms of cognitive decline (Arends, et al., 2000; Rozemuller, et al., 2005). Interestingly, it appears that microglia and astrocytes are highly activated around amyloid-laden capillaries, while in large CAA-affected vessels, in the absence of dyshoric changes, we only observed reactive astrocytes, no activated microglia. Activation of glial cells is mainly related to the presence of dyshoric Aβ deposits in capCAA. These deposits induce recruitment and activation of microglia cells around the affected blood vessels, in contrast with the mild glial response observed around vessels with dense and compact globular Aβ deposits (chapter 2).

A similar pattern was observed when we analyzed the distribution of hyperphosphorylated tau and ubiquitin, which accumulate in dystrophic neurites. In all cases the parenchyma surrounding capCAA contains numerous dystrophic neurites showing similarities with the disturbances occurring around classical plaques in AD. Remarkably, dystrophic neurites are rarely seen in close proximity to large Aβ-laden vessels without dyshoric changes.
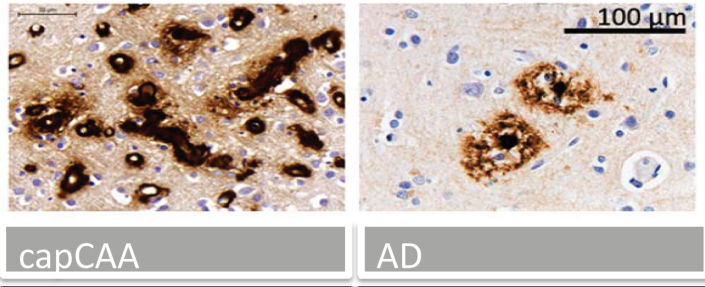
	capCAA	AD
Aβ deposition	vascular	parenchymal
Aβ40:Aβ42	Aβ40>Aβ42	Aβ40<Aβ42
tau	+	++
glia activation	+	+
CD45+ microglia	- (proinflammatory phenotype)	+
ApoE4	++ (frequency 0.54)	+ (frequency 0.36)
Clusterin	++	+
SAP	++	+
Complement	++	+
Lamininβ2	++	-
tight junctions	-	+
RAGE	++	+
P-gp	-	+
BCRP	-	+

Figure 2. Summary of the characteristics of capCAA and AD studied in this thesis.

Both glia activation and neuritic changes strictly correlate with the severity of Aβ load in the tissue and vasculature. Microglia clustered around capCAA capillaries not only appear morphologically activated but show a marked expression of the reactive oxygen species (ROS) generating enzyme NADPH oxidase-2 (NOX-2), suggesting increased production of ROS and consequent oxidative stress around capCAA (chapter 4).

It is reasonable to hypothesize that the parenchymal reaction associated with capCAA (or more generally with dyshoric changes) is related to the amyloid conformational structure rather than the Aβ species. Similar inflammatory reactions can be found in other forms of amyloidosis. Interestingly, also prion amyloid fibrils lead to severe tauopathy and microglia

accumulation (Gonzalez-Mariscal, et al., 2011; Overgaard, et al., 2011).

Another peculiar observation we came across analyzing glia activation, and particularly the microglia, is the absence or low expression of CD45 by microglia in patients with capCAA. CD45 is an immunomodulator which reduces the proinflammatory phenotype of microglia cells, switching them to a more phagocytic mode, as demonstrated in an AD mouse model (Biffi, et al., 2010). The lack of CD45 might not only be involved in an impaired removal of Aβ by microglia, but also fuel the development of a severe inflammatory response around capCAA, inducing the microglia to secrete proinflammatory cytokines. Although these are preliminary observations, studying the phenotype of glial cells recruited around Aβ deposits can potentially be very interesting and deserves further investigation.

The abnormal production of pro-inflammatory cytokines, chemokines and the complement system, as well as ROS, by microglia, can disrupt nerve terminals causing dysfunction and loss of synapses, which correlates with memory decline (Hensley, 2010). These inflammatory mediators are produced by activated microglia and reactive astrocytes, but also neurons and vascular endothelial cells can further contribute to the production of pro-inflammatory cytokines, acute phase proteins and complement.

Vascular-derived products of a permanently dysfunctional endothelium could result in neuronal injury in neurodegenerative disease states. In the Aβ loaded brain, an injured/altered brain endothelial cell can also release factors that are injurious or toxic to neurons (Biffi and Greenberg, 2011; Glenner and Wong, 1984a).

To summarize, in capCAA both activated glial cells and endothelium can release proinflammatory cytokines and ROS, which compromise not only neuronal function but also BBB function and integrity (chapter 2 and 4).

BBB alterations in capCAA

An important function of the BBB that may go awry in AD and capCAA is the regulation of the brain pool of Aβ. Brain Aβ levels, which are in equilibrium with plasma and CSF Aβ concentrations, are modulated by influx and efflux of soluble Aβ across the BBB via interaction with specific receptors and transporters located on brain endothelium.

In capCAA accumulation of Aβ occurs exactly at the interface of the CNS and the systemic circulation, affecting those locations responsible for transport and clearance of Aβ into the venous or CSF compartments. The role of capCAA in altering and modulating BBB function and integrity, which directly affects Aβ clearance, is of particular relevance in understanding AD pathophysiology.

Brain endothelial cells regulate the neuronal milieu both by their synthetic functions as well as by their BBB function. Therefore, disturbance in cerebrovascular metabolic or transport functions could result in a noxious neuronal environment in the capCAA brain.

Disturbed clearance of Aβ

Aβ is mainly produced in neurons and astrocytes and then released into the brain interstitial fluid (Revesz, et al., 2002). Under normal conditions Aβ is cleared or removed, keeping Aβ concentrations low and thereby avoiding aggregation. Several pathways involved in Aβ clearance have been described: (1) Aβ endocytosis by astrocytes and microglial cells; (2) Aβ enzymatic degradation (e.g., by neprilysin or the insulin-degrading enzyme (IDE); (3) Aβ transport across the BBB and/or (4) Aβ drainage along perivascular spaces (Thal, et al., 2008). If any of these mechanisms fail the result is an increased retention of Aβ within the brain and consequently Aβ aggregation and deposition as either plaques or (cap)CAA.

In capCAA the deposition of Aβ occurs at the level of the BBB; it is therefore feasible that the mechanism principally altered in capCAA patients is Aβ transport across the BBB. Accumulating evidence from patients and animal models of AD suggests that vulnerable brains may suffer from an increase in Aβ influx receptors and/or a decrease in Aβ efflux receptors (Bell and Zlokovic, 2009; Deane, et al., 2004).

The involvement of RAGE (receptor for advanced glycation endproducts) appears to be very

important in the development of the AD and capCAA pathology, since RAGE mediates the influx of Aβ into the brain parenchyma and consequently in an unbalanced situation enhances Aβ accumulation. RAGE is also known to be critical regarding the effects exerted by Aβ through its binding to the transporter. Aβ/RAGE interaction has been reported to activate NOX and a cascade of effects such as NF-κB-mediated endothelial activation resulting in secretion of proinflammatory cytokines, the expression of adhesion molecules and suppression of cerebral blood flow (Zlokovic, 2008), fueling not only Aβ accumulation but also oxidative stress and inflammatory responses associated with capCAA.

While RAGE is expressed at relatively low levels in the microvasculature under physiological conditions, its expression is upregulated with increasing ligand concentration, including Aβ (Donahue and Johanson, 2008). In AD brains, RAGE is upregulated and found in neurons, astrocytes, and microglia particularly in proximity to Aβ plaques and neurofibrillary tangles (Deane and Zlokovic, 2007; Donahue, et al., 2006). We confirmed that Aβ induces a local upregulation of RAGE in capCAA cases as well. In chapter 4 we have shown a striking increase in RAGE expression in capCAA-affected capillaries and demonstrated that Aβ cytotoxic effects on endothelial cells are exerted at least partially by its binding to RAGE.

Low density lipoprotein receptor/related protein 1 (LRP-1) is also expressed in the cerebral microvasculature and is a major Aβ efflux transporter (Shibata, et al., 2000). ApoE4, but not ApoE3 or ApoE2, blocks LRP1mediated Aβ clearance from the brain and, hence, promotes its retention (Di Paolo and Kim, 2011). Reduced LRP1 levels in brain microvessels, perhaps in addition to altered levels of other efflux transporters like P-glycoprotein (P-gp), are associated with Aβ cerebrovascular and brain accumulation during ageing in rodents, non-human primates, and humans. In addition, LRP1 levels are increased in transgenic AD mice models as well as patients with Alzheimer's disease (Abbott, et al., 2010).

In fact, we have shown that the expression of two other efflux transporters for Aβ at the BBB, P-gp and breast cancer resistance protein (BCRP), is severely affected when we compare capCAA with controls and AD lacking microvascular amyloid pathology (chapter 5). These transporters are thought to facilitate the release of Aβ into the blood stream, subsequent to Aβ uptake mediated by LRP-1 in the endothelial cells of the capillaries. If one of these proteins is downregulated, cerebral Aβ levels are bound to rise. It has been demonstrated that mice lack-

ing P-gp at the BBB have reduced clearance of Aβ from the CNS and lower levels of LRP1 in brain capillaries (Cirrito, et al., 2005).

We also showed that P-gp loss in capCAA can be related to clusterin. The effects of clusterin on Aβ aggregation have significant repercussions on P-gp expression, as Aβ/clusterin complexes might have a peculiar interaction with cell membranes or other molecules inducing a stronger downregulation of P-gp than Aβ aggregates alone. This may represent an additional detrimental role for clusterin in the pathogenesis of capCAA.
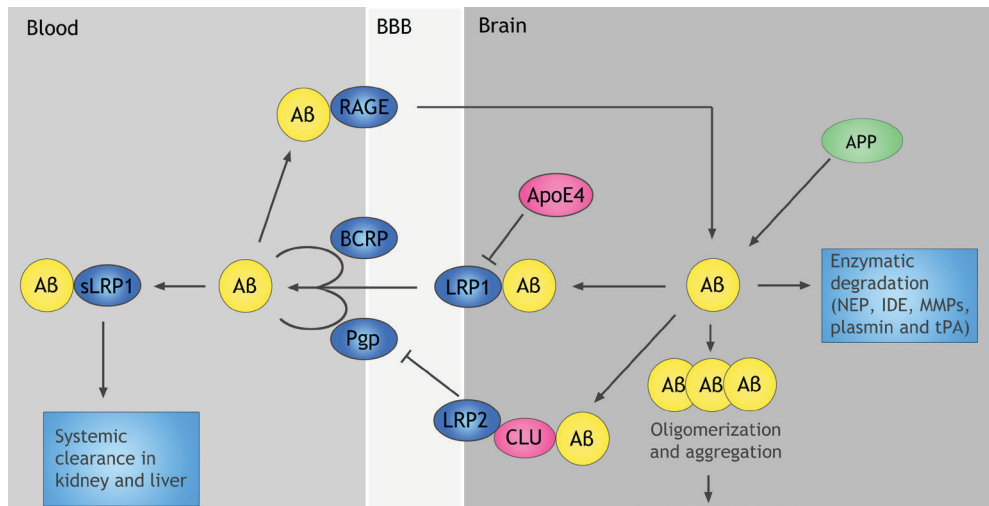
Figure 3. The role of blood–brain barrier transport in brain homeostasis of Aβ. Aβ is produced from the Aβ precursor protein (APP), both in the brain and in peripheral tissues. Clearance of Aβ from the brain normallymaintains its low levels in the brain. This peptide is cleared across the blood– brain barrier (BBB) by the lowdensity lipoprotein receptor-related protein 1 (LRP1). LRP1 mediates rapid efflux of a free, unbound form of Aβ and of Aβ bound to apolipoprotein E2 (ApoE2), ApoE3 from the brain's interstitial fluid into the blood, and ApoE4 inhibits such transport. LRP2 eliminates Aβ that is bound to clusterin (CLU) by transport across the BBB. ATPbinding cassette P-gp and BCRP mediates Aβ efflux from the brain endothelium to blood across the luminal side of the BBB. Cerebral endothelial cells, pericytes, vascular smooth muscle cells, astrocytes, microglia and neurons express different Aβ-degrading enzymes, including neprilysin (NEP), insulin-degrading enzyme (IDE), tissue plasminogen activator (tPA) and matrix metalloproteinases (MMPs), which contribute to Aβ clearance. In the circulation, Aβ is bound mainly to soluble LRP1 (sLRP1), which normally prevents its entry into the brain. Systemic clearance of Aβ is mediated by its removal by the liver and kidneys. The receptor for advanced glycation end products (RAGE) provides the key mechanism for influx of peripheral Aβ into the brain across the BBB. Faulty vascular clearance of Aβ from the brain and/or an increased re-entry of peripheral Aβ across the blood vessels into the brain can elevate Aβ levels in the brain parenchyma and around cerebral blood vessels. At pathophysiological concentrations, Aβ forms neurotoxic oligomers and also self-aggregates, which leads to the development of Aβ plaques and cerebral amyloid angiopathy (modified from Zlokovic, *Nature Reviews Neuroscience* 12, 723-738).

The accumulation of clusterin and clusterin/Aβ complexes on the abluminal side of the BBB is possibly due to a reduction in the expression of the receptor that transports them across the BBB, LRP2.

The transport of Aβ across the BBB is a delicate and intricate mechanism mediated by proteins (transporters) the expression of which is modulated by several factors, first of all Aβ itself. It is quite remarkable that Aβ induces upregulation of the influx transporter RAGE and downregulation of the Aβ efflux transporters, meaning that initial subtle increases in Aβ concentration would degenerate in a more profound Aβ brain retention due to impaired clearance. We postulate that AAPs involved in the clearance of Aβ (like apoE and clusterin) are responsible to initiate this cascade slowing the rate of Aβ removal. In this scenario, the local environment surrounding the capillaries is subjected to increased levels of Aβ, which eventually aggregate in the microvasculature.

Multiple pathogenic cascades, possibly more than the ones described in this thesis, in the neurovascular unit may contribute to faulty clearance of amyloid across the BBB and amplify neuronal dysfunction and injury in capCAA.

Breaking the barrier

BBB disruption is a common feature of virtually all neurodegenerative disorders and so, along with neuroinflammation, can be viewed as a key component in the process of neurodegeneration. Changes in the cerebral microvasculature have been reported in brains of AD subjects (Abbott, et al., 2010; Blasig, et al., 2011; Claudio, 1996; Farkas and Luiten, 2001; Perlmutter and Chui, 1990). However, the mechanisms that underlie massive deposition of Aβ aggregates in cerebral blood vessels and brain parenchyma are poorly understood. Likewise, processes involved in Aβ-driven neuroinflammation and associated BBB malfunction are largely unknown.

In vitro studies support the idea that Aβ deposition affects BBB integrity since different Aβ peptides are able to increase endothelial permeability (Blanc, et al., 1997; Tai, et al., 2009) and induce altered expression and translocation of tight junctions (TJs) proteins in human and animal endothelial cells (Gonzalez-Velasquez, et al., 2008; Marco and Skaper, 2006).

When analyzing TJs we observed a marked loss of key TJ proteins, such as occludin, claudin-5 and ZO-1 in Aβ-laden microvessels (Carrano, et al., 2011), which was confirmed later by

Hartz and colleagues (Hartz, et al., 2012).

To unravel pathways involved in BBB damage and Aβ-induced oxidative stress in brain endothelial cells, an *in vitro* approach was taken using a validated human brain endothelial cell line. We showed a significant dose-dependent downregulation of TJ proteins occludin and ZO-1 mRNA levels upon Aβ treatment. Such downregulation is due to the release of reactive oxygen species mediated by the binding of Aβ to RAGE, which in turn activates NOX. The role of RAGE in contributing to BBB disruption is not only limited to the modulation of TJs expression but also affecting TJs integrity through induction of matrix metalloproteases (Coisne and Engelhardt, 2011).

Together, our data suggest that Aβ contributes to the loss of barrier integrity in capCAA by decreasing TJ protein expression. Likely consequences are barrier leakage and radiological cortical cerebral microhaemorrhages (accumulation of iron loaded macrophages)(Gonzalez-Velasquez, et al., 2008; Zipfel, et al., 2009), which are commonly associated with CAA (Menon and Kidwell, 2009; Raposo, et al., 2011).

Damaged BBB has been confirmed by immunohistochemical examination of capCAA brains revealing leakage of fibrinogen into the brain parenchyma. Fibrinogen was found as a diffuse staining throughout the parenchyma surrounding affected vessels and we frequently detected colocalization of fibrinogen with fibrillar capillary Aβ deposits. In the most severe cases fibrinogen immunoreactivity was present in tissue surrounding all Aβ-laden vessels, suggesting an ongoing disruption of BBB integrity. The histopathological changes, including reduced TJ expression, glia cell activation and fibrinogen leakage, all correlated with severity of capCAA pathology. Blood proteins, such as fibrinogen, have essential functions in the maintenance of integral vasculature homeostatic processes involved in blood clotting. However, under pathological conditions a weakened BBB could allow extravasation of plasma proteins into parenchymal regions of the brain. A likely consequence of increased infiltration of proteins is the exacerbation of inflammatory responses mediated by the resident immune responding cells, microglia.

Microglia may not only initiate an inflammatory response to Aβ but also amplify and sustain inflammation in response to fibrinogen extravasation (Ryu and McLarnon, 2009). In this case a chronic inflammatory environment could be maintained by reciprocal signaling between

activated microglia and perturbed vasculature. Concomitant to cognitive decline, the inflammatory reaction associated with capCAA could impair the function and integrity of the BBB and decrease Aβ removal, which contributes to disease progression. The inflammatory reaction associated with the vasculature exacerbates Aβ effects on the BBB, and specifically the impairment of the BBB integrity. Such damage of the BBB may play a significant, if not critical role in the pathogenesis of AD and capCAA, especially in terms of any distortions of the homeostatic balance of the brain, and in particular of cerebral Aβ levels.

Therapeutic strategies and search for biomarkers

Considerable effort has been made in recent years toward gaining a better understanding of the pathogenesis of AD, and in developing novel therapeutic approaches. However to date, there is no effective treatment that can prevent, delay or cure the disease and most of the latest clinical trials focusing on decreasing Aβ load in the brain have been unsuccessful. Interestingly, anti-Aβ immunization therapies resulted in reduced numbers of plaques in the brain parenchyma. However, in some patients this led to an increase in vascular amyloid and subsequent vasogenic edema (Alzheimer, 1907; Dierksen, et al., 2010). It is interesting that the risk of developing vascular side effects are strongly correlated to the ApoE4 allele, implying that an impaired Aβ clearance results in an ineffective treatment. Differential response to therapy, in such cases, might be due to the presence of ongoing (cap)CAA pathology. In AD cases with a certain degree of capCAA, or with an increased risk of developing capCAA (apoE4 carriers), plaque burden might be reduced, inducing the movement of Aβ from the parenchyma toward the vasculature district, in the attempt to be cleared via the blood stream. We have shown that in capCAA cases, clearance through the BBB is impaired because of altered expression of transporters and amyloid associated proteins, leading to build up of Aβ in and around the vasculature and consequent vascular complications.

Clinical diagnosis of "probable AD" is based on neuroimaging and biochemical analysis of the cerebrospinal fluid (CSF), together with neuropsychological examination. Reduced CSF Aβ42 levels are consistently observed in AD patients (Mulder, et al., 2010), while, in contrast, levels of the more soluble CSF Aβ40 are normal (Bibl, et al., 2008). Furthermore, the increased CSF total tau and phosphorylated tau concentrations in AD (de Jong, et al., 2007) are likely related to the pathological accumulation of these proteins in neurofibrillary tangles. AD pa-

tients with many microbleeds have even lower CSF Aβ42 levels than AD patients without microbleeds, potentially due to additional amyloid deposition in cerebral vessel walls (Goos, et al., 2009) and CAA patients, presenting with lobar hemorrhage, exhibit lowered CSF levels of both Aβ42 and Aβ40 compared with controls and even to AD (Verbeek, et al., 2009). CapCAA cases would likely show lower levels of CSF Aβ42 and Aβ40 together with slightly increased CSF tau, reflective of the pathological features observed in the brain and how they compare to classical AD pathology. This remains an assumption as a comparative CSF analysis of AD, capCAA and CAA cases has yet to be performed, possibly due to the difficulties in differentially diagnosing these diseases during life.

Although guidelines to diagnose CAA during life exist (Boston criteria) (Knudsen, et al., 2001), these are not specific for capCAA. Hence currently, it is not possible to clinically define whether an AD case has capCAA pathology. Clinical evaluation of capCAA is very difficult, and although severe capCAA is associated with rapidly progressive dementia (Eurelings, et al., 2010), ApoE4 genotype (Richard, et al., 2010; Thal, et al., 2008) and occurrence of microbleeds (Dierksen, et al., 2010; Goos, et al., 2012), these findings are also observed in AD, or to be precise, in the heterogeneous population that we clinically define as AD.

Identifying biomarkers capable of discriminating subgroups in the AD population during life, in first instance cases affected by microvascular amyloidosis, is critical for the diagnosis of capCAA and the design of clinical trials, in terms of inclusion or exclusion of specific sub-populations for determined treatments. It also appears obvious that two sub-populations of AD, as diverse as we have described in this thesis, could benefit from different therapeutic approaches.

With our proteomics analysis of *post-mortem* tissue (chapter 3) we aimed to identify markers that could discriminate capCAA from AD. We have shown that proteins involved in Aβ aggregation and clearance at the BBB are severely modulated in capCAA, while these processes are marginally affected in AD. The ideal biomarker should be specific for capCAA and easily measurable *in vivo*, either in CSF (or even better, in plasma) or by brain imaging. Although we are still far from being able to pinpoint "the biomarker" for capCAA or AD, we have shown that cases with predominant microvascular (capCAA) or parenchymal (AD) Aβ are different enough to show significant differences in a small cohort using a proteomics approach.

In this thesis we have described common and different neuropathological features between AD and capCAA and pioneered the proteome analysis of capCAA and compared it with classical AD in *post mortem* tissue (chapter 3) describing pathways subjected to differential modulations, in first instance BBB related alterations. It is now important to continue in the direction of assessing the validity and feasibility of such proteins for use as biomarkers, for instance analyzing their modulation *in vivo* during disease progression in animal models and in human cases, e.g. by CSF analysis and brain imaging.

Conclusion

CapCAA is a distinct entity that defines sub-groups of both CAA and AD and whose pathogenesis is specifically associated with decreased transendothelial clearance of Aβ. CapCAA has a considerable influence on the BBB, affecting its integrity and function, and thereby affecting the homeostasis of the ageing brain.

We have demonstrated here that although capCAA and AD share some pathological hallmarks, several proteins involved in Aβ clearance are differentially deregulated. Proteins specifically up or down regulated in capCAA (and not in AD) might underscore altered pathogenic pathways explaining why Aβ accumulates around the brain vasculature instead of depositing as plaques in the brain parenchyma, as observed in AD. Furthermore, the identification of proteins that are clearly different between AD and capCAA cases could be used as biomarkers for the diagnosis of capCAA during life.

References

Abbott, N.J., Patabendige, A.A., Dolman, D.E., Yusof, S.R., Begley, D.J. 2010. Structure and function of the blood-brain barrier. *Neurobiol Dis* 37(1), 13-25.

Akiyama, H., Barger, S., Barnum, S., Bradt, B., Bauer, J., Cole, G.M., Cooper, N.R., Eikelenboom, P., Emmerling, M., Fiebich, B.L., Finch, C.E., Frautschy, S., Griffin, W.S., Hampel, H., Hull, M., Landreth, G., Lue, L., Mrak, R., Mackenzie, I.R., McGeer, P.L., O'Banion, M.K., Pachter, J., Pasinetti, G., Plata-Salaman, C., Rogers, J., Rydel, R., Shen, Y., Streit, W., Strohmeyer, R., Tooyoma, I., Van Muiswinkel, F.L., Veerhuis, R., Walker, D., Webster, S., Wegrzyniak, B., Wenk, G., Wyss-Coray, T. 2000. Inflammation and Alzheimer's disease. *Neurobiol Aging* 21(3), 383-421.

Alzheimer, A. 1907. Über eine eigenartige Erkrankung der Hirnrinde. *Allgemeine Zeitschrift für Psychiatrie* 64, 146-8.

Arends, Y.M., Duyckaerts, C., Rozemuller, J.M., Eikelenboom, P., Hauw, J.J. 2000. Microglia, amyloid and dementia in alzheimer disease. A correlative study. *Neurobiol Aging* 21(1), 39-47.

Bell, R.D., Sagare, A.P., Friedman, A.E., Bedi, G.S., Holtzman, D.M., Deane, R., Zlokovic, B.V. 2007. Transport pathways for clearance of human Alzheimer's amyloid beta-peptide and apolipoproteins E and J in the mouse central nervous system. *J Cereb Blood Flow Metab* 27(5), 909-18.

Bell, R.D., Zlokovic, B.V. 2009. Neurovascular mechanisms and blood-brain barrier disorder in Alzheimer's disease. *Acta Neuropathol* 118(1), 103-13.

Bibl, M., Mollenhauer, B., Esselmann, H., Schneider, M., Lewczuk, P., Welge, V., Gross, M., Falkai, P., Kornhuber, J., Wiltfang, J. 2008. Cerebrospinal fluid neurochemical phenotypes in vascular dementias: original data and mini-review. *Dement Geriatr Cogn Disord* 25(3), 256-65.

Biffi, A., Greenberg, S.M. 2011. Cerebral amyloid angiopathy: a systematic review. *J Clin Neurol* 7(1), 1-9.

Biffi, A., Sonni, A., Anderson, C.D., Kissela, B., Jagiella, J.M., Schmidt, H., Jimenez-Conde, J., Hansen, B.M., Fernandez-Cadenas, I., Cortellini, L., Ayres, A., Schwab, K., Juchniewicz, K., Urbanik, A., Rost, N.S., Viswanathan, A., Seifert-Held, T., Stoegerer, E.M., Tomas, M., Rabionet, R., Estivill, X., Brown, D.L., Silliman, S.L., Selim, M., Worrall, B.B., Meschia, J.F., Montaner, J., Lindgren, A., Roquer, J., Schmidt, R., Greenberg, S.M., Slowik, A., Broderick, J.P., Woo, D., Rosand, J. 2010. Variants at APOE influence risk of deep and lobar intracerebral hemorrhage. *Ann Neurol* 68(6), 934-43.

Blanc, E.M., Toborek, M., Mark, R.J., Hennig, B., Mattson, M.P. 1997. Amyloid beta-peptide induces cell monolayer albumin permeability, impairs glucose transport, and induces apoptosis in vascular endothelial cells. *J Neurochem* 68(5), 1870-81.

Blasig, I.E., Bellmann, C., Cording, J., Del Vecchio, G., Zwanziger, D., Huber, O., Haseloff, R.F. 2011. Occludin protein family: oxidative stress and reducing conditions. *Antioxid Redox Signal* 15(5), 1195-219.

Calero, M., Rostagno, A., Matsubara, E., Zlokovic, B., Frangione, B., Ghiso, J. 2000. Apolipoprotein J (clusterin) and Alzheimer's disease. *Microsc Res Tech* 50(4), 305-15.

Carrano, A., Hoozemans, J.J., van der Vies, S.M., Rozemuller, A.J., van Horssen, J., de Vries, H.E. 2011. Amyloid beta Induces Oxidative Stress-Mediated Blood-Brain Barrier Changes in Capillary Amyloid Angiopathy. *Antioxid Redox Signal*.

Cirrito, J.R., Deane, R., Fagan, A.M., Spinner, M.L., Parsadanian, M., Finn, M.B., Jiang, H., Prior, J.L., Sagare, A., Bales, K.R., Paul, S.M., Zlokovic, B.V., Piwnica-Worms, D., Holtzman, D.M. 2005. P-glycoprotein deficiency at the blood-brain barrier increases amyloid-beta deposition in an Alzheimer disease mouse model. *J Clin Invest* 115(11), 3285-90.

Claudio, L. 1996. Ultrastructural features of the blood-brain barrier in biopsy tissue from Alzheimer's disease patients. *Acta Neuropathol* 91(1), 6-14.

Coisne, C., Engelhardt, B. 2011. Tight junctions in brain barriers during central nervous system inflammation. *Antioxid Redox Signal* 15(5), 1285-303.

de Jong, D., Kremer, B.P., Olde Rikkert, M.G., Verbeek, M.M. 2007. Current state and future directions of neurochemical biomarkers for Alzheimer's disease. *Clin Chem Lab Med* 45(11), 1421-34.

Deane, R., Wu, Z., Zlokovic, B.V. 2004. RAGE (yin) versus LRP (yang) balance regulates alzheimer amyloid beta-peptide clearance through transport across the blood-brain barrier. *Stroke* 35(11 Suppl 1), 2628-31.

Deane, R., Zlokovic, B.V. 2007. Role of the blood-brain barrier in the pathogenesis of Alzheimer's disease. *Curr Alzheimer Res* 4(2), 191-7.

DeMattos, R.B., O'Dell M, A., Parsadanian, M., Taylor, J.W., Harmony, J.A., Bales, K.R., Paul, S.M., Aronow, B.J., Holtzman, D.M. 2002. Clusterin promotes amyloid plaque formation and is critical for neuritic toxicity in a mouse model of Alzheimer's disease. *Proc Natl Acad Sci U S A* 99(16), 10843-8.

Di Paolo, G., Kim, T.W. 2011. Linking lipids to Alzheimer's disease: cholesterol and beyond. *Nat Rev Neurosci* 12(5), 284-96.

Dierksen, G.A., Skehan, M.E., Khan, M.A., Jeng, J., Nandigam, R.N., Becker, J.A., Kumar, A., Neal, K.L., Betensky, R.A., Frosch, M.P., Rosand, J., Johnson, K.A., Viswanathan, A., Salat, D.H., Greenberg, S.M. 2010. Spatial relation between microbleeds and amyloid deposits in amyloid angiopathy. *Ann Neurol* 68(4), 545-8.

Divry, P. 1927. Etude histochimique des plaques séniles. *J Belge Neurol Psychiatry* 27, 643-57.

Donahue, J.E., Flaherty, S.L., Johanson, C.E., Duncan, J.A., 3rd, Silverberg, G.D., Miller, M.C., Tavares, R., Yang, W., Wu, Q., Sabo, E., Hovanesian, V., Stopa, E.G. 2006. RAGE, LRP-1, and amyloid-beta protein in Alzheimer's disease. *Acta Neuropathol* 112(4), 405-15.

Donahue, J.E., Johanson, C.E. 2008. Apolipoprotein E, amyloid-beta, and blood-brain barrier permeability in Alzheimer disease. *J Neuropathol Exp Neurol* 67(4), 261-70.

Eikelenboom, P., Stam, F.C. 1982. Immunoglobulins and complement factors in senile plaques. An immunoperoxidase study. *Acta Neuropathol* 57(2-3), 239-42.

Eikelenboom, P., Veerhuis, R. 1996. The role of complement and activated microglia in the pathogenesis of Alzheimer's disease. *Neurobiol Aging* 17(5), 673-80.

Eurelings, L.S., Richard, E., Carrano, A., Eikelenboom, P., van Gool, W.A., Rozemuller, A.J. 2010. Dyshoric capillary cerebral amyloid angiopathy mimicking Creutzfeldt-Jakob disease. *J Neurol Sci* 295(1-2), 131-4.

Farkas, E., Luiten, P.G. 2001. Cerebral microvascular pathology in aging and Alzheimer's disease. *Prog Neurobiol* 64(6), 575-611.

Glenner, G.G., Wong, C.W. 1984a. Alzheimer's disease and Down's syndrome: sharing of a unique cerebrovascular amyloid fibril protein. *Biochem Biophys Res Commun* 122(3), 1131-5.

Glenner, G.G., Wong, C.W. 1984b. Alzheimer's disease: initial report of the purification and characterization of a novel cerebrovascular amyloid protein. *Biochem Biophys Res Commun* 120(3), 885-90.

Gonzalez-Mariscal, L., Quiros, M., Diaz-Coranguez, M. 2011. ZO proteins and redox-dependent processes. *Antioxid Redox Signal* 15(5), 1235-53.

Gonzalez-Velasquez, F.J., Kotarek, J.A., Moss, M.A. 2008. Soluble aggregates of the amyloid-beta protein selectively stimulate permeability in human brain microvascular

endothelial monolayers. *J Neurochem* 107(2), 466-77.

Goos, J.D., Kester, M.I., Barkhof, F., Klein, M., Blankenstein, M.A., Scheltens, P., van der Flier, W.M. 2009. Patients with Alzheimer disease with multiple microbleeds: relation with cerebrospinal fluid biomarkers and cognition. *Stroke* 40(11), 3455-60.

Goos, J.D., Teunissen, C.E., Veerhuis, R., Verwey, N.A., Barkhof, F., Blankenstein, M.A., Scheltens, P., van der Flier, W.M. 2012. Microbleeds relate to altered amyloid-beta metabolism in Alzheimer's disease. *Neurobiol Aging* 33(5), 1011 e1-9.

Greenberg, S.M., Grabowski, T., Gurol, M.E., Skehan, M.E., Nandigam, R.N., Becker, J.A., Garcia-Alloza, M., Prada, C., Frosch, M.P., Rosand, J., Viswanathan, A., Smith, E.E., Johnson, K.A. 2008. Detection of isolated cerebrovascular beta-amyloid with Pittsburgh compound B. *Ann Neurol* 64(5), 587-91.

Harold, D., Abraham, R., Hollingworth, P., Sims, R., Gerrish, A., Hamshere, M.L., Pahwa, J.S., Moskvina, V., Dowzell, K., Williams, A., Jones, N., Thomas, C., Stretton, A., Morgan, A.R., Lovestone, S., Powell, J., Proitsi, P., Lupton, M.K., Brayne, C., Rubinsztein, D.C., Gill, M., Lawlor, B., Lynch, A., Morgan, K., Brown, K.S., Passmore, P.A., Craig, D., McGuinness, B., Todd, S., Holmes, C., Mann, D., Smith, A.D., Love, S., Kehoe, P.G., Hardy, J., Mead, S., Fox, N., Rossor, M., Collinge, J., Maier, W., Jessen, F., Schurmann, B., van den Bussche, H., Heuser, I., Kornhuber, J., Wiltfang, J., Dichgans, M., Frolich, L., Hampel, H., Hull, M., Rujescu, D., Goate, A.M., Kauwe, J.S., Cruchaga, C., Nowotny, P., Morris, J.C., Mayo, K., Sleegers, K., Bettens, K., Engelborghs, S., De Deyn, P.P., Van Broeckhoven, C., Livingston, G., Bass, N.J., Gurling, H., McQuillin, A., Gwilliam, R., Deloukas, P., Al-Chalabi, A., Shaw, C.E., Tsolaki, M., Singleton, A.B., Guerreiro, R., Muhleisen, T.W., Nothen, M.M., Moebus, S., Jockel, K.H., Klopp, N., Wichmann, H.E., Carrasquillo, M.M., Pankratz, V.S., Younkin, S.G., Holmans, P.A., O'Donovan, M., Owen, M.J., Williams, J. 2009. Genome-wide association study identifies variants at CLU and PICALM associated with Alzheimer's disease. *Nat Genet* 41(10), 1088-93.

Hartz, A.M., Bauer, B., Soldner, E.L., Wolf, A., Boy, S., Backhaus, R., Mihaljevic, I., Bogdahn, U., Klunemann, H.H., Schuierer, G., Schlachetzki, F. 2012. Amyloid-beta contributes to blood-brain barrier leakage in transgenic human amyloid precursor protein mice and in humans with cerebral amyloid angiopathy. *Stroke* 43(2), 514-23.

Hensley, K. 2010. Neuroinflammation in Alzheimer's disease: mechanisms, pathologic consequences, and potential for therapeutic manipulation. *J Alzheimers Dis* 21(1), 1-14.

Knudsen, K.A., Rosand, J., Karluk, D., Greenberg, S.M. 2001. Clinical diagnosis of cerebral amyloid angiopathy: validation of the Boston criteria. *Neurology* 56(4), 537-9.

Lambert, J.C., Heath, S., Even, G., Campion, D., Sleegers, K., Hiltunen, M., Combarros, O.,

Zelenika, D., Bullido, M.J., Tavernier, B., Letenneur, L., Bettens, K., Berr, C., Pasquier, F., Fievet, N., Barberger-Gateau, P., Engelborghs, S., De Deyn, P., Mateo, I., Franck, A., Helisalmi, S., Porcellini, E., Hanon, O., de Pancorbo, M.M., Lendon, C., Dufouil, C., Jaillard, C., Leveillard, T., Alvarez, V., Bosco, P., Mancuso, M., Panza, F., Nacmias, B., Bossu, P., Piccardi, P., Annoni, G., Seripa, D., Galimberti, D., Hannequin, D., Licastro, F., Soininen, H., Ritchie, K., Blanche, H., Dartigues, J.F., Tzourio, C., Gut, I., Van Broeckhoven, C., Alperovitch, A., Lathrop, M., Amouyel, P. 2009. Genome-wide association study identifies variants at CLU and CR1 associated with Alzheimer's disease. *Nat Genet* 41(10), 1094-9.

Lehner, C., Gehwolf, R., Tempfer, H., Krizbai, I., Hennig, B., Bauer, H.C., Bauer, H. 2011. Oxidative stress and blood-brain barrier dysfunction under particular consideration of matrix metalloproteinases. *Antioxid Redox Signal* 15(5), 1305-23.

Marco, S., Skaper, S.D. 2006. Amyloid beta-peptide1-42 alters tight junction protein distribution and expression in brain microvessel endothelial cells. *Neurosci Lett* 401(3), 219-24.

Menon, R.S., Kidwell, C.S. 2009. Neuroimaging demonstration of evolving small vessel ischemic injury in cerebral amyloid angiopathy. *Stroke* 40(12), e675-7.

Mulder, C., Verwey, N.A., van der Flier, W.M., Bouwman, F.H., Kok, A., van Elk, E.J., Scheltens, P., Blankenstein, M.A. 2010. Amyloid-beta(1-42), total tau, and phosphorylated tau as cerebrospinal fluid biomarkers for the diagnosis of Alzheimer disease. *Clin Chem* 56(2), 248-53.

Oppenheim, G. 1909. Über 'drusige Nekrosen' in der Großhirnrinde. *Neurol Zbl* 8, 410-3.

Overgaard, C.E., Daugherty, B.L., Mitchell, L.A., Koval, M. 2011. Claudins: control of barrier function and regulation in response to oxidant stress. *Antioxid Redox Signal* 15(5), 1179-93.

Perlmutter, L.S., Chui, H.C. 1990. Microangiopathy, the vascular basement membrane and Alzheimer's disease: a review. *Brain Res Bull* 24(5), 677-86.

Raposo, N., Viguier, A., Cuvinciuc, V., Calviere, L., Cognard, C., Bonneville, F., Larrue, V. 2011. Cortical subarachnoid haemorrhage in the elderly: a recurrent event probably related to cerebral amyloid angiopathy. *Eur J Neurol* 18(4), 597-603.

Revesz, T., Holton, J.L., Lashley, T., Plant, G., Rostagno, A., Ghiso, J., Frangione, B. 2002. Sporadic and familial cerebral amyloid angiopathies. *Brain Pathol* 12(3), 343-57.

Richard, E., Carrano, A., Hoozemans, J.J., van Horssen, J., van Haastert, E.S., Eurelings, L.S., de Vries, H.E., Thal, D.R., Eikelenboom, P., van Gool, W.A., Rozemuller, A.J. 2010.

Characteristics of dyshoric capillary cerebral amyloid angiopathy. *J Neuropathol Exp Neurol* 69(11), 1158-67.

Rozemuller, A.J., van Gool, W.A., Eikelenboom, P. 2005. The neuroinflammatory response in plaques and amyloid angiopathy in Alzheimer's disease: therapeutic implications. *Curr Drug Targets CNS Neurol Disord* 4(3), 223-33.

Rozemuller, J.M., Eikelenboom, P., Stam, F.C., Beyreuther, K., Masters, C.L. 1989. A4 protein in Alzheimer's disease: primary and secondary cellular events in extracellular amyloid deposition. *J Neuropathol Exp Neurol* 48(6), 674-91.

Ryu, J.K., McLarnon, J.G. 2009. A leaky blood-brain barrier, fibrinogen infiltration and microglial reactivity in inflamed Alzheimer's disease brain. *J Cell Mol Med* 13(9A), 2911-25.

Shibata, M., Yamada, S., Kumar, S.R., Calero, M., Bading, J., Frangione, B., Holtzman, D.M., Miller, C.A., Strickland, D.K., Ghiso, J., Zlokovic, B.V. 2000. Clearance of Alzheimer's amyloid-ss(1-40) peptide from brain by LDL receptor-related protein-1 at the blood-brain barrier. *J Clin Invest* 106(12), 1489-99.

Tai, L.M., Holloway, K.A., Male, D.K., Loughlin, A.J., Romero, I.A. 2009. Amyloid-beta-induced occludin down-regulation and increased permeability in human brain endothelial cells is mediated by MAPK activation. *J Cell Mol Med*.

Thal, D.R., Griffin, W.S., de Vos, R.A., Ghebremedhin, E. 2008. Cerebral amyloid angiopathy and its relationship to Alzheimer's disease. *Acta Neuropathol* 115(6), 599-609.

Verbeek, M.M., Kremer, B.P., Rikkert, M.O., Van Domburg, P.H., Skehan, M.E., Greenberg, S.M. 2009. Cerebrospinal fluid amyloid beta(40) is decreased in cerebral amyloid angiopathy. *Ann Neurol* 66(2), 245-9.

Vinters, H.V., Wang, Z.Z., Secor, D.L. 1996. Brain parenchymal and microvascular amyloid in Alzheimer's disease. *Brain Pathol* 6(2), 179-95.

Zipfel, G.J., Han, H., Ford, A.L., Lee, J.M. 2009. Cerebral amyloid angiopathy: progressive disruption of the neurovascular unit. *Stroke* 40(3 Suppl), S16-9.

Zlokovic, B.V. 2008. The blood-brain barrier in health and chronic neurodegenerative disorders. *Neuron* 57(2), 178-201.

Appendices

Nederlandse samenvatting

De ziekte van Alzheimer

De ziekte van Alzheimer (AD) is een irreversibele, progressieve hersenaandoening die langzaam het geheugen en denkvermogen en uiteindelijk het zelfs het vermogen om eenvoudige taken uit te voeren, aantast. AD is de meest voorkomende oorzaak van dementie onder oudere personen. Dementie is het verlies van cognitief handelen – denken, herinneren en redeneren. Het leidt onder meer tot gedragsveranderingen, en heeft sterke invloed op het dagelijks leven en dagelijkse activiteiten.

Hoewel de oorzaak of oorzaken van AD nog niet volledig duidelijk zijn, is het gevolg van AD in de hersenen overduidelijk. AD beschadigt en vernietigt hersencellen (neuronen). Een door AD aangetast brein telt veel minder cellen en veel minder verbindingen tussen de overgebleven hersencellen dan een gezond brein. Door het voortschrijdende verlies van neuronen, zorgt AD voor significante krimpt van de hersenen.

Wanneer doktoren hersenmateriaal van een AD patiënt onder een microscoop bekijken, zien ze drie soorten afwijkingen, die de typische kenmerken van AD worden genoemd:

Kluwen (*tangles*). Hersencellen zijn afhankelijk van een intern ondersteuning- en transportsysteem, dat essentiële bouwstenen en voedingsstoffen door de uitgestrekte axonen van de neuronen kan transporteren. Dit systeem staat of valt bij het goed functioneren van het eiwit tau. In de neuronen van een door AD aangetast brein binden lange slierten van dit eiwit samen tot een kluwen, waardoor het transportsysteem in de cel tot stilstand komt. Dit falen van het transportsysteem wordt sterk in verband gebracht met de afname van het aantal hersencellen bij AD.

Eiwit ophopingen *(amyloïde plaques)*. De samenklontering van het eiwit beta-amyloid kan hersencellen op meerdere manieren beschadigen en vernietigen, ondermeer door het verstoren van de communicatie tussen de cellen. Hoewel de uiteindelijke oorzaak van het afsterven van hersencellen bij AD niet bekend is, is de ophoping van beta-amyloid één van de meest voornaamste verdachten.

Eiwit ophoping in de vaatwand *(vascular amyloid deposits)*. Staat ook wel bekend als cerebrale amyloïde angiopathie (CAA) en is de ophoping van beta-amyloid op de wanden van

de bloedvaten in de hersenen. Er kunnen twee vormen van CAA worden beschreven: CAA type 1 wordt gekarakteriseerd door de eiwit ophoping in capillairen en wordt daarom vaak capillaire CAA (capCAA) genoemd. CapCAA komt voor in 51% van alle AD gevallen en correleert met de ernst van de dementie; CAA type 2 wordt gekarakteriseerd door beta-amyloid ophopingen in de grotere bloedvaten.

De amyloïde ophopingen vergroten de kans dat de aangetaste vaten slecht functioneren en verhogen daarmee de kans op hersenbloedingen en tasten de functionaliteit van de bloed-hersen barrière (BBB) aan.

Amyloïde ophoping

Een verminderde klaring van beta-amyloid uit de hersenen via de bloedvaten en/of een verhoogde terugstroom van beta-amyloid vanuit de perifere vaten leidt tot een verhoogd niveau van beta-amyloid in het hersenweefsel – het parenchym – als plaques en rondom de hersenvaten, als CAA. Bij pathofysiologische concentraties vormt beta-amyloid neurotoxische oligomeren en aggregeert op zichzelf verder wat uiteindelijk leidt tot CAA en parenchymale plaques. Omdat de klaring een cruciale rol speelt in de handhaving van beta-amyloid concentraties in de hersenen, en daarmee in de formatie van plaques en CAA, kan het feitelijke transport van het eiwit over de bloed-hersen barrière een hoofdrol spelen in de pathologische cascade welke leidt tot AD.

De bloed-hersen barrière

De bloed-hersen barrière (BBB) is de scheiding tussen het circulerende bloed en de hersenen dier ervoor zorgt dat de hersenen een sterk gereguleerd (micro-)milieu kan onderhouden, hetgeen noodzakelijk is voor efficiënte neurotransmissie. De BBB is semi-permeabel; wat wil zeggen dat het sommige stoffen doorlaat, terwijl het andere stoffen selectief de toegang weigert. In de meeste weefsels in het lichaam zijn de kleinste bloedvaten, de capillairen, omgeven door endotheel cellen met kleine openingen – fenestrae – tussen de cellen. Door deze openingen kunnen (voedings-) stoffen eenvoudig de bloedvaten in en uit. Echter, in de hersenen zijn deze fenestrae afwezig en sluiten de endotheelcellen strak op elkaar aan. Ze vormen een zogenaamd *tight junction*, waardoor stoffen niet zomaar de bloedvaten uit kunnen gaan. Ontwrichting van de BBB is een gemeenschappelijk kenmerk van vrijwel alle neurodegeneratieve stoornissen en kan zo, samen met neuronale inflammatie, gezien worden als één van de be-

langrijkste componenten in het proces van neurodegeneratie. Omdat in capCAA beta-amyloid aggregeert op de vaatwanden, op het grensvlak van de hersenen en de bloedsomloop, daar waar beta-amyloid juist uit de hersenen verwijdert dient te worden, is de rol van capCAA op de werking en integriteit van de BBB en daarmee samenhangend de klaring van beta-amyloid, van bijzonder belang in het begrijpen van de pathofysiologie van AD.

Doelstellingen

De aanwezigheid van uitgebreide capCAA onderscheidt een subgroep van AD gevallen met weinig tot geen parenchymale plaques, waarvan de eigenschappen en kenmerken in dit proefschrift zijn onderzocht en beschreven. Identificatie van differentieel tot expressie gebrachte eiwitten in klinische gevallen met capCAA pathologie, zou specifiek inzicht kunnen geven in de achterliggende moleculaire mechanismes welke leiden tot de verstoorde klaring van beta-amyloid over de BBB. Tevens kunnen hierdoor specifieke bio-markers geidentificeerd worden voor capCAA.

Gezien de centrale rol van de vasculaire en BBB compartimenten in de regulatie van beta-amyloid klaring is het doel van de studies, zoals beschreven in dit proefschrift, het onderzoeken en beschrijven van de rol van beta-amyloid transport eiwitten, evenals de expressie van specifieke BBB/endotheel eiwitten in de ADCAA hersenen en het uitzoeken van de vermeende rol van CAA in de ontwikkeling van de AD pathologie. Hiertoe is mijn proefschrift gericht op de vasculaire veranderingen welke plaats vinden in de capillaire vorm van CAA. Op zowel de gemeenschappelijke als de onderscheidende eigenschappen met "klassiek" AD, op de eiwitten welke een rol spelen in het transport van beta-amyloid over de BBB, waaronder amyloid-beta transporters en amyloid geassocieerde eiwitten, en een aantal eiwitten welke een significante rol kunnen spelen bij de algemene homeostase en onderhoud van de vasculaire endotheel en BBB compartimenten.

Voor het uiteindelijke doel van dit proefschrift zijn de volgende algemene doelstellingen geformuleerd:
- Beschrijf de neuropathologische eigenschappen van capCAA, en de gemeenschappelijke en onderscheidende eigenschappen met klassiek AD.
- Onderzoek de veranderingen aan de BBB in capCAA en diens achterliggende pathologische trajecten.

Hoofdstuk 2 beschrijft de pathologische eigenschappen van capCAA, de relatie tussen amyloïde afzettingen in capCAA, CAA en parenchymale plaques en de verspreidingspatronen van neurofibrillaire veranderingen, inflammatoire markers en ApoE rondom amyloïde laesies.

Om de differentiële eiwit expressie tussen AD en capCAA in de hersenen te bestuderen, wordt in **Hoofdstuk 3** een proteomics studie beschreven. We hebben verschillende eiwitten geïdentificeerd welke specifiek meer tot expressie komen in capCAA, hetgeen vervolgens verder onderzocht is middels immunohistochemische technieken. We hebben de expressie onderzocht van de eiwitten laminin, clusterin en SAP en van de activatie van het complement systeem in capCAA en AD hersenen. Zowel laminin, clusterin, SAP en de complement eiwitten colocaliseren met beta-amyloid aggregaten in CAA en capCAA hersenweefsel. Opvallend is dat we een sterkere colocalisatie aantroffen met de vasculaire beta-amyloid afzetting in vergelijking met de parenchymale ophopingen in AD hersenen.

Hoofdstuk 4. We onderzochten BBB veranderingen in capCAA met de nadruk op de veranderingen in de *tight junction (TJ)* alsmede tekenen van neuronale inflammatie. We hebben aangetoond dat beta-amyloid schadelijk is voor de endotheel cellen in de hersenen via de binding aan RAGE en de daaropvolgende oxidatieve stress, wat uiteindelijk leidt tot verstoring van de TJs en verlies van BBB integriteit, wat zichtbaar is door de aanwezigheid van fibrinogeen in capCAA weefsel.

De expressie en functie van ABC transporters is mogelijk cruciaal in de ontwikkeling van AD en capCAA. We laten in **Hoofdstuk 5** zien dat P-gp en BCRP minder sterk tot expressie komen in capCAA, maar niet minder in AD, en dat beta-amyloid en clusterin invloed hebben op de mate van expressie van P-gp. Dit speelt mogelijk een cruciale rol in de ontwikkeling van verschillende amyloïde afzettingen.

Samenvatting

CapCAA is een afzonderlijke entiteit die subgroepen van zowel CAA en AD identificeert en de bijbehorende pathogenese is specifiek geassocieerd met een verminderde klaring van beta-amyloid bij de BBB. CapCAA heeft een significante invloed op de BBB, tast zijn integriteit en functie aan en draagt daarmee bij aan een verstoorde homeostase van het verouderende brein. We hebben hier aangetoond dat hoewel capCAA en AD een aantal gemeenschappelijke

pathologische kenmerken delen, verscheidende eiwitten wel degelijk verschillend zijn ontregeld. Eiwitten die specifiek meer of juist minder tot expressie komen in capCAA (en niet in AD) tonen mogelijke veranderde pathogene cascades aan. Dit zou kunnen verklaren waarom beta-amyloid aggregeert rond de hersenvaten in plaats van in het brein parenchym, zoals bij AD. Verder zouden de eiwitten, waarvan aangetoont is dat ze duidelijk anders tot expressie komen in capCAA ten opzichte van AD, gebruikt kunnen worden voor de ontwikkeling van biomarkers voor de differentiele diagnose van capCAA bij nog in leven zijnde patiënten.

List of abbreviations

Aβ   amyloid β

AD   Alzheimer's Disease

APOE   apolipoprotein E

APOJ   apolipoprotein J

APP   amyloid precursor protein

ARS   antigen retrieval step

BACE   β-site AAP-cleaving enzyme

BBB   blood brain barrier

BCRP   breast cancer resistance protein

C1q   Complement factor 1q

C3d   Complement factor 3d

C5-9   Complement factor 5-9

CAA   cerebral amyloid angiopathy

capCAA   capillary cerebral amyloid angiopathy

CERAD   consortium to establish a registry for Alzheimer's disease

CJD   Creutzfeldt-Jakob disease

CNS   central nervous system

DAB   diaminobenzidine

DPI   diphenylene iodonium

ECs   endothelial cells

EOAD   early onset Alzheimer's disease

ELISA   Enzyme linked immuno-sorbent assay

EM   Electron microscopy

EV   EnVision Method

FBS	fetal bovine serum
GAPDH	Glyceraldehyde-3-phosphate dehydrogenase
GFAP	glial fibrillaryacidic protein
HCMEC	human cerebral microvascular endothelial cell
HRP	horseradish peroxidase
LA	lipoic acid
LRP	Low-density lipoprotein receptor related protein
MRP	multidrug resistance-associated protein
MTT	3-(4,5-dimethylthiazol-2-yl)-2,5-diphenyltetrazolium bromide
NFκB	nuclear factor kappa-light-chain-enhancer of activated B cells
NFT	neurofibrillary tangles
NOX	NADPH oxidase
O/N	over night
PET	Positron emission tomography
P-gp	P-glycoprotein
PIB	Pittsburgh compound-B
PMD	post mortem delay
PS	presenilin
RAGE	receptor for advance glycation end products
ROS	reactive oxygen species
SAP	serum amyloid P component
SMC	smooth muscle cells
TJ	tight junction
ZO	zona occludens

List of publications

Carrano A, Hoozemans JJ, van der Vies SM, van Horssen J, de Vries HE, Rozemuller AJ. Neuroinflammation and Blood-Brain Barrier Changes in Capillary Amyloid Angiopathy. Neurodegener Dis. 2012 Feb 1.

Carrano A, Hoozemans JJ, van der Vies SM, Rozemuller AJ, van Horssen J, de Vries HE. Amyloid beta Induces Oxidative Stress-Mediated Blood-Brain Barrier Changes in Capillary Amyloid Angiopathy. Antioxid Redox Signal. 2011 Sep 1;15(5):1167-78. Epub 2011 Mar 23

Carrano A, Richard E, Hoozemans JJ, van Horssen J, van Haastert ES, Eurelings LS, de Vries HE, Thal DR, Eikelenboom P, van Gool WA, Rozemuller AJ., Characteristics of Dyshoric Capillary Cerebral Amyloid Angiopathy. J Neuropathol Exp Neurol. 2010 Oct 11.

Rozemuller AJ , Jansen C, **Carrano A**, van Haastert ES, Hondius D, van der Vies SM, Hoozemans JJM. Neuroinflammation and Common Mechanism in Alzheimer's Disease and Prion Amyloidosis: Amyloid-Associated Proteins, Neuroinflammation and Neurofibrillary Degeneration. Neurodegener Dis. 2012 Mar 2.

Bruinsma IB, de Jager M, **Carrano A**, Versleijen AA, Veerhuis R, Boelens W, Rozemuller AJ, de Waal RM, Verbeek MM. Small heat shock proteins induce a cerebral inflammatory reaction. J Neurosci. 2011 Aug 17;31(33):11992-2000.

Eurelings LS, Richard E, **Carrano A**, Eikelenboom P, van Gool WA, Rozemuller AJ. Dyshoric capillary cerebral amyloid angiopathy mimicking Creutzfeldt-Jakob disease. J Neurol Sci. 2010 Aug 15;295(1-2):131-4.

Carrano A, Kooij G, van der Pol S, van Horssen J, Veerhuis R, Hoozemans JJ, Rozemuller AJ, de Vries HE. ABC transporters P-gp and BCRP are reduced in capillary cerebral amyloid angiopathy. Submitted

Curriculum vitae

Anna Carrano was born on September 12th, 1983, in northern Italy. She studied Medical Biotechnology and Molecular Medicine at the University of Milan with a curriculum focused on Neuroscience. Anna always dreamt to pursue a career abroad and during her MSc studies she was awarded with an Erasmus Scholarship in The Netherlands, which allowed her to obtain research experience in a foreign country. After successfully completed her studies in Italy, she returned to the Netherlands and started her PhD project within the Neuropathology group at the department of Pathology at the VU medical center, Amsterdam in March 2008, under the supervision of A.J. Rozemuller, H.E. de Vries, J.M. Hoozemans and J. van Horssen. During her PhD training her scientific interest focused on neuropathological changes occurring in Alzheimer's disease cases with severe amyloid deposition in the brain vasculature, also known as cerebral amyloid angiopathy. Since March of this year she works as a postdoctoral researcher at the Department of Neuroscience of the Mayo Clinic in Jacksonville, Florida in the United States of America.

Acknowledgements

This book is finally finished and this is the very last chapter that needs to be written. I dreaded this moment and procrastinated it indefinitely, not so much because I don't want to say thank you to all the amazing people that helped me get here, but because this is like saying goodbye, and I never liked it much. It is so difficult to write my acknowledgements from the other side of the ocean, away from everyone, from every single person I am going to name, without feeling emotional. But I am thankful, nonetheless, with my teary eyes, to all the people that made this project a success and the writing of this thesis possible.

My immense gratitude goes to all my supervisors, promotors and co-promotors, to Annemieke, Elga, Jeroen and Jack. It goes without saying that none of this would have been possible without you. You have thought, inspired, supported, and guided me all the way through. You are not only excellent scientists, you are amazing people and I am honored I have got to learn from you all and be part of your lives. Thank you also to Saskia, Rob and Piet, for your precious inputs and suggestions, and for sharing your wise knowledge with me.

Thank you to all the lab people, at the dept. of Pathology and Molecular cell biology and immunology, that helped with the bench work, when my two hands were not enough and my weeks too short. To everybody that contributed to make my experiments successful, and we all know it is not always the case.

Thanks to all my friends, to the PhD fellows, to the undergrad students, to the technicians, for making the lab (and The Netherlands in general) a better place to be, for sharing a laugh, a chat over a coffee and scientific frustrations (especially!) more often than we would like to admit. A special word for my Italian mates, the Netherlands feels a much sunnier place with you guys around!

Thanks to my family, the Italian and the Dutch one, moms and dads, sisters and husband, near and far, for staying close to me no matter what, no matter where. It made all the difference.

Thank you to Tineke and my furry babies for keeping me sane while going through the odys-

sey of writing this thesis. For giving me love and attention when I needed it the most.

And last thank you to my husband Maarten, who has been there all the way since my first day in the Netherlands. There is not enough space here to thank you and not enough words.

I miss you all and I long for the day I will see you again.